VOLUME 123 NUMBER 1

THE ASTROPHYSICAL JOURNAL

AN INTERNATIONAL REVIEW OF SPECTROSCOPY AND ASTRONOMICAL PHYSICS

JANUARY 1956

SOLAR SPECTROSCOPY WITH A VACUUM SPECTROGRAPH — *Robert R. McMath* — 1

THE TOTAL ECLIPSE OF THE SUN, FEBRUARY 25, 1952: LIGHT-CURVE NEAR MID-ECLIPSE — *Charles C. Batchelder, Katharine Batchelder, Richard Hargreaves, and James Hargreaves* — 9

RADIO REFLECTION AND REFRACTION PHENOMENA IN THE HIGH SOLAR CORONA — *Ronald N. Bracewell and George W. Preston* — 14

RADIO OBSERVATIONS OF INTERSTELLAR NEUTRAL HYDROGEN CLOUDS — *Robert S. Lawrence* — 30

SPECTROPHOTOMETRY OF GAMMA LEONIS — *William H. Wehlau* — 34

AN INTERPRETATION OF AE AQUARII — *John A. Crawford and Robert P. Kraft* — 44

A SPECTROSCOPIC STUDY OF THE PLEIADES — *Eugenio E. Mendoza V* — 54

THE GALACTIC CLUSTER NGC 2169 — *J. Cuffey and S. W. McCuskey* — 59

SOME REMARKS ON THE (*U, B, V*) SYSTEM — *Victor M. Blanco* — 64

A PHOTOMETRIC INVESTIGATION OF THE SHORT-PERIOD ECLIPSING BINARY, NOVA DQ HERCULIS (1934) — *Merle F. Walker* — 68

DIMENSIONS OF CONTACT SURFACES IN CLOSE BINARIES — *G. P. Kuiper and Jeannette R. Johnson* — 90

THE DEBYE-HÜCKEL EFFECT AND STATISTICAL THEORIES FOR COLLISION BROADENING — *Frank N. Edmonds, Jr.* — 95

RADIATIVE TRANSFER AND THERMODYNAMICS — *Rupert Wildt* — 107

ATMOSPHERES OF THE B STARS. I. THE SUPERGIANT EPSILON CANIS MAJORIS — *Lawrence H. Aller* — 117

ATMOSPHERES OF THE B STARS. II. THE SUPERGIANT 55 CYGNI — *Lawrence H. Aller* — 133

MODEL ATMOSPHERES — *Thomas L. Swihart* — 139

MODEL ATMOSPHERES AND THE SOLAR CONTINUUM — *Thomas L. Swihart* — 143

MODEL ATMOSPHERES WITH HIGH HYDROGEN-METAL RATIO — *Thomas L. Swihart* — 151

THE SURFACE-TEMPERATURE CLIMATE OF MARS — *Frank Gifford, Jr.* — 154

LABORATORY EXCITATION OF THE BLUE-GREEN BANDS OBSERVED IN THE SPECTRA OF N-TYPE STARS — *Bengt Kleman* — 162

ANALYSIS OF THE (0, 1) AND (1, 2) BANDS OF THE $^1\Delta$–$^3\Pi$ SYSTEM OF CH — *Norman H. Kiess and Herbert P. Broida* — 166

THE HYDROGEN-LINE RED SHIFT OF RADIO SOURCE CYGNUS A — *A. E. Lilley and E. F. McClain* — 172

NOTES

THE PHASE VARIATION OF URANUS — *Robert L. Talley and Henry G. Horak* — 176

THE HALO DISTRIBUTION OF RADIO EMISSION AND EXTENDED MAGNETIC FIELDS IN OUR GALAXY AND M31 — *G. R. Burbidge* — 178

RELATIVISTIC DEFLECTION OF SUN'S LIGHT BY THE MASS OF THE SUN — *S. N. Milford* — 182

ABSTRACTS OF ASTROPHYSICAL JOURNAL SUPPLEMENT SERIES

NUCLEAR REACTIONS AND ELEMENT SYNTHESIS IN THE SURFACES OF STARS — *W. A. Fowler, G. R. Burbidge, and E. Margaret Burbidge* — 183

A CATALOGUE OF HIGH-VELOCITY STARS — *Nancy G. Roman* — 184

REVISED LIST OF ABSORPTION LINES IN THE SPECTRUM OF R ANDROMEDAE — *Paul W. Merrill and Jesse L. Greenstein* — 186

PHOTOMETRY OF SOLAR FLARES — *Helen W. Dodson, E. Ruth Hedeman, and Robert R. McMath* — 186

ERRATA — 188

THE UNIVERSITY OF CHICAGO PRESS
CHICAGO, ILLINOIS, U.S.A.

January 1956 Vol. 123, No. 1

THE ASTROPHYSICAL JOURNAL

AN INTERNATIONAL REVIEW OF SPECTROSCOPY AND ASTRONOMICAL PHYSICS

Founded in 1895 by George E. Hale and James E. Keeler

Published in Collaboration with the American Astronomical Society

S. CHANDRASEKHAR
Managing Editor
Yerkes Observatory of the University of Chicago

EDITORIAL BOARD

HAROLD F. WEAVER (1956-60)
Berkeley Astronomical Department
University of California

MARTIN SCHWARZSCHILD (1954-58)
Princeton University Observatory

LEO GOLDBERG (1955-59)
The Observatory of the University of Michigan

HORACE W. BABCOCK (1953-57)
Mount Wilson Observatory of the Carnegie Institution of Washington

G. HERZBERG (1952-56)
National Research Council, Ottawa

The Astrophysical Journal is published bimonthly by the University of Chicago at the University of Chicago Press, 5750 Ellis Avenue, Chicago 37, Illinois, during January, March, May, July, September, and November. ¶Two volumes are published per year, one beginning with the January issue and the other beginning with the July issue. On all orders from the United States and its possessions the subscription price is $7.50 per volume or $15.00 per year; the price of single copies is $3.50. ¶On all orders from Canada the subscription price is $8.00 per volume or $16.00 per year; the price of single copies is $3.65. On all orders from all other countries the subscription price is $8.25 per volume or $16.50 per year; the price of single copies is $3.75. (Orders for service of less than a volume will be charged at the single-copy rate.) ¶Subscriptions are payable in advance. Please make all remittances payable to The University of Chicago Press, in United States currency or its equivalent by postal or express money orders or bank drafts. (Exception: members of The American Astronomical Society must send their subscriptions and remittances to the Treasurer of the Society.)

The following is an authorized agent:

For the British Commonwealth, except North America and Australasia: The Cambridge University Press, Bentley House, 200 Euston Road, London, N.W. 1, England. Prices of yearly subscriptions and of single copies may be had on application.

Claims for missing numbers should be made within the month following the regular month of publication. The publishers expect to supply missing numbers free only when losses have been sustained in transit, and when the reserve stock will permit.

Business correspondence should be addressed to The University of Chicago Press, Chicago 37, Illinois.

Communications for the editors and manuscripts should be addressed to: S. Chandrasekhar, Editor of THE ASTROPHYSICAL JOURNAL, Yerkes Observatory, Williams Bay, Wisconsin.

Line drawings and photographs should be made by the author, and all marginal notes such as co-ordinates, wave lengths, etc., should be included in the cuts. It will not be possible to set up such material in type.

One copy of the corrected galley proof should be returned as soon as possible to the editor, Yerkes Observatory, Williams Bay, Wisconsin. Authors should take notice that the manuscript will not be sent to them with the proof.

The cable address is "Observatory, Williamsbay, Wisconsin."

The articles in this journal are indexed in the *International Index to Periodicals*, New York, N.Y.

Applications for permission to quote from this journal should be addressed to The University of Chicago Press, and will be freely granted.

Microfilms of complete journal volumes are available to regular subscribers only and may be obtained at the end of the year. Orders and inquiries should be addressed to University Microfilms, 313 North First Street, Ann Arbor, Michigan.

Notice to subscribers: If you change your address, please notify us and your local postmaster immediately.

Entered as second-class matter, July 31, 1940, at the Post-Office at Chicago, Ill., under the Act of March 3, 1879.
Acceptance for mailing at special rate of postage provided for in United States Postal Act of October 3, 1917, Section 1103, amended February 28, 1925.
Copyright 1956 by the University of Chicago.

[PRINTED IN U.S.A.]

THE ASTROPHYSICAL JOURNAL

AN INTERNATIONAL REVIEW OF SPECTROSCOPY AND ASTRONOMICAL PHYSICS

VOLUME 123 JANUARY 1956 NUMBER 1

SOLAR SPECTROSCOPY WITH A VACUUM SPECTROGRAPH*

ROBERT R. MCMATH
McMath-Hulbert Observatory, University of Michigan
Received August 23, 1955

One of the first attempts to use solar spectrum observations in a quantitative way was made by a distinguished member of the staff of the Princeton University Observatory, Professor Henry Norris Russell. On the basis of estimated line intensities in the *Revised Rowland* tables, Professor Russell (1929) determined the relative chemical composition of the sun. In the succeeding twenty-five years his results have been refined but not greatly modified. Professor Russell's great work demonstrated the inherent power in quantitative studies of line intensities and stimulated attempts at more precise intensity measurements. Studies of the chemical composition of the sun were followed by analyses that derived the parameters of the physical state of an average solar atmosphere. Curve-of-growth methods provided information on states of excitation, kinetic temperatures, and pressures. Such methods are based on the measurement of a kind of average, the equivalent width, and, as is often the case, much important information is lost in the use of an average.

Today improvement in knowledge of the sun depends largely upon securing measurements of intensities in the solar spectrum that are sufficiently precise for the determination of accurate line profiles. At the present time, profiles of varying degrees of reliability have been determined for a total of about fifty *strong* lines in the solar spectrum (Pierce 1954). These refer to ten chemical elements. However, fewer than one-quarter of these measurements are precise enough to be useful in critical comparisons of theory and observation. The profiles of *faint* lines are almost unknown.

The reasons for this unsatisfactory state of our knowledge are not hard to find. Most of them originate in various imperfections in the spectroscopes that have been used in solar spectroscopy. The majority of solar spectroscopes in use today were designed originally for the measurement of accurate wave lengths rather than reliable intensities. Although these instruments show more than adequate resolution of close lines for position work, in all but a few cases stray light in the spectrum has not been controlled.

These considerations point toward the need for a large-grating instrument, designed especially to eliminate scattered light. With the successful ruling, in recent years, of

* Address of the retiring president of the American Astronomical Society at Princeton, N.J., April 5, 1955. The work described here was supported in part by Contract N6-onr-232V with the Office of Naval Research.

highly perfected gratings, there are no optical defects that will interfere with the precise measurement of intensity. There are, however, many other problems that must be overcome before the full performance of the practically perfect gratings, such as those produced by the Babcocks (1951), actually can be obtained.

For example, soon after the installation of one of the new Babcock gratings in our monochromator in the Snow telescope on Mount Wilson, it became evident that convection currents within the spectroscope limited the performance of the grating. The difficulty first appeared during the measurement of wave lengths of spectrum lines on direct intensity tracings. Air currents caused the spectrum lines to move in random fashion through a range of 0.06 A when conditions were good, and as much as 0.2 A when conditions were poor.

Elimination of bad seeing that is caused by motion of air within the instrument is the strongest argument for the construction of a vacuum spectroscope. There are, however, other considerations that favor a large vacuum instrument. Such a spectroscope is insensitive to changes in air pressure and temperature and thus makes possible closer

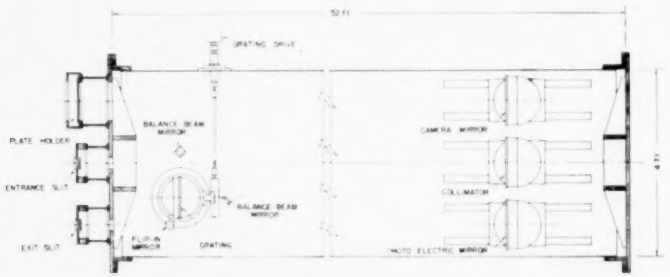

FIG. 1.—Schematic plan of the McMath-Hulbert 50-foot focal length vacuum spectroscope

control and repetition of observing conditions. A high-dispersion spectroscope operating in air must include compensation for pressure changes as small as 3 mm of mercury. Changes in temperature not only initiate air currents in air-filled spectrographs but also effect changes in the collimator, the image-forming elements, the mounting, and the grating. In a 15000-groove/inch grating on a Pyrex blank, a temperature change of 1° C will shift a spectrum line by one part in 300000 of its wave length. In a vacuum instrument, all these temperature effects are either eliminated or greatly reduced. When the spectrograph is evacuated, heat is transferred chiefly by radiation or by conduction along poor thermal paths, and the rate of contraction or expansion of any optical part must therefore be very small indeed. Nevertheless, the change in length of the instrument may be appreciable during a long period of observation, and it must be possible to control continuously the position of the focal point.

Several new inconveniences arise when a large spectroscope must be confined within a vacuum tank. All controls for the adjustment of the optical parts must be brought outside the tank through airtight seals. At least one window must be provided to let light into the instrument, and often a second is needed to let the light out. Unless windows are carefully selected and placed in the optical path, they can be troublesome sources of dust lines and interference fringes.

With these considerations in mind, preliminary designs for a large-scale vacuum spectroscope were begun at the McMath-Hulbert Observatory in November, 1953. The McGregor tower telescope, with its solar images, 6 and 12 inches in diameter, is so located that it can send light to several positions suitable for a large spectroscope. The best of these sites, lying to the east of the tower, was selected for the new instrument.

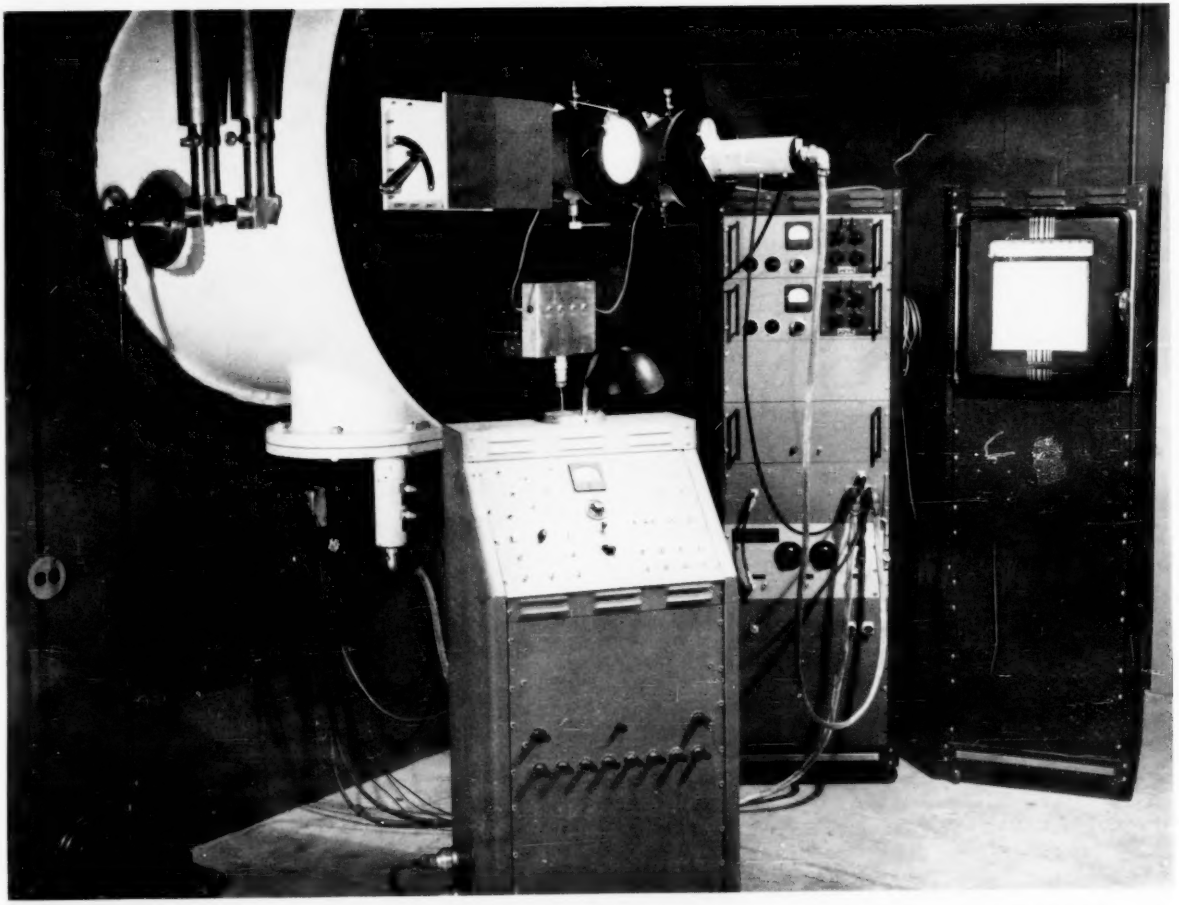

FIG. 2. — Working head of vacuum spectroscope. *From left to right:* air lock for photographic plates; entrance slit; and exit slit with E.M.I. photomultiplier in place.

No changes in the telescope were required. A focal length of at least 50 feet was needed for the new spectroscope, in order to illuminate completely the large gratings now available for use in solar spectroscopy. The choice of a 50-foot focal length also provided a correct matching of the resolving power of the 6 × 8-inch Babcock grating with the resolving power of existing photographic plates. In order to avoid chromatic aberration, it was decided to use an all-mirror optical system.

Figure 1 is a schematic drawing of the plan finally adopted. It shows the relative positions of the single collimator mirror, the grating mounting that can be rotated to move the spectrum, and two image-forming mirrors, one for use in a spectrographic arrangement, the other for a monochromator. It was decided that special temperature regulation other than that provided by evacuation would not be required. It was also thought that deep concrete piers, based in sand, would provide a sufficiently stable foundation for the instrument without additional antivibration mounting.

The general features of the large spectroscope began to materialize with the delivery to the observatory of a cylindrical tube, 52 feet long and 4 feet in diameter. The tube was delivered on April 13, 1954; but, before its arrival, underground concrete footings had

TABLE 1

COINCIDENT WAVE LENGTHS AND DISPERSION FOR DIFFRACTION ANGLE 55°.68

Wave Length	Order	Dispersion (mm/A)	Wave Length	Order	Dispersion (mm/A)	Wave Length	Order	Dispersion (mm/A)
27531	I	1.62	6883	IV	6.48	3933	VII	11.34
13766	II	3.24	5506	V	8.10	3441	VIII	12.96
9177	III	4.86	4588	VI	9.72	3059	IX	14.58

been prepared. Two-inch-thick, heavily ribbed steel plates for closing the ends of the tube had been machined at the observatory. The tube was manufactured by the Whitehead and Kales Company, of River Rouge, Michigan. Two sections of $\frac{1}{4}$-inch-thick steel plate were rolled and welded into two tubes, each 26 feet long. After delivery to the observatory, the two sections were welded together to form one continuous tube. The two end-plates are demountable. In addition, two portholes provide access to the inside of the tube. The steel end-plates are attached by bolts to two rings, machined at the observatory, and welded to the cylinder.

The air seal for the two end-plates is provided by a rubber gasket that is cemented into a groove in the end-plate and seals by pressure against the bolt ring on the end of the tube. Individual features of the spectroscope become clear if the path of a beam of light is traced through the instrument. In normal operation the telescope projects an image of the sun on the entrance slit of a small-prism spectroscope. This predisperser, in turn, images a spectrum on the entrance slit of the vacuum spectroscope (Fig. 1). The purpose of the predisperser is to exclude from the main instrument all sunlight except the narrow band of wave lengths under investigation. The dispersion of the predispersing spectroscope is such that a slit opening of 0.1 mm will admit only 69 A of the spectrum near Hα to the collimator of the vacuum spectrograph.

This use of a small-prism spectroscope not only reduces the intensity of stray light but also eliminates overlapping orders and permits selection of wave length and order desired. Table 1 shows as an example, in the seventh-order K region, the mixture of radiation emergent from the exit slit of the vacuum spectroscope if the prism spectroscope is not used. Table 1 also shows the variation of dispersion with wave length for a constant angle of diffraction, 55°.68. The change of dispersion with angle of diffraction

is large. The wave length 5000 A appears at the angles of diffraction and dispersions listed in Table 2. The rapid change of dispersion with angle of diffraction produces a linear dispersion of 26 mm/A for fifth-order Hα at an angle of 79°.88!

A field lens that images the telescope objective on the collimator is placed just in front of the entrance slit of the grating instrument. This lens provides part of the vacuum seal and, at the same time, admits light to a cylindrical air lock surrounding the slit mechanism. The air lock makes it possible to adjust the slit jaws without destroying the vacuum in the main tank. With the slits in vacuum, a small electric motor is used to open and close the slit jaws. The slits are 2 inches long, are made of optically polished chromium carbide, and are tilted so that light reflected from them can be used for guiding.

TABLE 2

ANGLES OF DIFFRACTION AND DISPERSIONS FOR λ 5000 A

Order	Angle of Diffraction	Dispersion (mm/A)	Order	Angle of Diffraction	Dispersion (mm/A)	Order	Angle of Diffraction	Dispersion (mm/A)
I	8°.63	0.92	III	26°.74	3.07	V	48°.59	6.91
II	17.46	1.92	IV	36.87	4.57	VI	64.16	12.59

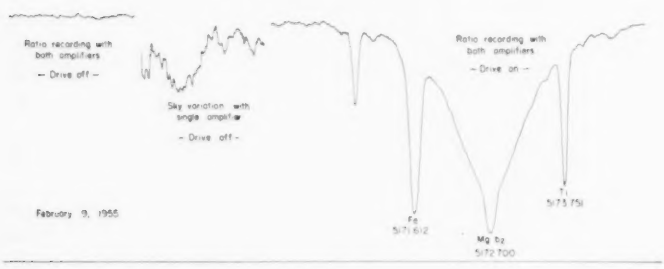

FIG. 3.—Sample tracings to illustrate ratio recording

The light proceeds from the entrance slit (Fig. 1) along the axis of the large vacuum tank to a 12-inch collimating mirror. All the final adjustments of this and all mirrors in the tank must be made after the air has been pumped out. The necessary motions are provided by electric motors, controlled from the observer's station. The collimator returns a parallel beam along the tube to the grating near the entrance slit (Fig. 1). All final grating adjustments and means for changing the wave-length region under observation are brought outside the vacuum tank either mechanically or electrically. The angle of rotation of the grating can be read with a périscope.

Satisfactory performance of the spectroscope as a direct recording monochromator is dependent upon the precision motion of the grating. Fortunately, a well-tested unit for providing the desired slow rotational motion of the grating was available in the McGregor infrared spectroscope. Its transfer to the vacuum spectroscope greatly expedited the construction of the new instrument. The rate of continuous rotation of the grating can be varied from 0°.01 per hour to a maximum rate of 0°.5 per hour. The rota-

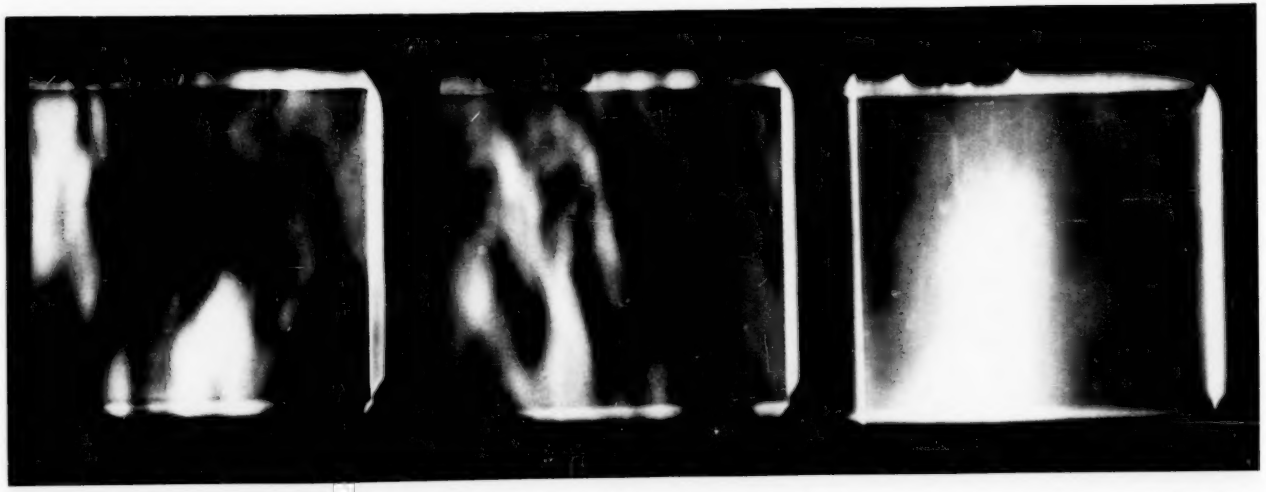

FIG. 4.—Foucault knife-edge tests to show disturbances by air currents in the spectrograph. *Left*, spectrograph at normal air pressure; *center*, spectrograph at half normal air pressure; *right*, spectrograph at 50 μ air pressure.

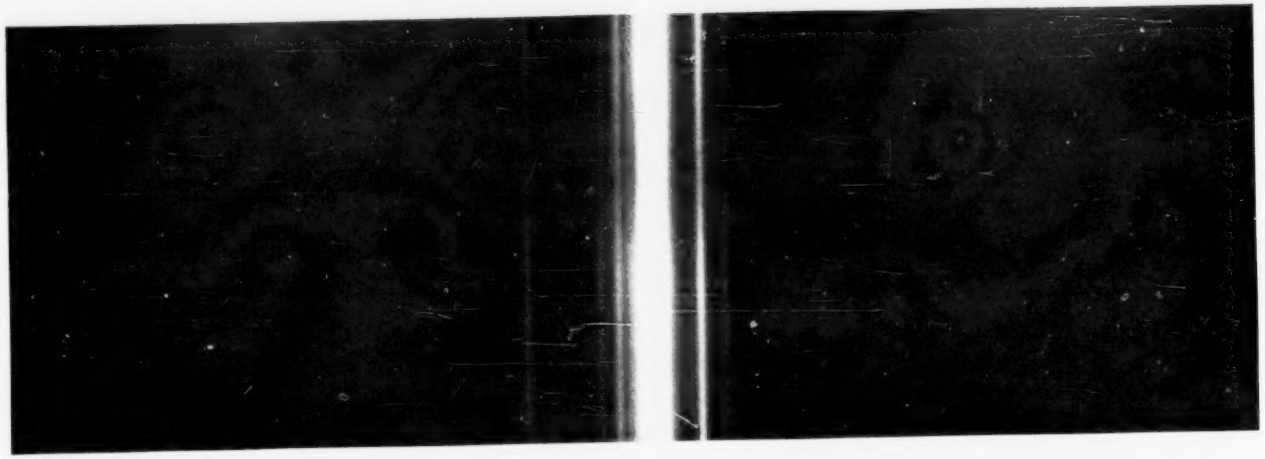

FIG. 5.—Photograph of 5461 Å line of natural mercury

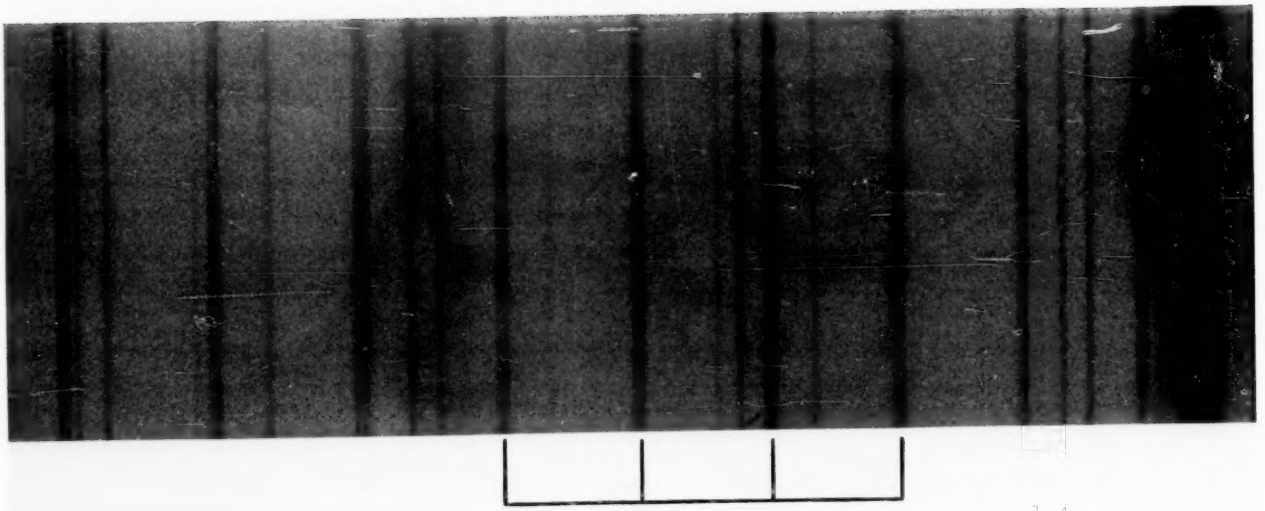

FIG. 6.—Photograph of iodine lines superposed on the solar spectrum at 5331 A. The four labeled pairs of lines have an average separation of 0.33 A

tion of the grating and the consequent variation in wave length of the emergent radiation are controlled by the frequency of the current driving the synchronous motors of the spectrograph. The same current is used to drive the recording chart, and in this way precise proportionality between grating rotation and linear distance on photometric tracings can be maintained.

The grating disperses the light and diffracts it back along the vacuum tank to either of two image-forming mirrors placed symmetrically on either side of the collimator (Fig. 1). One of the mirrors images a spectrum on an area to the left of the entrance slit, where it can be used for spectrum photography. The other mirror images a spectrum on an exit slit to the right of the entrance slit, thus forming a powerful grating monochromator which can be used for direct photoelectric recording. A small flip-in mirror (Fig. 1) can be tilted in to the beam to send light to a periscope for direct visual check of the wave-length region on the exit slit. Light baffles and traps have been installed throughout the tank to absorb stray light and keep it from reaching either the photographic plate or the exit slit. The camera mirror and photoelectric mirror may be covered by an absorbing shutter to eliminate reflection of unused light. The radiation that emerges from the exit slit can be used for various nonphotographic methods of detecting and recording intensities. With the grating set to provide a high-order spectrum, the energy that emerges from the exit slit is an almost monochromatic band that has a width of only 0.008–0.010 A.

The photographic plate and its holder are located in an air lock to make possible the changing of plates without loss of the spectroscope vacuum (Fig. 2). The single plateholder is supplemented by a magazine plateholder that permits the exposure of a dozen plates in rapid succession.

In principle, any detector can be used to measure the energy of the emergent beam. Up to the present time only E.M.I. No. 6262 photomultipliers have been tried. These have performed well. The output of the photomultiplier has been amplified by a Kron-type amplifier and the output recorded on a Leeds and Northrup G Speedomax.

Ratio recording will be attempted with most of the electrical detectors, to minimize effects of changes in sky transparency. A reference signal is obtained by reflecting a part of the collimated beam of sunlight from just in front of the grating to an auxiliary photomultiplier (see "Balance Beam Mirror," Fig. 1). A change in sky transmission will change both spectrum and reference beams by the same factor, but their recorded ratio will be unchanged. Figure 3 shows the effectiveness of ratio recording during an interval of variable sky transparency. The ratio of the outputs of the two cells is very nearly constant, even though the variation in output of one cell is large. Under these conditions, with the aid of ratio recording, the tracing (Fig. 3) of the magnesium line at 5173 was made.

Air was pumped out of the new spectroscope for the first time on May 21, 1954. The first photographs were made with a temporary camera on November 9, and the first tracings, with E.M.I. photomultipliers as detectors, were obtained on December 21. All these observations made use of some temporary equipment and can be improved as the instrument is completed. Nevertheless, they indicate that the initial performance of the spectroscope is good enough to permit profitable attack on solar problems.

The Foucault knife-edge test offers a way of observing the effect of pumping the air out of the tank (Fig. 4). The photographs made with air in the tank show the image badly distorted by air currents, but the photograph made with no air in the tank is free from this disturbance. The tank can be evacuated to the limiting pressure of the pump, 30 μ, but it is almost impossible to detect any convection currents after the pressure has been reduced to less than 3 or 4 mm.

The lines of natural mercury are sometimes used to test the performance of spectroscopes. Figure 5 is a photograph, taken with the vacuum spectrograph, of the 5461 line.

It was made in the fifth order of Babcock grating No. 96B, and it reveals most of the components of the hyperfine structure.

The lines of iodine provide another group of useful test objects for spectroscopes. The iodine spectrum contains many closely packed double lines in the green part of the spectrum. The four double lines shown near the center of Figure 6 have an average separation of 0.009 A. The ratio of the mean wave length of the lines to their average separation is 600000. The significance of a resolving power of 600000 can be made clearer by comparing a normal tracing of solar lines, as in the top line of Figure 7, with the much

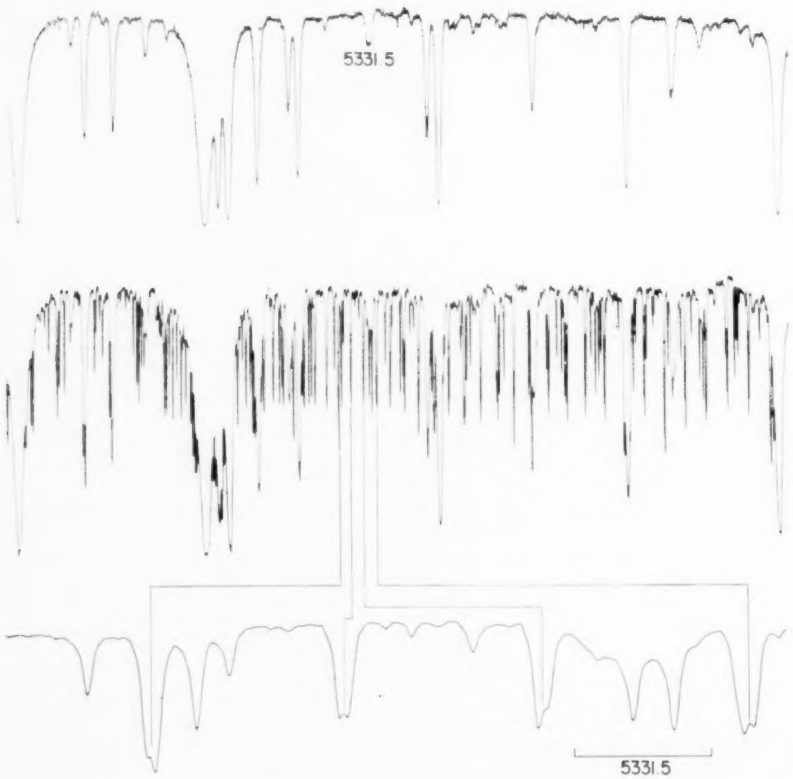

FIG. 7.—Direct tracings of solar spectrum and superposed lines of iodine

sharper iodine lines. The second line of Figure 7 shows the same part of the solar spectrum with the absorption lines of iodine superposed. Lastly, on a greatly expanded scale, the resolution of the previously mentioned close double iodine lines is shown. The scale of the last tracing, necessary to show the effects of a resolving power of 600000, can be judged by comparing the 5331 A solar line in the top tracing with the broad depression in the lower right that is the same line.

Figure 8 is a sample photograph of the solar spectrum made with the vacuum spectroscope. The tracing of the photograph reveals the high resolving power in the depth

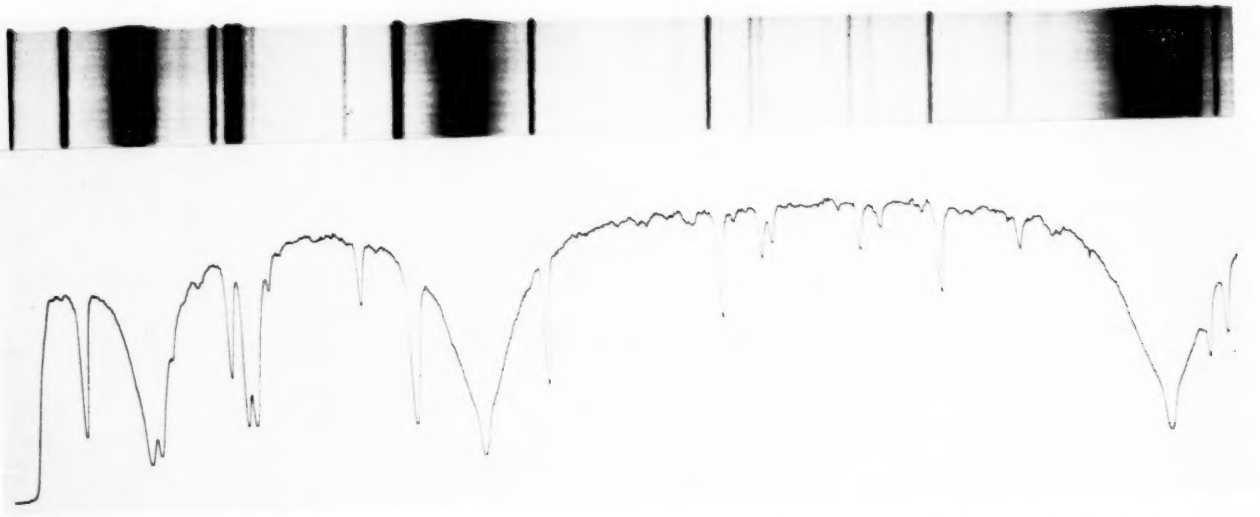

FIG. 8.—Photograph and tracing of magnesium b lines. The variations in the continuous background parallel to the dispersion and the displacements in the absorption lines are real solar features.

and sharpness of the lines of the heavy elements that flank the broad magnesium lines.

It is possible to compare some uncorrected direct photoelectric tracings from the vacuum spectroscope with results from the use of high-resolution instruments in line-profile work by Evans (1940) and Shane (1941). The greatest differences are in the central intensities, and even here the differences average less than 3 per cent (Fig. 9).

The K line of calcium is particularly interesting to all who use the results from spectroheliographs. New material for detailed study of this line can be obtained with the

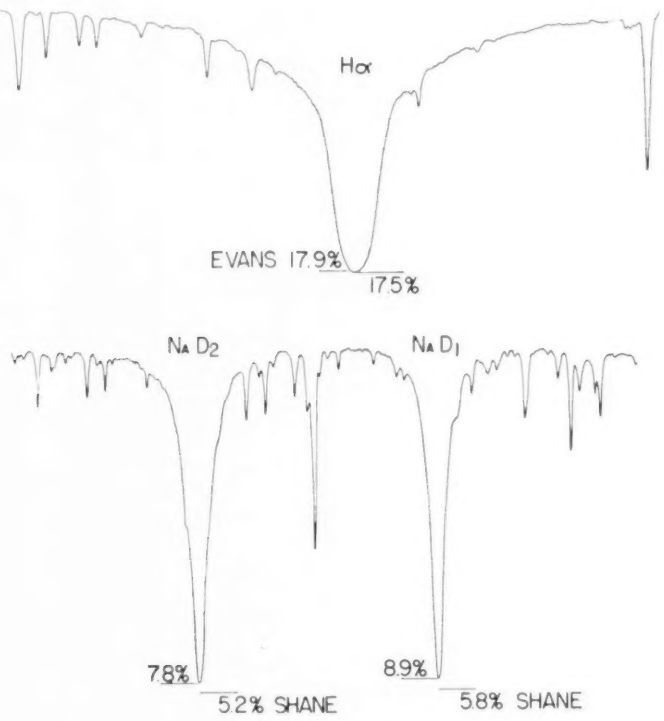

FIG. 9.—Direct photoelectric tracings of Hα and the sodium D line

vacuum spectrograph. The complex structure in the center of the line is revealed on a scale that should make precision measurements more easily obtainable than before (Fig. 10).

The programs planned for the vacuum spectrograph are extensive, and our hopes are high. Precision measurements should lead to improvement in abundance determinations. The evaluation of large-scale motions, turbulence, and kinetic temperatures as a function of height can be attempted. Molecular lines and the central intensities of the very strong absorption lines will give clues to the values of these quantities in the outermost solar layers. Lines with high excitation potential will be useful for the deeper layers.

Many of the programs for the new instrument will be connected with those of the spectroheliographs in the 50-foot tower. Provision has been made for placing monochromatic features of the sun on the slit of the vacuum spectroscope with the aid of a Lyot filter. Velocity and intensity changes in the spectra of spots, plages, and associated active phenomena will be intensively studied. The vacuum spectroscope will provide observations of higher precision than those previously recorded for large numbers of solar spectrum features. It is hoped that the number and quality of the observations that can be obtained will be of significant help in extending our knowledge of the sun.

The vacuum spectroscope has been a team project, and I could not overstate the contribution which has been made by my colleagues, Drs. Mohler and Pierce. Mr. John Brodie has made every drawing, and our instrument-maker, Mr. Sanderson, has converted the drawings into operating assemblies of steel and nonferrous metals. Everybody without exception in the group at Lake Angelus has helped when needed. The construction of this spectroscope was made possible by generous grants-in-aid by the Arthur Curtis James Foundation, The Detroit Edison Company, and McGregor Fund of Detroit, to whom I offer my grateful thanks.

REFERENCES

Babcock, H. D., and Babcock, H. W. 1951, *J. Opt. Soc. America*, **41**, 776.
Evans, D. S. 1940, *M.N.*, **100**, 150.
Pierce, A. K. 1954, *Proc. N.S.F. Conference on Stellar Atmospheres*, p. 4.
Russell, H. N. 1929, *Ap. J.*, **70**, 11.
Shane, C. D. 1941, *Lick Obs. Bull.*, **19**, 119.

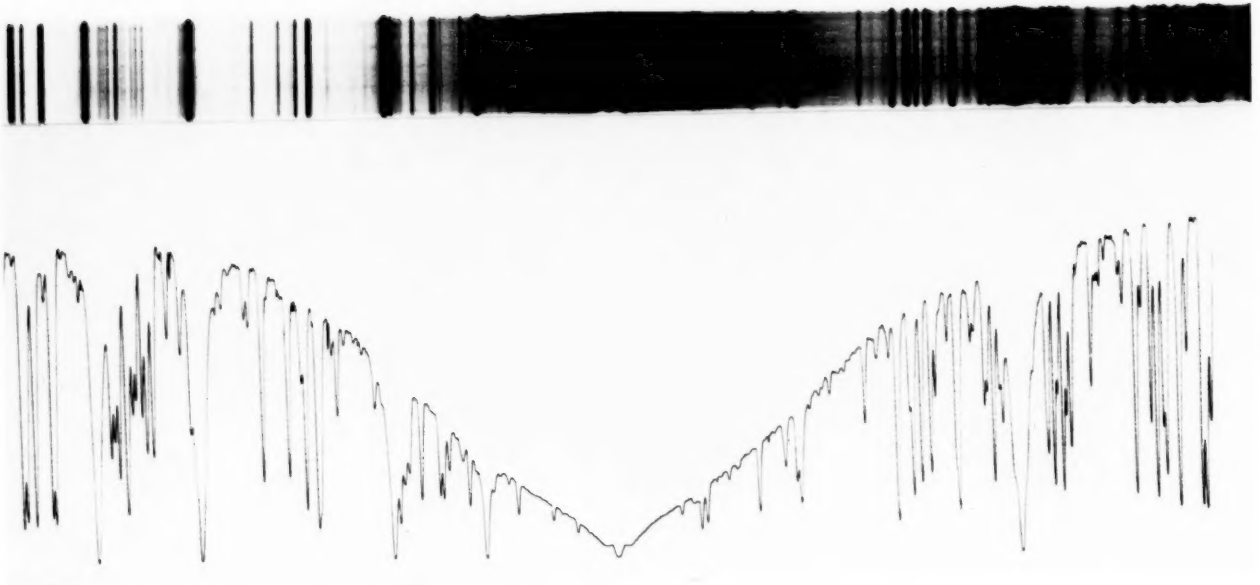

FIG. 10.—Photograph and tracings of the K line of calcium

THE TOTAL ECLIPSE OF THE SUN, FEBRUARY 25, 1952

LIGHT-CURVE NEAR MID-ECLIPSE

CHARLES C. BATCHELDER, KATHARINE BATCHELDER,
RICHARD HARGREAVES, AND JAMES HARGREAVES
University of Ottawa Astronomical Research Expedition
Received December 1, 1954; revised January 25, 1955; revised July 29, 1955

ABSTRACT

Observations obtained with an electric telephotometer during the total eclipse of February 25, 1952, show (1) that the light-curve was not symmetrical before and after mid-eclipse; (2) that during totality the luminance of the sky varied with time and zenith distance; and (3) that the zenithal intensities were equal at mid-eclipse and when the sun was at 95°28′ zenith distance, during evening twilight of the same day. It is suggested that for this eclipse the terrain over which the penumbra passed was an important cause of the irregularities noted.

EQUIPMENT

The electric telephotometer of the University of Ottawa sky photometer was used to measure the variation of the diffuse light of the sky during the total solar eclipse of February 25, 1952. The observing position was near Jebel Dabachi, 18°32′.5 N. and 35°32′.6 E. at an elevation of 650 meters above sea-level.

The telephotometer consists of an optical pile containing neutral density and color filters on a movable slide, but with no light-gathering optics. The receiver located directly below the optical pile is a 1P21 electron multiplier. The galvanometer scale was brought into the plane of the chronometer face with a prism and was either photographed or observed visually. For this program the instrument was set to receive from an unobstructed field of 1°.3 radius.

THE OBSERVATIONS

Table 1 gives the observations at the zenith near mid-eclipse which were recorded photographically. The film was read first in a viewer and then under a microscope, insuring that the galvanometer deflections were accurate to one unit in the second decimal place and the time to the beat of the chronometer ($\frac{1}{2}$ sec).

An arbitrary scale of relative radiant intensity was derived by adjusting the galvanometer deflections for dark current and multiplying by a factor for each neutral density filter used. This has been taken as ordinate for Figure 1; and as abscissa we have used the parameter x

$$x = \frac{1000\,(L_2 + m)}{L_1 + L_2},$$

where L and m are as defined in the *American Ephemeris*, Part III. There is a well-defined minimum and a distinct lack of symmetry, the intensity being greater after mid-eclipse.

The dark current on other days was found to rise with increasing temperature. We are satisfied that in the period of these observations it did not change by more than 0.1 unit of the galvanometer scale. The change may have been much less, since there was no noticeable fall in temperature near mid-eclipse.

The color filter used was Wratten 15 and the filter-receiver response to an equal-energy spectrum, calculated from the manufacturer's specifications, should have a maximum near 5400 A. We are less confident about the neutral density-filter factors, determined on the optical bench many months later. Therefore, we rely principally on a comparison between observations made with the same filter.

Another series of observations was made without benefit of photographic recording. This has served as a check on the filter number, which could not be shown on the photographs. Prior to $9^h15^m54^s$ and after $9^h26^m54^s$ three color filters were in use, with specified response maxima at 4300, 5400, and 6000 A. But the blue filter shows some discoloration of the balsam, which would shift the response toward the red.

The color-work indicates a shift in the blue/red ratio, rising to a 30 per cent change toward the red for the observations nearest mid-eclipse. This is symmetrical. Measurements before first and after fourth contact show that there was more than average dust in the air, evidently due to fall-out from the storm of February 22.

During totality, observations were made in twenty-six positions surrounding the sun. This series shows a distinct gradient from the horizon to the zenith, which is not the same for all position angles and varies with time.

For comparison with the work of some earlier observers (Mitchell 1924), we made a series of twilight observations. This shows that the luminance at the zenith and in the spectral range of the filter-receiver combination was equal for mid-eclipse and for

TABLE 1

PHOTOGRAPHICALLY RECORDED OBSERVATIONS OF THE ZENITH SKY*

Universal Time	Neutral Density Filter No.	Galvanometer Deflection	Radiant Intensity	x
$9^h18^m27^s$	3	0.90	188.5	+25.9
$55\frac{1}{2}$	3	0.56	139	+20.3
19 31	2	7.10	81.8	+13.5
$56\frac{1}{2}$	2	3.70	45	+ 8.5
20 30	2	0.50	9.8	+ 1.8
Second contact				
39.7				0.0
$44\frac{1}{2}$	1	3.50	3.90	− 0.9
21 1	1	2.96	3.36	− 4.0
12	1	2.80	3.20	− 6.1
not recorded	1	2.70	3.1	
Greatest phase				
22 12.5				−16.25
$59\frac{1}{2}$	1	4.00	4.4	− 9.1
23 $29\frac{1}{2}$	1	6.4/5	6.9	− 3.1
$35\frac{1}{2}$	1	7.00	7.4	− 2.1
Third contact				
36.7				0.0
24 $5\frac{1}{2}$	2	1.80	24	+ 3.7
$18\frac{1}{2}$	2	3.10	38	+ 6.2
$43\frac{1}{2}$	2	6.00	70	+11.1
25 6	2	8.55	97.6	+15.4
$13\frac{1}{2}$	2	9.72	110.3	+16.9
30	3	0.56	139	+20.1
46	3	0.73	164	+23.2
$48\frac{1}{2}$	3	0.80	174	+23.7
$53\frac{1}{2}$	3	0.82	177	+24.6
59	3	0.91	190	+25.7
26 3	3	0.98	200	+26.5
9	3	1.05	210	+27.7
17	3	1.17	228	+29.3
25	3	1.29	245	+30.8
39	3	1.49	274	+33.5
$58\frac{1}{2}$	3	1.77	315	+37.3

* After the photograph made at 21^m12^s the camera did not advance properly for seven exposures. At $19^m56\frac{1}{2}^s$ the definition of the galvanometer scale was poor.

16^h2^m of the same day. That was 20 minutes after sunset, when the sun was at a zenith distance of 95°28′ (not allowing for refraction). Ross, at Wallal on the northwest coast of Australia in 1922, derived an equivalence at zenith distance 97°29′, using a photographic plate exposed to the region of the southern pole. It is possible that the amount of actinic light would have been less than yellow light as measured by our photometer.

METEOROLOGICAL CONDITIONS

On the day of the eclipse the wind was calm or very light from the northeast; horizontal visibility[1] was 7 to the north and 8 to the south. There was no cloud until after mid-eclipse, but then thin and high cirrus was seen; during the afternoon and evening the amount of cirrus increased. There were no dense clouds at any time. On February 22 there had been a dust storm, reducing visibility to 6, but the dust had settled to low levels by sunrise on the eclipse day. It should be noted that a visibility of 7 and 8, while not the best that the Sudan can give, still indicates a transparency above the average.

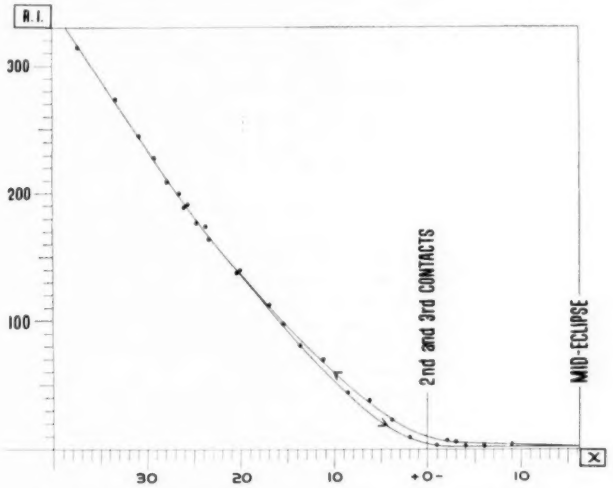

FIG. 1.—The variation of relative radiant intensity during the eclipse

TOPOGRAPHY

The Red Sea Hills are predominantly steep, deeply cleft mountains, which rise sharply out of the coastal plain bordering the Red Sea and then fade out slowly toward the Nile. The peaks become fewer and the valleys between them wider until the hills are left behind and there is only a flat, pebbled desert. Our observation site was located on the western edge of the mountainous region, with minor peaks to the northeast and only a few outcrops to the west. At second contact the full shadow was over the open desert, with the nearest zone of partial eclipse over the mountains. Here there were many high peaks and much broken ground to obstruct low-level scattering. At third contact the nearest zone of partial eclipse was over open desert, with only a few small peaks near by.

[1] Relevant code figures for horizontal visibility: 6 = objects visible at 4 km but not at 10 km; 7 = objects visible at 10 km but not at 20 km; 8 = objects visible at 20 km but not at 50 km; 9 = objects visible at 50 km but not at 150 km. Mountain peaks were used as visibility marks, the most distant was 75 km (cf. Middleton 1947).

We were informed by the airline plying between Port Sudan and Khartoum that a haze-top was often seen by their pilots about the level of the main peaks of the Red Sea Hills.

DISCUSSION

We must first consider the possibility of instrumental error. Unsteadiness in the galvanometer is improbable because the definition of the photographs was generally good. After much discussion we dismissed the dark current as the cause of any large error. The temperature within the instrument could not be measured; but during the three months following the eclipse, when much higher temperatures were experienced, it appeared that it was radiation from the rocks surrounding the observatory rather than air temperatures which caused the dark current to rise. During the eclipse the normal daily heating of the rocks was checked, but they did not have time to cool. If the temperature of the instrument had dropped, the dark current would have become more negative, and failure to allow for this would have made the readings too small. A temperature drop with time lag would have diminished the asymmetry. We feel, therefore, that objective causes should be sought.

A band of high luminance near the horizon has been recognized as typical of solar eclipses since the earliest times. Minnaert (1940) has described the horizon light as "a warm orange." Butler (Mitchell 1924) during the 1918 eclipse noted, 1 minute before totality, a greenish pallor overspreading the landscape before it was dark; and during the last half-minute before totality, the lower part of the sky turning to "a rich yellow inclining to orange," while the sky above darkened rapidly. He also noted a warm tone in the clouds, and his paintings, as reproduced in Mitchell's book (1924), suggest a suffusion of pink.

Richardson and Hulburt (1949) set up a horizon photometer and measured the integrated light during the 1947 eclipse. They obtained a light-curve during totality similar to, but slightly deeper and more regular than, the curve of zenith brightness (their photometer was screened to make it respond approximately like the standard observer).

Sharp and his co-workers (1933) refer to a noteworthy band of high luminance near the horizon during the 1932 eclipse, seen under cloud in New Hampshire. Their measurements show that this moved during totality and that the range of brightness, from zenith to horizon, was approximately 1 to 10.

During the 1947 eclipse we made observations with a rather crude instrument under a cloudy sky in Brazil. It was then possible to show that some light had come from zones as far distant as 400 km from the observer (Hargreaves 1949). Richardson and Hulburt (1949), who had been observing the same eclipse under very thin cirrus, drew the conclusion that "the brightness of the zenith sky during totality was almost entirely due to scattered light from low levels of the atmosphere and almost negligibly to primary scattered light from high levels."

The light-curve for the 1952 eclipse, as measured in the Sudan, is much flatter than the curves derived from the 1947 observations. This suggests that more of the scattered light came from distant penumbral regions. The color changes noted appear to support this hypothesis, and the absence of cloud, with above-average horizontal visibility, makes it plausible.

To account for the asymmetry before and after mid-eclipse, several physical considerations may be advanced; but some of these have already been criticized by other workers. Sharp, Gray, Little, and Eckweiler (1933) and Betenska (1944) concluded independently that light from the corona is insignificant in the illumination of the sky. We understand from a conversation with Ohman that he was unable to detect the green line with a monochromator during the 1947 eclipse when observing under cloud. If the gross effect of the corona is negligible or even small, inequality from one limb to another would not account for an important asymmetry such as we have noted. Our conclusion is that ir-

regular reflection from the ground and irregular transmission from the distant sky, low on the horizon, remain to be considered.

Attention has already been focused on the importance of ground reflections by van de Hulst (1948), following the analysis of Chandrasekhar (1950). It would seem that for the 1952 eclipse, as seen from our camp, a study should be made based on primary scattering in penumbral regions, with different ground albedo on opposite sides of the observer and mountain peaks cutting off light from low on the horizon in some directions. These complications make further pursuit impossible in this place but challenge investigation.

REFERENCES

Betenska, N. 1944, *J.B.A.A.*, **54**, 124.
Chandrasekhar, S. 1950, *Radiative Transfer* (Oxford: Clarendon Press), chap. x.
Hargreaves, J. 1949, *J.R.A.S. Canada*, **43**, 229.
Hulst, H. C. van de. 1948, *Ap. J.*, **107**, 220.
Kuiper, G. (ed.). 1948, *The Atmospheres of the Earth and Planets* (Chicago: University of Chicago Press).
Middleton, W. E. K. 1947, *Visibility in Meteorology* (Toronto: University of Toronto Press).
Minnaert, M. 1940, *Light and Colour in the Open Air*, trans. H. M. Kremer-Priest and K. E. Brian Jay (London: G. Bell & Sons, Ltd.).
Mitchell, S. A. 1924*a*, *Eclipses of the Sun* (2d ed.; New York: Columbia University Press), p. 347.
———. 1924*b*, *ibid.*, p. 209.
Richardson, R. A., and Hulburt, E. O. 1949, *J. Geophys. Res.*, **54**, 229.
Sharp, C. H., Gray, S. McR., Little, W. F., and Eckweiler, H. F. 1933, *J. Opt. Soc. Amer.*, **23**, 234.

RADIO REFLECTION AND REFRACTION PHENOMENA IN THE HIGH SOLAR CORONA

RONALD N. BRACEWELL* AND GEORGE W. PRESTON

Berkeley Astronomical Department, University of California

Received July 11, 1955; revised August 19, 1955

ABSTRACT

At the lowest frequencies used in radio astronomy, e.g., at 18 Mc/s, the sun has not yet been observed; but if existing data are correct, it presents a number of curious features: (*a*) the size of the sun as a radio-frequency source is two to three times the size of the visible sun, but in place of a sharp limb, there is merely a gradual fading-away into the background; (*b*) a zone of sky is occulted by the sun, and, because significant effects of refraction reach farther out into the corona than the effects of absorption, the occulted zone is some nine times larger than the photosphere; (*c*) the sun exhibits an occulting disk whose diameter is six times that of the photosphere and which differs from the emitting disk in having a sharp limb; (*d*) the discrepancy in size between the occulted zone and the occulting disk is associated with apparent displacement of the unocculted sky toward the sun by refration; (*e*) within the occulting disk the sun behaves as a convex reflector, mirroring the whole of the unocculted sky. The reflection of the Galaxy, though greatly diminished in size, remains comparable as a radio source with the emitting sun itself. If observed with existing aerials, which are incapable of resolving the solar emission from the galactic reflection, the sun should apparently exhibit a marked annual variation of flux density.

I. INTRODUCTION

The phenomena accompanying the transfer of radio-frequency radiation in the high solar corona can best be displayed by considering the lowest radio frequencies, and in this paper attention is concentrated on a frequency of 18 Mc/s, which occupies a place of special importance in radio astronomy as representing the long-wave-length end of the atmospheric window. It is true that Jansky's original discovery of the radio emission of the Galaxy was made at a slightly lower frequency and that Higgins and Shain (1954) have succeeded in obtaining observations at 9 Mc/s, but the work which has recently proved most fruitful and offers promise of continuing to do so is that of Shain (1951, 1954), Shain and Higgins (1954), and Shain and Mitra (1954) on 18 Mc/s. For this reason we have adopted 18 Mc/s as a representative low frequency where necessary to carry our ideas to numerical conclusions.

Observation shows that at 18 Mc/s the Galaxy is the most conspicuous feature in the sky as studied with the low resolution afforded by a 17° beam. Thus at the galactic center the very high brightness temperature of 375000° K was measured by Shain. No correction was included for the smoothing effect of the aerial, and there is reason to believe that the true brightness temperature is even higher.

The poor resolving power hitherto obtainable at 18 Mc/s has allowed only a blurred view of the sky; Shain's array of 30 dipoles, which has a beamwidth of 17°, extends over half an acre. On account of its small angular size, the quiet sun does not make much contribution to a radiometer with such a wide beam, and it has therefore not yet been studied. Higher resolution is already needed to investigate an expected narrow absorption lane (due to interstellar gas) in the galactic emission. In the present paper it is shown that the sun, too, will prove of great interest.

Section II gives the primary calculations of ray paths and absorption integrals in the sun's atmosphere, using methods exemplified in work on higher frequencies by Burkhardt and Schlüter (1949), Denisse (1950), Jaeger and Westfold (1950), Smerd (1950), and Hagen (1951). Since this section augments the published calculations of ray paths and center-limb brightness distributions, by carrying them to lower frequencies, it is

* On leave from Radiophysics Laboratory, Commonwealth Scientific and Industrial Research Organization, Sydney, Australia.

presented in a form which permits its use as reference material. Published ray paths have, however, proved to be insufficiently detailed for some purposes, making it desirable that the calculations themselves should be brought within easier reach. Some attention is paid to this aspect here, it is believed, for the first time.

In Section III the primary results are used to demonstrate the existence of an occulting disk and to derive its size. For the sky outside the occulting disk the amount of refraction is given, and for the interior zone the reflection coefficient, magnification, and deviation due to the solar mirror are given.

In Section IV these results are applied in calculating the image of the Galaxy in the sun at different times of the year, with a view to exhibiting the various forms which the image can assume. The emission of the sun plus galactic image, which gives the sun's apparent flux density as measured with a radiometer incapable of resolving the two, is shown to depend on the season.

II. PRIMARY CALCULATIONS

For the purposes of the present calculations the corona is sufficiently specified by a statement of the electron density, N, and the kinetic temperature of the electrons, T_e, at all points. From these two quantities the two necessary subsidiary quantities—refractive index, n, and absorption coefficient, κ—can be deduced. The temperature will be taken as 10^6 degrees K, and the electron density will be assumed to depend on ρ, the distance from the sun's center in units of the photospheric radius, as follows:

$$N = 1.55 \times 10^{14} \rho^{-6} (1 + 1.93 \rho^{-10}) \text{ electrons/m}^3 .$$

This formula, which is based on photometry of the white light of the corona, is due to Baumbach (1937), save that a term has been omitted which represented zodiacal light (Allen 1947). In adopting this formula, we assume spherical symmetry, the consequences of which are discussed in Section V. An advantage of the formula is that numerical results become directly comparable with those of the many other authors who have used it. The refractive index n in a medium containing N free electrons/m^3, each making ν collisions/sec, is given by

$$n^2 = 1 - \frac{N e^2}{\epsilon_0 m (\omega^2 + \nu^2)} ,$$

as long as the right-hand side is not negative. This provision is fulfilled in the present work. The remaining symbols have their usual meanings (e and m, charge and mass of electron; ω, angular frequency of wave; ϵ_0, permittivity of free space $= 8.854 \times 10^{-12}$ F/m). In terms of ρ and taking $\nu \ll \omega$,

$$n^2 = 1 - 12400 f^{-2} \rho^{-6} (1 + 1.93 \rho^{-10}) ,$$

where f is in megacycles per second. When $\rho \gg 1$, we have the simpler form

$$n^2 = 1 - 12400 f^{-2} \rho^{-6} ,$$

and when $f = 18 \times 10^6$,

$$n^2 = 1 - 38.27 \rho^{-6} .$$

The correction factor $1 + 1.93\rho^{-10}$ depends on ρ as shown in the accompanying tabulation.

	ρ							
	1	1.1	1.2	1.3	1.4	1.5	1.6	1.7
$1+1.93\rho^{-10}$ . . .	2.93	1.74	1.31	1.14	1.07	1.03	1.02	1.01

At 18 Mc/s the refractive index falls to zero at $\rho = 1.84$ (see Fig. 1). All ray paths thus lie well out in the corona. From the refractive index variation with height, the path of a radio-frequency ray may be calculated by using Snell's laws, which take the form: (*a*) all rays lie in planes containing the center of the sun, and (*b*) for all points of a ray,

$$n\rho \sin i = a \ , \tag{1}$$

where a is a constant for that ray and i is the angle of incidence of the ray on the surface of constant refractive index (Emden 1907).

For any ray, such as that in Figure 2,

$$\frac{\rho d\theta}{d\rho} = -\tan i .$$

Therefore,

$$\frac{d\theta}{d\rho} = -\rho^{-1} \sin i \,(1 - \sin^2 i)^{-1/2} = -\rho^{-1}\left(\frac{a}{n\rho}\right)\left[1-\left(\frac{a}{n\rho}\right)^2\right]^{-1/2}$$

$$= \frac{-a}{\rho\,(n^2\rho^2 - a^2)^{1/2}} ,$$

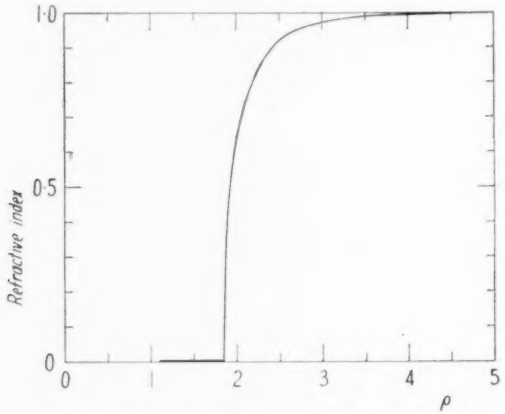

FIG. 1.—Refractive index of the corona at 18 Mc/s

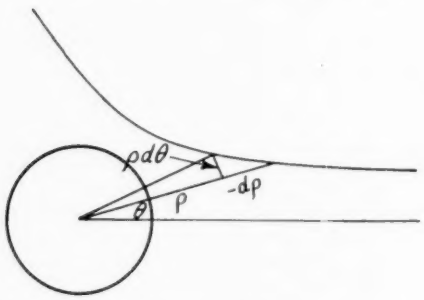

FIG. 2.—A radio-frequency ray path in the corona

and the equation of a ray is

$$\theta = a \int_{\rho}^{\infty} \frac{d\rho}{\rho\,(n^2\rho^2 - a^2)^{1/2}}, \tag{2}$$

The meaning of the constant a may be seen by going to large ρ, where $n \doteq 1$. Then $\rho \sin i = a$ = distance of the asymptote of the ray from the parallel line through the sun's center. This is shown on Figure 3, which also introduces ρ_a and θ_a, the polar coordinates of the turning point of a ray, and the deviation of a ray, Δ. We need the important relation,

$$n_a \rho_a = a \ , \tag{3}$$

and we may also note that

$$\Delta = \pi - 2\,\theta_a \ . \tag{4}$$

Throughout this work a and ρ will be reckoned in units of the phospheric radius.

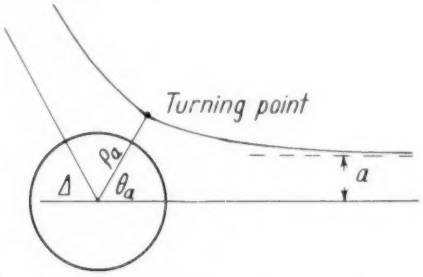

FIG. 3.—The parameters of a ray path

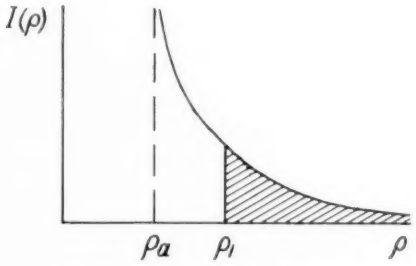

FIG. 4.—The integrand of equation (2)

Ray paths must be calculated by numerical integration of equation (2) with successively different values of a. The nature of the integrand $I(\rho) = a\rho^{-1}(n^2\rho^2 - a^2)^{-1/2}$ for a particular ray is as shown in Figure 4. The value of θ where $\rho = \rho_1$ is given by the shaded area, and the value of θ_a is the whole area under the curve.

For some purposes, a knowledge of the turning point and asymptotes of each ray might be sufficient. Given a, one can calculate ρ_a from equation (3) simply from a knowledge of the refractive index variation, and the result of this calculation is shown in Figure 5; but to get θ_a requires the integration of equation (2). Thus

$$\theta_a = a \int_{\rho_a}^{\infty} \frac{d\rho}{\rho\,(n^2\rho^2 - a^2)^{1/2}}. \tag{5}$$

The integration may be reduced to a summation as follows. Calculate $I(\rho)$ for $\rho = \rho_a + h, \rho_a + 2h, \rho_a + 3h, \ldots$, as far as ρ_m, where h is a small interval and ρ_m is a large value of ρ. The sum

$$h \sum_{\rho_a + h}^{\rho_m} I(\rho)$$

will approach the required integral indefinitely as $h \to 0$ and $\rho_m \to \infty$. But in practice it is desirable for the interval h to be as coarse, and for ρ_m to be as small, as is compatible with accuracy. This leaves two end corrections. The area under the tail may be seen from physical reasoning to be arcsin $[a/(\rho_m + \frac{1}{2}h)]$, and the area of the strip in which the

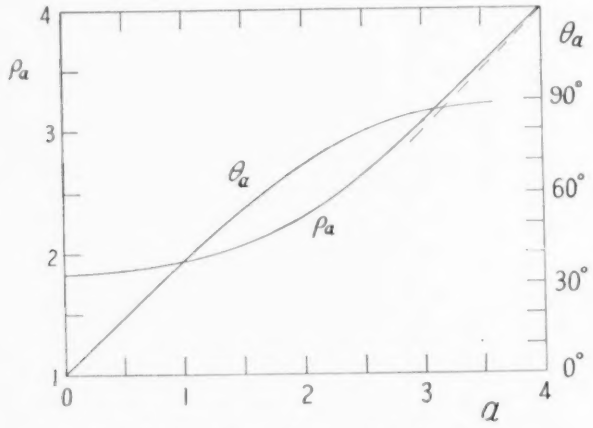

FIG. 5.—Co-ordinates of the turning points of rays

integrand goes infinite may be evaluated by a method given by Jeffreys and Jeffreys (1946). Then we have the following closed formula in place of the integral (5):

$$\theta_a = h\,[3.77I(\rho_a + h) - 0.96I(\rho_a + 2h) + 1.12I(\rho_a + 3h)] + h \sum_{\rho_a + 4h}^{\rho_m} I(\rho) + \arcsin \frac{a}{\rho_m + \frac{1}{2}h}. \tag{6}$$

In almost every case it has been found sufficient to take $h = 0.1$ and to extend the summation, Σ, over only six terms. The values of θ_a so obtained are given, with ρ_a, in Figure 5. The ray paths themselves are shown in Figure 6.

If κ is the absorption coefficient of the corona, the optical length of a ray will be given by

$$\tau = \int \kappa \, ds\,, \tag{7}$$

where the integral is taken along the whole ray. The element of path ds can be expressed in terms of the photospheric radius $R_\odot$ as

$$ds = R_\odot \left[1 + \left(\rho \frac{d\theta}{d\rho}\right)^2\right]^{1/2} d\rho\,. \tag{8}$$

The absorption coefficient of an ionized medium depends on the collision frequency, ν, and the electron density, N, as follows:

$$\kappa = \frac{2\sqrt{2}\pi f}{c}\left\{\left[\frac{(1-x)^2+z^2}{1+z^2}\right]^{1/2} - \frac{(1+z^2-x)}{1+z^2}\right\}^{1/2}, \tag{9}$$

where x and z are the dimensionless magneto-ionic parameters,

$$x = \frac{Ne^2}{m\epsilon_0\omega^2}, \qquad z = \frac{\nu}{\omega},$$

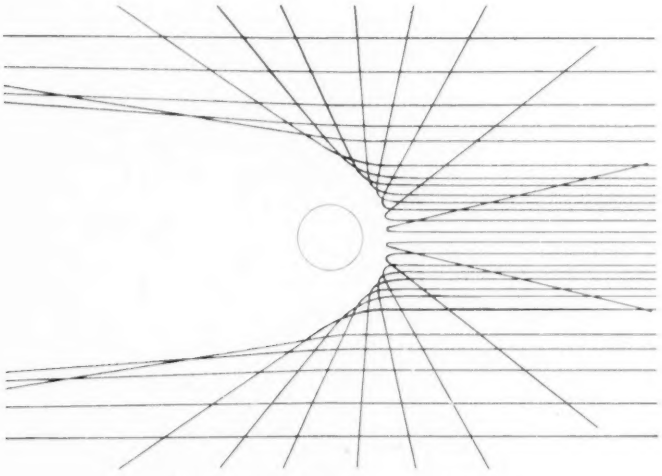

FIG. 6.—Ray paths in the corona at 18 Mc/s

In place of this cumbersome expression, one can use the approximation

$$\kappa \doteq \frac{\nu x}{n c}, \tag{10}$$

provided that the refractive index n is not near zero. As n approaches zero, the absorption coefficient rises to a finite value, given approximately by

$$\kappa_{n=0} = \frac{2\sqrt{2}\pi f z^{1/2}}{c},$$

which is obtainable from equation (9) by putting $x = 1$ and $z \ll 1$. The approximate expression (10), however, becomes infinite. A corresponding approximation under which we took $n^2 = 1 - x(1+z^2)^{-1}$ in Section I is not subject to this difficulty. The full expression is

$$n^2 = \frac{1}{2}\left\{\left[\frac{(1-x)^2+z^2}{1+z^2}\right]^{1/2} + \frac{1+z^2-x}{1+z^2}\right\}^{1/2}.$$

Since it is proposed to consider the optical length of rays which pass close to the level of zero refractive index, it is necessary to examine the validity of expression (10) in the course of the numerical work. This is done below. Meanwhile, adopting the approxima-

tion, and using Smerd and Westfold's (1949) formula for the collision frequency in ionized hydrogen, we have

$$\kappa = \frac{10^{-11} N^2}{n f^2 T_e^{3/2}},$$

where T_e is the electron temperature of the medium. Taking the electron temperature of the corona to be constant over the region where absorption is important, we obtain

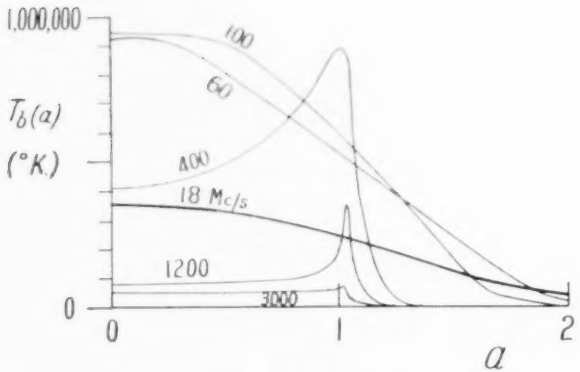

FIG. 8.—Solar brightness temperature distribution over the disk at 18 Mc/s (*heavy line*) compared with that calculated for other frequencies.

the following basic equation for calculating the optical thickness of the corona taken along a ray path:

$$\tau = \frac{2 \times 10^{-11} R_\odot}{f^2 T_e^{3/2}} \int_{\rho_a}^{\infty} \frac{N^2 \rho \, d\rho}{(n^2 \rho^2 - a^2)^{1/2}}. \tag{11}$$

The absorption integrals may be performed in the same way as the ray-path integrals since the integrand becomes infinite at $\rho = \rho_a$ and tapers away to zero as ρ approaches infinity, just as in Figure 4. The result is shown in Figure 7. It may be seen that the corona is optically thin for all 18-Mc/s rays, the absorption integral being always less than half a neper.

The validity of equation (10) must now be discussed. Assuming that $T_e = 10^6$ degrees K and $f = 18$ Mc/s, the value of the absorption coefficient when $x = 1$ comes to 10^{-4} nepers/m. The approximate formula gives an infinite result for $x = 1$, but for

$x = 1\text{–}10^{-14}$ this drops to 10^{-4}. The inaccurate range of the approximate formula is thus confined to levels infinitesimally close to the level where $x = 1$; and in the course of the calculations leading to Figure 7 it was confirmed that the approximation does not lead to error even for extremely small values of a.

As calculations of the kind described here have been carried out for shorter wave lengths, it is of interest to make a comparison. In Figure 8 we see solar brightness distributions calculated for the same solar model by Smerd. The lowest frequency considered was 60 Mc/s. The present result for brightness temperature $T_b(a)$, calculated from the formula

$$T_b(a) = T_e(1 - e^{-\tau}),$$

is shown as a heavy line. On 18 Mc/s the extension of the sun is seen to be greater than on higher frequencies, which continues the trend already shown and is due to the level of origin rising with decreasing frequency. On the other hand, the earlier calculations

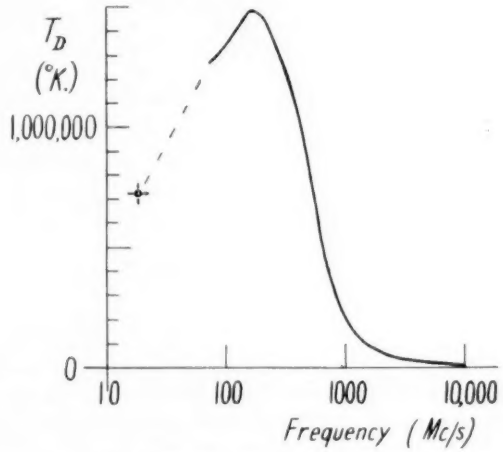

FIG. 9.—Sun's apparent disk temperature

showed, as far as they went, that the central brightness temperature of the sun increased steadily from 10^4 up to 10^6 degrees K, with decreasing frequency. However, this trend must reverse at about 60 Mc/s, since at 18 Mc/s the central brightness temperature is only 375000° K. The decreasing of the brightness temperature is due to the thinning-out of electrons as the level of origin rises with decreasing frequency.

The apparent disk temperature, T_D, which is a measure of the sun's flux density and therefore suitable for comparison with observation, is given by

$$T_D = 2\int_0^\infty T_b(a)\, a\, da\,.$$

The value obtained is 720000, and Figure 9 shows how this fits in with the results at other frequencies. The curve is the theoretical one calculated by Smerd and is well supported by observation (Pawsey and Smerd 1953). The point calculated for 18 Mc/s shows that, in spite of the greater extension of the emitting sun, the total radiation at 18 Mc/s would be expected to be well below the maximum. This has not yet been verified by observation.

III. GEOMETRICAL OPTICAL PHENOMENA

The envelope to the rays shown in Figure 6 may be termed the "limit-of-escape surface" for radiation reaching an observer at infinity on the right-hand side, since radiation originating within this enveloping surface will not be able to escape in the direction of the observer. The occulted volume cannot usefully be described in terms of an occulting disk, since the size of the disk depends on the distance of the source. If, however, we consider a family of rays which, instead of converging at infinity, converge at a finite distance, e.g., at the earth's distance from the sun, then a useful concept may be isolated. Although the appearance of Figure 6 would hardly be altered, the enveloping surface would become asymptotic to a cone having its vertex at the earth. Then, although the size of the occulting disk would increase with distance as before, its angular size would approach a constant value for sources not in the immediate vicinity of the sun. Several studies (Machin and Smith 1952; Hewish 1955) of occultation of the discrete radio source in Taurus have been made experimentally on meter wave lengths, but the only published theoretical work is that of Link (1952).

To obtain an equation for the angular size of the occulting disk, consider a family of rays passing through the earth and making angles α with the sun-earth line (Fig. 10). Let each ray make an angle β with the sun-earth line, well away from the sun on the side remote from the earth. Taking the rays in order of increasing α, we see that their inter-

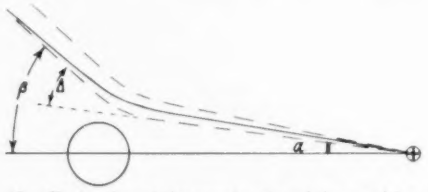

FIG. 10.—Derivation of the angular size of the occulting disk

sections with the celestial sphere have a stationary position. The locus of such points, taken in all position angles, is the rim of the occulted zone of the celestial sphere, and its position is given by

$$\frac{d\beta}{d\alpha} = 0 .$$

Since $\beta = \alpha + \Delta$ and $\alpha \doteq a\Omega$, where $\Omega = 0.0046$ = angular radius of photosphere, we have, in terms of quantities available from Section II,

$$\frac{d\Delta}{da} = -\Omega ,$$

or, from equation (4),

$$\frac{d\theta_a}{da} = \tfrac{1}{2}\Omega . \tag{12}$$

Reference to Figure 5 reveals that $d\theta_a/da$ does not fall to the required low value of 0.0023 in the range of a shown. We can extend the data on θ_a to larger values of a without resorting to numerical integration by utilizing the fact that for large ρ_a the ray path is not very curved. If we integrate $d\theta/d\rho$ along the straight line tangential to the ray at its turning point, we have, instead of equation (5),

$$\theta_a \doteq a \int_{\rho_a}^{\infty} \frac{d\rho}{\rho\,(\rho^2 - a^2)^{1/2}} \tag{13}$$

$$= \arcsin n_a .$$

The approximate expression arcsin n_a will be found to give the great bulk of the accurate value in equation (5). If we now subtract equation (13) from equation (5), we have, without approximation,

$$\theta_a = \arcsin n_a + a\int_{\rho_a}^{\infty}\left[\frac{1}{\rho\,(n^2\rho^2 - a^2)^{1/2}} - \frac{1}{\rho\,(\rho^2 - a^2)^{1/2}}\right]d\rho\,.$$

The integral on the right-hand side is small and, if evaluated approximately, leads to

$$\theta_a \doteq \arcsin n_a + \frac{\pi}{2\sqrt{2}}(1 - n_a)^{1/2}\,.$$

From the assumed data on refractive index variation we have $1 - n_a \doteq 19a^{-6}$; hence

$$\theta_a \doteq \frac{\pi}{2} - 1.3a^{-3}\,;$$

and from equation (12) we find that, for the occulting ray,

$$a \doteq 6.4\,.$$

The occulting disk therefore subtends an angle of 3°.2 at the earth, and, since the deviation of the occulting ray is 0°.6, the zone of sky occulted has a diameter of 4°.4.

To an observer on the earth, a distant source in the occulted zone would not be visible. A source just outside this zone would appear to be shifted toward the sun by an amount Δ, which could be as high as 0°.6. Accompanying this shift there would be a lateral compression $\sin\alpha/\sin\beta$ and a radial expansion $d\alpha/d\beta$, with a resultant average magnification,

$$\left(\frac{\sin\alpha}{\sin\beta}\,\frac{d\alpha}{d\beta}\right)^{1/2}.$$

The flux density of a small discrete source would be increased by this factor.

Inside the occulting disk the terrestrial observer would see a reflection of the whole of the unocculted sky. The distortion and magnification would continue to be represented by the foregoing expression, but the magnification would now be much less than unity. The average magnification is the square root of the ratio of the solid angle subtended by the occulting disk to 4π, since almost the whole of the sky will appear reflected within the disk. This is very small, in the present case 0.014. The magnification at the center of the disk is 0.0035. This is deduced from the value of $d\theta_a/da$ at $a = 0$ (0.66), obtainable from Figure 5. As well as suffering diminution in angular size, the reflected image of a source is subject to attenuation by the amounts given in Figure 7.

To summarize this section we may say that the sun at 18 Mc/s acts as a diffuse radiating disk with a central temperature of 375000° K, about 1° in diameter. It occults a zone of sky 4°.4 in diameter and magnifies and distorts discrete sources just outside the occulted zone. Each point of the unocculted sky is seen in two places, once via the direct ray and once via the reflected ray. The situation is closely analogous to a mirage, in which an inverted image is seen by reflected rays. Though it is not often stressed in connection with the mirage, there must also be an occulted zone hidden behind the area occupied by the image.

IV. THE IMAGE OF THE GALAXY

Radio-frequency radiation from the Galaxy, reflected in the solar corona, will have a brightness temperature virtually the same as the brightness temperature of the direct radiation from the Galaxy. It is true that there will be a reduction due to absorption in the corona, and Figure 7 may be used to calculate the reduction, but for most rays it is small. In the direction of the galactic center the brightness temperature of the direct

radiation is known from the work of Shain and Higgins (1954) to be 300000° K at least. It may well be more, since the value stated is an average over a zone 17° in diameter. Now the sun itself, at the center of the disk where it is brightest, has a brightness temperature of 375000° K, as calculated previously, so it follows that the reflected image of the Galaxy is about as bright as the sun itself. Observational studies of the sun at 18 Mc/s will therefore be complicated by the reflected galactic radiation, and it is of interest to consider what the principal effects will be.

The observations of the galactic radiation are fragmentary but adequate for the present purpose, since they show the general shape of the contours of equal brightness temperature in the vicinity of the brightest part. Table 1 gives the galactic and equatorial co-ordinates of points on three representative lines of equal brightness temperature surrounding the galactic center ($l = 330°$; $b = 0$). A comparison of Table 1 with

TABLE 1

300,000 K.	l(deg.)	330	320	330	340
	b(deg.)	2.5	0	−2.5	0
	R.A.	17^h30^m	17^h15^m	17^h50^m	18^h05^m
	δ(deg.)	−23	−35	−27.5	−17.5
200,000 K.	l	330	270	330	30
	b	15	0	−15	0
	R.A.	16^h48^m	12^h40^m	18^h43^m	19^h43^m
	δ	−18	−62	−33	27
150,000 K.	l	330	240	330	60
	b	22.5	0	−22.5	0
	R.A.	16^h23^m	9^h20^m	19^h18^m	21^h20^m
	δ	−13	−50	−36	50

the published observations will show that the departures from symmetry about the galactic center have not been preserved. It would have been possible to do so, but the nature of the principal phenomena is better displayed by retaining only the best-established attributes of the radiation.

When the observer looks at an angular distance α (see Fig. 10) from the center of the sun's disk in position angle P measured eastward from the south point of the disk, his line of sight passes through the point on the celestial sphere which is in the same position angle but at an angular distance β from the center of the disk. Let T_G be the galactic brightness temperature at that point, τ the optical length of the ray, and T_S the contribution of solar emission to the brightness temperature. Then the observed brightness temperature T in the direction (α, P) will be given by

$$T(\alpha, P) = T_G(\beta, P)\, e^{-\tau} + T_S(\alpha).$$

Since for small values of α there is no distinction between α and a, we may replace $T_S(\alpha)$ by $T_b(a)$, as given in Figure 8, and take τ directly from Figure 7. To calculate $T_G(\beta, P)$, one might first use Figure 5 and the relation $\beta = \alpha + \pi = 2\theta_a$ to obtain β from α, and then convert the co-ordinates (β, P) to galactic co-ordinates (l, b), taking account of the co-ordinates of the sun, and interpolate in Table 1 to find T_G. It is in this last step that practical difficulties arise, but a very neat procedure has been found which is based on the preliminary construction of two charts, Figures 11 and 12.

Figure 11 represents the relation

$$T = T_G e^{-\tau} + T_S$$

in terms of a and T_G as independent variables, the data on τ and T_S being incorporated.

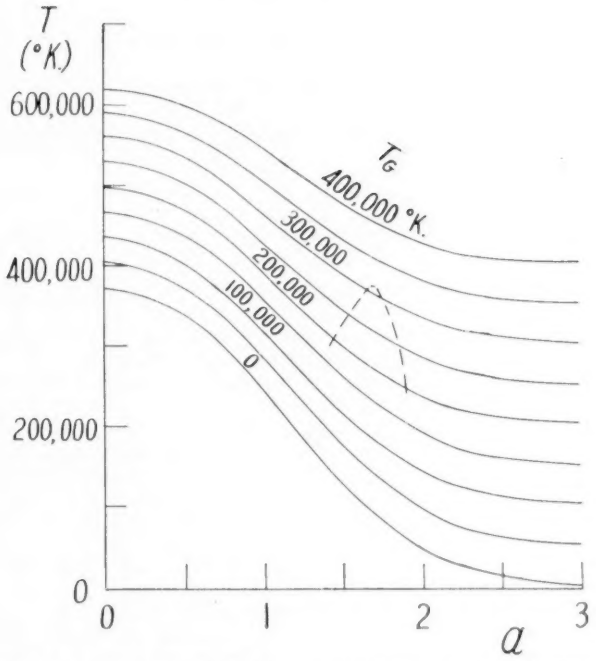

FIG. 11.—The brightness temperature, T, of a ray a which emerges from the Galaxy with brightness temperature, T_G.

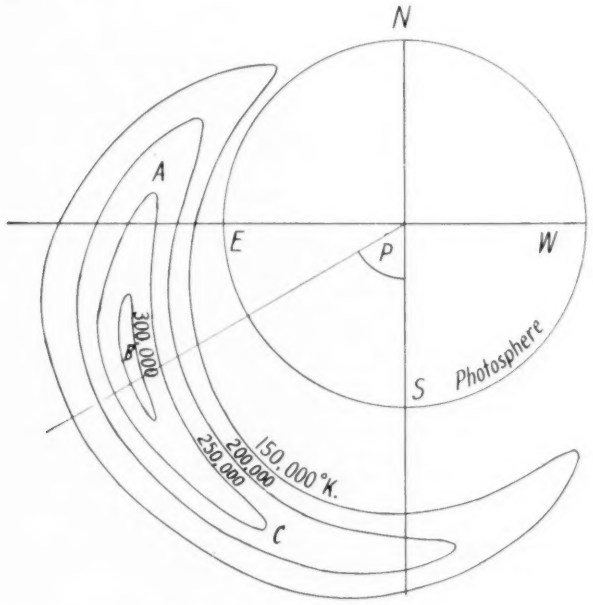

FIG. 12.—The image of the Galaxy before allowing for solar emission and absorption (October 21)

Figure 12 shows the image of the Galaxy, as calculated before allowance for solar emission and absorption. The co-ordinates of the solar center were fixed as for October 21, and then the pair of values of right ascension and declination from Table 1 were converted to α and P by the relations

$$\cos \alpha = \sin \text{dec.} \sin \text{dec.}_\odot + \cos \text{dec.} \cos \text{dec.}_\odot \cos (\text{R.A.} - \text{R.A.}_\odot),$$

$$\cot P = \tan \text{dec.} \cos \text{dec.}_\odot \operatorname{cosec} (\text{R.A.} - \text{R.A.}_\odot) - \sin \text{dec.}_\odot \cot (\text{R.A.} - \text{R.A.}_\odot),$$

the latter of which is conveniently reduced to addition and subtraction by the use of Norie's nautical tables.

Now consider a cross-section of the image along any line such as that shown in position angle P and plot it on Figure 11 to the curvilinear co-ordinates T_θ and a. The broken line, which shows the result, is then a cross-section of the desired distribution, and it enables one to mark the points where any contour $T = \text{Const.}$ crosses the section line.

In this way one rapidly builds up the contour diagram of brightness temperature over the sun and vicinity (Fig. 13). The distribution obtained shows a region exceeding 350000° K at the center of the disk and a further region which, from its brightness and extent, is clearly comparable in flux density with the sun alone. The contour on which the brightness is half the central value (*shown broken*) is roughly circular, but distinctly eccentric, though not in the direction of the galactic center.

Observation of the sun with limited resolving power should therefore reveal the following effects: (*a*) flux density increased, (*b*) position shifted, and (*c*) symmetry, if observable, impaired. All these effects depend on the season and, to some extent, on the resolution of the aerial. The dependence on season may be exhibited roughly by showing the distance of the galactic image from the sun's center and its orientation, as in Figure 14. For the purposes of this figure a segment of the galactic equator, 120° long, is shown in its reflected position. No allowance is made for solar emission and absorption; thus for October 21 the arc shown is the same as *ABC* in Figure 12. It is probably correct to deduce from Figure 14 that the flux density of sun plus image goes through a deep minimum in June, since in that month the image is smallest and subject to the greatest attenuation.

It is possible that solar flux density measurements already in progress on higher frequencies contain a small contribution from the Galaxy, but the extent to which the reflection effects persist at higher frequencies remains to be studied.

V. DISCUSSION

Several assumptions have been made in the foregoing analyses, and we here consider to what extent they could modify the conclusion that the sun should present an appearance like that shown in Figure 13. The main assumptions are (*a*) the corona is isothermal at 10^6 degrees K; (*b*) the electron density is given by the Baumbach-Allen formula as far out as six solar radii; and (*c*) the corona is spherically symmetrical.

The assumed temperature of the corona affects the solar emission and the attenuation of the galactic radiation in such a way that if the corona were hotter, the solar emission would be less and the galactic reflection brighter, thus emphasizing the image phenomenon. The evidence that the corona is kept fairly isothermal by its high thermal conductivity and that it is at a temperature which cannot be below about a million degrees is based on independent radio and optical observations, and there is now little question that this broad fact is established. Should the temperature fall off at the large distances here discussed, the solar emission would be unaffected, and the increased absorption of the image would, because of the small electron density, be negligible.

As regards the electron-density distribution, there is no sound basis for extrapolating the distribution established for the inner corona to a value of $\rho = 6$. There is evidence,

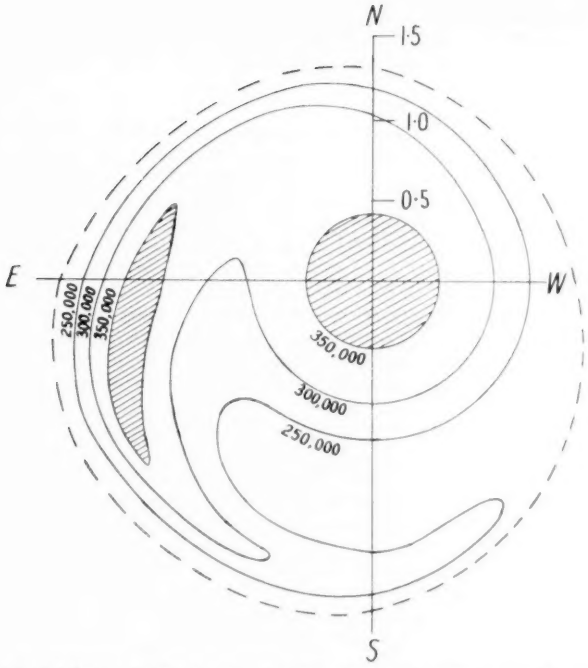

FIG. 13.—Solar brightness distribution showing the reflection of the Galaxy. Brightness temperatures in degrees Kelvin. The approximate half-central-brightness contour is shown in broken outline.

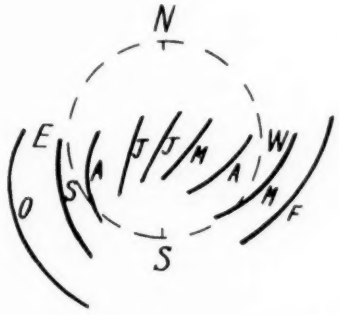

FIG. 14.—The position of the galactic image in different months of the year. The photosphere is shown in broken outline.

however, that at these greater distances the electron density is larger than the value given by the formula (Machin and Smith 1952). The result of such a modification to the present theory would be to enlarge the occulting disk and the angular dimensions of the image of the Galaxy. Therefore, as far as the temperature and electron-density data are concerned, the phenomena described here are likely to be, if anything, more pronounced than we have calculated.

Departures of the corona from symmetry may introduce major modifications to the present results. For example, a coronal streamer in which the electron density was ten times greater than the surrounding value could displace the level of zero refractive index by a substantial fraction of a solar radius. This seems to be the most probable major cause of discrepancy between theory and future observation and, under adequate resolution, could permit electron-density studies in the outer parts of the coronal streamers. The necessary modifications to the theory, in the sector affected, should not be much more arduous than at present, since in any case we are forced to use numerical methods; so it is probable that gross departures of the observations from the simple theory could be interpreted. In considering this subject, the analogy with the mirage is useful for suggesting the types of distortion to be expected. The phenomena of towers, duplicated images both erect and inverted, indentations, and detached occulating patches are all to be expected under various kinds of variation of refractive index.

A different type of departure from symmetry has been invoked by Hewish (1955) to explain the occultation observations on the discrete source in Taurus. He finds radio evidence for a cloudy structure of the corona probably associated with the fine visible structure. The effect on a point source of radio waves is to spread it out over a disk a few minutes of arc in diameter; but unless the instrument used had extremely high resolution, as did his interferometer, this effect would not be distinguishable from the inherent blurring due to the instrument. To what extent regular refraction was affected is not clear, but one can imagine that, in the case of extreme non-uniformity of ionization, regular refraction phenomena could be obliterated. The solar reflector would become a diffuse reflector. It does not seem worth while at present to consider this theoretically, since the likelihood on present evidence is that reflection will be partly diffuse over the whole sun and possibly very diffuse in places.

It would seem that the major features of the visible white-light corona would be the major causes of asymmetry of the 18-Mc/s reflector. However, it may be remembered that, on account of the rapid decrease of electron density with ρ, the contours of equal electron density are not distorted very much from the spherical form by coronal features which are visually quite marked.

The general conclusion from this discussion of assumptions is that we are likely to have covered the principal effects on 18 Mc/s. These are in themselves so interesting that forthcoming observations with high resolution on 18 Mc/s will be awaited with impatience, and it may be expected that in due course such observations will lead to definite knowledge about the electron density and its degree of uniformity in the outer solar corona, under both quiet and disturbed conditions.

REFERENCES

Allen, C. W. 1947, *M.N.*, **107**, 426.
Baumbach, S. 1937, *A.N.*, **263**, 121.
Burkhardt, G., and Schlüter, A. 1949, *Zs. f. Ap.*, **26**, 295.
Denisse, J.-F. 1950, *Ann. d'ap.*, **13**, 181.
Emden, R. 1907, *Gaskugeln* (Leipzig: B. G. Teubner Verlag), p. 296.
Hagen, J. P. 1951, *Ap. J.*, **113**, 547.
Hewish, A. G. 1955, *Proc. R. Soc. London, A*, **228**, 238.
Higgins, C. S., and Shain, C. A. 1954, *Australian J. Phys.*, **7**, 460.
Jaeger, J. C., and Westfold, K. C. 1950, *Australian J. Sci. Res. A*, **3**, 376.

Jeffreys, H., and Jeffreys, B. S. 1946, *Methods of Mathematical Physics* (Cambridge: At the University Press), p. 264.
Link, F. 1952, *Bull. Centr. Astr. Inst. Czechoslovakia*, **3**, 6.
Machin, K. R., and Smith, F. G. 1952, *Nature*, **170**, 319.
Pawsey, J. L., and Smerd, S. F. 1953, *The Sun*, ed. G. P. Kuiper (Chicago: University of Chicago Press), chap. 7.
Shain, C. A. 1951, *Australian J. Sci. Res. A*, **4**, 258.
———. 1954, *Australian J. Phys.*, **7**, 150.
Shain, C. A., and Higgins, C. S. 1954, *Australian J. Phys.*, **7**, 130.
Shain, C. A., and Mitra, A. P. 1954, *J. Atm. and Terr. Phys.*, **5**, 316.
Smerd, S. F. 1950, *Australian J. Sci. Res. A*, **3**, 34.
Smerd, S. F., and Westfold, K. C. 1949, *Phil. Mag.*, **40**, 831.

RADIO OBSERVATIONS OF INTERSTELLAR NEUTRAL HYDROGEN CLOUDS

ROBERT S. LAWRENCE*

National Bureau of Standards, Boulder, Colorado

Received August 29, 1955

ABSTRACT

A detailed relationship is found to exist between optical interstellar absorption lines and 21-cm observations. Six stars not in the vicinity of the galactic plane were selected from a list of stars which exhibit complex absorption spectra of Ca II. In the directions of two of these stars a weak hydrogen line appears, which agrees in radial velocity with an intense component of the optical spectrum.

The presence of sharp, well-separated components in the interstellar absorption lines of some stellar spectra proves the existence of definite concentrations, or clouds, of interstellar gas moving with various radial velocities. From optical measurements it is difficult to infer the dimensions and distribution of these clouds. The radio telescope, using the 21-cm emission line of neutral hydrogen, may be useful in this respect if it can record

TABLE 1

COMPARISON OF 21-CM AND OPTICAL INTERSTELLAR LINES

STAR	GALACTIC CO-ORDINATES		TYPE	MAG.	RADIAL VELOCITY (KM/SEC RELATIVE TO THE SUN)		
	l	b			21-Cm	Optical Components of Ca II (in Order of Decreasing Intensity)	
HD 219188	52°	−51°	B2n	6.9	− 9	− 7, +18, (−29?)	
HD 215733	54	−37	B2	7.7	−10	−26, −11, −44,	−57
HD 203664	30	−28	B3n	8.3	+ 5	− 8, +66, (−28?)	
HD 119608	289	+42	cB0	7.3	−10	− 3, +18, (−11?,	+33?)
HD 91316	204	+54	cB0	3.8	. .	−13, − 4, +16	
HD 93521	150	+64	B3n	6.9	. . . . .	−11, −53, + 5,	−34

and delineate the same individual clouds. The absorption lines of Ca II and Na I may be expected to be formed in the same regions of space where the emission of neutral hydrogen takes place. The present investigation shows that a detailed relationship between optical and radio measurements of interstellar clouds does indeed appear.

Radio measurements of interstellar clouds cannot be strictly comparable to optical observations because of the necessarily great disparity in angular resolution of the two methods. The optical observations are concerned only with those portions of clouds that happen to lie between the disk of a star and the observer, while the radio observations average over all clouds that lie in the acceptance cone of the radio telescope. The two methods of observation will be most nearly comparable in regions of the sky where the density of clouds is low. For this reason, the present observations were limited to intermediate galactic latitudes.

Dr. Guido Münch, of the Mount Wilson and Palomar Observatories, provided the list of six intermediate-latitude stars shown in Table 1. The spectra of these stars all

* This work was done at Harvard College Observatory, Cambridge, Massachusetts.

show complex absorption lines due to interstellar Ca II. The 24-foot comparison-type radiometer at the G. R. Agassiz Station of Harvard Observatory provides a means of measuring the 21-cm radiation from the regions of the sky surrounding the six stars. The half-power beamwidth of the antenna is 1°.7. The bandwidth of 15 kc/sec corresponds to a range in radial velocity of about 3 km/sec.

The 21-cm line is measurable in four of the six regions, although the peak intensity is low in each case. Table 1 gives, for comparison, the radial velocities of the radio and optical lines. It is noteworthy that for the first two stars on the list the radio velocity agrees closely with the velocity of an intense optical component. In view of the great difference in angular resolution, the failure to find correspondence in every case is not surprising.

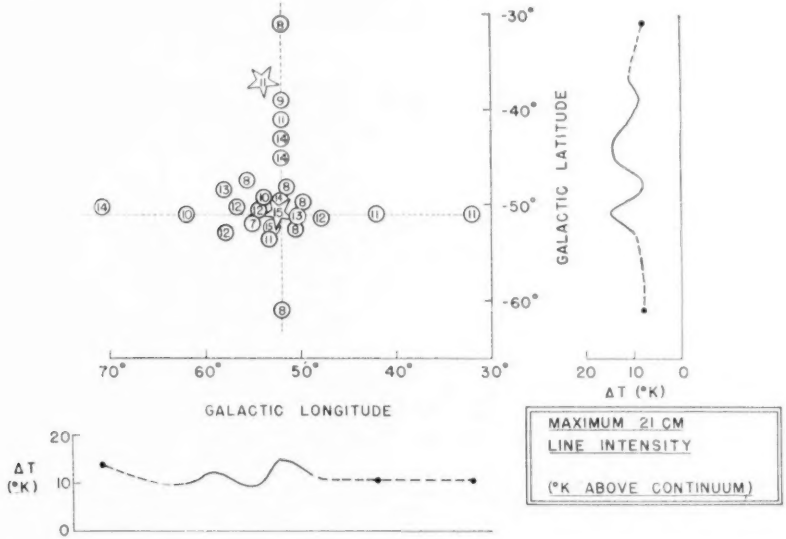

FIG. 1.—Positions and observed intensities of the 21-cm line. The curves show the dependence of intensity near HD 219188 upon longitude and latitude.

The map of Figure 1 shows, in galactic co-ordinates, the region included in the radio measurements for the first two stars. The circles represent settings of the radio beam, and the numbers give the peak antenna temperature of the line at each setting. The variations over the region seem not to be systematic, but both stars appear at local maxima of intensity. This is illustrated by the supplementary curves showing the intensity variation with longitude and latitude. The latitude-curve is particularly striking, as it shows that a minimum of intensity lies between this complex and the galactic equator.

Figure 2 shows, in as much detail as the measurements permit, the velocity structure of the hydrogen complex near HD 219188. The three maps give, for the same area, contours of 21-cm intensity as measured at three frequencies, corresponding to three radial velocities. The central map represents hydrogen moving with the radial velocity (-7 km/sec) of the intense optical component in the spectrum of HD 219188. Velocities differing from this by -5 and $+5$ km/sec are represented on the other two maps. The black dot indicates the position of the star. Although the velocities shown by the maps differ

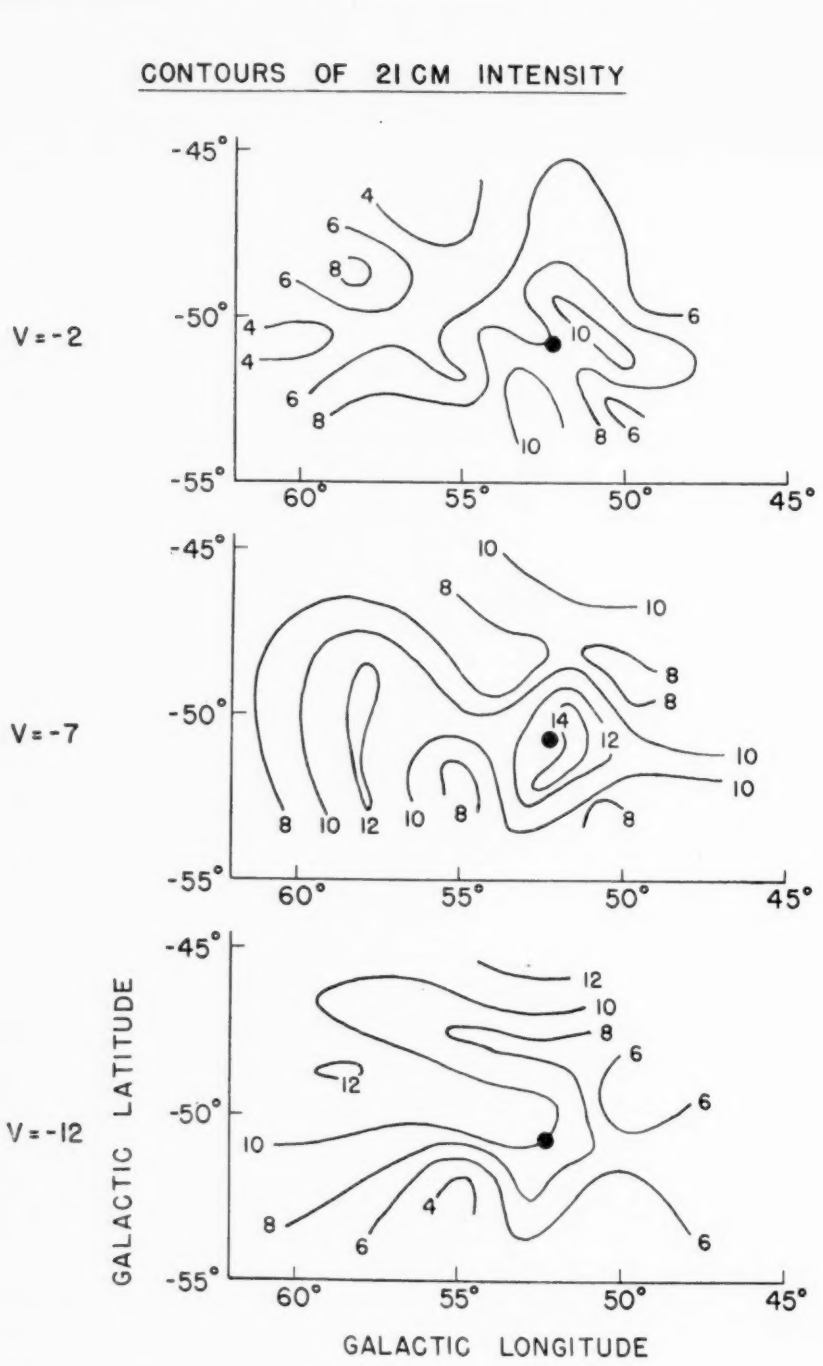

FIG. 2.—Contour maps of 21-cm intensity in the vicinity of HD 219188. Each map shows only the contribution of hydrogen moving with a specific radial velocity. The velocity (−7 km/sec) of the hydrogen in the middle map is the same as that of an intense component in the optical spectrum.

by only 5 km/sec, the maximum near the star is much more pronounced on the map for which the radio and optical velocities agree. The correspondence in both position and velocity indicates strongly that the radio observations pertain to the same cloud as the intense component of the optical absorption line of Ca II.

The contour maps show that the details of the hydrogen structure change rapidly with frequency (or radial velocity of the hydrogen), and yet the general patchy appearance of all three maps is similar. These observations are consistent with a tentative model of the hydrogen complex, consisting of many clouds moving with different radial velocities. The clouds are probably too small to be resolved by the 25-foot Agassiz Station radio telescope. We estimate that the diameter of a unit cloud is not likely to be far in excess of 10 pc (for an assumed distance of 650 pc for the star) and that its mass is not in excess of 50 solar masses. An obvious way to learn more about the size of these clouds is to repeat the observations with a radio telescope of greater aperture, at least 50 or 60 feet.

I wish to acknowledge the encouragement, and original suggestion of the problem, by Drs. Bart J. Bok and Guido Münch. In addition, I express thanks to Dr. Münch for the optical data, and to Dr. Bok for making available the facilities of the Agassiz Station radio-astronomy project.

SPECTROPHOTOMETRY OF GAMMA LEONIS

WILLIAM H. WEHLAU*

Berkeley Astronomical Department, University of California

Received August 8, 1955

ABSTRACT

The atmospheres of both components of this high-velocity binary were studied, using the curve-of-growth method. Excitation and ionization temperatures were derived for iron and titanium. Rotational temperatures for CH were also obtained. The values of the effective surface gravity derived from the ionization temperatures and electron pressures are lower than the values obtained from the parameters of the system. The equivalent widths, line widths, and central depths were used to study the turbulence in the atmospheres. The turbulent velocities are too small to account for the discrepancies in the values of the surface gravity.

Gamma Leonis is a high-velocity visual binary. With low dispersion the individual components show spectral peculiarities similar to those found for other high-velocity stars, particularly a weakening of the CN lines. Data for the system are summarized in Table 1. The abundances of the elements and the excitation temperatures for

TABLE 1

PARAMETERS OF γ LEONIS

Period	619 years*
Parallax	
Trigonometric	$0''.019 \pm 0''.006$†
Spectroscopic	$0''.017$‡
Visual magnitude	
A	2.61§
B	3.80
Spectral type	
A	K0 III−‡
B	G7 III+

* E. Rabe, given by P. Muller, 1953, *J. Obs.*, **36**, 61.

† L. Jenkins, 1952, *General Catalogue of Trigonometric Stellar Parallaxes* (New Haven: Yale University Observatory).

‡ P. C. Keenan and G. Keller, 1953, *Ap. J.*, **117**, 241.

§ *Harvard Ann.*, **64**, 165, 1912.

γ Leo A have been compared by Gratton (1953) with the values for other late-type giants. The present investigation considers primarily the curves of growth, the temperatures obtained in several different ways, and the turbulent velocities.

Two spectrograms with a dispersion of 2.8 A/mm were obtained for each component by O. Struve at the Mount Wilson Observatory. Microphotometer tracings of the plates were made from 4020 to 4540 A, where the densities are suitable for photometry on all plates. These tracings were reduced to intensity tracings with the equipment at Berkeley.

The position of the continuum is subject to the usual uncertainty for such late-type stars. To locate the continuum, the highest points on the density tracings were measured and plotted as a function of wave length. A smooth curve was drawn through these points, and this curve was adopted for the position of the continuum. The satisfactory agreement of points on the curves of growth described later indicates that this method yielded consistent values over the wave-length region considered. However,

* Now at the Warner and Swasey Observatory, Case Institute of Technology.

in the neighborhood of λ 4215, where the plates are broken into two sections, some uncertainty remains, and there are appreciable systematic differences between the equivalent widths determined from the two plates of the same star. Minnaert's (1935) method for locating the position of the continuum from the wings of strong lines was applied to the Ca I line at λ 4227 and gave results consistent with the adopted position.

To determine the equivalent widths, each line was drawn individually, and the areas were measured with a planimeter. Equivalent widths of lines in the wings of strong lines were corrected by Thackeray's (1936) method. The values of log $W/\lambda \times 10^6$ for each star are listed in Table 2. The values of the half-widths and the central depths are also listed in this table.

Curves of growth were constructed for each star, using the Fe I equivalent widths and Wright's (1948) log X_f-values. For a number of weaker lines no log x_f values were available. For these lines Allen's (1934 and 1938) solar equivalent widths were used to evaluate log X_f. The equivalent widths given by him were corrected to Wright's system and the log X_f-values read from Wright's solar curve of growth.

The Fe I excitation temperatures were evaluated from the deviations of the individual points from the mean curves of growth. If the deviations are designated by log X − log X_f, then the temperatures may be evaluated from

$$\log X - \log X_f = -5040\chi_i\left(\frac{1}{T}-\frac{1}{T_\odot}\right) + \text{constant}. \tag{1}$$

Least-squares solutions for the temperatures of each component, employing only points for which log X_f-values were available from Wright, gave the following values:

$$\gamma \text{ Leo A:} \quad \Delta\theta = 0.264 \pm 0.025; \quad T = 3868° \pm 74°,$$

$$\gamma \text{ Leo B:} \quad \Delta\theta = 0.210 \pm 0.025; \quad T = 4035° \pm 82°.$$

Within the accuracy of the data, all excitation potentials appeared to give the same difference from the solar value.

New values of log X were computed from equation (1), using the excitation temperatures given above. Curves of growth for Fe I, using these log X-values, are shown in Figure 1. The parameters of the curves of growth are given in Tables 3, 4, and 5.

Curves of growth were also constructed for Fe II, Ti I, and Ti II. For Ti I, excitation temperatures were also derived, as follows:

$$\gamma \text{ Leo A:} \quad \Delta\theta = 0.420 \pm 0.104; \quad T = 3300° \pm 220°,$$

$$\gamma \text{ Leo B:} \quad \Delta\theta = 0.208 \pm 0.098; \quad T = 3830° \pm 290°.$$

The empirical curves of growth were fitted with the Fe I-curves by shifting them horizontally. From the displacements of the curves of growth relative to the solar curve, the numbers of atoms in the ground state of each stage of ionization relative to the values for the sun were derived. These values, log $N_* - \log N_0$, are listed in Table 5.

Using the Milne-Eddington model, $N_{r,s}$, the number of atoms above the optical depth, τ_0, for the continuum, which contribute to the formation of a line, is given by

$$N_{r,s} = \frac{\zeta_{r,s}}{\mu_0 m_H}\frac{\tau_0}{\kappa} \tag{2}$$

(Unsöld 1938, eq. [68.7], with slightly different notation). Here $\mu_0 m_H$ is the average mass per atom, κ the continuous absorption coefficient per gram, and $\zeta_{r,s}$ the ratio

TABLE 2

EQUIVALENT WIDTHS, HALF-WIDTHS, AND CENTRAL DEPTHS

λ	Log W/λ×10⁶		D/λ×10⁶		R_0	
	A	B	A	B	A	B
Fe I						
4035.25	1.19	0.96	32	31	0.50	0.32
4036.37	1.25	1.06	32	34	.56	.37
4037.72	1.14	0.91	33	32	.42	.29
4044.61	1.74	1.61	56	59	...	...
4045.82	2.63	2.37	...	...	...	...
4062.45	1.60	1.51	50	39	.84	.76
4063.60	2.42	2.19	...	...	...	...
4065.40	1.43	1.31	39	36	.71	.58
4069.08	...	1.22	...	38	...	.48
4070.77	1.57	1.48	50	42	...	.70
4071.74	2.40	2.19	...	...	...	...
4072.52	1.51	1.36	34	37	...	.61
4082.12	1.45	1.30	40	38	.68	.54
4084.50	1.61	1.56	52	51	.80	.74
4085.31	1.66	1.61	58	53	.82	.77
4085.98	...	1.16	...	33	...	.40
4087.09	1.43	1.32	41	37	.68	.57
4088.57	1.29	1.23	33	37	.63	.45
4091.56	1.40	1.28	35	34	.66	.51
4099.99	1.06	0.98	31	33	.34	...
4100.74	1.70	1.66	52	49	...	...
4114.45	1.57	1.44	42	37	.80	.70
4114.96	1.32	...	36	...	.58	...
4116.97	1.30	...	33	...	.62	...
4117.32	0.59	0.50	18	19	.22	.16
4126.68	1.36	1.19	35	39	.60	.40
4132.06	2.09	2.03	...	...	...	...
4132.90	1.63	1.50	51	44	.76	.71
4133.87	1.58	1.50	47	48	.80	.70
4139.93	1.54	1.45	43	39	.80	.66
4143.87	...	1.98	...	...	...	.90
4147.67	1.78	1.59	58	50	.96	.78
4154.50	1.64	1.54	52	49	.87	.74
4156.80	...	1.60	...	52	...	.76
4160.56	1.19	1.10	31	34	.55	.40
4174.92	1.78	1.64	65	57	.92	.80
4175.64	1.60	1.57	50	50	.80	.73
4183.02	1.13	1.13	33	32	...	.42
4191.44	1.80	1.70	71	57	.88	.84
4191.68	1.61	1.44	56	41	.78	.66
4202.03	1.94	1.84	...	78	...	.90
4206.70	1.82	1.68	72	60	.89	.76
4208.61	...	1.47	...	41	...	...
4216.19	1.78	1.68	68	57	0.93	0.80
4222.22	1.70	1.56	59	48	...	...
Fe I						
4233.61	1.75	1.65	64	55	0.92	0.79
4243.79	1.29	1.18	32	33	.56	.46
4247.43	1.76	1.71	67	64	.85	.80
4249.32	0.88	0.77	27	30	.28	.20
4250.12	1.89	1.74	91	70	.85	.83
4250.79	2.03	1.86	...	85	...	.88
4260.48	1.90	1.80	79	72	...	.89
4271.16	1.89	1.81	83	75	.93	.85
4271.76	2.31	2.17	...	...	...	...
4276.68	1.48	1.30	48	41	.65	.50
4281.60	...	0.42	...	20	...	.13
4282.41	1.70	1.62	53	50	.90	.79
4283.87	1.19	0.64	33	25	.46	.18
4291.47	1.71	1.52	56	44	.90	.76
4325.76	2.36	2.19	...	...	...	...
4337.05	1.75	1.59	61	52	.94	.80
4347.24	1.51	1.36	40	38	.78	.60
4365.90	1.31	1.17	35	30	.60	.49
4377.80	1.27	1.17	34	37	.52	.42
4383.55	2.60	2.38	...	...	...	...
4389.24	1.65	1.47	48	39	.89	.72
4404.75	2.35	2.16	...	...	...	...
4415.12	2.12	1.94	...	86	...	.88
4427.31	1.79	1.69	63	53	.95	.84
4430.62	1.66	1.58	56	52	.84	.74
4432.57	1.30	1.15	37	31	.54	.46
4439.64	1.15	0.80	33	29	.42	.24
4439.88	1.37	1.22	36	32	.62	.52
4442.34	1.81	1.73	73	64	.86	.81
4447.72	1.78	1.67	67	55	.87	.78
4472.52	...	0.73	...	33	...	.15
4478.04	1.16	0.93	32	27	.47	.32
4487.74	1.03	0.78	32	26	.36	.24
4489.74	1.66	1.53	53	44	.84	.76
4494.57	1.86	1.72	84	66	.88	.82
4502.59	1.15	0.92	33	32	.45	.28
4504.84	1.40	1.25	47	39	.54	.45
4510.82	0.95	0.67	33	30	.28	.16
4517.53	1.53	1.39	48	41	.69	.59
4523.40	1.25	1.08	34	29	.58	.42
4525.88	1.20	0.90	34	30	0.47	.29
4528.62	2.04	1.94	...	...	...	0.86
4536.51	1.04	0.72	34	25	...	...

TABLE 2—*Continued*

λ	log W/λ×10⁶		D/λ×10⁶		R_0	
	A	B	A	B	A	B
Ti I						
4060.26	1.39	1.23	36	32	0.70	0.50
4065.09	1.55	1.36	48	42		.54
4112.71	1.51	1.30	42	36	.78	.54
4166.31	1.24	1.09	35	35	.50	.29
4186.12	1.51	1.31	46	40	.72	.50
4276.44	1.27	1.00	38	29	.52	.33
4281.37	1.38	1.16	37	33	.66	.41
4284.99	1.48	1.40	45	41	.71	.60
4287.40	1.51	1.39	43	38	.73	.62
4295.75	1.54		45		.77	
4326.36		1.26		36		
4334.84	1.37		41		.56	
4355.31	1.13	1.02	32	34	.40	.31
4417.27	1.44		41		.68	
4436.59	1.25		36		.48	
4441.27	1.12	0.78	32	26	.39	.22
4449.14	1.43	1.28	41	34	.68	.54
4450.90	1.43	1.28	39	38	.67	.52
4453.31	1.46	1.36		37		.57
4453.71	1.40	1.20	37	37	.65	.46
4465.81	1.35	1.18	38	35	.60	.45
4480.60	1.27	1.08	35	32	.52	.37
4481.26	1.48	1.41	46	43	.71	.59
4495.01	1.14	0.67	36	22	.38	.22
4503.76	1.09		31		.38	
4512.73	1.56	1.37	47	36	.75	.63
4518.02	1.56	1.41	48	40	.74	.64
4527.30	1.72	1.54	64	51	.81	.66
4533.24	1.63	1.49	50	42	.84	.72
4534.78	1.62	1.48	50	40	.83	.71
Fe II						
4128.74	1.14	1.23	33	42	.39	.42
4233.17	1.58	1.55	53	50	.71	.71
4369.40	1.11	1.22	31	36	.43	.44
4416.82	1.49	1.42	49	43	.64	.62
4489.18	1.52	1.43	48	44	.70	.60
4491.40	1.33	1.32	39	40	.56	.55
4508.28	1.35	1.37	41	39	.57	.60
4515.34	1.41	1.35	43	39	.60	.59
4520.22	1.37	1.36	42	40	.58	.58
Ti II						
4028.33	1.57		49		.70	
4287.89	1.66	1.64	54	55	.81	.76
4316.81	1.32	1.27	38	43	0.54	0.47
Ti II						
4320.96		1.44		39		0.68
4330.26	1.31	1.25	36	36	0.51	.49
4337.92	1.60	1.53	48	44	.81	.76
4341.37	1.60	1.48	52	44		
4344.29	1.48	1.40	38	38	.72	.64
4394.06	1.54	1.40	45	39	.75	.65
4395.85	1.49	1.42	43	40	.70	.62
4398.31	1.33	1.20	40	36	.56	.44
4417.72	1.62	1.56	52	48	.74	.73
4443.80	1.67	1.60	53	53	.82	.76
4450.49	1.50	1.45	40	40	.75	.69
4464.46	1.44	1.43	38	41	.72	.62
4468.49	1.68	1.65	55	57	.82	.76
4469.16	1.46	1.35	40	38	.67	.58
4470.86	1.48	1.36	42	38	.68	.58
4488.32	1.29	1.23	35	35	.50	.48
4493.53		1.20		33		.46
4501.27	1.70	1.61	56	53	.82	.76
4524.73	1.26	1.11	37	31	.51	.40
CH						
4218.72	1.39	1.35	44	42	.54	.53
4224.86	1.48	1.34	44	39		.53
4255.25	1.36	1.33	43	40	.53	.53
4255.82	1.50	1.45	46	47	.70	.64
4261.23	1.56	1.43	63	54	.60	.54
4267.38	1.35	1.30	49	41	.50	.48
4281.97	1.39	1.39	43	45	.54	.53
4343.96	1.20	1.17	36	39	.44	.39
4347.54	1.30	1.15	48	39	.40	.39
4348.34	1.28	1.24	40	41	.45	.43
4355.71	1.30	1.19	42	42	.46	.40
4356.37	1.29	1.23	46	41	.44	.44
4356.61	1.30	1.20	49	42	.42	.39
4374.22	1.53	1.50	51	45	.69	.62
4380.07	1.38	1.34	45	37	.54	.51
4387.08	1.31	1.30	40	43	.50	.47
4388.88	1.20	1.22	32	40	.44	.40
4396.07	1.21	1.13				
4396.96	1.16	1.19	40	41	.37	.36
4397.16	0.98	0.89	32	33	.28	.23
4402.85	0.86	0.77	32	38	0.22	0.15

of the number of atoms contributing to the formation of the line to the total number of atoms of all elements, N. Equation (2) may be written for the sun and the star. The ratio of these gives

$$\Delta \log N_{r,s} = \Delta \log \zeta_{r,s} + \Delta \log \tau_0 - \Delta \log \kappa . \tag{3}$$

The values of $\Delta \log N_{r,s}$ are given for the ground state by the curves of growth. The quantity $\zeta_{r,s}$ may be written

$$\zeta_{r,s} = \frac{N_{r,s}}{\sum_r \sum_s N_{r,s}} \frac{\sum_r \sum_s N_{r,s}}{N} . \tag{4}$$

The ratio

$$\frac{N_{r,s}}{\sum_r \sum_s N_{r,s}}$$

is obtained from Saha's and Boltzmann's equations, while

$$\frac{\sum_r \sum_s N_{r,s}}{N}$$

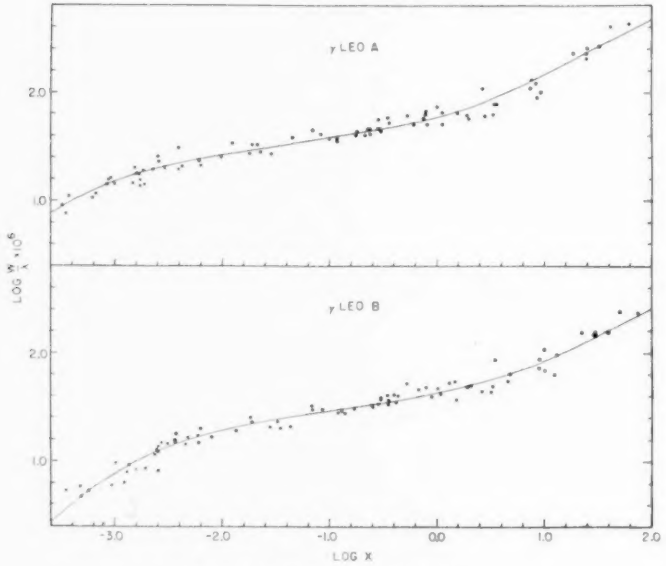

FIG. 1.—Curves of growth for Fe I

TABLE 3

TEMPERATURE DETERMINATIONS

Temperature	$\Delta\theta$		T	
	A	B	A	B
Excitation:				
Fe I	0.264 ± 0.025	0.210 ± 0.025	3868° ± 74°	4035° ± 82°
Ti I	.420 ± 0.104	.208 ± 0.098	3300 ± 220	3830 ± 290
CH	.184	.066	3770 ± 150	4130 ± 160
Ionization:				
Fe	.277	.170	4110	4500
Ti	0.303	0.178	4020	4470
Effective ($\tau = 0.3$)	.....	.....	3870	4160

TABLE 4

TURBULENT VELOCITIES (KM/SEC)

Velocity	Fe I		CH	
	A	B	A	B
Instrumental	3.7			
Curve of growth	2.2	2.0	.....	.....
Line width	4.5	4.5	6.8	6.8
Central depth	5.5	4.6	6.6	6.2
Curve of line-width correlation				
ξ_1	4.2	4.2	.....	.....
ξ_2	4.5	4.5	.....	.....
Thermal	1.1	1.1	2.0	2.1

TABLE 5

PARAMETERS OF THE ATMOSPHERES

Quantity	A	B
$\Delta \log N$ (star − sun)		
Fe I	1.89	1.24
Fe II	1.29	1.28
Ti I	1.89	1.12
Ti II	1.65	1.22
$\log Sf$ (CH)	14.85	14.72
Γ/γ_{CH}	1.0	1.4
$\log P_e$		
Fe	− 0.90	− 0.60
Ti	− 1.19	− 0.55
$\log g$		
Fe	1.5	1.8
Ti	0.9	1.9
Mass and radius	2.2	2.7

gives the chemical composition of the atmosphere. If it is assumed that the chemical composition of the sun and the star are the same and that τ_0, the optical depth for the formation of the lines, is the same for the sun and the star, then these terms drop out of equation (3). Also, if the continuous opacity is due to the negative hydrogen ion, it will be proportional to the number of negative hydrogen ions, which is given by Saha's equation. Under these assumptions equation (3) and Boltzmann's and Saha's equations may be solved for the electron pressure and the ionization temperature in the manner given by Koelbloed (1953). The values of $\Delta\theta_{ion}$ and $\Delta \log P_e$ obtained for iron and titanium are shown in Tables 3 and 5.

The effective surface gravity may be determined from the ionization temperature and the electron pressure. For the determination of $\log g$, the solar values of $\log P_e$ and θ_{ion} have both been taken as 0.95. The values read from Koelbloed's graph are listed in Table 5. These values may be compared with those computed from the masses and radii of the stars. The radii are obtained from the effective temperatures and the bolometric magnitudes. The effective temperatures and bolometric corrections are taken from Kuiper (1938). The absolute magnitudes were computed from the apparent magnitudes and the parallax given by Keenan and Keller (1953), which is in good agreement with the trigonometric parallax. The masses were computed from the elements of the visual orbit, and the mass ratio was obtained from the mass-luminosity relation corresponding to the absolute magnitudes derived. The surface gravity derived in this manner is given in Table 5.

For both stars the effective surface gravity is smaller by a factor of about 8 than the surface gravity derived from the dimensions of the stars. This is in agreement with the results found for other late-type giant stars. To investigate the contribution of the turbulent velocities to this discrepancy, the widths and central depths of a number of the least-distorted lines were measured.

To determine the turbulent velocities, the methods given by Huang and Struve (1955) were used. It was assumed that the velocity distribution of large eddies is that given by a Gaussian function. Graphs of central depth and line width versus equivalent width yield velocities corresponding to a combination of large eddies, small eddies, thermal motion, and instrumental width. These velocities are summarized in Table 4.

The graphs for Fe I are shown in Figures 2 and 3. Within the uncertainties of the data, both methods yield the same result, averaging 5.0 km/sec for γ Leo A and 4.5 km/sec for γ Leo B. The lower part of the curve of line-width correlation gives ξ_1, the velocity for small eddies, and ξ_2, the velocity for small and large eddies combined. The value of ξ_1 obtained here is 4.2 km/sec for both stars. The value obtained for large eddies is 1.6 km/sec; however, the difference between ξ_1 and ξ_2 is small and indicates that the velocity for large eddies is too small to be significant in comparison with the other effects.

The instrumental profile was determined from the iron comparison lines on the plates. The width corresponds to a Doppler velocity of 3.7 km/sec. When this is taken into account, the velocity derived for small eddies is 3.1 km/sec for γ Leo A and 2.3 km/sec for γ Leo B, in agreement with the values obtained from the curves of growth. The pressure due to the turbulent velocities is quite inadequate to account for the differences between the effective surface gravity and the values determined from the dimensions of the stars.

The turbulent velocities have also been investigated by using the central depths and half-widths of the CH lines. For both stars slightly higher values for the velocities than those found for Fe I were obtained by both methods, although the number of CH lines is smaller and the results are more uncertain. When the instrumental width and the velocity due to thermal motion are removed, the turbulent velocities for CH are larger than the Fe I values by 2.1 km/sec for γ Leo A and 2.6 km/sec for γ Leo B. No variation of the turbulent velocity with excitation potential was found for the

Fe I lines. The velocities derived from the titanium and Fe II lines were found to be approximately the same as the Fe I values.

The equivalent widths of a number of CH lines that appeared to be relatively free of blending were measured to obtain the relative concentrations of the molecule in the two stars and to evaluate the rotational temperatures. The effective number of molecules contributing to the formation of each line was obtained from the Fe I curves of growth. Since CH is lighter than Fe I, the thermal motion for the molecules will be larger than for the Fe I atoms. Before using the Fe I curves of growth to evaluate log Nf for CH, they were displaced to account for the difference in the velocities of the molecules and the atoms. It was assumed that the turbulent velocities for the molecules were the same as those for the atoms.

The values of log Nf obtained for each line are related to the rotational temperature by the equation

$$\log \frac{Nf}{i} = -\frac{F''(J'')}{8068}\,\frac{5040}{T} + \text{constant}\,, \tag{5}$$

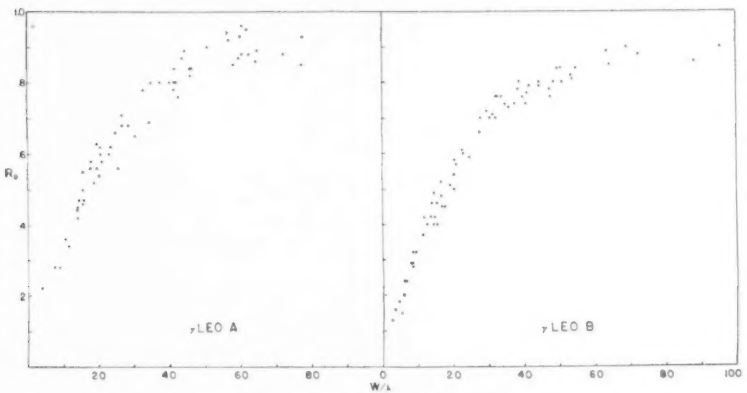

FIG. 2.—The relation between central depth and equivalent width for Fe I

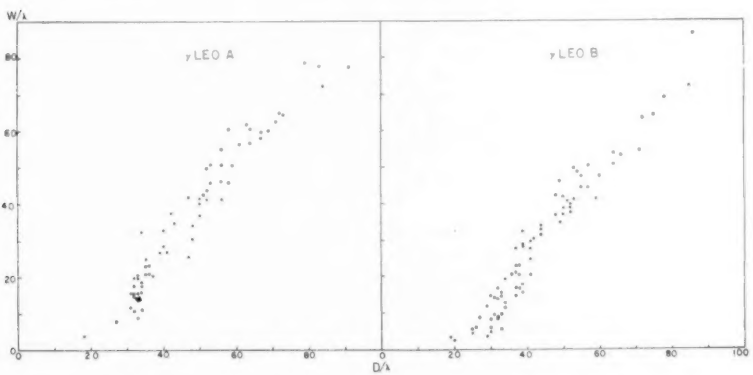

FIG. 3.—The relation between line width and equivalent width for Fe I

where $F''(J'')$ is the rotational-term value and i is the intensity factor. The intensity factors were computed from the formulae given by Jevons (1932) for doublets, Hund's coupling case b. The rotational temperatures were obtained from equation (5) by a least-squares solution. The values obtained are

$$\gamma \text{ Leo A:} \quad T = 3770° \pm 150°,$$

$$\gamma \text{ Leo B:} \quad T = 4130° \pm 160°.$$

These values are more uncertain than is indicated by the probable errors. The temperatures depend to a large extent on a few lines with high rotational quantum numbers in the P branch. These lines are weak, and any blending with atomic lines would lead to a higher value for the temperature than the true one. In addition, any error in the position of the continuum in this region would have a large systematic effect on the equivalent widths of these lines.

From the number of molecules contributing to the formation of each line, Nf, it is possible to obtain the total population for the level K'' from the relative transition probabilities for the lines arising from that level. The molecular abundance given by $\log Sf$ (Roach 1939) may be evaluated from the equation

$$\log Sf = \log N_{K''} f + \log G, \tag{6}$$

where G is given by

$$G = \frac{Z(T)}{g\, e^{-E_\kappa/kT}}, \tag{7}$$

with $Z(T)$ the partition function, g the statistical weight of the level, and E_κ the excitation potential. The value of $\log Sf$ for γ Leo A is 14.85 and for γ Leo B, 14.72, giving a ratio of 1.4 for the number of molecules of CH in the atmospheres of the two stars. These values may also be compared with the $\log Sf$-value of 13.96 for the sun given by Hunaerts (1947).

All the temperatures which have been derived, except the CH rotational values, have been obtained by adding the difference measured to the solar values. In comparing the various determinations for γ Leo, any differences in the corresponding solar values should also be taken into account. For the excitation tmeperatures for Fe I and Ti I, which depend on the $\log X_f$-values, Wright's temperatures of 4850° and 4550° for the sun have been used. For the determination of the ionization temperatures, 5300° has been assumed for the solar value. This is reflected in the higher temperatures obtained from the ionization than from the excitation. A comparison of $\Delta\theta$ is more satisfactory, although $\Delta\theta_{\text{ion}}$ depends to some extent on the θ_{ion} assumed for the sun. The values of $\Delta\theta$ obtained from the ionization are slightly smaller than the ones obtained from the excitation. If $\Delta\theta_{\text{ion}}$ is computed by using a lower value for the ionization temperature than the assumed one, the values of $\Delta\theta_{\text{ion}}$ increase. The temperatures obtained from titanium are generally lower than those obtained from iron.

For comparison, the temperatures computed from the equation

$$T^4 = T_{\text{eff}}^4 \left(\tfrac{1}{2} + \tfrac{3}{4}\tau\right) \tag{8}$$

have been included in Table 3. The values of T_{eff} have been taken from Keenan and Morgan (1951), and τ has been taken as 0.3.

For the sun, the rotational temperatures of the molecules have been found to be appreciably lower than the excitation temperatures of the atoms. This might also be expected for the two components of γ Leo; however, the differences in the stratification of the atmospheres as compared with the sun could alter this effect. Although no differences were found for either γ Leo A or γ Leo B, additional determinations of rotational temperatures are required to remove the uncertainty.

It is a pleasure to express my appreciation to Dr. O. Struve and Dr. H. F. Weaver for their advice and encouragement in this study.

REFERENCES

Allen, C. W. 1934, *Mam. Commonwealth Solar Obs. Canberra*, Vol. **1**, No. 5.
———. 1938, *ibid.*, Vol. **2**, No. 6.
Gratton, L. 1953, *Les Processus nucléaires dans les astres* (5th Colloque international d'astrophysique), pp. 419–448.
Huang, S., and Struve, O. 1955, *Ap. J.*, **121**, 84.
Hunaerts, J. 1947, *Ann. d'ap.*, **10**, 237.
Jevons, W. 1932, *Band Spectra of Diatomic Molecules* (London: Physical Society), p. 136.
Keenan, P. C., and Keller, G. 1953, *Ap. J.*, **117**, 241.
Keenan, P. C., and Morgan, W. W. 1951, *Astrophysics: A Topical Symposium*, ed. J. A. Hynek (New York: McGraw-Hill Book Co.), chap. 1.
Koelbloed, D. 1953, *Pub. Astr. Inst. U. Amsterdam*, No. 10.
Kuiper, G. P. 1938, *Ap. J.*, **88**, 472.
Minnaert, M. 1935, *Zs. f. Ap.*, **10**, 40.
Roach, F. E. 1939, *Ap. J.*, **89**, 99.
Thackeray, A. D. 1936, *Ap. J.*, **84**, 433.
Unsöld, A. 1938, *Physik der Sternatmosphären* (Berlin: Julius Springer).
Wright, K. O. 1948, *Pub. Dom. Ap. Obs. Victoria*, Vol. **8**, No. 1.

AN INTERPRETATION OF AE AQUARII

JOHN A. CRAWFORD AND ROBERT P. KRAFT*

Berkeley Astronomical Department, University of California

Received August 8, 1955; revised September 19, 1955

ABSTRACT

The spectrum of AE Aquarii is discussed on the basis of spectrograms taken at the Lick Observatory, giving a dispersion of 130A mm at Hγ. The late-type component of this double star, classified on the Morgan-Johnson system, is found to be K5 IV–V. This classification, taken together with Joy's minimum value of $1\odot$ for the mass of the star, indicates that a rapid evolutionary expansion may already have brought it to the point of filling one lobe of the zero-velocity surface passing through the inner Lagrangian point of the system. On this hypothesis, supported by the presence of narrow Ca II emission lines, the K star is found to eject material, some of which is collected by the blue companion. The order of magnitude of the rate of this transfer of mass is estimated by three independent methods: (1) the theoretical Sandage-Schwarzschild rate of evolutionary expansion; (2) the observed luminosity of the blue star; and (3) the intensities of the narrow and broad emission features in Hδ. These estimates agree, yielding a rate of $\sim 10^{25}$ g/year. The density of material in the region surrounding the blue star is found to be, accordingly, $\sim 10^{-13}$ g/cc. It is suggested that the accretion of mass by the blue star is related to the outbursts of 2 mag. found by Zinner, and a possible connection with the U Geminorum type variables is pointed out.

I. INTRODUCTION

The recent discovery by A. H. Joy (1954*a*, *b*) that the flaring variable AE Aquarii is a spectroscopic binary of short period has led us to attempt an interpretation of this system. Joy has found that AE Aquarii consists of a pair of dwarf stars, one of spectral type K, having relatively narrow emission lines of H and Ca II, the other possessing a continuous spectrum with superimposed broad emission lines of H, He I, and Ca II. Two stars of the U Geminorum class, SS Cygni and RU Pegasi, were reported by him (1954*a*) to show similar spectral features and large radial-velocity variations, suggesting the possibility of binary motion. Thus it is not impossible that the explosive U Geminorum phenomenon requires, in some unexplained fashion, two stars in a short-period orbit as a necessary, though not sufficient, condition.

Despite the spectral similarity of these three stars, it should be noted that AE Aquarii does not appear to be a typical U Geminorum star when judged by its light-variability. Zinner (1938) found outbursts of 2 mag. (photographic) with a possible period of about 1 year. Henize (1949), Lenouvel (1952), and Lenouvel and Golay (1954) observed a strong tendency for "flickering" at minimum, with occasional flares up to 1 mag. The A.A.V.S.O. detected no major outbursts during 1953, its "AE Aquarii year" (Mayall 1954). If we suppose that the period-amplitude relation found by Kukarkin and Parenago (1933), as modified by Kopylov (1954), applies, the outburst corresponding to 1 year should be 5 or 6 mag. We would then conclude that either the period is more nearly of the order of 5–10 days or that AE Aquarii does not have bona fide U Geminorum outbursts. In either case the spectrum found by Joy certainly suggests that AE Aquarii is a close relative of such variables as SS Cygni and RU Pegasi.

The present discussion consists of an attempt to obtain a self-consistent model designed to explain the major spectroscopic features of AE Aquarii. The interpretation given here may be thought of as an alternative to that advanced by Joy. Briefly, the argument is as follows: It is proposed in Section II that the late-type star lies above the main sequence at K5 by such an amount that it fills one lobe of the inner zero-velocity surface surrounding the system. In Sections III and IV we follow the motion of material

* National Science Foundation predoctorial fellow.

FIG. 1.—The spectrum of AE Aquarii compared with MK standards. The spectral type is thought to be K4 or K5 from the absence of the G band and the ratio of λ 4290 to λ 4299. The weakness of Ca I (λ 4226) and Cr I (λ 4254) suggests that the star is slightly above the main sequence.

flowing into the lobe surrounding the blue star. The density of gaseous material in this lobe (or, equivalently, the rate of accretion) is derived from the intensity of the broad Hδ emission and independently from the rate of accretion of this material by the blue star, the luminosity of which is found to be largely supplied by the kinetic energy of infall. An additional check on the density is obtained from the Sandage-Schwarzschild (1952) rate of evolutionary expansion of the K star. In Section V a possible process is briefly discussed through which the accretion of ionized material onto the blue component might engender, under suitable conditions, sudden releases of energy in the envelope, identifiable with the outbursts of U Geminorum stars.

II. THE SPECTRUM

The observational material is derived in part from the study made by Joy (1954*b*) and also from spectrograms taken at the Lick Observatory by G. H. Herbig, who has generously supplied them to us for use in this investigation. These spectrograms, giving a dispersion of about 130 A/mm at Hγ, were obtained with two prisms and a $3\frac{1}{2}$-inch camera attached to the 36-inch refractor. Suitable MK standards (Johnson and Morgan 1953; Johnson and Harris 1954) were taken for comparison purposes by one of us (R. P. K.) with the same prisms, camera, and slit-width.

One of these spectrograms of AE Aquarii, together with certain standard comparison stars, is reproduced in Figure 1. The general spectroscopic features pointed out by Joy, including the broad, unsymmetrical emission lines of hydrogen as well as the late-type absorption spectrum, are clearly seen. (The Ca II emission also is faintly present but is not reproduced.) Owing to the increasing opacity of the 36-inch objective toward the violet, the spectra of AE Aquarii are all very weak to the shortward of λ 4150 but are sufficiently dense in the vicinity of the G band to permit spectral classification. The spectrum reproduced in Figure 1, having the weakest continuous emission of the series, is the most suitable plate for the classification of the late-type star. Joy assigns it to dK0; we do not, however, find the corresponding classification K0 V when the star is placed on the MK system. The spectrum seems to be slightly anomalous, yielding different results from different line ratios. It can most nearly be described as K4 IV–V or K5 IV–V for the following reasons: (1) the G band is altogether absent; (2) the ratio λ 4290: λ 4299 is that of dK4 or dK5; (3) the resonance lines of Cr I, λ 4254, and Ca I, λ 4226, are too weak for K4 V–K5 V.

Possible systematic differences between the Mount Wilson and MK systems of spectral classification do not apparently account for the inconsistency, since, in general, the Mount Wilson system tends to classify K stars *later* than the MK system, e.g., HD 154363 is Mount Wilson dM0 (Wilson 1953); MK: K5 V. An inspection of Figure 1 shows that the ratio λ 4254:λ 4260 and the weakness of λ 4226 are closely that of K2 V, properties which seem inconsistent with criteria 1 and 2. These contradictions can, however, be removed by assuming that the star is slightly above the main sequence at K4 or K5. One might, of course, adopt the point of view that K0–K3 is the basically correct classification. Then the absence of the G band would again suggest that the star should be placed above the main sequence in that range. Thus, whether the star lies in the interval K0–K3 or the interval K4–K5, the properties of the spectrum seem to indicate a luminosity somewhat greater than class V. Further evidence on this point would be furnished by spectrograms reaching λ 4077 of Sr II.

We shall proceed, for illustrative purposes, on the assumption that the spectral classification is K5 IV–V, attempt to anticipate some objections that might be raised against it, and show how they may be answered. In the first place, it might be argued that the spectrum is composite; the filling-in by the blue star tends to wipe out such incipiently weak features as the G band, so that the late-type component is actually earlier than K5. Moreover, the weakness of Cr I and Ca I is in support of a classification of about dK0–dK2. The blue-star veiling, however, can have little effect on the ratio of the

moderately strong features described in 2, and these lead to a classification at least as late as dK4.

A different kind of objection to the classification K5 IV–V might be looked for in the role played by the ionizing radiation of the blue star. Should the radiation field at the substellar surface of the K star be controlled by the blue star, a weakening of the lines of neutral metals, owing to ionization, might be thought to occur. This argument appears to be strengthened by the observed presence of hydrogen emission lines arising in an extended atmosphere associated with the K component, presumably excited by the radiation of the blue companion. We shall now consider the refutation of this objection.

Despite the dilution factor of the order of 10^{-4}, the blue star will control the radiation field at the substellar surface of the K companion and, in particular, should be responsible for a high degree of ionization of metals. The fractional projected area of the K-star disk exposed to the blue star is about one-fifth at elongation, the plate illustrated in Figure 1 having been taken just prior to that phase, K star receding. The net result will be that the K-star surface is divided into two parts, one large region controlled by the K star and a small one of totally foreign character. In no case can we think of this small ionized region as producing a *perturbation* on the spectrum of the star as a whole: its spectral properties are altogether different from those of the major portion of the surface. It therefore seems clear that the spectral classification obtained must be an integral property of the star.

A K5 V star has $T_e = 4400°$ K, $M_v = +7.8$ (Keenan and Morgan 1951), and a radius of 0.58 $R_\odot$, using Kuiper's (1938) empirical bolometric correction. From Joy's work, the minimum masses of the K star and blue star are 0.94 $\odot$ and 0.97 $\odot$, respectively, using the second of his two solutions (the first solution leads to even larger minimum masses). It does not appear likely that a K5 star can have a minimum mass of the order of 1 $\odot$ and remain on the main sequence. Present ideas of stellar evolution would lead to the belief that such a star is in a state of rapid expansion, proceeding essentially on the same time scale as that of a gravitationally contracting star of the same mass, luminosity, and radius. It is reasonable to suppose that the maximum attainable volume, namely, that of one lobe of the inner zero-velocity surface, has already been reached, and we shall go ahead on this assumption, which further results seem to justify.

There is, however, some direct observational evidence suggesting that the K star is surrounded by a turbulent gas envelope, an event to be expected if it is in a state of expansion through an inner zero-velocity surface. This evidence is the presence, in Joy's spectra, of narrow H and K emission lines sharing the radial velocity of the K star. These features are 2–5 A wide. The velocity of gases moving in the rotating frame of reference between the inner and outer zero-velocity surfaces can be readily estimated from the difference of potential of these surfaces, using the masses and separation of the stars adopted in this article. This gives a value of about 200 km/sec, in good agreement with Joy's observed width for the narrow emission features.

Generally speaking, Ca II emission is characteristic of SS Cygni stars and of objects in which considerable turbulence is believed to exist (supergiants of late spectral type, certain long-period variables, cepheid variables). It seems that turbulence is a likely mechanism for the production of such emission lines. It is also of interest to consider the case of TW Draconis. This is an eclipsing binary whose secondary is a subgiant listed by Crawford (1955) as filling the inner zero-velocity surface. Miss Roman has found Ca II emission lines, associated with the subgiant component, on a Yerkes spectrogram (Bidelman 1954). Several other eclipsing binaries with subgiant secondaries are known to show Ca II emission (RZ Eri, WW Dra, RT Lac, AR Lac), as are also several binaries with periods less than 1 day (W UMa, RW Com, RT And, FG Hya) (Bidelman 1954). It will be proposed in this article that the blue component of AE Aquarii is surrounded by a highly turbulent gas cloud. It is interesting to note that a strong, broad Ca II emission

line shows the same radial velocity as the blue star, in agreement with the general idea that Ca II emission is a characteristic of turbulence.

In order to proceed further, we shall arbitrarily adopt Joy's second solution, which gives a mass ratio of unity (1.0) and a minimum mass of 1 $\odot$ for each star. On the other hand, the mass of the K star can hardly exceed 1.5 $\odot$ if it is to be classified as K5 IV–V. The system is not known to eclipse, but this may very well be disguised by the persistent flickering, of the order of 0.3 mag. (Henize 1949; Lenouvel 1952; Lenouvel and Golay 1954). For a mass ratio of 1.0, the dimensions of the inner zero-velocity surface given by Kopal (1954) permit an avoidance of eclipse if the masses of the stars are not less than 1.3 $\odot$. We shall therefore adopt this value in the discussion to follow. It should be emphasized that none of the conclusions reached in this article are affected by the exact

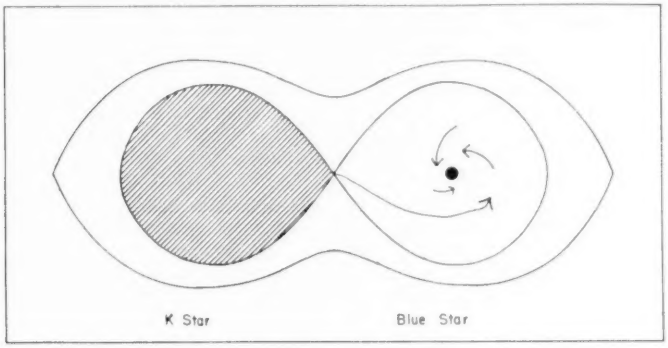

FIG. 2.—The system of AE Aquarii (schematic). The view is pole-on, and the inner and outer zero-velocity surfaces are indicated. Turbulent gas streams are represented by arrows.

choice of the mass in the interval 1.0–1.5 $\odot$. The "physical radius" (Kuiper 1941) of the K5 star would then be 1.2×10^{11} cm = 1.7 $R_\odot$ (about three times the radius of a main-sequence star of the same spectral type), the separation between the centers of mass 3.2×10^{11} cm = 4.5 $R_\odot$, and $i = 64°$. The absolute bolometric magnitude of the K5 star becomes +4.8 if $T_e = 4300°$ K, and $M_v = +5.5$, i.e., the star is 2.3 mag. above the main sequence. The parallax is then 0".013, and we have, according to Joy, $M_v = +6.5$, with $R = 6.6 \times 10^9$ cm for the blue star.

The model as viewed "pole-on" is shown in Figure 2. As has already been suggested, two consequences of the filling of one lobe by the K star are the following: (1) A stream of gas will be ejected from the K star into the region surrounding the blue star, in a manner analogous to the "ejection of type A" described by Kuiper (1941) in connection with his interpretation of β Lyrae. The simultaneous ejection of material into the region between the inner and outer zero-velocity surfaces can, however, by no means be ruled out and is probably to be expected. (2) The K star will suffer a decrease in surface gravity when compared with a single star of the same mass and radius. Such a reduction will tend to increase the degree of ionization, and, in particular, the conversion of chromium from Cr II to Cr I and calcium from Ca II to Ca I will be delayed as one passes from K0 to K5. Thus Cr I, λ 4254, and Ca I, λ 4226, are weakened, as we have already indicated.

Dr. Joy (private communication) has expressed the opinion that the K star is certainly earlier than K5. In this connection it should be pointed out that the spectrum reproduced in Figure 1 is rather narrow. There is also some question regarding the use of

the MK system of classification in attempting to detect comparatively small luminosity effects. It seems that this disagreement over the assignment of spectral class is in a large part due to the fact, recognized by Joy and the authors, that the late-type spectrum is peculiar. This in itself lends plausibility to the hypothesis that the star is somewhat swollen. It should be emphasized in particular that, if Joy's classification (dK0) is adopted, the average radius of such a star would be about half that of the inner lobe, and an increase in this radius by a factor of 2 would be beyond the limit of spectroscopic detectability at low dispersion. There is, therefore, in any case, no obstacle to the hypothesis that the K star does indeed fill a lobe of the inner zero-velocity surface.

III. DISCUSSION OF THE PROCESS OF MASS TRANSFER

According to modern ideas on stellar evolution, the expansion of a star is intimately related to the gravitational contraction of a hydrogen-depleted central core, the luminosity being due chiefly to the conversion of hydrogen in a thin shell surrounding the core (Schönberg and Chandrasekhar 1942; Sandage and Schwarzschild 1952). The expansion occurs at a rate given essentially by the gravitational time scale, meaning that a certain fraction of the total energy released is converted into potential energy of the outer regions of the stellar mass. When, as in the present case, the size of the star is limited by a zero-velocity surface, the consequence of the tendency to expand must be the outpouring of mass through this surface, especially through the conical tip of the star at the inner Lagrangian point, where a natural sink for the flow of material exists. This ejected material will then be accelerated in the gravitational field of the companion star (here the blue star) and captured, as will be shown later.

In order to estimate roughly the rate σ at which mass is emitted by the K star, we can equate the order of magnitude of the rate of increase of potential energy to the luminosity thus:

$$\frac{G}{2R}\frac{d}{dt}(\mathfrak{M}^2) = \frac{G\mathfrak{M}\sigma}{R} \sim L. \tag{1}$$

The potential of the ejected material is that associated with the inner Lagrangian surface and is significantly smaller in magnitude than the mean potential energy per unit mass of the star. We are therefore justified in neglecting to include it in the order-of-magnitude relationship expressed by equation (1). This relationship presumably gives the order of magnitude of σ. We obtain in this way the value 6.7×10^{25} g/year, using the adopted values of L, $\mathfrak{M}$, and R for the K star. However, for an isolated expanding star, the results of Sandage and Schwarzschild (1952) indicate that, for a mass of 2 $\odot$, the total rate of increase of potential energy is about thirty times smaller than the luminosity. It is not possible to state whether or not a factor of this order is applicable in the present case. If this were so, the accretion rate would become 0.2×10^{25} g/year, a value which is smaller than, but closer to, the two independent estimates of σ obtained later.

As a check on this procedure, an alternative estimate was made on the basis of the radial expansion of the models of Sandage and Schwarzschild (1952). Although given only for masses 1 $\odot$, 2 $\odot$, and 4 $\odot$, the physical characteristics of these models can be readily interpolated for intermediate masses. This was done for the adopted value, 1.3 $\odot$. If $\dot{R}_m$ is the rate at which the radius of the (single-star) model increases, an estimate of the corresponding rate of mass loss σ of our (double-star) component filling the inner Lagrangian surface is given roughly by

$$\sigma = 4\pi R_m^2 \bar{\rho} \dot{R}_m ,$$

where $\bar{\rho}$ is the mean density of the model. This can be written

$$\sigma = 3\mathfrak{M}\frac{\dot{R}_m}{R_m}.$$

Values of $\dot{R}_m$ were obtained by numerical differentiation for all but one of the models considered by Sandage and Schwarzschild, and the corresponding values of σ listed in Table 1 are in general agreement with the previous estimate. It is hard to see physically how the rate of mass loss by an expanding member of a close binary system can ever greatly exceed the value given by equation (1).

The inner zero-velocity surface surrounding the blue star will contain the matter ejected from the K star in the neighborhood of the inner Lagrangian point L_1. This matter will be accelerated by the blue star to velocities of several hundred kilometers per second. Kuiper (1941) has discussed a similar system (type A) and states that the material ejected from the expanding star forms a ring around the companion. The high angular momentum of the infalling material relative to the blue star appears, at first, to offer an obstacle to a significant rate of accretion. It is easy to show, however, that for AE Aquarii the collision mean-free path in the region around the blue star is very much smaller than the dimensions of the zero-velocity surface. As a consequence, the material moves like a gas. The Reynolds number is extremely high, and it is quite certain that the gas is turbulent. If, in fact, a ring is formed, as Kuiper suggests, the inner

TABLE 1

	Model No.					
	I	II	III	IV	V	VI
$\sigma \times 10^{-25}$ g/year	0.19	0.87	1.35	1.66	2.42	4.90

portions of the ring must rotate more rapidly than the outer portions, as both describe essentially circular Keplerian orbits around the blue star. The velocity gradient will cause a very rapid turbulent exchange of angular momentum, so that the inner part of the ring will lose angular momentum and move in closer, while the outer part gains angular momentum and spreads out. The constant infall of new material keeps the expansion of the ring in equilibrium, and the net effect is that matter accretes onto the surface of the blue star, which acts as a sink for the angular momentum as well. The mixing length in the ring is extremely large, being, according to Prandtl's theory, of the order of the dimensions of the ring itself. It is of some interest to estimate the size that the ring would have, were it not for the dissipative effect of turbulence. A particle of unit mass, falling out of the K star at the inner Lagrangian point, will possess initially an angular momentum relative to the blue star equal to Va, where V is the velocity of the star and a the radius of its orbit. The order of magnitude of this angular momentum cannot be expected to change during the time it takes for the particle to come close to the blue star. If p is the distance of nearest approach to the blue star, and v is the velocity of the particle, we can write

$$Va \sim p\,v = p\sqrt{2G\mathfrak{M}p^{-1}}.$$

We find in this way $p \sim a/8 = 2 \times 10^{10}$ cm, a value about three times larger than the radius of the blue star. This represents the order of magnitude of the periastron distance of the infalling matter, neglecting the effects of turbulence. Finally, to support our statement that the material forms a turbulent gas, we shall estimate the collision mean-free path. A lower limit to the density is obtained by assuming that the blue star forms a perfect sink. In this case, at a typical distance of 6×10^{10} cm from the blue star, the velocity acquired is about 760 km/sec. This must also be the order of magnitude of the accretion velocity. Assuming this and an accretion rate of 10^{25} g/year, the continuity condition for the steady state yields a density of $\sim 10^{-13}$ g/cc. As the gas is ionized, the cross-sections will be larger than those for neutral atoms, which are about 10^{-16} cm^2. Even in this

case, however, the mean free path is only 10^5 cm. The Reynolds number is extremely high, being about 10^7.

Finally, the repulsive force exerted on the infalling gas by the blue-star radiation is estimated to be smaller than the gravitational attraction by a factor $\sim 10^{-3}$. There appears, therefore, to be no obstacle to the hypothesis that the blue star collects material ejected by its companion.

If, in fact, as the foregoing considerations suggest, mass is accreted by the blue star at a rate of the order of 10^{25} g/year, we would expect that the kinetic energy of the tenuous infalling material would be dissipated into heat by viscosity in the turbulent motion and by impact with the denser material of the star's atmosphere. The heat thus liberated should then appear as a contribution to the luminosity of the blue star of about the amount $L = G\mathfrak{M}\sigma R^{-1}$.

The adopted luminosity for the blue star is 4.9×10^{33} ergs/sec. The value of σ obtained by substituting this figure in the relation $L = G\mathfrak{M}\sigma/R$ is 0.6×10^{25} g/year. The agreement of this value with the other estimates suggests that the observed luminosity of the blue star is essentially due to the energy released by the accreted material. This view is strengthened also by the fact that the blue star occupies a peculiar position in the H-R diagram. It lies 10.5 vis. mag. below the main sequence but about 4 mag. above the most luminous white dwarfs, whose effective temperature it exceeds by about 8000° K. Unless the blue star is essentially degenerate, it can readily be shown that the small radius implies such a high internal temperature that electron scattering is the principal source of opacity. A simple calculation based on the standard model then yields a luminosity 8 mag. brighter than is observed.

AE Aquarii is an example among many other close binary systems in which the ages of the two components appear to differ greatly. The process of mass loss by expansion through an inner zero-velocity surface (Kopal 1955) affords a possible explanation for this apparent anomaly in the case of eclipsing systems with subgiant components (Crawford 1955).[1] The history of AE Aquarii, according to this view, could be described as follows: Originally the blue star was the more massive component. As evolution proceeded, it began expansion earlier than its companion, losing the hydrogen-rich material from its outer layers. Eventually it became essentially depleted of hydrogen and contracted to its present state. Later on, the companion, which must have been more massive and more luminous than it appears at present, also expanded until it reached the inner zero-velocity surface and initiated the process of mass loss which is still going on. The existence of evolutionary sequences of this type in close binary systems is strongly suggested by the currently accepted theories of stellar evolution.

IV. THE HYDROGEN-EMISSION LINES

A third way of estimating the accretion rate, which yields about the same value as the other two, is provided by the total intensity of the hydrogen-emission lines, which show the radial velocity of the blue star. For this purpose the line Hδ, in the spectrum reproduced in Figure 1, was utilized. Allowing for a correction due to the contribution of the K5 star to the continuous spectrum, the effective width $\Delta\lambda$ of Hδ was found to be 23 A for a height set equal to the intensity of the blue-star continuum. The hydrogen was assumed to be completely ionized (in agreement with the fact that the observed emission lines show no self-absorption) at constant density in a sphere of radius S surrounding the blue star. The assumption of constant density was, of course, made for convenience. However, because of the difficulties caused by the effects of turbulence, a better guess would be hard to make. It is probably true that turbulence tends to make the density more uniform than it would otherwise be. The temperature of the blue star being 20000° K, an electron temperature of 10000° K was arbitrarily assumed.

[1] The process of mass ejection and its effect on the period have also been discussed by F. B. Wood (1950; see also Dadaev 1954).

The rate of radiative recombination of ionized hydrogen into different energy levels has been calculated by Cillié (1932) for several assumed temperatures. The rate of recombination per cubic centimeter at 10000° K into the sixth level is given by him as $1.45 \times 10^{-14} N^2$, where N is the density of hydrogen nuclei, assuming that all electrons come from the ionization of hydrogen. The probability that the excited atom will emit a quantum in Hδ is 0.221. The density N is then given by the expression

$$0.221 \times 1.45 \times 10^{-14} \times \frac{4\pi}{3} S^3 N^2 = \frac{8\pi^2 R^2 c}{e^{hc/\lambda k T} - 1} \frac{\Delta\lambda}{\lambda^4},$$

where T is the effective temperature, R the radius of the blue star, and λ the wave length of Hδ. We obtain in this way

$$N^2 S^3 = 1.3 \times 10^{56}. \tag{2}$$

This figure is overestimated because of the neglect of the effect of captures in levels higher than the sixth, followed by cascading into the sixth level. If, at the other extreme, we assume that all captures in levels above the sixth result in cascades to this level, we obtain the value 1.9×10^{55} for $N^2 S^3$. Strömgren's theory (1939) gives a relation between the density of hydrogen and the radius of the largest sphere, S_S, ionized by the blue-star radiation:

$$N^2 S_S^3 = 1.0 \times 10^{55}. \tag{3}$$

As this value is perhaps significantly smaller than the one given by equation (2), there is an indication that another mechanism besides blue-star radiation is at work keeping the gas ionized, in fact, all the way to the neighborhood of the K star, where the narrow hydrogen emission arises. Turbulence may very well provide such a mechanism. The fact that Hδ is observed and shows no self-absorption makes it clear that no H I region envelops the ionized zone, so that S should be taken as the effective radius of the outer zero-velocity surface, beyond which the density can be assumed to decrease abruptly. This radius is about 1.6×10^{11} cm. Substituting this value in equation (2), we get for N the value 1.8×10^{11} atoms/cc, yielding the value 4.0×10^{-13} g/cc for the density ρ on the assumption of a hydrogen abundance of 75 per cent. The velocity v given by the Hδ line at half-maximum is 400 km/sec, corresponding to a free-fall distance r from the blue star of 8×10^{10} cm. The order of magnitude of the accretion rate is given by the relation

$$\sigma = 4\pi r^2 \rho v.$$

In this way we obtain for σ the value 4.4×10^{25} g/year. This is overestimated, owing to the neglect of cascading. If all cascading is assumed to populate the sixth level of hydrogen, we obtain for N the value 2.6×10^{10} H atoms/cc and for σ the value 0.6×10^{25} g/year.

There is also a narrow Hδ component in emission (2–5 A). Its radial velocity was not measured by Joy but is apparently similar to that of the K star. Its intensity on the spectrogram in Figure 1 seems about one-fifth that of the broad line. This is in agreement with the mass-transfer picture of AE Aquarii, according to which the region between the inner and outer zero-velocity surfaces surrounding the K star is expected to be filled with material of about the same density as the gas in the lobe surrounding the blue companion. This is, of course, because of the condition for the continuity of gas flow, since the velocities characteristic of the two regions are of the same order of magnitude.

It seems possible that turbulence keeps hydrogen ionized even in the shadow cone behind the K star. If not, we would expect the radial velocity of the narrow hydrogen-emission features to be systematically smaller than that of the K component. Spectrograms taken with a higher dispersion than was available to us are needed to settle this question.

To summarize, we have obtained values of the accretion rate from three independent lines of approach: (1) the theory of expansion; (2) the luminosity of the blue star; and (3) the recombination of hydrogen and have found them to have the same order of magnitude. This agreement seems to constitute a good argument in favor of this proposed model of AE Aquarii.

V. FURTHER DISCUSSION

In a recent publication (1954) Ambarzumian has reviewed the observational evidence relating to sources of stellar energy and has concluded that thermonuclear processes in stellar interiors are insufficient to explain a wide variety of unusual stars (T Tauri stars, comet-like nebulae, certain irregular variables of low luminosity, etc.). He has suggested that additional energy sources should be looked for in the outer regions of such objects. This general point of view seems to receive some further support from our conclusion that the luminosity of the blue component of AE Aquarii is mostly the result of the infall of material onto the surface.

The discovery of outbursts in AE Aquarii by Zinner (1938) hints at a possible relationship between this star and the U Geminorum group. What is further suggested by the preceding model is a connection between the process of mass transfer and the existence of outbursts. There is evidence that the outbursts are probably associated with the blue star: the spectrum is similar to that of an old nova; the magnitude fluctuations observed by Lenouvel (1952) in the photographic region are probably associated with the blue star; and, finally, there is no evidence that other systems in which one component fills the inner zero-velocity surface and the other component is a main-sequence star or a subgiant exhibit outbursts.

With regard to the process through which outbursts in the luminosity of the blue star result from the accretion of matter, a suggestion by Greenstein (1950) in connection with the T Tauri variable BD $-6°1253$ is of interest. The density and velocity of the dark cloud in the immediate vicinity of this star have values quite close to those found by us in the region surrounding the blue component of AE Aquarii. Greenstein points out that the magnetic field whipped up by the turbulent motion of the accreted ionized gas will itself be accreted, with the possibility of resulting intense electrical discharges identifiable with the flares observed in this T Tauri object. A similar mechanism may be operating in AE Aquarii.

In this connection the work of Kopylov (1954) is of interest. He has shown that the period-amplitude relation for certain recurrent novae is not necessarily a simple extrapolation of that for the U Geminorum variables. It would therefore seem possible that the mechanism responsible for the outbursts of AE Aquarii and stars of the U Geminorum class need not be identical in kind with that responsible for the explosions of repeating novae.

We wish to record our appreciation to Dr. G. H. Herbig for making available to us his spectrograms of AE Aquarii and also to thank Dr. W. P. Bidelman for a valuable discussion. We are indebted also to Dr. A. H. Joy, to Dr. J. L. Greenstein, and to Dr. A. R. Sandage for reading the manuscript and commenting on it. We are especially grateful to Professor O. Struve for his criticism.

REFERENCES

Ambarzumian, V. A. 1954, *Contr. Burakan Obs.*, No. 13.
Bidelman, W. P. 1954, *Ap. J. Suppl.*, **1**, No. 7, 223.
Cillié, M. 1932, *M.N.*, **92**, 820.
Crawford, J. A. 1955, *Ap. J.*, **121**, 71.
Dadaev, A. N. 1954, *Izvestia, Central Obs. Poulkovo*, Vol. **19**, Part 5, No. 152.
Greenstein, J. L. 1950, *Pub. A.S.P.*, **62**, 156.
Henize, K. G. 1949, *A.J.*, **54**, 89.

Johnson, H. L., and Harris, D. L. 1954, *Ap. J.*, **120**, 196.
Johnson, H. L., and Morgan, W. W. 1953, *Ap. J.*, **117**, 313.
Joy, A. H. 1954*a*, *Pub. A.S.P.*, **66**, 5.
———. 1954*b*, *Ap. J.*, **120**, 377.
Keenan, P. C., and Morgan, W. W. 1951, *Astrophysics*, ed. J. A. Hynek (New York: McGraw-Hill Book Co., Inc.), pp. 20 and 23.
Kopal, Z. 1954, *Jodrell Bank Ann.*, **1**, 37.
———. 1955, "Trans. I.A.U. Report of Commission 42" (unpublished).
Kopylov, I. 1954, *Doklady Akad. Nauk. U.S.S.R.*, Nov. ser., **99**, 515.
Kuiper, G. P. 1938, *Ap. J.*, **88**, 429.
———. 1941, *ibid.*, **93**, 133.
Kukarkin, B., and Parenago, P. 1933, *Akad. Nauk. S.S.S.R., Astr. Sovet. Peremmennye Zvezdy*, **4**, 251.
Lenouvel, F. 1952, *C.R.*, **235**, 1282.
Lenouvel, F., and Golay, M. 1954, *C.R.*, **237**, 1215.
Mayall, M. 1954, *J.R.A.S., Canada*, **48**, 22.
Sandage, A., and Schwarzschild, M. 1952, *Ap. J.*, **116**, 475.
Schönberg, M., and Chandrasekhar, S. 1942, *Ap. J.*, **96**, 161.
Strömgren, B. 1939, *Ap. J.*, **89**, 533.
Wilson, R. E. 1953, *General Catalogue of Stellar Radial Velocities* ("Carnegie Institution of Washington Publications," No. 601 [Washington: Carnegie Institution]), p. 197.
Wood, F. B. 1950, *Ap. J.*, **112**, 196.
Zinner, E. 1938, *A.N.*, **265**, 345.

A SPECTROSCOPIC STUDY OF THE PLEIADES

EUGENIO E. MENDOZA V*

Yerkes Observatory

Received July 5, 1955; revised August 28, 1955

ABSTRACT

A spectroscopic study of 78 stars of the Pleiades has been made. Spectra of 59 members are combined with the photoelectric observations of Johnson. After eliminating the effects of interstellar absorption, a two-color diagram and an H-R diagram were constructed. The discontinuity in the color index $(B-V)$ shown by the near-by stars is not present in the Pleiades. The F stars in the Pleiades appear, on the average, to be relatively fainter in the ultraviolet than stars of similar type and luminosity in the neighborhood of the sun.

Measures of color indices in the (U, B, V) system for near-by stars by Johnson and Harris (cf. Johnson and Morgan 1953; Morgan, Harris, and Johnson 1953) show a deficiency of stars with $(B-V)$ color index in the interval from $+0.20$ to $+0.30$ mag. Strömgren (1956) has discussed this problem. The $(B-V)$ color-index observations of the Pleiades (Johnson and Morgan 1953) do not indicate any conspicuous discontinuity between $+0.20$ and $+0.30$ mag. in $(B-V)$. The present paper is an investigation of the combined photoelectric and spectroscopic material of members of the Pleiades cluster, to eliminate the effects of interstellar absorption for each star individually.

Spectra of 78 members of the Pleiades were taken with the one-prism spectrograph attached to the 40-inch telescope of the Yerkes Observatory. The dispersion is about 125 A/mm at Hγ. All plates were taken during the fall and winter of 1953–1954 and the fall and winter of 1954–1955. Spectral types and luminosity classes were assigned to these stars according to the criteria of the Yerkes revised atlas system (MK type) outlined by Morgan (see Johnson and Morgan 1953). Among these spectra, 59 are the cluster members studied photoelectrically by Johnson (*ibid.*). The remaining 19 stars were taken from Hertzsprung's catalogue (1947) of the Pleiades region. In this catalogue they are marked as cluster members according to their proper motions.

The results of the spectroscopic observations are summarized in Tables 1 and 2. The columns of Table 1 give, first, the Hertzsprung number (see Hertzsprung 1923); second, third, and fourth, the values of V, $(B-V)$, and $(U-B)$, from Johnson's photoelectric observations (*ibid.*); fifth, the type on the MK system; sixth, the value of $(B-V)_0$, the intrinsic color index; seventh, the value of $(U-B)_0$, the intrinsic color index; eighth, the value of V_0, the V magnitude corrected for interstellar absorption; ninth, Remarks.

The first, fourth, and fifth columns of Table 2 are similar to the first, fifth, and sixth columns of Table 1. The second column of Table 2 gives m, the photographic magnitude (see Binnendijk 1946); the third column lists $(B-V)_c$, the computed color index (see below).

The star Hz 146, which may be a borderline metallic-line star, has been considered to have the photometric characteristics of an A8 star. The star Hz 225 shows a weaker G band than other stars of the cluster of similar spectral type. The star Hz 310 was classified as a giant by Schwassmann (1930). Our plate indicates a spectrum fainter than luminosity class IV.

The intrinsic color indices $(B-V)_0$, which have been used for stars in Table 1, are given in Table 3. Because of the discontinuity in $(B-V)$ observed near the gap in the case of the near-by stars, the intrinsic colors in this region are uncertain; the procedure adopted was as follows: between B6 and A4, $(B-V)_0$ was taken from Table 3 of the

* Fellow of the University of Mexico.

TABLE 1

OBSERVATIONS OF THE PLEIADES

Hz	V	$(B-V)$	$(U-B)$	MK	$(B-V)_0$	$(U-B)_0$	V_0	Remarks
28	8.24	+0.235	+0.14	A7 V	+0.20	+0.11	8.13	
43	8.05	+ .197	+ .15	A5 V	+ .15	+ .12	7.91	
88	9.06	+ .458	+ .10	F2 V	+ .38	+ .04	8.83	
92	8.16	+ .265	+ .09	A8 V	+ .23	+ .06	8.06	
108	9.82	+ .537	+ .05	F9 V	+ .56	+ .07	9.89	
117	5.45	− .046	− .33	B7 IV	− .12	− .38	5.23	Celaeno
126	3.69	− .107	− .41	B6 III	− .14	− .43	3.59	Electra
133	10.37	+ .627	+ .13	G0 V	+ .60	+ .11	10.29	
146	8.57	+ .331	+ .16	A m ?	+ .23	+ .09	8.27	
150	5.64	− .075	− .36	B8 V	− .09	− .37	5.60	18 Tau
156	4.29	− .106	− .46	B6 V	− .14	− .48	4.19	Taygeta
169	8.98	+ .439	+ .08	F3 V	+ .41	+ .06	8.89	
187	8.02	+ .216	+ .18	A3 V	+ .09	+ .09	7.64	
206	8.58	+ .352	+ .11	A9 V	+ .27	+ .05	8.33	
213	10.12	+ .602	+ .13	F9 V	+ .56	+ .10	9.99	
216	7.16	+ .159	+ .08	A1 V	+ .03	− .01	6.77	
219	9.70	+ .548	+ .05	F9 V	+ .56	+ .06	9.74	
227	9.43	+ .520	+ .11	F5 V	+ .45	+ .06	9.22	
242	3.86	− .068	− .40	B7 III	− .12	− .44	3.70	Maia
251	7.84	+ .192	+ .16	A2 V	+ .06	+ .06	7.44	
255	5.75	− .044	− .23	B8 V	− .09	− .26	5.61	Asterope
265	6.41	− .028	− .15	B9 V	− .06	− .17	6.31	
323	4.16	− .056	− .43	B6 IV nn	− .14	− .49	3.91	Merope
329	10.42	+ .640	+ .15	G0 V	+ .60	+ .12	10.30	
341	7.34	+ .097	+ .12	A2 V	+ .06	+ .09	7.23	
371	8.09	+ .353	+ .28	A0 V	.00	+ .03	7.03	
385	10.20	+ .724	+ .31	G6 V	+ .70	+ .29	10.13	
388	9.28	+ .457	+ .05	F4 V	+ .42	.00	9.17	
428	10.52	+ .638	+ .16	G0 V	+ .60	+ .13	10.43	
436	6.80	+ .025	− .07	B9.5 V	− .03	− .11	6.63	
457	8.38	+ .294	+ .08	A9 V	+ .27	+ .06	8.31	
468	9.44	+ .468	+ .02	F6 V	+ .46	+ .01	9.42	
510	6.98	+ .030	+ .05	A1 V	+ .03	+ .05	6.98	
513	7.64	+ .206	+ .12	A4 V	+ .12	+ .06	7.38	
520	7.26	+ .035	+ .05	A2 V	+ .06	+ .07	7.34	
534	7.76	+ .153	+ .12	A3 V	+ .09	+ .07	7.57	
540	6.80	+ .063	+ .02	A0 V	.00	− .03	6.61	
542	2.86	− .090	− .33	B7 III	− .12	− .35	2.77	Alcyone
620	9.86	+ .540	+ .11	F8 V	+ .53	+ .10	9.84	
681	9.24	+ .548	+ .12	F6 V	+ .46	+ .06	8.88	
693	8.25	+ .361	+ .11	A9 V	+ .27	+ .04	7.98	
695	9.12	+ .470	+ .07	F4 V	+ .42	+ .03	8.97	
708	10.69	+ .558	+ .07	F9 V	+ .56	+ .07	10.10	
722	5.44	− .072	− .32	B8 V	− .09	− .33	5.39	HR 1172
736	10.02	+ .556	+ .09	F8 V	+ .53	+ .07	9.96	
742	6.94	+ .125	+ .09	A1 V	+ .03	+ .02	6.66	
760	10.34	+ .614	+ .13	G0 V	+ .60	+ .12	10.30	
792	8.36	+ .284	+ .13	A8 V	+ .23	+ .11	8.20	
870	3.62	− .085	− .36	B8 III	− .09	− .36	3.60	Atlas
878	5.08	− .078	− .28	B8 pec	− .09	− .29	5.04	Pleione
885	8.11	+ .22	+ .13	A7 V	+ .20	+ .12	8.05	
891	7.51	+ .097	+ .11	A2 V	+ .06	+ .08	7.40	
910	6.59	− .028	− .12	B9.5 V	− .03	− .12	6.58	
924	7.96	+ .175	+ .13	A3 V	+ .09	+ .07	7.70	
948	9.08	+ .434	+ .02	F3 V	+ .41	.00	9.01	
977	6.16	− .052	− .19	B9 V	− .06	− .20	6.14	HR 1183
996	7.53	+ .077	+ .08	A2 V	+ .06	+ .07	7.48	
1129	6.92	+ .086	+ .03	A2 V	+ .06	+ .01	6.84	
1184	8.81	+0.384	+0.05	F2 V	+0.38	+0.05	8.80	

paper by Morgan, Harris, and Johnson (1953). From it the color excesses, $E_{(B-V)}$, follow. These color excesses were plotted on a chart of the Pleiades to obtain $E_{(B-V)}$ for stars with spectra later than A4 and earlier than F2; the $E_{(B-V)}$ of each star in this spectral range is defined as the mean color excess of the neighboring stars. This determination is based only on stars with accurately defined intrinsic colors, e.g., the late B- and early A-type stars.

TABLE 2

PLEIADES STARS WITH COMPUTED $(B-V)$

Hz	m	$(B-V)_c$	MK	$(B-V)_0$	Hz	m	$(B-V)_c$	MK	$(B-V)_0$
8	9.91	+0.48	F5 V	+0.45	313	8.18	+0.25	A7 V	+0.20
27	8.18	+ .37	A9 V	+ .31	396	9.81	+ .41	F5 V	+ .45
29	10.03	+ .47	F5 V	+ .45	447	8.61	+ .37	A9 V	+ .31
44	10.21	+ .56	F6 V	+ .46	484	9.12	+ .48	F3 V	+ .41
123	9.37	+ .36	F3 V	+ .41	501	8.48	+ .24	A7 V	+ .20
145	9.31	+ .39	F2 V	+ .38	508	6.19	+ .03	A0 V	.00
176	10.15	+ .48	F5 V	+ .45	757	9.52	+ .49	F4 V	+ .42
225	10.16	+ .60	G0 V*	+ .60	975	8.28	+ .19	A7 V	+ .20
248	6.54	+ .27	A0 V	.00	1003	6.74	+0.03	A0 V	0.00
310	9.19	+0.56	G0 V	+0.60					

* Weak G band.

TABLE 3

INTRINSIC COLORS

MK	$(B-V)_0$	MK	$(B-V)_0$	MK	$(B-V)_0$	MK	$(B-V)_0$
B6	−0.14	A1	+0.03	A8	+0.23	F5	+0.45
B7	− .12	A2	+ .06	A9	+ .27	F6	+ .46
B8	− .09	A3	+ .09	(A9	+ .31)*	F8	+ .53
B9	− .06	A4	+ .12	F2	+ .38	F9	+ .56
B9.5	− .03	A5	+ .15	F3	+ .41	G0	+ .60
A0	0.00	A7	+0.20	F4	+0.42	G6	+0.70

* This star is included in Table 2.

The intrinsic color index, $(U-B)_0$, was computed from the formula

$$(U-B)_0 = (U-B) - 0.72E_{(B-V)}, \tag{1}$$

where

$$\frac{E_{(U-B)}}{E_{(B-V)}} = 0.72 \tag{2}$$

is the slope of the reddening path. This value has been taken from Johnson and Morgan (1953). For stars of Table 2 the procedure was as follows: The color indices, CI, of Binnendijk's catalogue were compared with stars of known $(B-V)$ and MK type; this permitted the determination of computed values of $(B-V)$, which have been labeled $(B-V)_c$. When corrected for local values of $E_{(B-V)}$, the quantity $(B-V)_0$ was determined for stars having no directly observed (U, B, V) photometry. The intrinsic color of the A9 stars is poorly determined. In Table 2 the value of +0.31 mag. is used for class A9.

Figure 1 is a plot of $(U-B)_0$ of the Pleiades (*upper part*) and the near-by stars (*lower part*). In the upper part, filled circles refer to stars of Table 1 and open circles those of Table 2; for the latter the ordinates are arbitrary. For the near-by stars the observed

colors are taken to be equal to the intrinsic colors. Some values provided by Dr. Harris in advance of publication were included. These values differ very slightly from those used to define the color index listed in Table 3. The diagram indicates that there is no gap between +0.20 and +0.30 mag. in the $(B-V)_0$ color index for the Pleiades.

The stars with $(B-V)_0$ greater than +0.4 mag. and smaller than +0.6 mag. show a remarkable difference when compared with the near-by stars; the Pleiades members have, on the average, fainter $(U-B)_0$ than the near-by stars. In the former the stars tend to be below the line $(U-B)_0 = 0.00$ mag.; in the latter they are, in general, above this

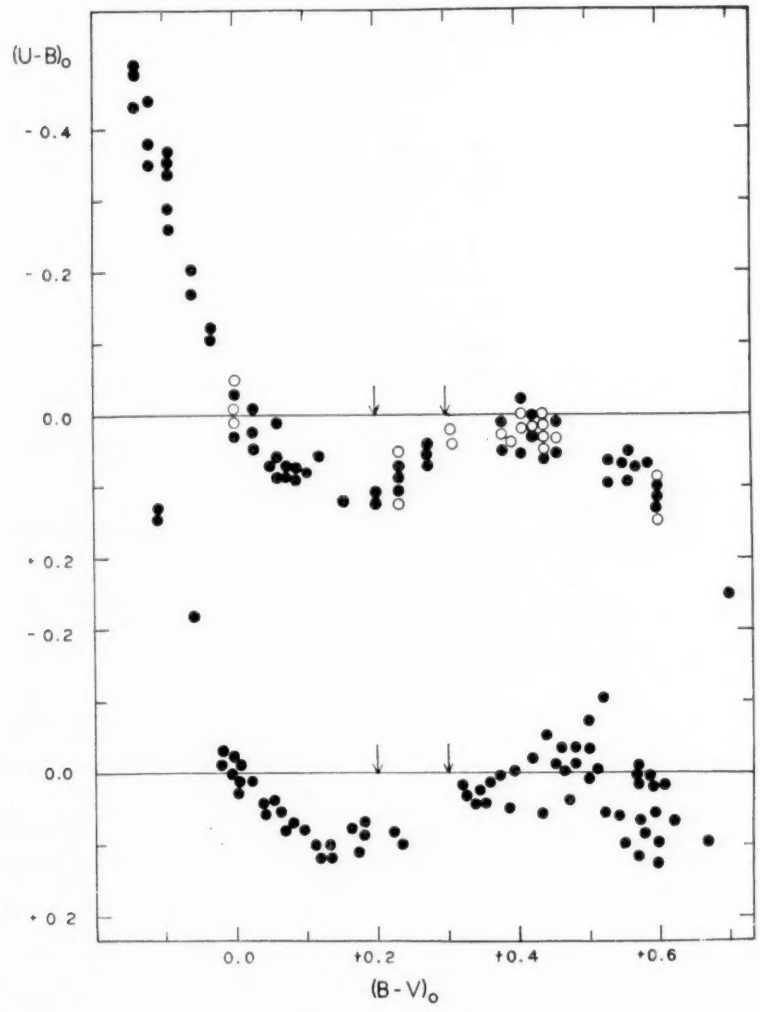

FIG. 1.—Two-color diagram of the Pleiades (*upper*) and the near-by stars (*lower*). For the Pleiades, filled circles refer to stars of Table 1 and open circles to those of Table 2.

line. The Pleiades, on the average, are fainter in the ultraviolet than the near-by stars in the range from F5 to G0.

The results for the Pleiades thus are opposite to the ultraviolet excess found by Johnson and Sandage for certain globular clusters (1955). It appears that the stars in the solar neighborhood are intermediate in this characteristic between the globular clusters, on the one hand, and the Pleiades, on the other. An opposite effect has been found for

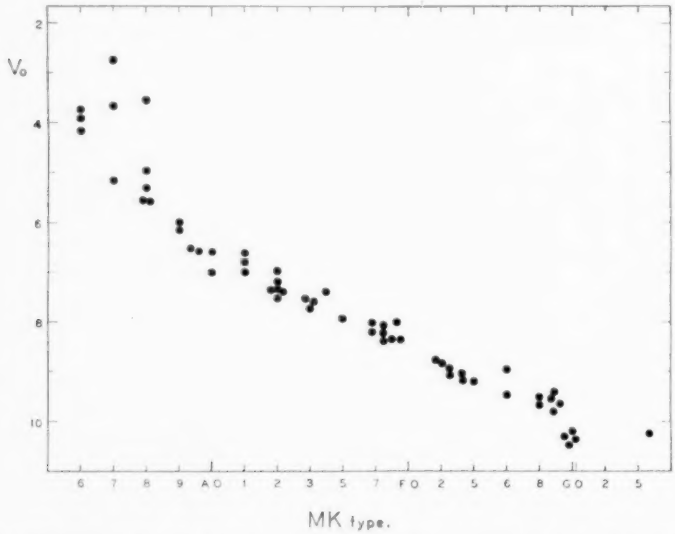

FIG. 2.—Hertzsprung-Russell diagram for the Pleiades. The quantity V_0 is the V magnitude corrected for interstellar absorption.

NGC 752 by Johnson (1953). The latter cluster is probably one of the oldest galactic clusters known. The star Hz 146, a possible metallic-line star, has an intrinsic color which lies in the gap shown by the near-by stars. The H-R diagram is shown in Figure 2. The V magnitudes have been corrected to V_0 by use of a factor of $3.0E_{(B-V)}$.

We wish to make acknowledgment to the following: to Professor B. Strömgren for permission to read his paper in manuscript; to Professor W. W. Morgan, who proposed to me this problem, for suggestions; and to Dr. D. L. Harris III for his unpublished data and friendly criticism.

REFERENCES

Binnendijk, L. 1946, *Leiden Ann.*, Vol. **19**, Part II.
Hertzsprung, E. 1923, *Effective Wavelengths of Stars in the Pleiades* (Mém. Acad. r. Sci. Lettres de Danemark, Copenhague).
Hertzsprung, E., *et al.* 1947, *Leiden Ann.*, Vol. **19**, Part I.
Johnson, H. L. 1953, *Ap. J.*, **117**, 356.
Johnson, H. L., and Morgan, W. W. 1953, *Ap. J.*, **117**, 313.
Johnson, H. L., and Sandage, A. R. 1955, *Ap. J.*, **121**, 616.
Morgan, W. W., Harris, D. L., and Johnson, H. L. 1953, *Ap. J.*, **118**, 92.
Schwassmann, A. 1930, *Mitt. Hamburger Sternw.*, **6**, 129.
Strömgren, B. 1956, *The Hertzsprung-Russell Diagram* (in press).

THE GALACTIC CLUSTER NGC 2169

J. CUFFEY
Goethe Link Observatory, Indiana University

AND

S. W. MCCUSKEY
Warner and Swasey Observatory, Case School of Applied Science

Received May 18, 1955; revised July 8, 1955

ABSTRACT

Photoelectric colors, magnitudes, and objective-prism spectral types in NGC 2169 are presented in Table 1, Figure 2, and Figure 3. Bright-blue B stars and a few main-sequence A stars appear to characterize the cluster's total population. Absence of dust and of nebulosity lends additional interest to the cluster. Selective absorption is 0.17 mag., and general absorption of yellow light is 0.51 mag. The cluster's distance is estimated as 2000 pc.

NGC 2169 is a galactic cluster located in Orion at the co-ordinates $\alpha = 6^{h}03^{m}$, $\delta = +14°00'$; $l = 163°$, $b = -1°.4$ (1900). In physical structure and population it seems unusually interesting. The nucleus, 7′ in diameter, contains two distinct groups of bright stars, and a long streamer of similar stars extending 70′ in position angle N. 120 E. appears likely to be related to the cluster. Thus NGC 2169 differs from the nearly spherical groupings typical of most galactic clusters and appears to lack the numerous faint red stars typical of a well-populated main sequence. In these respects, NGC 2169 resembles objects described in recent literature by Ambarzumian, Blaauw, Morgan, and others as stellar associations.

Complete absence of interstellar dust and of gas clouds associated with the cluster is another interesting aspect. No nebulosity, either bright or dark, appears on blue or red exposures with the 24–36-inch Warner and Swasey Schmidt telescope or on plates taken with the 36-inch and 10-inch telescopes at the Link Observatory. In view of the statement by Baade (1950) describing spiral nebulae—"No dust, no population I, particularly no O and B stars"—the lack of nebulosity makes objects like NGC 2169 strategic ones for study, for here we have associations of B stars with no evident trace of associated dust or gas clouds. It is interesting to speculate that if the B stars have been formed out of gas and dust relatively recently, as some astronomers believe, then, in NGC 2169, the gas and dust must have been used up efficiently in star formation, with almost none left over for the interstellar medium.

The photoelectric colors and magnitudes in Table 1 were determined with the 36-inch reflector of the Goethe Link Observatory. A discussion of the photoelectric equipment used would be too lengthy for inclusion here because of numerous changes during the interval. The most recent observations, made with a dry-ice-refrigerated 1P21 photomultiplier, an M.I.T. amplifier circuit, and comparison of each star observation with a radium-paint source of proved stability, were given greatest weight. Each series of observations made with a given instrumental arrangement included measures of polar-sequence stars for calibration, and they were used to reduce the outside-atmosphere magnitudes and colors to the International System as represented by the photoelectric P and $P - V$ system of Stebbins, Whitford, and Johnson (1950). Although ten polar-sequence stars were originally used in relating our $B - V$ colors to the $P - V$ system, stars 6, 10, 2R, and 4R eventually received the greatest weight because they were most often observed during the process of checking instrumental changes.

Since the filters used throughout (see *Ap. J.*, **115**, 18, 1952) do not transmit appre-

ciable ultraviolet light, the color system of the present paper may be expected to be linearly related to other color systems. Thus observations of seventeen stars selected from the list by Johnson and Morgan (1953) obtained by R. L. Sears and others show that our natural color system, $(B-V)_{\text{Link}}$, is related to the $(B-V)_{\text{JM}}$ system of Johnson and Morgan by

$$(B-V)_{\text{JM}} = 1.046\,(B-V)_{\text{Link}} + 0.661$$

with remarkably good linearity throughout the color interval -0.20 to $+1.38$. The colors in Table 1, designated $(P-V)_{\text{Link}}$, were found to be related to the $(B-V)_{\text{JM}}$ system by

$$(P-V)_{\text{Link}} = 1.068\,(B-V)_{\text{JM}} - 0.104.$$

The cluster was observed on twelve nights between November 9, 1949, and November 15, 1953. For the first six nights, the polar-sequence stars mentioned were used in

TABLE 1

NGC 2169

No.	V	No. Meas.	$P-V$	No. Meas.	Sp.	No.	V	No. Meas.	$P-V$	No. Meas.	Sp.
1	6.902	5	−0.259	3	B3	13	11.150	3	−0.014	2	B5
2	8.098	13	−0.159	11	B5	14	9.326	3	+1.792	2	.....
3	8.58	2	−0.239	2	B3	15	11.740	3	+0.013	2	.....
4	8.749	11	−0.216	8	B3	A	11.08	1	+0.19	1	B9
5	9.11	2	−0.127	2	B3	B	9.37	2	+0.106	2	A2
6	8.438	8	+0.848	7	G2	C	9.995	6	−0.130	7	B3
7	10.56	2	−0.098	2	.....	D	8.84	2	−0.160	2	B3
8	10.74	2	−0.108	2	.....	E	8.97	1	+0.18	1	A0
9	10.73	2	−0.092	2	B5	F	10.08	1	−0.11	1	B8
10	10.866	3	+0.001	3	.....	G	7.68	1	−0.11	1	B8
11	9.93	2	+1.115	2	G8 III	H	8.72	1	−0.13	1	B9
12	11.06	2	+0.032	2	B8						

calibration. For the remaining nights the C-region stars C2 E, F, G, H, and C3 F, with the values of P and $P-V$ by A. N. Cox (1953), were used. A single measure, as given in Table 1, is usually based upon six yellow deflections (V), and upon six yellow and six blue deflections ($P-V$). Extinction and its dependence on color were satisfactorily determined on some of the nights, and all magnitudes and colors were referred to outside the earth's atmosphere. Linear relations were used to reduce the measures to the P and $P-V$ systems. Probable errors of the tabulated values are given in Table 2.

The spectra were observed on 4° objective-prism plates taken with the 24-36-inch Schmidt telescope of the Warner and Swasey Observatory. The dispersion was 283 A/mm. Two orientations of the prism were used to separate the spectra adequately. Observational results are summarized in Table 1. The numbering system refers to the chart in Figure 1.

The color-spectrum relation, Figure 2, is nearly linear, with little scatter. At *A0* the color index is +0.05. The cluster's color excess is then evident if the intrinsic colors of A0 stars on the P, V system are available. Recent work indicates that A0 stars have colors in the neighborhood of −0.12. This is probably a reliable value and results from the comparison by Eggen (1955) of the $P-V$ system with the $B-V$ system. The shift in zero point of the $B-V$ color system amounts essentially to a specification of the colors of six relatively near-by A0 V stars, among them Vega, and represents a close approach to the true colors of A0 stars. The color excess of NGC 2169, then, is 0.17, and the

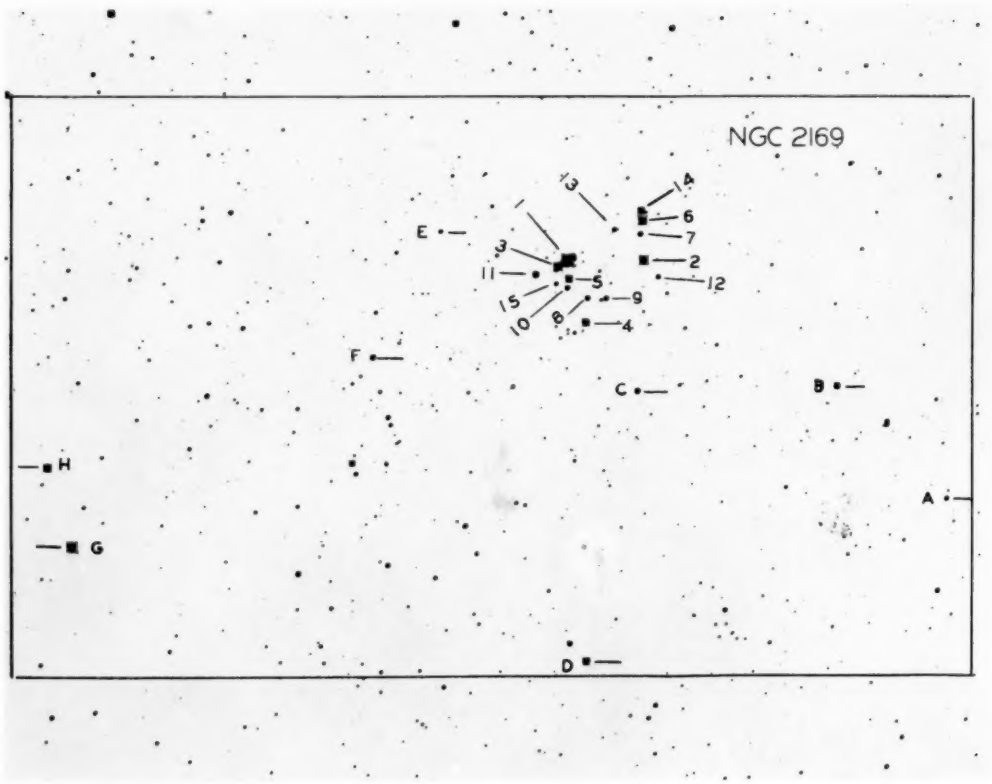

FIG. 1.—Star chart, NGC 2169

visual absorption 0.51. Other authors have suggested that A0 stars may have colors closer to −0.18, on the basis of various intercalibrations of the $P - V$, $B - V$, and C_1 color systems. If this value is used, the color excess of NGC 2169 becomes 0.23 mag., and the absorption 0.69 mag. However, the present authors regard the first set of data given here as probably most nearly correct.

The absorption in the direction NGC 2169 appears somewhat low, although some of the field stars show higher color excesses, such as those of A (0.34 mag.) and E (0.30 mag.). Areas of higher absorption undoubtedly exist in the region of the cluster when a large area of sky is considered and may explain the difference between the absorption found in the direction of NGC 2169 and that found by other workers in near-by fields. McCuskey (1949), in analyzing LF 8 ($\alpha = 6^h14^m$, $\delta = +14°$), which covers an area of 17.3 square degrees, found absorption starting at 500 pc and reaching 2.8 mag. (photographic) at 2500 pc. Bok, Boutelle, and Olmstead (1948) described the absorption as variable and the region between longitudes 160 and 175 as perhaps the least obscured of the anticenter region. They estimated the absorption to be 1.2 mag/kpc (photographic) in a field at $l = 165°$, $b = 0°$. Evidently the absorption is of a spotty nature over a region more widespread than that covered by the cluster data.

The color-magnitude relation, Figure 3, displays a nearly vertical giant branch, nar-

TABLE 2

PROBABLE ERRORS OF VALUES TABULATED IN TABLE 1

Nos.	INTERNAL (SCALE)		EXTERNAL (ZERO POINT)	
	V	$P-V$	V	$P-V$
2, 4	±0.006	±0.004	±0.014	±0.014
1, 6, C	.007	.004	.015	.014
A, E, F, G, H	.018	.011	.037	.033
All others	±0.013	±0.008	±0.026	±0.024

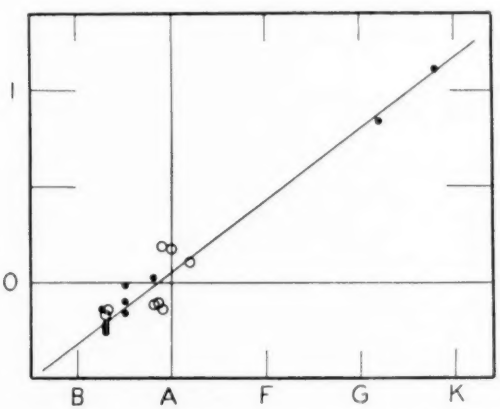

FIG. 2.—Color-spectrum relation for NGC 2169. Dots represent stars in the cluster's apparent nucleus; circles, stars outside the nucleus.

row and well defined, with a few stragglers and a slight tendency for the faintest stars to be redder. The color-magnitude diagram, in this case, is obviously poorly suited to distance determination. We have therefore turned to the individual spectral types, although in only one case, No. 11 (G8 III), was a luminosity class obtainable from the spectra. Because this star deviates from the cluster's color-magnitude relation, it may not be a cluster member and does not help in distance determination. When the absolute magnitudes of stars of given spectral types and luminosity classes given by Keenan and

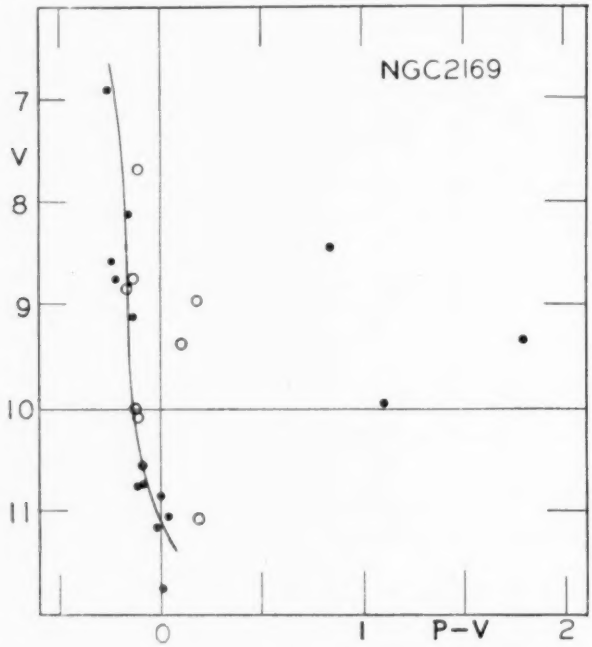

FIG. 3.—Color-magnitude relation for NGC 2169. Dots represent stars in the cluster's apparent nucleus; circles, stars outside the nucleus.

Morgan (1951) are considered, it is evident that the cluster stars represent a wide range in luminosity classes. If, for example, the cluster stars are assumed to be main-sequence stars of luminosity class V, the distance moduli derived show a strong dependence upon the apparent magnitude, in the sense that the brighter stars give systematically smaller distances. Trumpler's conclusion that the brightest stars in many clusters are unusually luminous for their spectral types is thus well confirmed. The color-magnitude relation indicates that the faintest cluster stars observed are likely to be main-sequence stars of class V, and we have selected Nos. 9, 12, and 13 as the best cases. The resulting distance modulus, corrected for absorption, is 11.50 mag., and the corresponding distance is 2000 pc.

Luminosity classes estimated for the cluster stars show that they range continuously from main-sequence A stars to a bright B giant of luminosity class II. No supergiants of classes *Ia* or *Ib* are present.

REFERENCES

Baade, W. 1950, *Pub. Obs. U. Michigan*, **10,** 10.
Bok, B. J., Boutelle, B. D., and Olmstead, M. 1948, *A.J.*, **53,** 197.
Cox, A. N. 1953, *Ap. J.*, **117,** 83.
Eggen, O. J. 1955, *A.J.*, **60,** 86.
Johnson, H. L., and Morgan, W. W. 1953, *Ap. J.*, **117,** 313.
Keenan, P. C., and Morgan, W. W. 1951, *Astrophysics*, ed. J. Hynek (New York: McGraw-Hill Book Co., Inc.), p. 23.
McCuskey, S. W. 1949, *Ap. J.*, **109,** 143.
Stebbins, J., Whitford, A. E., and Johnson, H. L. 1950, *Ap. J.*, **112,** 469.

SOME REMARKS ON THE (U, B, V) SYSTEM

VICTOR M. BLANCO*

Warner and Swasey Observatory, Case Institute of Technology

Received August 10, 1955

ABSTRACT

The variations of the total and selective absorptions with respect to spectral intensity distribution and total absorption are determined for the (U, B, V) photometric system.

A knowledge of the ratio of total to selective absorption is required in the determination of stellar distances by two-color photometric methods. Likewise, in three-color photometric studies the ratio between two different color excesses is often used. When wide-band photometry is used, these quantities are simultaneously affected by the spectral intensity distribution of the observed star and by the total amount of absorption. The present remarks deal with the nature of the variations expected in such cases.

Computations have been carried out to determine how the ratio of total to selective absorption in the Johnson-Morgan (1953) B, V system varies for different spectral classes and total absorptions. In a similar manner, the expected variations in the ratio between the $U-B$ and $B-V$ color excesses have been studied. The calculations are based on the filter transmissions published by these authors (1951), the interstellar absorption-curve as observed by Whitford (1948), and spectral intensity distributions as explained later. The "effective" wave lengths in the interstellar absorption-curve have been modified in the manner suggested by Schalén (1951), Van Rhijn (1953), and Borgman (1954). The principal uncertainty in the corrected curve is the zero point or Δm-value at $1/\lambda = 0$, which, as explained later, is probably 0.15 mag. lower than indicated by Whitford. In the computations of the ratio of total to selective absorption, several values for the zero point were assumed.

Letting $\phi(\lambda)$ be the transmission function of a given filter-cell combination, $I(\lambda)$ the star's spectral intensity distribution, and $\tau(\lambda)$ the transmission function of a unit amount of interstellar material, the total absorption observed with a given filter after correction for atmospheric extinction is given by

$$\Delta m = -2.5 \log \frac{\int_0^\infty \tau(\lambda)\,\phi(\lambda)\,I(\lambda)\,d\lambda}{\int_0^\infty \phi(\lambda)\,I(\lambda)\,d\lambda}. \tag{1}$$

The ratio R of visual absorption to $B-V$ color excess follows from

$$R = \frac{\Delta m_V}{\Delta m_B - \Delta m_V}, \tag{2}$$

while the ratio of color excesses in the (U, B, V) system follows from

$$\frac{E_{U-B}}{E_{B-V}} = \frac{\Delta m_U - \Delta m_B}{\Delta m_B - \Delta m_V}. \tag{3}$$

In the calculations the interstellar absorption-curve, with the Δm-values as given by Whitford, was assumed to hold for a unit amount of interstellar matter. For other

* John Simon Guggenheim Foundation fellow, 1954–1955.

amounts, say x units, one must raise $\tau(\lambda)$ to the x power in equation (1). The integrations were performed numerically. Among the various zero points tried in the calculations, the one was chosen (i.e., 0.15 mag. below that indicated by Whitford) which gave a ratio R of 3.0 for unreddened early-type stars. This is in agreement with the value proposed by Morgan, Harris, and Johnson (1953) and is also approximately predicted by van de Hulst's (1949) theoretical absorption laws if the observed curve is modified in the manner explained previously. This zero point, furthermore, is compatible with the mean value of total to selective absorption in the International System, derived in such a way as to be independent of Whitford's interstellar absorption-curve.

The ratio of total to selective absorption was determined for the following objects: (1) black bodies with temperatures of 25000°, 14300°, 8000°, and 3000°; (2) the star Vega, using the absolute intensity distribution determined by Kienle, Wempe, and Beileke (1940), with an extrapolation in the ultraviolet based on observations by J. Stock at this observatory; (3) the star β Peg (M2 III) from locally obtained spectrophotoelectric comparisons with the star α And and the absolute intensity distribution observed for α And by Kienle, Wempe, and Beileke. The results are summarized in Table 1, where the second column gives for each object the value Δm_v found from equation (1) for the yellow filter and either one or eight units of interstellar material.

TABLE 1

Object	Total Visual Absorption	R	Object	Total Visual Absorption	R	Object	Total Visual Absorption	R
25000°	1.02	3.00	Vega	7.86	3.28	3000°	0.97	3.44
25000	8.01	3.24	8000°	1.00	3.17	β Peg	0.99	4.01
Vega	1.01	3.07	8000	7.79	3.38	β Peg	7.69	4.12

The results for the 14300° black body were the same as for Vega and hence are excluded from Table 1. Since the ratio R varied linearly with the total absorption, only two values of the total absorption are presented. The results for the 3000° black body are of academic interest, since for a star of this temperature the TiO and metallic absorptions influence the ratio R appreciably. From the foregoing results, the following empirical formula may be obtained (it holds for stars of class of about G5 and earlier):

$$A_V = [3.1 + 0.3\,(B-V)_{\text{Int}}]\,\frac{E_{B-V}}{1 - 0.03\,A_V}. \tag{4}$$

The differences obtained by using this relation instead of a simple ratio of 3.0 are small except for heavily reddened early-type stars and for late-type stars. It should be pointed out that if the value of 3.1 in equation (4) were later found to be in error because of a different zero point in the interstellar absorption law, this would not seriously affect the values of the other constants. The effect on equation (4) caused by the use of the effective wave lengths previously indicated is to increase the coefficient of A_V by 0.013.

For computing the ratio E_{U-B}/E_{B-V}, the ultraviolet points of the interstellar absorption-curve must be used. A correction to these points has been found necessary by Divan (1954), because of differences between the Balmer discontinuities of ζ and ϵ Persei. This effect has also been found by J. Stock (1956). The ratio between selective absorptions has been computed both on the basis of Whitford's and Divan's results, for the star Vega, and for a 25000° black body. The results are plotted in Figure 1. The calculations show that E_{U-B}/E_{B-V} varies almost linearly with the total absorption and that the slopes of

the lines do not vary appreciably with the different ultraviolet transmissions and intensity distributions considered here. These results may be compared with the observations of Morgan, Harris, and Johnson (1953), who have plotted a "reddening path" for OB stars in a graph of $U-B$ versus $B-V$. Strictly speaking, the "reddening path" given by them is the locus of the end-points of the actual reddening paths, which have slightly different slopes, depending on the total absorption. The following relation was found to yield values of E_{U-V}/E_{B-V} which will represent their observations:

$$\frac{E_{U-B}}{E_{B-V}} = 0.76 + 0.03\,A_V\,. \tag{5}$$

The constant 0.76 in this equation is quite sensitive to the ultraviolet transmission properties of the interstellar material, but the constant 0.03 is not. The foregoing considera-

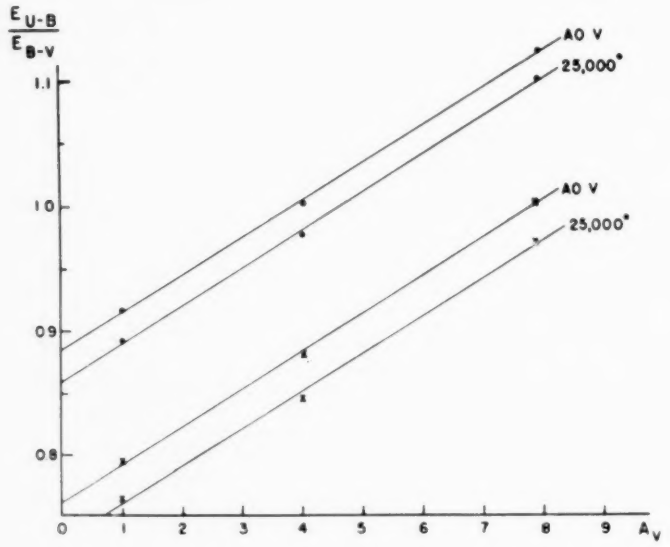

FIG. 1.—The dots refer to computations based on Divan's interstellar absorption-curve; the crosses, to Whitford's.

tions should be taken into account when deriving distance moduli of faint, reddened, early-type stars by wide-band, three-color methods.

As an illustration of the possible applications of these results, a recalibration has been made of the relationship between the quantity Q defined by Johnson and Morgan (1953) and the spectral type. Q is found to vary linearly with spectral type from -0.95 for class O5 to -0.90 for class B0. For class B0 0.5 the quantity changes to -0.83, and then varies linearly with spectral class to class A0, where, by definition, its value is zero.

As a further illustration, the total absorptions have been computed for the stars in the heavily obscured O-association in Cygnus studied by Johnson and Morgan (1954). The corrected distance modulus is found to be 10.6 instead of 10.9. The Q-values for the stars in this association average -1.05, low when compared to the normal Q-values quoted earlier. This difference may be an indication of a departure from the average absorption

law in the direction of this association. It is estimated that if the "S" point in Whitford's observations of the interstellar absorption-curve is diminished by 0.15 mag., it will be sufficient to produce the observed excess in Q.

Another application of these results is in the derivation of intrinsic color indices for reddened M-type supergiants. If, for the red supergiants associated with h and χ Persei, one estimates the total visual absorption from near-by blue members of the clusters and uses the ratio of total to selective absorption found for the M stars β Peg taken from Table 1, the intrinsic $B-V$ colors are found to be 1.85 for the type M2 I*ab*. The observations on which this result is based are described elsewhere (Blanco 1955).

REFERENCES

Blanco, V. M. 1955, *Ap. J.*, **123**, 434.
Borgman, J. 1954, *B.A.N.*, No. 457.
Divan, L. 1954, *Ann. d'ap.*, **17**, 456.
Hulst, H. van de. 1949, *Recherches astr. Obs. Utrecht*, Vol. **11**, Part 2.
Johnson, H. L., and Morgan, W. W. 1951, *Ap. J.*, **114**, 523.
———. 1953, *ibid.*, **117**, 313.
———. 1954, *ibid.*, **119**, 344.
Kienle, H., Wempe, J., and Beileke, F. 1940, *Zs. f. Ap.*, **20**, 91.
Morgan, W. W., Harris, D. L., and Johnson, H. L. 1953, *Ap. J.*, **118**, 98.
Rhijn, P. van. 1953, *B.A.N.*, **441**.
Schalén, C. 1951, *Uppsala Ann.*, **3**, 54.
Stock, J. 1956, *Ap. J.*, **123** (in press).
Whitford, A. E. 1948, *Ap. J.*, **107**, 102.

A PHOTOMETRIC INVESTIGATION OF THE SHORT-PERIOD ECLIPSING BINARY, NOVA DQ HERCULIS (1934)

MERLE F. WALKER*

Mount Wilson and Palomar Observatories
Carnegie Institution of Washington, California Institute of Technology

Received August 8, 1955

ABSTRACT

Nova DQ Her (1934) has been found to be an eclipsing binary having the shortest known period, 4^h39^m. During 1954, 1530 photoelectric observations of the system in three colors were obtained with the 100-inch Mount Wilson reflector. They indicate that, like UX UMa, the light-curve is of the Algol type, primary eclipse is partial, and no secondary eclipse is visible. Unlike UX UMa, the depth of primary decreases with decreasing wave length. Other similarities to UX UMa include a minimum in the light-curve at $0.7P$, occasional shoulders before and after eclipse, asymmetry of the rising branch of the eclipse-curve, and irregular intrinsic variations. A unique feature of the light-curve of DQ Her is the occurrence between phases $0.110P$ and $0.325P$ of rapid variations in light having a period of 1.180 minutes and a range of 0.07 mag. in the ultraviolet.

Provisional photometric elements have been derived for the system. The radii of the stars are about $0.10\ R_\odot$, while their masses are abnormally low, about $6 \times 10^{-3}\ m_\odot$. It is possible that the low mass of the secondary star results from various observational errors and that the star is actually a normal M-type dwarf. However, unless the system is so abnormal that the photometric elements have no meaning, the mass of the nova component must be very much less than the usually assumed value of $1.5\ m_\odot$. The resemblances between the light-curves of DQ Her and UX UMa suggest that the peculiarities of both systems may be explained by a similar model.

During the course of a program of photoelectric observations of old novae, the writer found that Nova DQ Her (1934) is an eclipsing binary with the shortest known period, 4^h39^m. A preliminary discussion of this system has appeared elsewhere (Walker 1954); the present paper gives a detailed analysis of the observations of the star secured during 1954.

Photometric observations of DQ Her were secured on six nights with a photoelectric photometer attached to the 100-inch Mount Wilson reflector. The photometer, filters, and technique of observation have been described previously (Walker and Herbig 1954). On the first night, July 9, the star was monitored for about 15 minutes in ultraviolet light in connection with the program of detecting short-period light-variations in old novae. These first observations indicated that DQ Her was rapidly variable in what appeared to be a nearly periodic manner, the average period of the fluctuations being about 1 minute. This was a rather surprising result, since the rapid light-variations found in other old novae all appear to be random. Consequently, DQ Her was reobserved on July 31 in order to confirm both the reality and the periodic nature of its light-variations; during the course of these observations the binary nature of the star was discovered. As on July 9, the star was monitored continuously in ultraviolet light; on all subsequent nights, yellow, blue, and ultraviolet light-curves were obtained. On July 31, owing to the fact that the star was monitored continuously, adequate comparison-star readings were not obtained. Comparison-star measuremnets are also lacking on August 1, since only a short run was obtained before the sky clouded over. On both these nights, the observations were reduced to no atmosphere by using average extinction coefficients and the readings of the standard radium source to correct for the drift in the sensitivity of the apparatus; an arbitrary zero point of the resulting magnitudes was adopted.

On the three remaining nights, DQ Her was referred to near-by comparison stars,

* Carnegie fellow, 1952–1954.

TABLE I

YELLOW OBSERVATIONS

Heliac JD 2434000+	Heliac Phase	Δ Mag.	Heliac JD 2434000+	Heliac Phase	Δ Mag.	Heliac JD 2434000+	Heliac Phase	Δ Mag.
955.6669	0.3330	-0.044	983.7078	0.5524	+3.716	984.6652	0.4970	+3.601
.6898	.8460	+0.028	.7092	.5596	+3.722	.6653	.4976	+3.646
.6913	.8557	+0.000	.7103	.5653	+3.705	.6655	.4986	+3.649
.6921	.8598	-0.013	.7117	.5725	+3.757	.6657	.4996	+3.629
.6944	.8717	-0.021	.7193	.6118	+3.760	.6669	.5058	+3.651
.6947	.8733	+0.014	.7230	.6309	+3.771	.6734	.5394	+3.651
.6957	.8784	+0.031	.7342	.6887	+3.764	.6746	.5456	+3.725
.6967	.8836	+0.024	.7358	.6970	+3.724	.6751	.5482	+3.672
.6976	.8882	-0.031	.7373	.7047	+3.743	.6793	.5699	+3.723
.6988	.8944	-0.003	.7416	.7269	+3.764	.6809	.5781	+3.704
.6997	.8991	+0.022	.7431	.7347	+3.741	.6831	.5895	+3.719
.7005	.9037	+0.092	.7516	.7786	+3.667	.6848	.5983	+3.745
.7015	.9084	+0.045	.7532	.7868	+3.676	.6900	.6251	+3.756
.7017	.9094	+0.104	.7573	.8080	+3.654	.6966	.6592	+3.764
.7044	.9234	+0.113	.7592	.8178	+3.633	.6987	.6701	+3.757
.7056	.9296	+0.186	.7607	.8256	+3.645	.7036	.6954	+3.817
.7065	.9342	+0.286	.7618	.8313	+3.661	.7109	.7331	+3.750
.7074	.9389	+0.384	.7628	.8364	+3.624	.7126	.7418	+3.770
.7085	.9445	+0.422	.7641	.8431	+3.647	.7145	.7517	+3.749
.7093	.9487	+0.567	.7684	.8653	+3.666	.7161	.7599	+3.769
.7106	.9554	+0.690	.7703	.8752	+3.644	.7164	.7615	+3.800
.7118	.9616	+0.746	.7731	.8896	+3.657	.7192	.7759	+3.815
.7128	.9667	+0.874	.7745	.8968	+3.654	.7249	.8054	+3.665
.7138	.9719	+0.976	.7793	.9216	+3.763	.7262	.8121	+3.678
.7149	.9776	+1.066	.7802	.9263	+3.803	.7275	.8188	+3.662
.7159	.9828	+1.177	.7806	.9284	+3.863	.7280	.8214	+3.746
.7169	.9879	+1.257	.7819	.9351	+3.917	.7294	.8286	+3.691
.7181	.9941	+1.327	.7821	.9361	+3.983	.7354	.8596	+3.671
.7190	.9988	+1.359	.7831	.9413	+4.071	.7371	.8684	+3.694
.7203	.0055	+1.309	.7842	.9469	+4.161	.7390	.8782	+3.649
.7217	.0127	+1.149	.7853	.9526	+4.295	.7407	.8870	+3.708
.7248	.0287	+0.958	.7867	.9599	+4.440	.7423	.8952	+3.710
.7262	.0360	+0.821	.7878	.9655	+4.625	.7430	.8989	+3.720
.7275	.0427	+0.661	.7908	.9810	+4.833	.7445	.9066	+3.770
.7287	.0489	+0.534	.7919	.9867	+4.958	.7475	.9221	+3.829
.7299	.0551	+0.491	.7933	.9939	+5.097	.7493	.9314	+3.963
.7310	.0607	+0.415	.7946	.0007	+5.007	.7505	.9376	+4.047
.7322	.0669	+0.329	.7959	.0074	+5.011	.7520	.9453	+4.158
.7333	.0726	+0.263	.7973	.0146	+4.891	.7534	.9526	+4.247
.7344	.0783	+0.186	.7995	.0260	+4.763	.7550	.9608	+4.471
.7359	.0860	+0.167	.8006	.0316	+4.683	.7564	.9681	+4.561
.7371	.0922	+0.054	.8018	.0378	+4.483	.7584	.9784	+4.640
.7383	.0984	+0.063	.8037	.0477	+4.284	.7595	.9841	+4.794
.7395	.1046	+0.003	.8049	.0539	+4.182	.7607	.9903	+4.879
.7408	.1114	+0.025	.8063	.0611	+4.098	.7618	.9960	+4.944
.7420	.1176	-0.076	.8078	.0688	+3.999	.7630	.0021	+4.913
.7424	.1196	+0.024	.8090	.0750	+3.905	.7644	.0094	+4.902
.7432	.1238	+0.014	.8110	.0859	+3.838	.7658	.0166	+4.831
.7470	.1434	-0.025	.8126	.0936	+3.743	.7673	.0244	+4.760
.7482	.1496	+0.042	.8131	.0962	+3.676	.7687	.0316	+4.661
.7497	.1573	+0.007	.8147	.1045	+3.640	.7690	.0331	+4.586
.7509	.1635	+0.016	.8159	.1107	+3.626	.7743	.0605	+4.194
.7522	.1702	-0.009	.8184	.1236	+3.606	.7756	.0672	+4.067
.7531	.1749	+0.026	.8190	.1267	+3.541	.7766	.0724	+3.974
.7541	.1800	+0.035	.8202	.1329	+3.597	.7781	.0801	+3.936
.7553	.1862	-0.001	.8205	.1344	+3.529	.7793	.0863	+3.899
.7569	.1945	-0.012	.8221	.1427	+3.519	.7804	.0920	+3.771
.7582	.2012	-0.012	.8238	.1515	+3.520	.7807	.0936	+3.814
.7591	.2059	-0.002	.8266	.1659	+3.634	.7818	.0992	+3.745
.7598	.2095	+0.018	.8269	.1675	+3.540	.7821	.1008	+3.786
.7607	.2141	+0.008	.8287	.1768	+3.576	.7834	.1075	+3.722
.7617	.2193	+0.000	.8308	.1876	+3.582	.7848	.1147	+3.734
.7628	.2250	+0.006	.8328	.1980	+3.574	.7864	.1230	+3.736
.7664	.2436	-0.019	.8440	.2558	+3.658	.7902	.1426	+3.622
.7679	.2513	+0.011	.8462	.2672	+3.654	.7905	.1442	+3.707
.7690	.2570	+0.001	.8568	.3219	+3.580	.7918	.1509	+3.662
.7726	.2756	-0.022	.8571	.3235	+3.656	.7932	.1581	+3.684
.7759	.2926	-0.029	.8589	.3327	+3.596	.7946	.1654	+3.765
983.6783	.4000	+3.541	.8604	.3405	+3.584	.7959	.1721	+3.714
.6787	.4021	+3.521	.8676	.3777	+3.550	.7973	.1793	+3.735
.6790	.4036	+3.536	.8693	.3865	+3.582	.7989	.1876	+3.737
.6794	.4057	+3.597	.8710	.3952	+3.565	.8005	.1958	+3.743
.6797	.4072	+3.562	.8724	.4025	+3.550	.8009	.1979	+3.666
.6810	.4139	+3.610	.8731	.4061	+3.584	.8041	.2144	+3.729
.6863	.4413	+3.600	.8801	.4422	+3.614	.8057	.2227	+3.708
.6885	.4527	+3.582	.8821	.4526	+3.630	.8146	.2686	+3.679
.6905	.4630	+3.592	.8846	.4655	+3.592	.8163	.2774	+3.686
.7015	.5198	+3.684	984.6648	.4950	+3.569	.8265	.3301	+3.712
.7031	.5281	+3.670	.6650	0.4960	+3.534	.8280	0.3379	+3.673
.7061	0.5436	+3.683						

TABLE 1

YELLOW OBSERVATIONS

Heliac JD 2434000+	Heliac Phase	Δ Mag.
984.8300	0.3482	+3.691
.8318	.3575	+3.691
.8334	.3657	+3.646
.8386	.3926	+3.617
.8405	.4024	+3.606
.8425	.4127	+3.664
.8441	.4210	+3.661
.8457	.4293	+3.680
.8471	.4365	+3.649
.8516	.4597	+3.681
.8536	.4701	+3.686
.8552	.4783	+3.699
.8624	.5155	+3.699
.8643	.5253	+3.749
.8662	.5351	+3.762
.8721	.5656	+3.780
.8748	.5796	+3.810
.8810	.6116	+3.827
985.6737	.7056	+3.820
.6757	.7160	+3.812
.6806	.7413	+3.774
.6826	.7516	+3.754
.6875	.7769	+3.769
.6956	.8187	+3.716
.6970	.8260	+3.694
.6974	.8280	+3.655
.6992	.8373	+3.638
.7060	.8725	+3.640
.7072	.8787	+3.593
.7084	.8849	+3.616
.7096	.8910	+3.635
.7106	.8962	+3.686
.7118	.9024	+3.705
.7133	.9102	+3.714
.7147	.9174	+3.782
.7186	.9375	+3.893
.7200	.9448	+4.005
.7211	.9504	+4.079
.7225	.9577	+4.213
.7238	.9644	+4.345
.7250	.9706	+4.574
.7262	.9768	+4.675
.7278	.9850	+4.928
.7293	.9928	+5.022
.7305	.9990	+5.121
.7318	.0057	+4.974
.7331	.0124	+4.884
.7348	.0212	+4.748
.7375	.0351	+4.518
.7390	.0429	+4.334
.7404	.0501	+4.258
.7421	.0589	+4.146
.7437	.0672	+3.961
.7452	.0749	+3.847
.7466	.0821	+3.860
.7480	.0894	+3.797
.7484	.0914	+3.746
.7500	.0997	+3.659
.7516	.1080	+3.693
.7527	.1136	+3.682
.7540	.1204	+3.731
.7552	.1266	+3.660
.7565	.1333	+3.641
.7577	.1395	+3.658
.7609	.1560	+3.602
.7626	.1648	+3.602
.7732	.2195	+3.574
.7745	.2262	+3.622
.7759	.2335	+3.727
.7773	.2407	+3.684
.7787	.2479	+3.734
.7803	.2562	+3.722
.7842	.2763	+3.650
.7856	.2836	+3.610
.7869	.2903	+3.623
.7891	.3016	+3.629
.7956	.3352	+3.673
.7973	.3440	+3.658
.7987	.3512	+3.640
.8002	.3745	+3.615
.8043	0.3801	+3.578

TABLE 2

BLUE OBSERVATIONS

Heliac JD 2434000+	Heliac Phase	Δ Mag.	Heliac JD 2434000+	Heliac Phase	Δ Mag.
955.6873	0.8350	-0.019	983.7068	0.5472	+3.201
.6876	.8366	-0.059	.7084	.5555	+3.209
.6901	.8495	-0.055	.7096	.5617	+3.191
.6916	.8573	-0.050	.7107	.5673	+3.221
.6922	.8604	-0.046	.7122	.5751	+3.249
.6925	.8619	-0.096	.7198	.6143	+3.207
.6950	.8748	-0.045	.7235	.6334	+3.207
.6960	.8800	-0.050	.7346	.6908	+3.248
.6969	.8846	-0.045	.7363	.6996	+3.212
.6978	.8893	-0.044	.7377	.7068	+3.213
.6991	.8960	-0.065	.7408	.7228	+3.219
.7001	.9012	-0.022	.7421	.7295	+3.229
.7009	.9053	-0.012	.7434	.7362	+3.214
.7019	.9104	+0.019	.7521	.7812	+3.099
.7047	.9249	+0.081	.7537	.7894	+3.119
.7058	.9306	+0.112	.7562	.8023	+3.119
.7067	.9352	+0.232	.7578	.8106	+3.068
.7077	.9404	+0.311	.7598	.8209	+3.031
.7087	.9456	+0.412	.7612	.8282	+3.076
.7096	.9502	+0.462	.7621	.8328	+3.041
.7101	.9528	+0.500	.7633	.8390	+3.049
.7111	.9580	+0.562	.7644	.8447	+3.049
.7120	.9626	+0.633	.7674	.8602	+3.086
.7131	.9683	+0.693	.7692	.8695	+3.046
.7141	.9735	+0.810	.7737	.8927	+3.019
.7151	.9786	+0.873	.7752	.9005	+3.052
.7163	.9848	+0.924	.7778	.9139	+3.107
.7173	.9900	+0.984	.7795	.9227	+3.186
.7183	.9952	+1.040	.7809	.9299	+3.195
.7194	.0008	+1.045	.7825	.9382	+3.324
.7210	.0091	+1.005	.7835	.9433	+3.445
.7220	.0153	+0.954	.7844	.9480	+3.547
.7242	.0256	+0.819	.7857	.9547	+3.612
.7250	.0298	+0.784	.7871	.9619	+3.789
.7267	.0385	+0.648	.7883	.9681	+3.880
.7279	.0447	+0.533	.7903	.9785	+3.976
.7291	.0509	+0.433	.7912	.9831	+4.026
.7301	.0561	+0.394	.7923	.9888	+4.086
.7314	.0628	+0.298	.7938	.9965	+4.158
.7326	.0690	+0.279	.7951	.0032	+4.147
.7336	.0742	+0.200	.7964	.0100	+4.210
.7349	.0809	+0.140	.7976	.0162	+4.049
.7363	.0881	+0.072	.7999	.0280	+3.951
.7374	.0938	+0.058	.8009	.0332	+3.915
.7376	.0948	+0.103	.8026	.0420	+3.743
.7386	.1000	+0.022	.8040	.0492	+3.600
.7399	.1067	+0.041	.8051	.0549	+3.526
.7410	.1124	+0.039	.8067	.0632	+3.418
.7413	.1139	-0.031	.8082	.0709	+3.279
.7426	.1207	-0.009	.8094	.0771	+3.304
.7435	.1253	+0.002	.8099	.0797	+3.276
.7462	.1392	-0.003	.8117	.0890	+3.182
.7474	.1454	+0.012	.8134	.0978	+3.099
.7483	.1501	+0.044	.8151	.1065	+3.066
.7486	.1516	-0.005	.8164	.1132	+3.026
.7501	.1594	-0.006	.8167	.1148	+3.086
.7511	.1646	-0.011	.8171	.1169	+3.025
.7524	.1713	+0.003	.8193	.1282	+3.051
.7535	.1769	-0.018	.8210	.1370	+3.015
.7544	.1816	-0.008	.8227	.1458	+3.014
.7560	.1899	+0.003	.8242	.1535	+3.054
.7573	.1966	+0.014	.8273	.1695	+3.069
.7584	.2023	-0.008	.8290	.1783	+3.059
.7592	.2064	-0.009	.8295	.1809	+3.003
.7600	.2105	+0.014	.8311	.1892	+3.009
.7610	.2157	+0.003	.8315	.1912	+3.047
.7621	.2214	+0.013	.8333	.2005	+3.069
.7633	.2276	-0.004	.8450	.2610	+3.105
.7655	.2389	+0.014	.8469	.2708	+3.081
.7669	.2462	+0.011	.8575	.3255	+3.065
.7683	.2534	+0.000	.8592	.3343	+3.051
.7695	.2596	+0.001	.8681	.3803	+3.062
.7731	.2782	+0.014	.8697	.3885	+3.065
.7764	.2952	-0.007	.8716	.3983	+3.076
983.6828	.4232	+3.058	.8739	.4102	+3.073
.6870	.4449	+3.077	.8780	.4314	+3.117
.6894	.4573	+3.070	.8807	.4453	+3.096
.6910	.4656	+3.072	.8856	.4706	+3.074
.7019	.5219	+3.161	984.6660	.5012	+3.103
.7037	.5312	+3.168	.6675	.5089	+3.163

TABLE 2

BLUE OBSERVATIONS

Heliac JD 2434000+	Heliac Phase	Δ Mag.	Heliac JD 2434000+	Heliac Phase	Δ Mag.
984.6723	0.5337	+3.193	984.8431	0.4158	+3.144
.6739	.5420	+3.165	.8445	.4231	+3.105
.6755	.5502	+3.195	.8462	.4319	+3.121
.6779	.5626	+3.215	.8476	.4391	+3.099
.6796	.5714	+3.227	.8505	.4541	+3.153
.6815	.5812	+3.219	.8522	.4628	+3.165
.6836	.5921	+3.237	.8541	.4727	+3.166
.6855	.6019	+3.227	.8558	.4814	+3.167
.6889	.6194	+3.258	.8630	.5186	+3.187
.6973	.6626	+3.255	.8649	.5289	+3.209
.6994	.6737	+3.234	.8668	.5382	+3.240
.7023	.6887	+3.269	.8704	.5568	+3.257
.7113	.7351	+3.199	.8729	.5697	+3.258
.7132	.7449	+3.167	.8756	.5837	+3.272
.7149	.7537	+3.205	.8815	.6142	+3.271
.7175	.7672	+3.205	985.6744	.7093	+3.318
.719[illegible]	.7790	+3.199	.6762	.7185	+3.285
.723[illegible]	.7997	+3.125	.6793	.7346	+3.257
.7252	.8069	+3.064	.6814	.7454	+3.266
.7266	.8142	+3.006	.6832	.7547	+3.246
.7284	.8235	+3.102	.6862	.7702	+3.170
.7300	.8317	+3.097	.6961	.8213	+3.144
.7358	.8617	+3.092	.6980	.8311	+3.095
.7375	.8704	+3.092	.6996	.8394	+3.113
.7378	.8720	+3.125	.7065	.8750	+3.062
.7397	.8818	+3.083	.7077	.8812	+3.045
.7412	.8896	+3.100	.7088	.8869	+3.031
.7434	.9009	+3.113	.7100	.8931	+3.079
.7450	.9092	+3.147	.7110	.8983	+3.113
.7480	.9247	+3.220	.7123	.9050	+3.089
.7495	.9324	+3.315	.7139	.9133	+3.106
.7508	.9391	+3.442	.7151	.9195	+3.190
.7524	.9474	+3.520	.7175	.9318	+3.263
.7540	.9557	+3.625	.7191	.9401	+3.294
.7555	.9634	+3.768	.7203	.9463	+3.395
.7571	.9717	+3.847	.7216	.9530	+3.469
.7588	.9805	+3.936	.7230	.9603	+3.612
.7599	.9861	+4.023	.7243	.9670	+3.736
.7611	.9923	+4.069	.7255	.9732	+3.857
.7623	.9985	+4.057	.7265	.9783	+3.949
.7634	.0042	+4.084	.7268	.9799	+4.077
.7648	.0114	+4.044	.7284	.9881	+4.082
.7661	.0182	+4.012	.7296	.9943	+4.160
.7678	.0269	+3.961	.7309	.0011	+4.119
.7696	.0362	+3.829	.7321	.0073	+4.117
.7722	.0497	+3.601	.7336	.0150	+4.011
.7734	.0559	+3.557	.7363	.0289	+3.913
.7746	.0621	+3.464	.7367	.0310	+3.792
.7759	.0688	+3.406	.7380	.0377	+3.735
.7772	.0755	+3.336	.7396	.0460	+3.657
.7786	.0827	+3.312	.7407	.0517	+3.617
.7796	.0879	+3.263	.7411	.0537	+3.537
.7811	.0956	+3.200	.7412	.0543	+3.502
.7825	.1029	+3.203	.7425	.0610	+3.484
.7838	.1096	+3.168	.7429	.0630	+3.389
.7854	.1178	+3.179	.7441	.0692	+3.339
.7869	.1256	+3.157	.7456	.0770	+3.276
.7890	.1364	+3.197	.7471	.0847	+3.228
.7891	.1369	+3.127	.7488	.0935	+3.208
.7893	.1380	+3.073	.7506	.1028	+3.129
.7907	.1452	+3.111	.7521	.1106	+3.153
.7923	.1535	+3.135	.7530	.1152	+3.172
.7939	.1617	+3.195	.7543	.1219	+3.140
.7951	.1679	+3.150	.7557	.1291	+3.097
.7961	.1731	+3.191	.7570	.1359	+3.128
.7980	.1829	+3.180	.7582	.1421	+3.104
.7995	.1907	+3.187	.7613	.1581	+3.061
.8013	.2000	+3.201	.7630	.1668	+3.076
.8045	.2165	+3.201	.7633	.1684	+3.034
.8067	.2278	+3.155	.7737	.2221	+3.071
.8152	.2717	+3.133	.7751	.2293	+3.129
.8168	.2800	+3.156	.7765	.2366	+3.140
.8270	.3327	+3.170	.7779	.2438	+3.175
.8286	.3410	+3.170	.7793	.2510	+3.213
.8307	.3518	+3.135	.7807	.2583	+3.200
.8324	.3606	+3.107	.7848	.2794	+3.082
.8341	.3694	+3.138	.7861	.2861	+3.084
.8374	.3864	+3.077	.7895	.3037	+3.084
.8393	.3962	+3.099	.7961	.3378	+3.120
.8409	0.4045	+3.101	.7979	.3471	+3.124
			.7992	.3538	+3.098
			.8022	.3693	+3.084
			.8036	0.3765	+3.072

TABLE 3

ULTRAVIOLET OBSERVATIONS

Heliac JD 2434000+	Heliac Phase	Δ Mag.
954.7106	0.7907	+0.001
.7120	.7979	−0.013
.7127	.8016	−0.014
.7134	.8052	−0.001
.7137	.8067	−0.016
.7141	.8088	+0.024
.7144	.8103	−0.018
.7148	.8124	−0.006
.7151	.8139	+0.007
.7155	.8160	−0.017
.7158	.8175	+0.027
.7162	.8196	−0.030
.7165	.8212	+0.014
.7169	.8232	+0.014
.7172	.8248	+0.008
.7176	.8268	−0.002
.7179	.8284	−0.005
.7183	.8305	+0.007
.7186	.8320	+0.006
.7190	.8341	+0.022
.7193	.8356	+0.009
.7197	.8377	−0.005
.7200	.8392	−0.013
.7204	.8413	−0.014
.7207	.8428	+0.007
.7210	.8444	+0.008
.7212	.8454	−0.042
.7216	.8475	+0.006
.7220	.8056	+0.003
.7224	.8516	−0.007
.7227	.8532	−0.014
.7231	.8552	+0.010
.7234	.8568	−0.022
.7238	.8589	−0.045
.7241	.8604	−0.062
.7245	.8625	−0.060
.7248	.8635	−0.055
.7252	.8661	−0.050
.7255	.8676	−0.053
.7259	.8697	−0.062
.7262	.8713	−0.070
.7266	.8733	−0.042
.7269	.8749	−0.107
.7273	.8769	−0.072
.7287	.8842	−0.091
.7290	.8857	−0.102
.7294	.8878	−0.117
.7297	.8893	−0.066
.7301	.8914	−0.062
.7304	.8929	−0.056
.7308	.8950	−0.048
.7311	.8966	−0.064
.7315	.8986	−0.055
.7318	.9002	−0.095
.7322	.9022	−0.072
.7325	.9038	−0.047
.7327	.9048	−0.097
.7329	.9059	−0.077
.7332	.9070	−0.056
.7335	.9090	−0.043
.7338	.9105	−0.023
.7342	.9126	−0.022
.7346	.9146	−0.012
.7349	.9162	−0.012
.7350	.9167	−0.044
.7352	.9177	−0.027
.7356	.9198	−0.023
.7360	.9219	−0.004
.7363	.9234	+0.018
.7366	.9250	+0.034
.7370	.9270	+0.058
.7374	.9291	+0.078
.7379	.9317	+0.097
.7387	.9358	+0.152
.7391	.9379	+0.156
.7394	.9394	+0.194
.7398	.9415	+0.209
.7402	.9436	+0.247
.7405	.9451	+0.277
.7419	0.9523	+0.344

TABLE 3

ULTRAVIOLET OBSERVATIONS

Heliac JD 2434000+	Heliac Phase	Δ Mag.	Heliac JD 2434000+	Heliac Phase	Δ Mag.	Heliac JD 2434000+	Heliac Phase	Δ Mag.
954.7422	0.9539	+0.387	954.7870	0.1853	−0.019	954.8231	0.3717	+0.129
.7426	.9560	+0.402	.7875	.1879	+0.025	.8234	.3733	+0.206
.7430	.9580	+0.417	.7880	.1904	−0.023	.8238	.3753	+0.280
.7433	.9596	+0.437	.7884	.1925	+0.002	.8242	.3774	+0.306
.7436	.9611	+0.467	.7888	.1946	−0.038	.8245	.3789	+0.308
.7440	.9637	+0.476	.7891	.1961	−0.015	.8248	.3805	+0.104
.7443	.9647	+0.523	.7896	.1987	−0.063	.8256	.3846	+0.216
.7450	.9684	+0.550	.7900	.2008	−0.020	.8259	.3862	+0.081
.7464	.9756	+0.636	.7905	.2033	−0.076	.8266	.3898	+0.128
.7467	.9771	+0.666	.7908	.2049	−0.061	.8271	.3924	+0.173
.7470	.9787	+0.686	.7912	.2070	−0.091	.8273	.3934	+0.101
.7474	.9807	+0.708	.7913	.2075	−0.043	.8276	.3950	+0.220
.7565	.0277	+0.641	.7918	.2101	−0.049	.8281	.3975	+0.154
.7568	.0293	+0.611	.7920	.2111	−0.112	.8287	.4006	+0.252
.7572	.0314	+0.595	.7925	.2137	−0.053	.8292	.4032	+0.426
.7576	.0334	+0.552	.7930	.2163	−0.113	.8294	.4043	+0.229
.7579	.0350	+0.530	.7933	.2178	−0.064	.8298	.4063	+0.145
.7582	.0365	+0.507	.7938	.2204	−0.089	.8301	.4079	+0.103
.7586	.0386	+0.482	.7942	.2225	−0.073	.8308	.4115	+0.097
.7590	.0407	+0.451	.7946	.2245	−0.099	.8318	.4166	+0.204
.7593	.0422	+0.431	.7950	.2266	−0.075	.8322	.4187	+0.134
.7596	.0438	+0.419	.7954	.2287	−0.110	.8326	.4208	+0.224
.7599	.0453	+0.393	.7958	.2307	−0.073	.8329	.4223	+0.282
.7602	.0469	+0.371	.7960	.2318	−0.136	.8346	.4311	+0.071
.7606	.0489	+0.339	.7965	.2343	−0.076	.8352	.4342	+0.097
.7610	.0515	+0.309	.7968	.2359	−0.120	.8356	.4363	+0.029
.7613	.0525	+0.291	.7971	.2374	−0.079	.8361	.4389	+0.125
.7616	.0541	+0.270	.7977	.2405	−0.179	.8364	.4404	+0.076
.7620	.0562	+0.260	.7981	.2426	−0.104	.8369	.4430	+0.153
.7624	.0582	+0.252	.7984	.2442	−0.109	.8371	.4440	−0.003
.7627	.0598	+0.250	.7995	.2498	−0.135	.8377	.4471	+0.025
.7630	.0613	+0.232	.7998	.2514	−0.091	.8384	.4507	+0.066
.7634	.0634	+0.212	.8002	.2534	−0.122	.8389	.4533	−0.039
.7638	.0655	+0.200	.8009	.2571	−0.102	.8391	.4544	+0.016
.7641	.0670	+0.197	.8012	.2586	−0.098	.8398	.4580	+0.007
.7644	.0686	+0.199	.8016	.2607	−0.122	.8400	.4590	+0.100
.7648	.0706	+0.197	.8020	.2627	−0.159	.8405	.4616	+0.092
.7652	.0727	+0.197	.8023	.2643	−0.123	.8412	.4652	+0.041
.7659	.0763	+0.191	.8026	.2658	−0.184	.8415	.4667	+0.016
.7662	.0778	+0.188	.8030	.2679	−0.134	.8416	.4673	+0.093
.7666	.0799	+0.178	.8036	.2710	−0.177	.8419	.4688	+0.085
.7669	.0815	+0.160	.8040	.2731	−0.150	.8422	.4704	+0.093
.7672	.0830	+0.107	.8043	.2746	−0.163	.8426	.4724	+0.028
.7676	.0851	+0.165	.8047	.2767	−0.111	.8433	.4760	+0.023
.7680	.0871	+0.154	.8050	.2782	−0.190	.8434	.4766	+0.047
.7683	.0887	+0.148	.8055	.2808	−0.130	.8439	.4791	+0.003
.7686	.0902	+0.137	.8059	.2829	−0.157	.8444	.4817	+0.046
.7690	.0923	+0.114	.8064	.2855	−0.107	.8448	.4838	+0.019
.7694	.0944	+0.147	.8067	.2870	−0.156	.8454	.4869	+0.077
.7697	.0959	+0.065	.8072	.2896	−0.071	.8460	.4900	+0.053
.7700	.0975	+0.106	.8075	.2911	−0.089	.8462	.4910	+0.043
.7704	.0995	+0.055	.8081	.2942	−0.077	.8467	.4931	+0.085
.7707	.1011	+0.052	.8082	.2948	−0.125	.8474	.4972	+0.076
.7710	.1026	+0.037	.8088	.2979	−0.071	.8488	.5044	−0.045
.7714	.1047	+0.025	.8092	.2999	−0.094	.8493	.5070	−0.001
.7717	.1063	+0.015	.8096	.3020	−0.084	.8499	.5101	−0.018
.7721	.1083	−0.038	.8099	.3035	−0.083	.8505	.5132	−0.014
.7724	.1099	+0.003	.8103	.3506	−0.102	.8509	.5153	+0.017
.7730	.1130	−0.055	.8106	.3072	−0.094	.8516	.5189	+0.082
.7734	.1155	+0.012	.8113	.3108	−0.073	.8520	.5210	+0.040
.7738	.1171	−0.003	.8114	.3113	−0.064	.8627	.5762	−0.033
.7743	.1197	+0.017	.8116	.3123	−0.096	.8634	.5799	−0.010
.7747	.1217	−0.005	.8120	.3144	−0.041	.8641	.5835	−0.012
.7752	.1243	+0.001	.8126	.3175	−0.098	.8648	.5871	+0.011
.7755	.1259	−0.037	.8130	.3196	−0.039	.8652	.5892	−0.026
.7760	.1285	+0.002	.8133	.3211	−0.105	.8655	.5907	+0.014
.7763	.1300	−0.031	.8134	.3216	−0.095	.8658	.5922	−0.022
.7767	.1321	+0.013	.8138	.3237	−0.061	.8683	.6052	+0.022
.7772	.1347	−0.020	.8141	.3252	+0.007	.8690	.6088	+0.022
.7777	.1372	+0.020	.8144	.3268	+0.049	.8697	.6124	+0.026
.7780	.1378	−0.036	.8148	.3288	+0.067	.8704	.6160	+0.015
.7784	.1409	+0.011	.8162	.3361	+0.078	.8709	.6186	−0.006
.7788	.1429	−0.025	.8166	.3381	+0.058	.8712	.6201	+0.042
.7794	.1460	−0.001	.8169	.3397	+0.059	.8713	.6207	+0.027
.7801	.1496	+0.018	.8172	.3412	+0.089	.8717	.6227	+0.025
.7804	.1512	−0.002	.8176	.3433	+0.039	.8724	.6263	+0.022
.7818	.1584	+0.009	.8180	.3454	+0.091	.8728	.6284	−0.018
.7822	.1605	−0.021	.8183	.3469	+0.067	.8731	.6300	+0.006
.7826	.1625	+0.015	.8186	.3485	+0.098	.8738	.6336	−0.005
.7829	.1641	+0.026	.8190	.3506	+0.105	.8745	.6372	+0.031
.7832	.1656	+0.050	.8194	.3526	+0.115	.8752	.6408	+0.040
.7835	.1672	+0.015	.8196	.3536	+0.045	.8756	.6429	+0.009
.7838	.1687	−0.003	.8197	.3542	+0.039	.8759	.6444	+0.032
.7841	.1703	+0.037	.8204	.3578	+0.063	.8762	.6460	+0.057
.7843	.1713	+0.013	.8210	.3609	+0.057	.8766	.6480	+0.034
.7849	.1744	+0.053	.8214	.3629	+0.081	.8773	.6516	+0.033
.7853	.1765	+0.023	.8217	.3645	+0.050	.8801	.6661	+0.064
.7859	.1796	+0.049	.8221	.3666	+0.098	.8808	.6697	+0.059
.7862	.1811	+0.010	.8224	.3681	+0.068	.8835	.6837	+0.049
.7866	.1832	+0.021	.8228	.3702	+0.109	.8842	.6873	+0.049

TABLE 3

ULTRAVIOLET OBSERVATIONS

Heliac JD 2434000+	Heliac Phase	Δ Mag.
954.8849	0.6909	+0.037
.8856	.6945	+0.029
.8863	.6981	+0.011
.8870	.7017	+0.030
.8877	.7054	+0.037
.8882	.7079	+0.027
.8887	.7105	+0.075
.8890	.7121	+0.050
.8894	.7141	+0.109
.8898	.7162	+0.080
.8905	.7198	+0.069
.8912	.7234	+0.067
.8919	.7270	+0.066
.8926	.7307	+0.031
.8933	.7343	+0.037
.8940	.7379	+0.009
.8947	.7415	++0.058
.8961	.7487	+0.016
.8968	.7524	+0.015
.8975	.7560	+0.022
.8982	.7596	+0.010
.8989	.7632	-0.006
.8996	.7668	-0.009
.9002	.7699	-0.021
.9009	.7735	-0.021
.9016	.7771	-0.048
.9023	.7808	-0.030
.9028	.7833	+0.002
.9031	.7849	-0.033
.9037	.7886	+0.004
.9044	.7916	-0.008
.9051	.7952	-0.007
.9058	.7988	-0.005
.9065	.8023	+0.000
.9072	.8061	+0.007
.9079	.8097	-0.006
.9086	.8133	-0.002
.9093	.8169	-0.013
.9100	.8205	+0.001
.9106	.8236	+0.000
.9110	.8257	+0.029
.9113	.8272	-0.003
.9120	.8309	-0.031
.9127	.8345	-0.034
.9134	.8381	-0.034
.9138	.8402	-0.014
.9132	.8474	-0.070
.9135	.8489	-0.062
.9142	.8526	-0.062
.9166	.8646	-0.084
.9169	.8662	-0.081
.9176	.8698	-0.056
.9183	.8634	-0.009
.9186	.8649	-0.018
.9190	.8670	-0.058
.9194	.8691	-0.113
.9197	.8706	-0.156
.9200	.8722	-0.117
.9204	.8742	-0.170
.9208	.8763	-0.158
.9211	.8779	-0.150
.9214	.8794	-0.140
.9218	.8820	-0.126
.9222	.8835	-0.119
.9225	.8851	-0.112
.9228	.8866	-0.107
.9232	.8887	-0.102
.9236	.8908	-0.108
.9239	.8923	-0.109
.9242	.8939	-0.110
.9246	.8959	-0.113
.9250	.8980	-0.112
.9253	.8995	-0.101
.9236	.9011	-0.066
.9259	.9026	-0.052
.9262	.9042	-0.091
.9265	.9057	-0.038
.9266	.9063	-0.075
.9270	.9083	-0.081
.9273	.9099	-0.085
.9276	.9114	-0.102
.9280	.9135	-0.098
.9284	.9156	-0.091
.9287	.9171	-0.060
.9290	.9187	-0.032
.9294	.9207	-0.012
.9298	.9228	+0.027
.9301	.9243	+0.055
.9304	.9259	+0.062
.9308	0.9280	+0.087
954.9312	0.9300	+0.119
.9315	.9316	+0.125
.9318	.9331	+0.150
.9322	.9352	+0.161
.9326	.9378	+0.188
.9328	.9383	+0.224
.9332	.9403	+0.244
.9335	.9419	+0.269
.9338	.9434	+0.292
.9356	.9527	+0.467
.9360	.9548	+0.498
.9363	.9564	+0.519
.9366	.9579	+0.528
.9370	.9600	+0.538
.9374	.9620	+0.545
.9377	.9636	+0.592
.9380	.9651	+0.622
.9384	.9672	+0.663
.9387	.9688	+0.672
.9391	.9708	+0.693
.9394	.9724	+0.716
.9398	.9744	+0.728
.9401	.9760	+0.760
.9405	.9781	+0.801
.9408	.9796	+0.825
.9412	.9817	+0.858
.9415	.9832	+0.900
.9419	.9853	+0.921
.9422	.9868	+0.979
.9426	.9889	+1.066
.9429	.9904	+1.025
.9433	.9925	+0.913
.9436	.9941	+0.945
.9440	.9966	+0.978
.9443	.9977	+0.910
.9447	.9997	+0.892
.9450	.0013	+0.900
.9464	.0085	+0.902
.9468	.0106	+0.894
.9471	.0121	+0.859
.9475	.0142	+0.871
.9478	.0158	+0.923
.9482	0178	+0.860
.9485	.0194	+0.802
.9507	.0307	+0.781
.9510	.0323	+0.728
.9513	.0338	+0.622
.9516	.0354	+0.614
.9519	.0369	+0.626
.9523	.0390	+0.598
.9526	.0405	+0.515
.9530	.0426	+0.513
.9533	.0442	+0.484
.9537	.0462	+0.455
.9540	.0478	+0.406
.9544	.0498	+0.410
.9547	.0514	+0.405
.9551	.0535	+0.399
.9554	.0550	+0.398
.9558	.0571	+0.388
.9568	.0622	+0.356
.9572	.0643	+0.325
.9575	.0659	+0.321
.9579	.0679	+0.336
.9582	.0695	+0.301
.9586	.0715	+0.269
.9593	.0751	+0.260
.9596	.0767	+0.229
.9599	.0782	+0.203
.9602	.0798	+0.162
.9606	.0819	+0.144
.9610	.0839	+0.113
.9613	.0855	+0.080
.9616	.0870	+0.107
955.6877	.8371	-0.054
.6881	.8392	-0.028
.6905	.8516	-0.059
.6906	.8521	+0.002
.6909	.8536	-0.031
.6919	.8588	-0.057
.6926	.8624	-0.052
.6929	.8640	-0.033
.6940	.8696	-0.006
.6943	.8712	-0.037
.6954	.8769	-0.013
.6964	.8820	-0.010
.6971	.8857	-0.030
.6974	.8872	-0.050
.6981	.8908	-0.048
.6986	0.8934	-0.087
955.6995	0.8981	-0.043
.7003	.9022	+0.032
.7014	.9079	+0.021
.7024	.9135	+0.025
.7040	.9213	+0.036
.7051	.9270	+0.026
.7052	.9275	+0.113
.7061	.9321	+0.150
.7071	.9373	+0.263
.7081	.9425	+0.329
.7090	.9471	+0.432
.7103	.9538	+0.458
.7114	.9595	+0.514
.7124	.9647	+0.568
.7134	.9698	+0.665
.7144	.9750	+0.763
.7155	.9807	+0.776
.7165	.9859	+0.855
.7176	.9915	+0.891
.7187	.9972	+0.917
.7199	.0034	+0.925
.7214	.0112	+0.828
.7224	.0163	+0.788
.7244	.0267	+0.707
.7253	.0313	+0.639
.7272	.0411	+0.565
.7274	.0421	+0.518
.7284	.0473	+0.463
.7294	.0525	+0.429
.7306	.0587	+0.362
.7317	.0644	+0.302
.7328	.0700	+0.249
.7331	.0716	+0.196
.7341	.0762	+0.169
.7351	.0819	+0.132
.7356	.0845	+0.091
.7367	.0902	+0.109
.7377	.0953	+0.064
.7379	.0964	+0.023
.7391	.1026	+0.062
.7405	.1098	+0.004
.7417	.1160	+0.039
.7429	.1222	+0.035
.7440	.1279	+0.042
.7465	.1408	+0.035
.7480	.1485	+0.018
.7490	.1537	+0.024
.7504	.1609	-0.003
.7516	.1671	+0.052
.7528	.1733	+0.003
.7538	.1785	+0.012
.7549	.1842	+0.045
.7565	.1924	+0.062
.7578	.1992	-0.001
.7588	.2043	+0.007
.7594	.2074	+0.014
.7604	.2126	+0.024
.7613	.2172	+0.012
.7624	.2229	+0.021
.7635	.2286	+0.003
.7660	.2415	+0.011
.7676	.2498	+0.000
.7686	.2549	-0.015
.7697	.2606	+0.030
.7699	.2616	-0.023
.7703	.2637	+0.059
.7708	.2663	-0.015
.7714	.2694	+0.001
.7722	.2735	+0.010
.7738	.2818	-0.017
.7745	.2854	-0.020
.7752	.2890	-0.029
.7769	.2978	-0.003
983.6840	.4294	+2.271
.6842	.4305	+2.290
.6846	.4325	+2.305
.6849	.4341	+2.314
.6853	.4362	+2.323
.6874	.4470	+2.292
.6877	.4486	+2.274
.6881	.4506	+2.240
.6901	.4609	+2.280
.6915	.4682	+2.281
.7026	.5255	+2.380
.7042	.5338	+2.383
.7075	.5508	+2.451
.7089	.5580	+2.460
.7099	.5632	+2.488
.7113	.5704	+2.480
.7128	0.5782	+2.479

TABLE 3

ULTRAVIOLET OBSERVATIONS

Heliac JD 2434000+	Heliac Phase	Δ Mag.	Heliac JD 2434000+	Heliac Phase	Δ Mag.	Heliac JD 2434000+	Heliac Phase	Δ Mag.
983.7203	0.6169	+2.494	984.6862	0.6055	+2.493	984.8547	0.4758	+2.434
.7242	.6371	+2.519	.6892	.6210	+2.534	.8565	.4850	+2.424
.7351	.6934	+2.505	.6896	.6231	+2.562	.8634	.5207	+2.497
.7368	.7021	+2.492	.6980	.6664	+2.543	.8656	.5320	+2.513
.7384	.7104	+2.507	.7000	.6768	+2.577	.8675	.5419	+2.536
.7412	.7249	+2.564	.7030	.6923	+2.580	.8711	.5605	+2.559
.7426	.7321	+2.534	.7120	.7387	+2.557	.8737	.5739	+2.538
.7439	.7388	+2.538	.7138	.7480	+2.538	.8761	.5863	+2.580
.7528	.7848	+2.437	.7154	.7563	+2.542	.8820	.6167	+2.601
.7541	.7915	+2.465	.7158	.7584	+2.564	985.6750	.7124	+2.611
.7568	.8054	+2.459	.7183	.7713	+2.582	.6766	.7206	+2.572
.7587	.8152	+2.397	.7203	.7816	+2.534	.6770	.7227	+2.525
.7603	.8235	+2.424	.7244	.8028	+2.476	.6800	.7382	+2.559
.7615	.8297	+2.465	.7258	.8100	+2.448	.6820	.7485	+2.546
.7625	.8349	+2.388	.7272	.8173	+2.481	.6839	.7583	+2.547
.7637	.8411	+2.421	.7289	.8260	+2.488	.6869	.7738	+2.518
.7648	.8468	+2.432	.7306	.8348	+2.478	.6966	.8239	+2.508
.7678	.8622	+2.450	.7363	.8643	+2.475	.6984	.8332	+2.408
.7699	.8731	+2.406	.7384	.8751	+2.439	.6987	.8348	+2.447
.7740	.8943	+2.387	.7402	.8844	+2.462	.6999	.8410	+2.444
.7758	.9036	+2.436	.7416	.8916	+2.464	.7069	.8771	+2.423
.7787	.9185	+2.494	.7420	.8937	+2.497	.7080	.8828	+2.412
.7801	.9258	+2.508	.7439	.9035	+2.500	.7092	.8890	+2.393
.7815	.9330	+2.583	.7456	.9123	+2.545	.7103	.8947	+2.465
.7828	.9397	+2.697	.7482	.9257	+2.594	.7114	.9003	+2.463
.7837	.9444	+2.791	.7488	.9288	+2.632	.7126	.9065	+2.435
.7849	.9506	+2.840	.7500	.9350	+2.695	.7130	.9086	+2.383
.7862	.9573	+2.927	.7502	.9360	+2.711	.7142	.9148	+2.492
.7875	.9640	+3.025	.7514	.9422	+2.786	.7155	.9215	+2.548
.7885	.9692	+3.172	.7530	.9505	+2.850	.7182	.9355	+2.533
.7905	.9795	+3.162	.7544	.9577	+2.974	.7196	.9427	+2.593
.7915	.9846	+3.217	.7561	.9665	+3.059	.7209	.9494	+2.717
.7928	.9914	+3.283	.7579	.9758	+3.106	.7220	.9551	+2.776
.7941	.9981	+3.335	.7591	.9820	+3.205	.7235	.9628	+2.856
.7953	.0043	+3.355	.7603	.9882	+3.222	.7246	.9685	+3.005
.7968	.0120	+3.459	.7614	.9939	+3.243	.7258	.9747	+3.067
.7979	.0177	+3.202	.7626	.0001	+3.234	.7273	.9825	+3.189
.8002	.0296	+3.165	.7639	.0068	+3.256	.7288	.9902	+3.274
.8014	.0358	+3.136	.7653	.0140	+3.244	.7300	.9964	+3.315
.8030	.0440	+2.966	.7666	.0207	+3.183	.7314	.0036	+3.262
.8044	.0513	+2.858	.7682	.0290	+3.169	.7327	.0104	+3.233
.8058	.0585	+2.781	.7702	.0393	+3.034	.7343	.0186	+3.148
.8072	.0657	+2.674	.7729	.0533	+2.875	.7368	.0315	+3.066
.8087	.0735	+2.626	.7737	.0574	+2.810	.7373	.0341	+2.992
.8106	.0833	+2.499	.7751	.0646	+2.755	.7384	.0398	+2.950
.8124	.0926	+2.411	.7764	.0714	+2.687	.7399	.0475	+2.914
.8141	.1014	+2.390	.7778	.0786	+2.584	.7417	.0568	+2.804
.8155	.1086	+2.355	.7789	.0843	+2.637	.7432	.0646	+2.685
.8176	.1194	+2.336	.7800	.0899	+2.576	.7446	.0718	+2.600
.8183	.1231	+2.326	.7803	.0915	+2.516	.7460	.0790	+2.519
.8196	.1298	+2.258	.7814	.0972	+2.561	.7475	.0868	+2.509
.8199	.1313	+2.300	.7817	.0987	+2.593	.7494	.0966	+2.446
.8214	.1391	+2.239	.7829	.1049	+2.522	.7510	.1049	+2.428
.8217	.1406	+2.282	.7843	.1122	+2.484	.7524	.1121	+2.449
.8231	.1479	+2.311	.7859	.1204	+2.490	.7536	.1183	+2.421
.8233	.1489	+2.348	.7874	.1282	+2.497	.7548	.1245	+2.418
.8246	.1556	+2.316	.7897	.1400	+2.412	.7563	.1322	+2.394
.8278	.1721	+2.433	.7911	.1473	+2.397	.7573	.1374	+2.395
.8282	.1742	+2.336	.7914	.1488	+2.428	.7586	.1441	+2.414
.8301	.1840	+2.328	.7928	.1561	+2.437	.7616	.1596	+2.347
.8321	.1943	+2.318	.7944	.1643	+2.481	.7617	.1601	+2.306
.8335	.2016	+2.324	.7954	.1695	+2.501	.7620	.1617	+2.404
.8339	.2036	+2.369	.7967	.1762	+2.470	.7634	.1689	+2.362
.8456	.2641	+2.381	.7985	.1855	+2.468	.7635	.1694	+2.308
.8478	.2754	+2.371	.7999	.1927	+2.503	.7638	.1710	+2.359
.8578	.3271	+2.301	.8002	.1943	+2.482	.7642	.1730	+2.297
.8584	.3302	+2.260	.8017	.2020	+2.479	.7643	.1736	+2.380
.8599	.3379	+2.277	.8020	.2036	+2.515	.7649	.1767	+2.296
.8686	.3828	+2.323	.8050	.2191	+2.491	.7653	.1787	+2.349
.8703	.3916	+2.326	9061	.2247	+2.480	.7658	.1813	+2.394
.8721	.4009	+2.341	.8157	.2743	+2.371	.7661	.1829	+2.343
.8746	.4138	+2.329	.8173	.2826	+2.397	.7666	.1854	+2.293
.8792	.4376	+2.378	.8274	.3348	+2.405	.7668	.1865	+2.342
.8814	.4490	+2.400	.8293	.3446	+2.405	.7673	.1891	+2.293
.8835	.4598	+2.400	.8310	.3533	+2.399	.7742	.2247	+2.328
.8865	.4753	+2.288	.8314	.3553	+2.343	.7757	.2324	+2.381
984.6661	.5017	+2.384	.8329	.3632	+2.388	.7769	.2386	+2.447
.6666	.5043	+2.401	.8347	.3725	+2.344	.7784	.2464	+2.325
.6681	.5120	+2.434	.8378	.3885	+2.287	.7799	.2541	+2.430
.6730	.5373	+2.465	.8383	.3911	+2.334	.7813	.2614	+2.440
.6742	.5435	+2.425	.8398	.3988	+2.330	.7852	.2815	+2.363
.6745	.5451	+2.464	.8412	.4060	+2.313	.7866	.2887	+2.329
.6759	.5523	+2.464	.8417	.4086	+2.392	.7900	.3063	+2.340
.6782	.5642	+2.483	.8419	.4096	+2.348	.7966	.3404	+2.429
.6786	.5662	+2.524	.8436	.4184	+2.367	.7984	.3497	+2.414
.6802	.5745	+2.493	.8451	.4262	+2.370	.7998	.3569	+2.376
.6820	.5838	+2.504	.8466	.4339	+2.346	.8028	.3724	+2.331
.6825	.5864	+2.462	.8482	.4422	+2.323	.8039	0.3781	+2.359
.6827	.5874	+2.482	.8509	.4561	+2.346			
.6843	0.5957	+2.495	.8528	0.4659	+2.396			

and these in turn were tied in to the U, B, V system of Johnson and Morgan (1953). The chart of the field of DQ Her in Fig 8 shows the locations of these stars, and their magnitudes and colors are listed in Table 4. Star B was used as the primary comparison star, and the magnitudes of DQ Her on August 29, 30, and 31 are given in terms of the instrumental magnitude difference in each color, DQ Her *minus* B, reduced to no atmosphere.

The (1530) observations of DQ Her in yellow, blue, and ultraviolet light are given in Tables 1, 2, and 3, respectively. For each observation, the tables list the heliocentric Julian date and the phase computed from the elements:

$$\text{Minimum} = \text{Helioc. JD } 2434954.94475 + 0^d1936223\,E\,.$$

The observed times of minimum light from which these elements were derived, together with the residuals, observed time *minus* time computed from the foregoing elements, are listed in Table 5.

TABLE 4

MAGNITUDES AND COLORS OF COMPARISON STARS

Star	V	$B-V$	$U-B$
A	15.82	+0.37	+0.01
B	10.56	+0.51	+0.01
C	11.53	+1.45	+1.68

TABLE 5

OBSERVED MINIMA OF DQ HERCULIS

Helioc. JD 2434+	O−C (Day)	Color	Helioc. JD 2434+	O−C (Day)	Color
954.7515	+0.0004	UV	983.79575	+0.00128	UV
954.94495	+ .00020	UV	984.76270	+ .00012	V
955.71887	− .00037	V	984.76295	+ .00037	B
955.71900	− .00024	UV	984.76329	+ .00071	UV
955.71931	+ .00007	B	985.72981	− .00089	B
981.665	.000	Pg*	985.72981	− .00089	UV
983.79431	− .00016	V	985.72985	− .00085	V
983.79483	+0.00036	B	989.797	0.000	Pg*

* Minimum observed photographically by J. B. Oke at Toronto.

The individual light-curves, plotted against phase, are shown in Figures 1–5. The observations on July 31 between phases $0.470P$ and $0.852P$ are of low weight, owing to difficulty with the offset guiding device. The light-curves display the following features:

1. Primary eclipse is partial and lasts about 1 hour, from $0.889P$ to $0.111P$. Its depth decreases as one goes to shorter wave lengths, being about 1.4 mag. in the yellow, 1.0 mag. in the blue, and 0.8 mag. in the ultraviolet. These depths vary from cycle to cycle. There is no trace of a secondary eclipse. A very shallow secondary would be obscured by the intrinsic variations of the star, discussed later; all we can say is that the depth of secondary must be ≤ 0.03 mag.

2. Shoulders sometimes occur both before and after eclipse; their structure and height vary from cycle to cycle. The one preceding eclipse begins at about $0.70P$, while that following eclipse, if it occurs, usually lasts until about $0.20P$, although there is considerable variation, as on July 31.

3. The rising branch of the eclipse curve is asymmetric between $0.050P$ and $0.111P$ (the end of eclipse), and during some cycles there is a definite stillstand, as on July 31.

4. Between $0.20P$ and $0.45P$ the light of the system is relatively constant or increases slightly. After $0.45P$, the light-level decreases, reaching a minimum at $0.70P$, and then increases again until the beginning of the next primary eclipse. The amount of this decrease is about 0.15 mag. in yellow light; the variation with wave length is discussed later. On most nights the occurrence of this minimum and of the shoulder before eclipse are confused. On these nights, following the minimum at $0.70P$, the brightness of the system does not surpass, and may not even attain, the level of "constant" light between

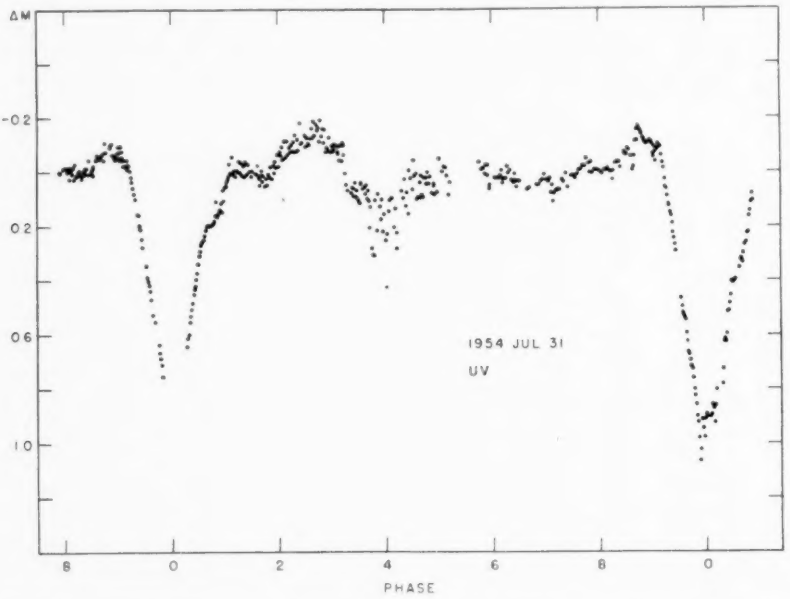

FIG. 1.—Photometric observations of DQ Her. The ordinate is the instrumental magnitude, reduced to no atmosphere. The zero point is arbitrary. The abscissa is the phase computed from zero phase = Minimum = Helioc. JD 2434954.94475 + $0^d1936223E$.

phases $0.20P$ and $0.45P$. Thus one could describe the light-curve as showing a decrease in light until $0.70P$, followed by a shoulder preceding eclipse or as displaying only a light-minimum between $0.45P$ and the beginning of the following eclipse at $0.89P$.

5. Intrinsic variations occur throughout the cycle of the system, with periods of from 1 to 40 minutes and amplitudes up to at least 0.15 mag. Over most of the cycle these periods and amplitudes appear to occur at random. However, one of the most striking features of the light-curve is that, between $0.110P$ and $0.325P$, there occur extremely rapid variations with a definite periodicity, which are superimposed upon the random fluctuations of longer period. The period of these variations, determined from the observations on July 31, is 1.180 minutes, and their amplitude is about 0.035 mag. in the ultraviolet. Some trace of these variations persists until about $0.50P$. Owing to the shortness of the period of these variations, they can be properly observed only by monitoring the star continuously in a single color. Altogether, DQ Her has been monitored on

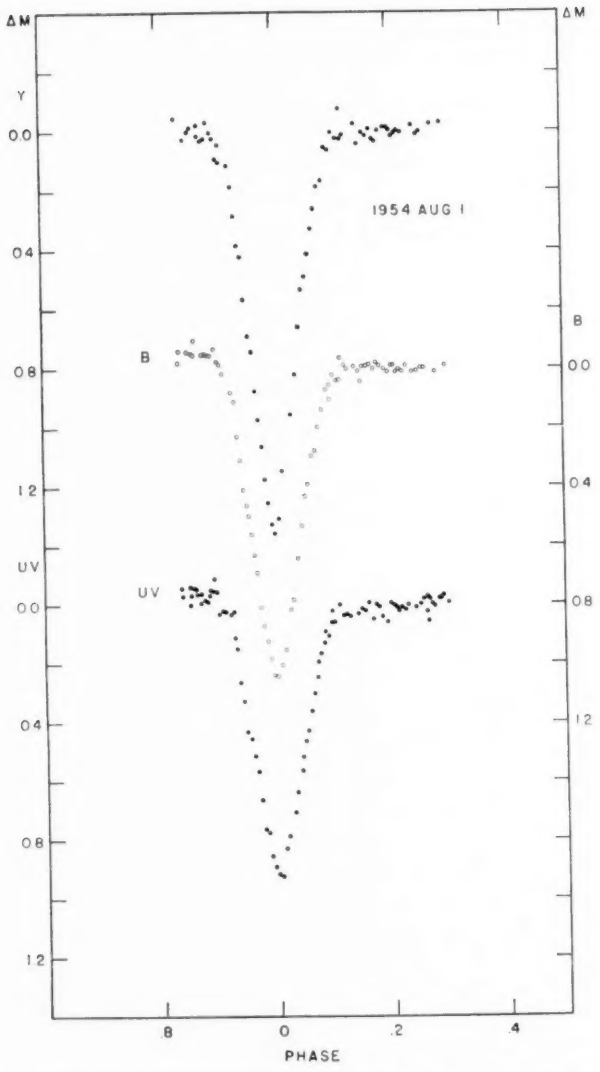

FIG. 2.—Photometric observations of DQ Her. Ordinate and abscissa as in Fig. 1

three nights during some part of the foregoing phase interval: July 9, when the variations were first discovered, July 31, and August 31, when again these periodic variations occurred. Sections of the light-curve have been traced from the Brown recorder sheets for these three nights and have been combined in Figure 6 according to the phase in the 4-hour period. These tracings are still in intensity units. However, a vertical distance corresponding to 0.10 mag. has been marked for each of the runs. The residuals, ob-

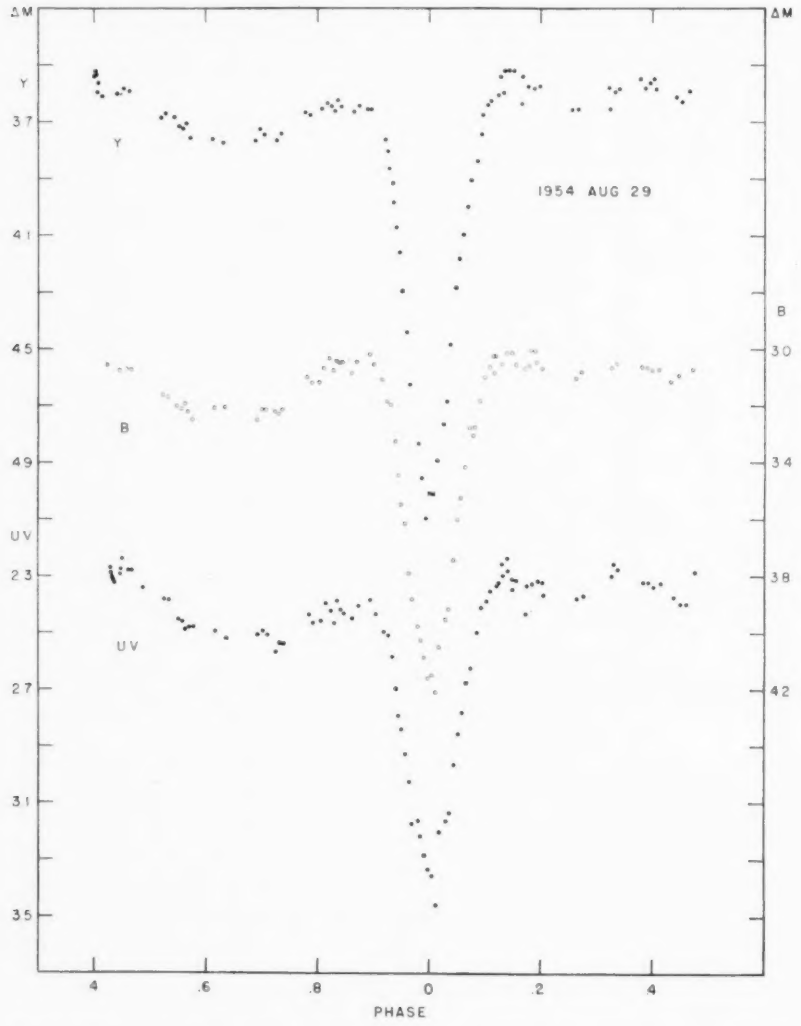

FIG. 3.—Photometric observations of DQ Her. The ordinate is the instrumental magnitude difference, DQ Her *minus B*, reduced to no atmosphere. Abscissa as in Fig. 1.

served maxima *minus* maxima computed with $P = 1.180$ minutes, for the observations of July 31 are shown in Figure 7. The accuracy in determining the observed times of maximum light was about ± 0.1 minute. While only a very limited amount of material is available, it suggests that these variations are a permanent feature of the light-curve. The fact that they occur during only a part of the 4-hour period indicates that they probably result in some way from the binary nature of the system and that only a portion of the star is involved in their production.

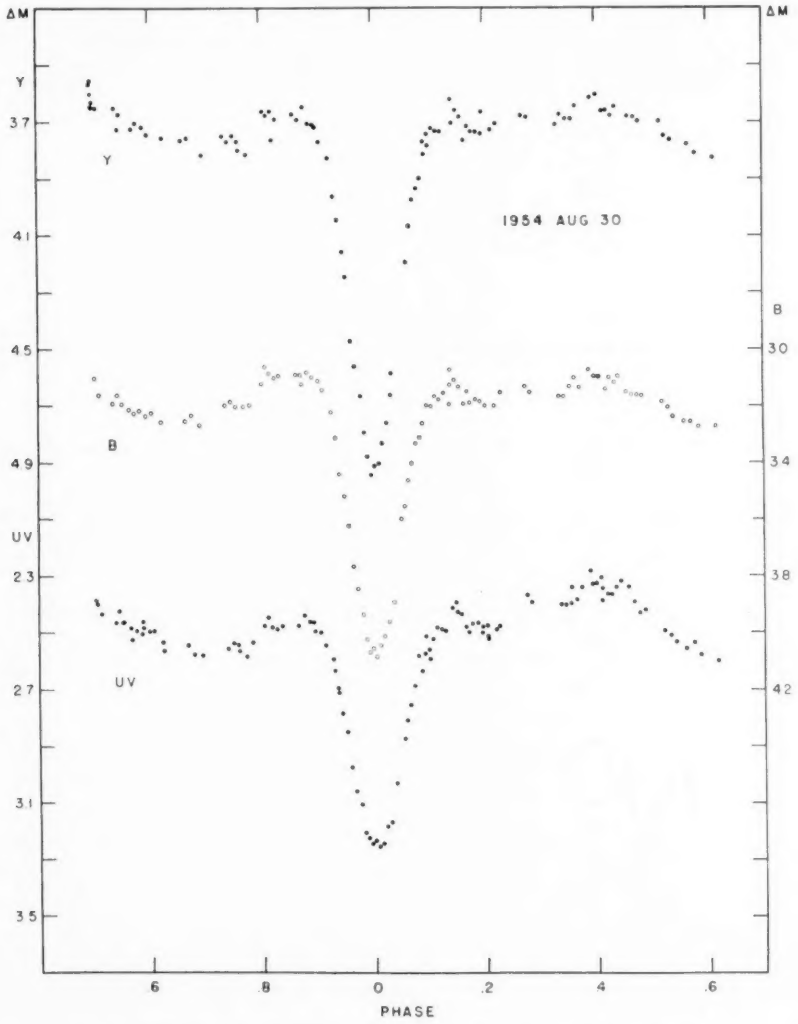

FIG. 4.—Photometric observations of DQ Her. Ordinate and abscissa as in Fig. 3

6. Adopting the color of the system as normal between $0.11P$ and $0.40P$, the $B-V$ color of the star remains constant until about $0.70P$, after which the star becomes bluer, maximum blueness outside eclipse occurring at the top of the shoulder preceding eclipse ($0.89P$). The amount of this blue excess is about 0.10 mag. The $U-V$ color of the system, on the other hand, increases slightly after $0.40P$, the star becoming about 0.05 mag. redder at $0.70P$ and about 0.07 mag. redder at $0.89P$. As mentioned previously, the

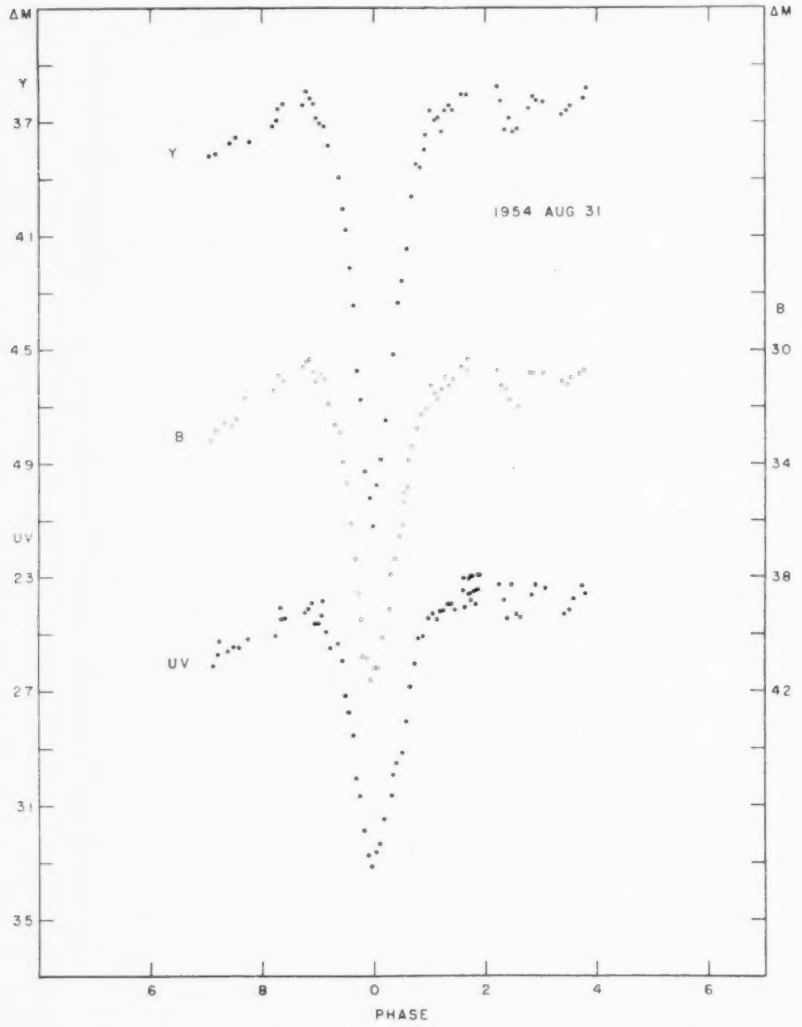

FIG. 5.—Photometric observations of DQ Her. Ordinate and abscissa as in Fig. 3

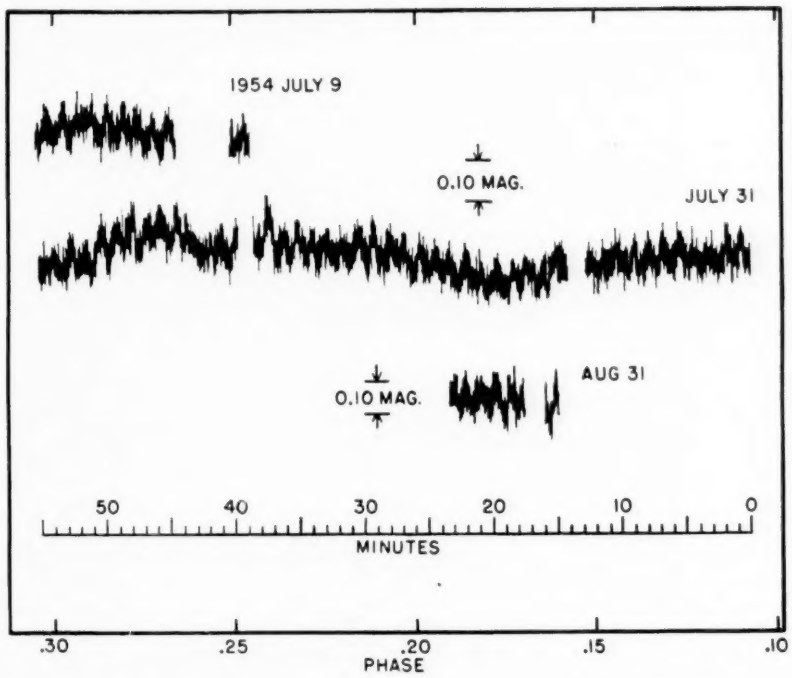

FIG. 6.—Tracings from Brown recorder sheets, showing rapid, periodic variations in ultraviolet light. The period of these fluctuations, determined from the observations on July 31, is $P = 1.180$ minutes. The abscissa is the phase in the 4-hour period.

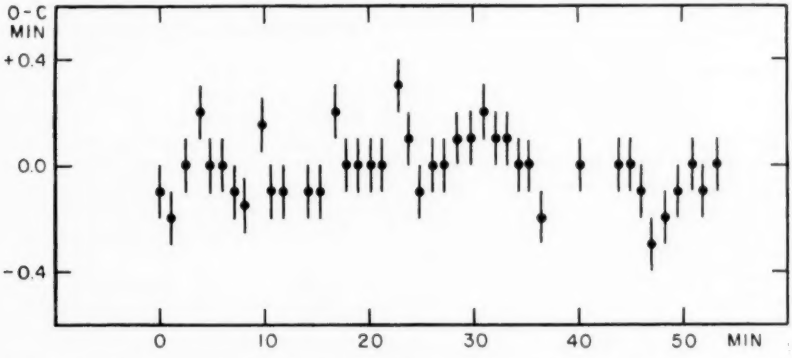

FIG. 7.—Residuals between the observed maxima of the 1-minute light-variations on July 31, shown in Fig. 6, and the maxima computed using $P = 1.180$ minutes.

depth of eclipse varies with wave length, so that the star is bluer than normal in both color systems during eclipse. Figure 8 shows that the nebulosity surrounding DQ Her is relatively bright photographically in comparison to the star. Consequently, it appears likely that the decreasing depth of eclipse with decreasing wave length results from the filling-in of the light-curve by radiation from the expanding shell. If we assume that the depth of eclipse is actually the same in all wave lengths and that the yellow light-curve is unaffected by light from the nebulosity, we find that this filling-in is probably responsible also for the peculiar color changes between $0.40P$ and $0.70P$; on these assumptions, the depths of the light-minimum at $0.70P$ become 0.15 mag. in the yellow, 0.26 in the blue, and 0.40 in the ultraviolet. However, this filling-in of the light-curve will not account for the anomalous brightness of the star in blue light at phase $0.89P$. At this time the system is brightest in the blue and faintest in the ultraviolet, relative to the light-levels between $0.11P$ and $0.40P$.

Since the magnitude differences, DQ Her *minus* B, were left on the instrumental system, the colors of DQ Her derived from the tabulated magnitude differences and the colors of star B will not be exactly on the U, B, V system. The magnitude and colors of DQ Her have therefore been converted to this system for three selected times on Aug 29 and are given in Table 6. Applying the corrections discussed for the effect of radiation from the nebulosity upon the measured blue and ultraviolet intensities of the star, we obtain the following corrections to the colors: $\Delta B-V = +0.092$ mag., and $\Delta U-B = +0.233$ mag. Thus the "corrected" colors of the star at $0.45P$ become $B-V = +0.09$ mag., and $U-B = -0.69$ mag.

Whether or not these corrections are applied, the star falls into the portion of the $U-B$ and $B-V$ diagram populated by the white dwarfs (Johnson and Morgan 1953). The occurrence of a star in this part of the diagram indicates either that the star is highly reddened by interstellar absorption or that it is intrinsically more luminous in the ultraviolet than a normal main-sequence star having the same $B-V$ color. Using either the corrected or the observed colors of DQ Her, a total visual absorption of about 1 mag. would be required to account for the location of the star in the diagram. The distance modulus of DQ Her has been determined by Baade (1940) from the linear expansion and radial velocity of the shell surrounding the star. From the major and minor axes of the elliptical shell, Baade derived distance moduli of 6.52 and 7.07 mag., or an average value of 6.8 mag. Combining this with the measured visual magnitude $V = 14.2$ from Table 6, the absolute visual magnitude of the nova is now $M_v = +7.4$. Thus the star is intrinsically faint and is so close to the sun that the amount of interstellar absorption should be fairly small; at the galactic latitude of DQ Her (25°), the average visual absorption for a star having a distance modulus of 6.8 mag. is only about 0.40 mag. Another possible source of absorption is provided by the debris of the nova explosion which surrounds the star. An estimate of this absorption can be made from the known size of the shell, the size of the star (discussed later), the amount of material ejected during the nova outburst (Whipple and Gaposchkin 1936), and the coefficients of interstellar absorption calculated by Greenstein (1937). Assuming that the composition of the ejected material is the same as that of the atmosphere of a normal star, the total absorption to be expected is only a few thousandths of a magnitude. It would seem, therefore, that the location of DQ Her in the $U-B$ and $B-V$ diagram must result primarily from an abnormal brightness of the star in the ultraviolet.

At the present time, very little is known concerning changes in the spectrum of the star during the 4-hour period. Figure 9 shows two spectra of DQ Her taken by Humason with the prime-focus nebular spectrograph on the 200-inch reflector. In general, the spectrum is still very similar in appearance to what it was in 1949 and 1950 (Swings and Jose 1949, 1952). The most striking change shown by Humason's plates is that the higher members of the Balmer series, which appear in emission at phase $0.57P$, have disappeared at $0.07P$. These lines thus must originate close to the stars and not in the sur-

FIG. 8.—Chart of the field surrounding nova DQ Her (1934), from a photograph with the 100-inch reflector. The scale is 6.78″/mm. DQ Her is indicated by the arrow. *A*, *B*, and *C* are the comparison stars referred to in the text.

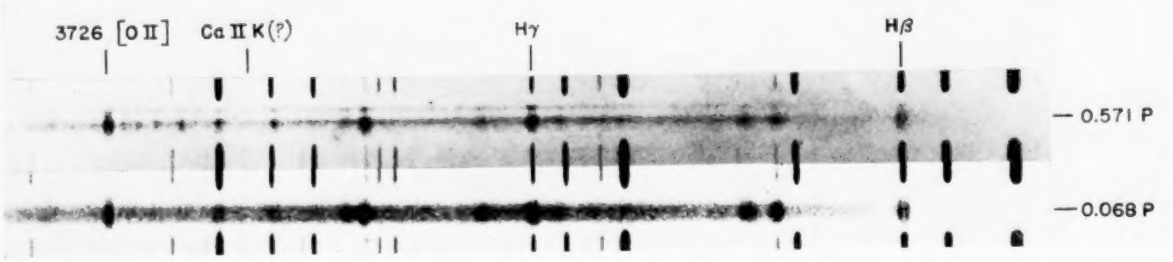

FIG. 9.—Spectra of DQ Her taken by M. L. Humason with the prime-focus nebular spectrograph on the 200-inch reflector. The upper plate was taken at JD 2434991.650, and the lower at JD 2434994.650.

rounding shell. Even so, velocities obtained from them might not reflect the true velocity of either of the stars. The Balmer continuum appears in emission at both phases. This is undoubtedly part at least of the explanation of the anomalous brightness of the star in the ultraviolet, as shown by the photoelectric observations. The spectrum shows practically no absorption features. There are indications of a few faint lines, but, with only a small number of plates available, their reality is very uncertain. One such feature occurs at the position of Ca II K. However, if it is real, it may be of interstellar origin; a weak interstellar K line was found by Williams (1935) during the outburst of the nova. Thus the prospects of obtaining the velocity-curve of the star do not appear very favorable. However, in view of the importance of this system, it is extremely desirable that velocity measurements be attempted.

We have already seen that the $B-V$ color of DQ Her is that of a star of spectral class A. On the other hand, if the spectrum were that of a normal A star, we should expect to see some trace of at least the wings of the strong hydrogen absorption lines. The absence of a strong Balmer absorption spectrum indicates either that the tempera-

TABLE 6

MAGNITUDES AND COLORS OF DQ HERCULIS

Helioc. JD 2434+	Phase ($P=1$)	V	$B-V$	$U-B$
983.688	0.450	14.18	0.00	−0.92
983.769	.870	14.24	− .11	− .73
983.872	0.400	14.16	+0.01	−0.84

TABLE 7

ADOPTED LEVELS OF UNIT INTENSITY

Date 1954	ΔM_y for Unit Intensity	Date 1954	ΔM_y for Unit Intensity
Aug. 1	0.000	Aug. 30	+3.700
29	+3.650	31	+3.650

ture of the star is much higher than that given by the color or that the hydrogen lines of the nova are abnormally weak. We have seen that the effect of interstellar reddening is too small to account for the observed color of the star. Consequently, the latter interpretation appears the more likely. It should be noted that the presence in the spectrum of emission lines such as He II 4686 also suggest a higher temperature than that of an A star. The cause of this discrepancy is not known. The abnormal brightness of the star in the ultraviolet might suggest that the lines of high excitation are somehow produced by very intense radiation in the far ultraviolet.

The photometric elements of the system have been derived from the yellow light-curve, since, as we have already discussed, it appears likely that this curve is least affected by the filling-in of radiation from the nebulosity surrounding the star. Owing to the variation in the brightness of the star outside eclipse, there is some uncertainty involved in choosing the proper unit of light-intensity. The adopted levels of unit intensity are given in Table 7. The elements were derived with the aid of the nomograms published by Merrill (1952, 1953*a*, *b*). In making the solution it was assumed that the secondary star is of zero brightness, that the coefficient of limb darkening is 0.6, and that the orbit is circular. Since the light-curve is of the Algol type, no corrections for ellipticity or reflection effect were required. Only the descending branch of the eclipse-curve was used in deriving the elements, owing to the asymmetry of the rising branch, discussed earlier.

Since the depth of eclipse and the shape of even the descending branch of the light-curve vary from cycle to cycle and since the depth of secondary eclipse is uncertain, there appeared to be little point in carrying out a very elaborate analysis of the eclipse-curve. In preparing the observations, the light-curve was obtained by simply drawing a free-hand curve through a plot of all the observations; normal points were not formed. The nomograms were then used to obtain only the first approximation to the elements. These elements are listed in Table 8, using Merrill's notation. Primary eclipse is an occultation. Consequently, the nova component has been designated throughout the remainder of the paper by the subscript s, while the slightly larger secondary star has been denoted by the subscript g. Figure 10 shows the fit of the elements to the observed light-curve. The ordinate of the eclipse-curve is intensity, in units of the uneclipsed light, while the abscissa is the phase in degrees. It appears from the figure that the representation of the observations is quite satisfactory, even from this first solution; the error of representation is less than the changes in the eclipse-curve from night to night, except possibly between phases $-23°$ to $-30°$. Some preliminary trials with other sets of elements and different

TABLE 8

ELEMENTS OF DQ HERCULIS

λ_1	0.286	e	0.00*
λ_2	1.000*	ρ_g	3.7 $\rho_\odot$†
Limb darkening	0.60*	ρ_s	6.6 $\rho_\odot$†
α_0^{∞}	0.716	Abs. vis. mag. of primary	+7.4
k	0.83 ± 0.07	Abs. vis. mag. of secondary	$\geq$ +10.7
L_g	< 0.05	T_e (primary)	10000° K‡
L_s	> 0.95	a	2.1×10^6 km§
J_g/J_s	< 0.0004	R_g	0.11 $R_\odot$§
r_g	0.366 ± 0.010	R_s	0.10 $R_\odot$§
r_s	0.30 ± 0.02	$m_g = m_s$*	6×10^{-3} $m_\odot$
i	76°.7 ± 1°.7		

* Assumed.

† Computed from the photometric elements, assuming equal masses.

‡ From observed $B - V$ color.

§ Calculated from absolute visual magnitude and T_e of primary.

degrees of limb darkening indicated that the fit of this part of the curve could not be materially improved. The discordance of this section of the curve is thus probably to be ascribed to some nongeometrical origin, such as gas streams surrounding the stars.

Interestingly, it is possible to fit a theoretical curve through the asymmetric rising branch. Using the same assumptions as before, one obtains the following elements for the rising branch: $k = 0.91$, $r_g = 0.38$, $i = 77°.3$. Since the light-curves show quite clearly that this branch of the eclipse-curve is abnormal, these elements have little weight. However, they suggest that even if the descending branch is also complicated by the presence of gas streams or clouds, the elements derived from it are not grossly in error.

If we assume a value of the mass ratio, the mean densities of the stars may be computed from the formulae given by Russell (1912). Taking the masses of the stars to be equal, their densities are $\rho_g = 3.7$ $\rho_\odot$, and $\rho_s = 6.6$ $\rho_\odot$.

As mentioned earlier, the color of the star is about $B-V = 0.00$, or $B-V = +0.09$ if some correction is made for light from the surrounding nebulosity, which cannot be excluded in measuring the star. For the purposes of this discussion, let us adopt the color $B-V = 0.00$, since the correction for the light of the nebula is rather uncertain and will be, to some extent, offset by the effect of any possible interstellar absorption. Owing to the abnormal brightness of the star in the ultraviolet, the $B-V$ color probably gives a more reliable estimate of the effective temperature of the star than would an

estimate which includes this ultraviolet radiation. If the other old novae are also anomalously bright in the ultraviolet, this could account for the extremely high temperatures which have been assigned to them (McLaughlin 1941), since these estimates have been based upon the length of the ultraviolet extension of the spectrum.

The effective temperature corresponding to $B-V = 0.00$ is about 10000° K. Adopting this value, the radius of the nova component may then be derived by means of the equation

$$\left(\frac{R}{R_\odot}\right)^2 = \frac{L}{L_\odot}\left(\frac{T_{e\odot}}{T_e}\right)^4.$$

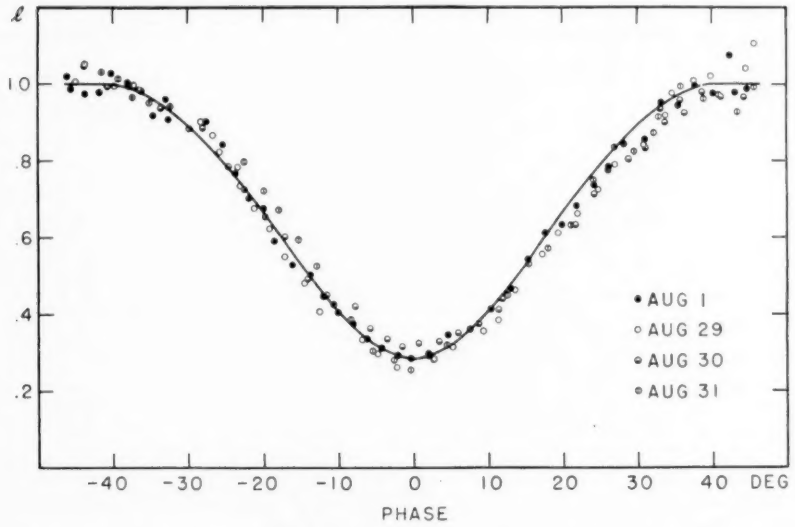

FIG. 10.—Primary eclipse of DQ Her in yellow light. The ordinate is the intensity in units of the uneclipsed light. The abscissa is the phase in degrees. The points represent individual observations. The solid line is the theoretical eclipse-curve computed from the elements given in Table 8.

Taking the absolute visual magnitude of the nova equal to +7.4, the radius of the nova becomes 0.10 $R_\odot$, while, from the ratio of the radii given by the photometric solution, the radius of the secondary star is 0.11 $R_\odot$, and the radius of the circular orbit becomes 0.31 $R_\odot$ or 2.1×10^5 km.

From the absence of a detectable secondary eclipse, we conclude that the secondary star must be at least 3.3 mag. fainter than the nova component. Thus its absolute visual magnitude must be $\geq +10.7$, which, for a main-sequence star, corresponds to a spectral type equal to or later than dM3. The radius derived here is also fairly consistent with that of a dwarf M star. However, the density is much too low and leads to a mass of only about 6×10^{-3} $m_\odot$. This is also the mass of the nova, since we have assumed that the mass ratio is unity. The mass of a late M dwarf is about 0.1 or 0.2 $m_\odot$, while the mass of an old nova has been assumed to lie in the range from 1.5 to 3 $m_\odot$ (McLaughlin 1941).

The possible sources of error in our determination of the masses of the components of DQ Her are: (1) an error in the distance modulus; (2) an error in the bolometric correction or in the effective temperature derived from the $B-V$ color, owing to the peculiar

energy distribution of the star; (3) an error in the assumed value of the mass ratio; and (4) an error in the photometric elements arising from some complication of the light-curve, either by the presence of detached clouds or streams of material in the system or by some unusual structure of the stars themselves, such as extended atmospheres.

While it might be possible to account for the discrepancy in the mass of the secondary star, it is very difficult to see how any of the first three of these sources of error could account for the smallness of the mass of the nova. For example, if we suppose that the distance modulus is in error and that the true mass of either star is 0.1 $m_\odot$ and that the densities given by the photometric elements are correct, then the error required in the distance modulus is 2.0 mag. Baade (1955) states that his estimate of the distance modulus (Baade 1940) could be in error by at least a magnitude. According to Baade, the relationship between absolute magnitude at maximum light and the rate of decline in brightness after maximum found by Arp for the novae in M31 gives a distance modulus for DQ Her of 7.8 mag., 1 mag. greater than the value derived from the expansion parallax. With this value of the distance, the radius of the nova is 0.14 $R_\odot$, the radius of the secondary is 0.17 $R_\odot$, and their masses are $m_s = m_g = 0.02\ m_\odot$. Thus an error in the distance modulus might account in large part for the discordance of the mass of the secondary star if, as we have assumed, it is actually a normal M dwarf. However, if the mass of the nova is to be 1.5 $m_\odot$, an error of 4.5 mag. is required in the distance modulus; an error of this size would appear to be completely out of the question. If the observed values of the distance and density are correct, the effective temperature would have to be 5450° K for a mass of 0.1 $m_\odot$ and 3600° K for a mass of 1.5 $m_\odot$. As we have seen, if any uncertainty exists, it is whether the temperature is still higher than the value of 10000° K used in these calculations. There remains the possibility of an error in the bolometric correction, because of the peculiar energy distribution of the old nova. Yet it is hard to see how such an error could be large enough to account for the abnormally small masses. Likewise, the small mass of the nova cannot be accounted for by an error in the assumed mass ratio. At most, this can amount to a factor of only 2.

Another explanation which can be ruled out is that the light-curve is produced by a dark spot on the surface of a single star. From the observed depth of eclipse in yellow light, it is clear that even if such a spot were completely dark, it would have to cover very nearly the entire hemisphere of the star. This, in turn, would require that the duration of the light-minimum be very nearly half the period. This conclusion would apply even if the star were completely darkened at the limb.

It is much more difficult to determine whether the small masses could result from an error in the photometric elements arising from some complication of the system. If the radius of the nova is 0.10 $R_\odot$ and the mass is 0.1 $m_\odot$, then the radius of the nova in terms of the radius of the orbit must be $r_s = 0.12$, while if the mass is 1.5 $m_\odot$, $r_s = 0.05$. These values are far outside the probable errors of the elements derived from the observed light-curve. It is easy to show that an error of this sort could not be introduced by the filling-in of the eclipse-curve by light from the shell. However, there is the possibility that the light-curve is not produced by a simple geometric eclipse of stars having sharp boundaries, whose distribution of surface brightness follows the ordinary law of limb darkening. It has already been pointed out that the detached material in the system, whose presence is indicated by the asymmetry of the eclipse-curve, probably has little effect upon the values of the elements. On the other hand, the discordance of the masses could very easily be accounted for if one or both of the stars were surrounded by an extended atmosphere. If this were so, one might expect that the light-curve could not be represented on the assumption of a simple geometric eclipse. The fact that the light-curve can be represented on this basis within the errors of observation means that if complications of some sort do exist, it is not possible to demonstrate that fact from the present material.

Thus we must conclude that if the photometric elements are reliable, the small mass

of the secondary star might be explained by the combined effects of errors in the distance modulus, temperature, bolometric correction, and mass ratio but that these sources of error are not sufficient to allow the mass of the nova to be as large at 1.5 $m_\odot$. The question of the reliability of the photometric elements must be left undecided; it is to be hoped that photoelectric observations over a period of years may help to clarify this problem.

Whipple and Gaposchkin (1936) have estimated the mass of material ejected by Nova Her up to the time of the great minimum to be between 3 and 13×10^{28} g. Even if the mass of the nova were only 6×10^{-3} $m_\odot$, this would amount only to between 2 and 11×10^{-3} of the mass of the nova. Consequently, despite the uncertainty in the mass of the nova, the fractional loss of mass remains very small; we are still correct in considering the nova phenomenon to be a rather "superficial" one which does not radically affect the structure of the star.

There are many striking similarities between DQ Her and the other known eclipsing binary of comparable period, UX UMa. The periods of the two systems are very nearly equal, that of UX UMa being only 4 minutes longer than the period of DQ Her. Both stars have Algol-type light-curves, and, in addition, both at times display shoulders before and after eclipse, asymmetry of the rising branch of the eclipse-curve, a minimum at about $0.7P$, and intrinsic variability (Linnell 1950; Johnson, Perkins, and Hiltner 1954; Walker and Herbig 1954). One difference is that the nearly continuous light-curves of UX UMa obtained in 1953 (Walker and Herbig 1954) show no trace of the 1-minute periodic fluctuations found in DQ Her; the variations in UX UMa appear to be completely random.

The colors of the two stars are also very similar. According to Harris (1955), provisional values of the average colors of UX UMa between $0.2P$ and $0.7P$ are: $B-V = +0.11$ mag., $U-B = -0.81$. The color variations throughout the 4-hour cycle are also somewhat similar. If one allows for the effect of light from the nebula around DQ Her, then both systems become redder during the minimum near $0.7P$ relative to their colors between phases $0.2P$ and $0.4P$. However, owing in all probability to the effect of light from the shell, DQ Her becomes bluer during primary eclipse, while UX UMa, whose light-curve is less obviously affected by extraneous radiation, becomes redder. The shape of the light-curves of DQ Her suggests the type of curve found by Johnson, Perkins, and Hiltner (1954) for UX UMa on May 29, 1952. Their curve for this date also appears to show the anomalous brightness of the system in blue light at $0.86P$ found in DQ Her. DQ Her does not show the anomalous brightness in the ultraviolet between phases $0.03P$ and $0.09P$ displayed by UX UMa (Walker and Herbig 1954); this feature may possibly be obscured in DQ Her by the effect of the nebular light upon the ultraviolet light-curve.

Linnell (1950) obtained densities for the components of UX UMa which are somewhat higher than those we have found for DQ Her. Assuming equal masses, Linnell obtained densities of 19 and 48 $\rho_\odot$ for the bright and faint components, respectively. We cannot accurately compare the luminosities or the values of the radii and masses of the two systems. No accurate value of the distance modulus is available for UX UMa. Moreover, the amplitude of the velocity-curve given by Struve (1948) has very low weight, since the spectroscopic observations of Walker and Herbig (1954) indicate that, at least at times, the observed velocities do not refer to the motions of the stars themselves.

In view of the similarities between the light-curves of the two systems, we are led to ask whether UX UMa could also be an old nova or a prenova. While we cannot answer this question at the present time, it appears likely that the features of the light-curve of DQ Her may be explained by the same sort of model that has been proposed by Walker and Herbig (1954) to account for the peculiarities of UX UMa—that is, that there exists a detached cloud of luminous material in the system which is occulted by the faint star during the asymmetric portion of the eclipse-curve. From the phase of the asymmetry,

the material must lie about $1\frac{1}{2}$ radii above the surface of the nova component. From the duration of the shoulder following eclipse, the luminous region must lie nearly at right angles to the line of centers of the stars. The diminution of light beginning at $0.5P$ could then be interpreted, as in UX UMa, as the result of absorption by a thin, dark extension of this luminous region which is seen projected against the disk of the nova. On this picture, the luminosity of the system ought to be greatest at $0.7P$, when the bright cloud is most favorably presented to view. To avoid this difficulty, we might suppose either that the cloud, though luminous, is cooler than the star and appears dark when seen projected against its surface or that the material is relatively opaque and that only the inner side next to the old nova is luminous. A complete spectroscopic and photometric analysis of the system will be required to determine whether either of these interpretations is possible.

It has been shown in connection with UX UMa (Walker and Herbig 1954) that if the foregoing model is correct, there should be a correlation between the bright shoulders and the asymmetry of the eclipse-curve, in that the asymmetry should never occur unless the bright shoulders are present, but that the converse might not always be true. Although only a small amount of material is available, there is some indication that this correlation occurs in DQ Her. This model does not account for the 1-minute periodic variations between $0.11P$ and $0.32P$.

It has been pointed out elsewhere (Walker 1954) that the binary nature of DQ Her raises several interesting questions regarding the evolution of a nova. Did a single star undergo fission during the nova stage in 1934, or has the present binary system existed since the initial formation of the stars? The fission hypothesis does not appear very plausible; the small fraction of the star's mass blown off in the nova explosion suggests that the phenomenon involves only the outer layers of the star. On the other hand, according to our present ideas of stellar evolution, a star which is now in the nova or post-nova stage must at one time have been a red giant. Thus, if the binary system has existed since the formation of the stars, we encounter the difficulty that during the time that the nova component was a red giant the secondary star, being very close to the primary, would have had to revolve deep within the expanded photosphere of the nova. Is it possible that somehow this star escaped going through the red giant stage in its evolution? Or was the system at one time more widely separated and the secondary, revolving in the resisting medium of the atmosphere of the red giant, slowed down by just the right amount to produce the close binary which we observe today? A theoretical investigation of these questions would be highly desirable.

Some of the answers to these problems might be provided by a thorough study of all the plates showing DQ Her taken before the 1934 explosion. It is to be noted that no perceptible light-variation was found by Boyd (1934), who examined the 19 pre-outburst plates of DQ Her in the Harvard collection; by Van Biesbroeck (1934), who examined two Yerkes plates; or by Morgenroth (1935), who examined 74 Sonnenberg plates taken between August 1, 1930, and November 3, 1934. However, it is impossible at this time to say how much significance should be attached to these results, since the dates and lengths of exposures are not given and since we do not yet have a sufficiently accurate value of the period to be able to predict when the minima should have occurred prior to the outburst. It will clearly be of great importance to obtain accurate times of minimum light for this system, both to investigate the question of eclipses prior to 1934 and to determine whether the length of the period is changing as a result of continued loss of mass since the nova stage.

The binary nature of DQ Her also raises the question whether all novae are binaries, the nova phenomenon resulting in some manner from the binary nature of the systems. The composite spectrum of T CrB shows that it is double, and Joy's (1954) recent spectroscopic study of the nova-like variable AE Aqr shows that it, too, is a spectroscopic binary. In addition, SS Cyg is known to have a variable radial velocity (Joy 1943)

and may also be a spectroscopic binary. However, this is no indication that all novae are binaries. Indeed, what we know concerning the evolution of stars suggests that the nova phenomenon is only one stage in the aging of any star having the proper initial configuration.

It is a pleasure to thank Dr. M. L. Humason for arranging for additional observing time with the 100-inch reflector in order to permit a more comprehensive investigation of the star; Dr. A. Sandage for assisting the writer at the telescope on three nights; and Dr. B. Oke for permission to publish two times of minimum light observed by him. The writer is also indebted to Drs. W. Baade and G. H. Herbig for several stimulating discussions of the problems raised by this system.

REFERENCES

Baade, W. 1940, *Pub. A.S.P.*, **52,** 386.
———. 1955, private communication.
Boyd C. 1934, *Harvard Anno. Card*, No. 321.
Greenstein, J. L. 1937, *Harvard Circ.*, No. 422.
Harris, D. L. 1955, private communication.
Johnson, H. L., and Morgan, W. W. 1953, *Ap. J.*, **117,** 313.
Johnson, H. L., Perkins, B., and Hiltner, W. A. 1954, *Ap. J. Suppl.*, **1,** 91 (No. 4).
Joy, A. H. 1943, *Pub. A.S.P.*, **55,** 283.
———. 1954, *Ap. J.*, **120,** 377.
Linnell, A. P. 1950, *Harvard Circ.*, No. 455.
McLaughlin, D. B. 1941, *Pop. Astr.*, **49,** 292.
Merrill, J. E. 1952, *Contr. Princeton U. Obs.*, No. 26.
———. 1953*a*, *ibid.*, No. 23.
———. 1953*b*, *ibid.*, No. 24.
Morgenroth, O. 1935, *A.N.*, Vol. **254,** Beilage to No. 6076.
Russell, H. N. 1912, *Ap. J.*, **36,** 54.
Struve, O. 1948, *Ap. J.*, **108,** 153.
Swings, P., and Jose, P. D. 1949, *Ap. J.*, **110,** 475.
———. 1952, *ibid.*, **116,** 229.
Van Biesbroeck, G. 1934, *Harvard Anno. Card*, No. 320.
Walker, M. F. 1954, *Pub. A.S.P.*, **66,** 230.
Walker, M. F., and Herbig, G. 1954, *Ap. J.*, **120,** 278.
Whipple, F., and Gaposchkin,C. P. 1936, *Harvard Circ.*, No. 413.
Williams, E. G., 1935, *M.N.*, **95,** 573.

DIMENSIONS OF CONTACT SURFACES IN CLOSE BINARIES

G. P. KUIPER AND JEANNETTE R. JOHNSON

Yerkes Observatory

Received July 27, 1955

ABSTRACT

In this paper the calculated dimensions are given of the innermost and outermost equipotential contact surfaces for close binaries of different mass ratios. They are based on the Roche model.

Two fields of study require a knowledge of the numerical properties of certain critical equipotential surfaces in close binary systems: (1) the binary stars themselves and (2) problems of planet and satellite formation. In the course of such studies a number of these surfaces were computed, and these data are collected here for ready reference.

The model considered is that of two finite masses having a specified mass ratio and moving in a circular relative orbit. Each mass is assumed to be sufficiently concentrated

TABLE 1

DIMENSIONS OF THE INNERMOST CONTACT SURFACE

μ	$x(L_1)$	$\Omega(L_1)$	$a_1' = x_1 - 1 + \mu$	$a_1'' = 1 - \mu - L_1$	b_1	c_1
0.50	0.0000000	2.0000000	0.404980	0.500000	0.374046	0.356131
.40	.1416175	1.9904543	.369575	.458382	.337554	.322723
1/3	.2374182	1.9727853	.345369	.429249	.312882	.299768
2/7	.3072332	1.9537420	.327202	.407053	.294526	.282532
.25	.3607434	1.9353294	.312786	.389257	.280065	.268874
.20	.4380760	1.9023266	.290871	.361924	.258267	.248176
.10	.6090351	1.7984766	.234931	.290965	.203733	.195972
.05	.7152254	1.7102082	.191180	.234775	.162307	.156092
.02	.8034656	1.6261631	.145838	.176534	.120671	.115952
.01	.8480787	1.5838206	.118672	.141921	.096439	.092603
.005	.8811683	1.5549648	.096381	.113832	.077013	.073901
.002	.9132185	1.5310240	.072978	.084781	.057119	.054771
.001	.9312870	1.51997439	.058996	.067713	.045514	.043624
.0001	.9680652	1.50449463	.028758	.031835	.021301	.020397
.00001	.9851267	1.50098751	.013817	.014863	.009926	.009500
0.000001	0.9930814	1.50021467	0.006569	0.006918	0.004615	0.004416

toward its center for the Roche model to apply on the outer surfaces of interest. The equipotential surfaces are then given by

$$-\Omega = \frac{1-\mu}{r_1} + \frac{\mu}{r_2} + \frac{x^2+y^2}{2}, \tag{1}$$

in which Ω is the (negative) potential and r_1 and r_2 are the distances of a point (x, y, z) to the mass centers, $M_1 = 1 - \mu$ and $M_2 = \mu$; the co-ordinate system is rotating with the binary, the z-axis is the axis of rotation, the x-axis runs through the two mass centers, and the origin is at the center of gravity. The units are the distance between the centers = 1; total mass = 1; angular velocity = 1 (or period = 2π).

On the axis there are three points where $\partial\Omega/\partial x = 0$; they correspond to the Lagrangian points L_1, L_2, and L_3 of the restricted three-body problem. The equipotential surface through L_1 (between the stars) is the *innermost contact surface;* that through L_2, the *outermost contact surface* (cf. Kuiper 1941*a*). The former gives the dimensions of the two

components that will just insure contact. It will also (for a given μ) define the largest possible dimension of a stable protoplanet moving around the sun or of a protosatellite near a planet (provided that the Roche approximation applies). The outer contact surface has found application in the study of flow within close binary systems (Kuiper 1941*b*).

The calculations proceed as follows: the conditions $\partial\Omega/\partial x = 0$ and $y = z = 0$ fix for each value of μ the x co-ordinates of L_1 and L_2. These values and equation (1) fix Ω_1 and Ω_2. Thereupon, the lengths of the axes a', a'', b, and c are found from equation (1); a' is the outward radius measured along the x-axis, and a'' is the inward radius. The shape of the surface can be further defined by the study of its three orthogonal sections parallel to the co-ordinate planes; for suitably chosen values of two co-ordinates, the third co-ordinate is found from equation (1). In this paper we give only the section in the xy-plane.

The results are contained in Tables 1–4 and Figures 1–2. The mass ratios listed are,

TABLE 2

DIMENSIONS OF THE OUTERMOST CONTACT SURFACE

μ	$x(L_2)$	$\Omega(L_2)$	$a_2' = L_2 - 1 + \mu$	b_2	c_2	$b(L_1)$	$c(L_1)$
0.50..	1.1984062	1.7283981	0.698406	0.482281	0.436616	0.326078	0.291108
.40...	1.2308138	1.7594673	.630814	.427135	.391841	.295611	.265766
1/3....	1.2490474	1.7737291	.582380	.390172	.360606	.273607	.246635
2/7....	1.2596665	1.7794671	.545381	.363015	.337123	.256583	.231509
.25...	1.2658581	1.7805970	.515858	.341888	.318579	.242821	.219129
.20...	1.2710487	1.7761966	.471049	.310575	.290699	.221565	.199819
.10...	1.2596999	1.7333422	.359700	.235529	.222325	.166493	.149289
.05...	1.2280937	1.6771971	.278094	.181991	.172544	.124133	.110482
.02...	1.1800779	1.6128666	.200078	.131245	.124833	.082911	.073147
.01...	1.1467650	1.5771597	.156765	.103077	.098186	.060451	.053058
.005...	1.1181889	1.5516319	.123189	.081186	.077414	.043751	.038254
.002...	1.0878645	1.5296905	.089864	.059382	.056677	.028293	.024652
0.001...	1.0699161	1.5193076	0.070916	0.046939	0.044825	0.020250	0.017613

first, the five values used before by one of us (Kuiper 1941*c*) and, second, a number of smaller μ-values, of interest primarily in planetary problems. The present results are computed to more decimals and, to that extent, supersede the earlier values.

The figures give the sections in the plane of the relative orbit (xy-plane). The shapes of the surfaces are remarkably similar for the very large range of mass ratios, though there is clearly an increase in the ellipticity toward the smaller values of μ. This is shown also in Table 5, which lists the values of b/a' and c/a' because of the ambiguity as to how to round off the point at L_1. If the motion of a particle, assumed to remain with the secondary mass, is zero in the rotating frame, its maximum allowed distance from the center of the secondary mass is given by the inner contact surface. If its motion in the rotating frame is not zero, as is true for a satellite moving around a planet, which, in turn, revolves around the sun, then the satellite must be closer to the planet, approximately by a factor of 2, as follows from energy considerations.

It is useful to have an interpolation formula giving the dimensions of the inner contact surface (or *radius of action*, R_A), as a function of μ. Because the surface is pointed at L_1, the definition of R_A is somewhat arbitrary. Table 6 gives the values of a found graphically by rounding off the point. Then R_A, computed for the xy-plane only, follows. The equation

$$\log \frac{R_A}{a_P} = 0.318 \log \mu - 0.327 \qquad (2)$$

TABLE 3

SECTION OF INNERMOST CONTACT SURFACE IN xy-PLANE

$\mu = 0.50$		$\mu = 0.40$		$\mu = 1/3$		$\mu = 2/7$	
x	$\pm y$	x	$\pm y$	x	$\pm y$	x	$\pm y$
−0.15	0.2041	0.0000	0.2023	0.1000	0.2028	0.15	0.2318
.00	.0000	.1416	.0000	0.2374	.0000	0.3072	.0000
+ .20	.2520	.35	.2467	0.40	.2022	0.50	.2205
+ .50	.3740	.60	.3376	2/3	.3129	5/7	.2945
+ .75	.2981	.85	.2520	0.85	.2606	0.95	.2069
+0.9050	0.0000	0.9696	0.0000	1.0120	0.0000	1.0415	0.0000

$\mu = 0.25$		$\mu = 0.20$		$\mu = 0.10$		$\mu = 0.01$		$\mu = 0.001$	
x	$\pm y$	x	$\pm y$	x	$\pm y$	x	$\pm y$	x	$\pm y$
0.20	0.2405	0.3500	0.1436	0.5000	0.1899	0.7750	0.1700	0.9100	0.05116
0.3607	.0000	0.4381	.0000	0.6090	.0000	0.8481	.0000	0.9313	.00000
0.55	.2131	0.6000	.1867	0.7250	.1371	0.9250	.07895	0.9550	.02869
0.75	.2801	0.8000	.2583	0.9000	.2037	0.9900	.09644	0.9990	.04551
0.90	.2483	1.0000	.1895	1.0500	.1576	1.0550	.07980	1.0300	.03767
1.0628	0.0000	1.0909	0.0000	1.1349	0.0000	1.1087	0.00000	1.0580	0.00000

TABLE 4

SECTION OF OUTERMOST CONTACT SURFACE IN xy-PLANE

$\mu = 0.5$		$\mu = 0.4$		$\mu = 1/3$		$\mu = 2/7$	
x	$\pm y$	x	$\pm y$	x	$\pm y$	x	$\pm y$
−0.15	0.3710	0.00	0.3545	0.10	0.3427	0.15	0.3510
−0.08	.3412	0.1416	.2956	0.18	.2931	0.23	.2922
0.00	.3261	0.30	.3377	0.2374	.2736	0.3072	.2566
+0.10	.3488	0.50	.4120	0.40	.3143	0.45	.2868
+0.25	.4175	0.60	.4271	0.55	.3706	0.60	.3438
+0.50	.4823	0.75	.4180	2/3	.3902	5/7	.3630
+0.70	.4658	0.95	.3403	0.85	.3706	0.90	.3401
+0.90	.3796	1.10	.2133	1.00	.3027	1.05	.2641
+1.05	.2506	1.2308	0.0000	1.10	.2224	1.15	.1732
+1.1984	0.0000			1.2490	0.0000	1.2597	0.0000

$\mu = 0.25$		$\mu = 0.20$		$\mu = 0.10$		$\mu = 0.01$		$\mu = 0.001$	
x	$\pm y$	x	$\pm y$	x	$\pm y$	x	$\pm y$	x	$\pm y$
0.20	0.3498	0.35	0.2776	0.50	0.2740	0.775	0.19724	0.91	0.06128
0.30	.2712	0.4381	.2216	0.55	.2137	0.82	.094669	0.92	.03468
0.3607	.2428	0.58	.2503	0.6090	.1665	0.8481	.06045	0.9313	.02025
0.50	.2707	0.68	.2888	0.70	.1772	0.89	.069878	0.9533	.03250
0.62	.3178	0.80	.3106	0.80	.2175	0.94	.094038	0.976	.04286
0.75	.3419	0.95	.2927	0.90	.2355	0.99	.1031	0.999	.04694
0.90	.3269	1.05	.2495	1.00	.2247	1.03	.098362	1.017	.04465
1.05	.2597	1.18	.1413	1.08	.1929	1.07	.081969	1.035	.03712
1.15	.1752	1.2710	0.0000	1.18	.1157	1.12	.039597	1.053	.02291
1.2659	0.0000			1.2597	0.0000	1.1468	0.000000	1.0699	0.00000

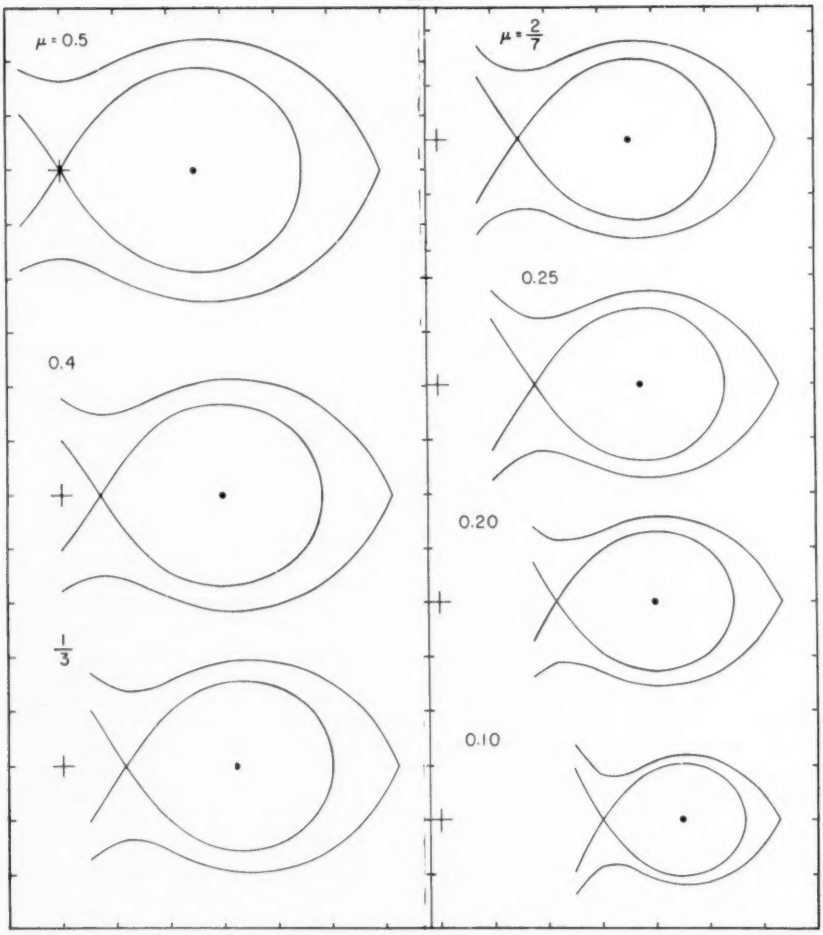

FIG. 1.—Inner and outer contact surfaces for secondary components of different μ-values. Marginal divisions are 0.2 apart. Cf. Tables 3 and 4. Each cross indicates the position of the center of mass.

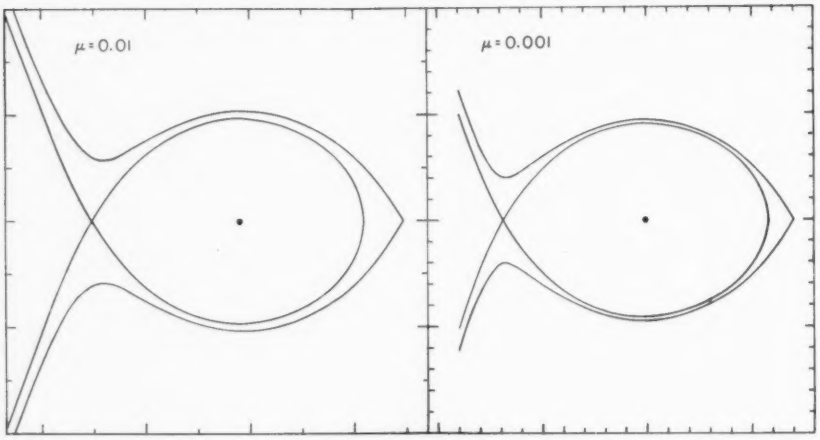

FIG. 2.—Same as Fig. 1, but divisions are 0.05 apart (*left*) or 0.01 (*right*)

TABLE 5

RATIOS OF AXES OF INNERMOST CONTACT SURFACE

μ	b/a'	c/a'	μ	b/a'	c/a'	μ	b/a'	c/a'
0.5	0.9236	0.8794	0.10	0.8672	0.8342	0.001	0.7715	0.7394
0.25	0.8954	0.8596	0.01	0.8127	0.7803	0.000001	0.7025	0.6722

TABLE 6

REPRESENTATION OF EQUATION (2)

μ	a	b	$R(x, y)$	Δ	μ	a	b	$R(x, y)$	Δ
0.5	0.415	0.374	0.395	+0.020	10^{-3}	0.0606	0.0455	0.053	+0.005
0.4	.38	.338	.359	+ .009	10^{-4}	.0295	.0213	.0254	+ .004
0.25	.325	.280	.302	− .001	10^{-5}	.0142	.0099	.0120	− .004
10^{-1}	.244	.204	.224	− .005	10^{-6}	0.0068	0.0046	0.0057	−0.009
10^{-2}	0.122	0.096	0.109	0.000					

was found to represent the R_A-values quite well (Kuiper 1951). This is shown in Table 6, where Δ represents the residual (left term − right term). Hence R_A can be found from equation (2) with a precision of 1 per cent or better in the range $10^{-5} < \mu < 0.3$.

REFERENCES

Kuiper, G. P. 1941*a*, *Ap. J.*, **93**, 137, 141.
———. 1941*b*, *ibid.*, pp. 150 f.
———. 1941*c*, *ibid.*, p. 140.
———. 1951, *Proc. Nat. Acad. Sci.*, **37**, 717.

THE DEBYE-HÜCKEL EFFECT AND STATISTICAL THEORIES FOR COLLISION BROADENING

FRANK N. EDMONDS, JR.

Department of Mathematics and Astronomy, University of Texas, Austin, Texas

Received June 27, 1955

ABSTRACT

The theory of Debye and Hückel for electrolytes is shown to be valid and pertinent for ionized gases of astrophysical interest. Corrections to statistical theories of collision broadening due to the Debye-Hückel effect are shown to be negligible in the cases of linear and quadratic Stark broadening of the spectral lines of ions. In Appendix I, Debye-Hückel effect corrections are calculated for the related problem of the average distance to the nearest charged particle.

I. INTRODUCTION

The collision broadening of certain stellar absorption lines can be described by the theories of statistical broadening. However, it is now evident that such descriptions are not entirely satisfactory. Kolb (1954) and Doherty and Aller (1954) have pointed out the inability of the Holtzmark theory to predict the linear Stark broadening of hydrogen lines, and Minnaert (1953) has summarized the adequacy of statistical-broadening descriptions for the sun. One possible improvement to the statistical theories of collision broadening would be to account for the Debye-Hückel effect of electrostatic forces between charged particles. This effect is the tendency of a charged particle to be surrounded by particles of opposite charge, to the exclusion of those of like charge. It seems probable that corrections to statistical-broadening theories due to the Debye-Hückel effect would be too small to explain discrepancies between theory and observations in astronomical spectra. Margenau and Meyerott (1955) have shown that polarization energies for hydrogen, in which account is taken of the Debye-Hückel effect, would produce very small corrections to statistical broadening.

In this paper corrections for linear or quadratic Stark broadening of spectral lines of ions are considered. The validity of the Debye-Hückel theory for ionized gases is established for values of density and temperature of astrophysical interest. Corrections to collision-broadening profiles as calculated by this theory are shown to be very small and restricted to the far wings of the profile, as would be expected. In Appendix I the Debye-Hückel theory is used to calculate the average distance to the nearest charged particle.

II. THE DEBYE-HÜCKEL EFFECT

The Debye-Hückel theory for solutions of electrolytes is discussed in some detail by Fowler and Guggenheim (1939). In §§ 910 and 911 of their discussion, an expression is derived for $\psi(r)$, the average electrostatic potential at a distance r from an ion of charge $Z_0\epsilon$, where ϵ is the electronic charge in electrostatic units and the sign of the charge is accounted for by the sign of Z_0. In this derivation two approximations are made which are fundamental to the Debye-Hückel theory. One expresses a relation, equation (910.1) in Fowler and Guggenheim's discussion, between $\psi(r)$ and the average "free energy" of another particle with charge $Z_j\epsilon$ located in the potential field $\psi(r)$. Of greater importance to present considerations is the mathematical approximation made in solving the Poisson-Boltzmann equation for $\psi(r)$. It is assumed that

$$\frac{|Z_j|\epsilon\psi(r)}{kT} \ll 1, \tag{1}$$

where k is Boltzmann's constant and T is absolute temperature; in this approximation all terms involving powers higher than the first of expression (1) are neglected. The expression for $\psi(r)$ obtained is

$$\psi(r) = \left(\frac{Z_0\epsilon\, e^{\kappa a}}{1+\kappa a}\right)\frac{e^{-\kappa r}}{r}, \tag{2}$$

where a is the effective radius or closest distance of approach for the ion and

$$\kappa = \left(\frac{4\pi\epsilon^2}{kT}\sum_j N_j Z_j^2\right)^{1/2}. \tag{3}$$

In equation (3) the summation over j represents summation over the various types of charged particles (ions and free electrons), with N_j being the number per cubic centimeter. Substitution of $\psi(r)$ in Poisson's equation gives a mean electrostatic charge density surrounding the ion of $-\kappa^2\psi(r)/4\pi$. Using this density, Fowler and Guggenheim, in § 912 of their discussion, show that the total charge surrounding the ion is $-Z_0\epsilon$, thereby satisfying the requirement of electrical neutrality. Also, in § 914 of their discussion, they show that $4\pi r^2$ times the charge density of this "ionic atmosphere" attains a maximum at

$$r_m = \kappa^{-1}. \tag{4}$$

This distance r_m is called the "mean radius of the ionic atmosphere" and represents the distance at which the concentration of charge in the atmosphere is a maximum.

The potential $\psi(r)$ as given by equation (2) holds only for $r \geq a$, and, as an additional meaning or definition of a, it is assumed that in the region $r \geq a$ classical mechanics is valid. It therefore follows from Boltzmann's principle that the probability of finding an ion or free electron of charge $Z_j\epsilon$ at a distance r is proportional to $\exp[-Z_j\epsilon\psi(r)/kT]$. The function describing this probability used in this discussion must be normalized so that it will approach unity (corresponding to a random distribution) as r approaches infinity. Hence such a probability function will be given by

$$\tau_j(r) = \exp\left[\frac{-Z_j\epsilon\psi(r)}{kT}\right] \tag{5}$$

$$= 1 - \frac{A_j}{r}\, e^{-\kappa r} \qquad (r \geq a),$$

and

$$\tau_j(r) \equiv 0 \qquad (r < a), \tag{6}$$

where

$$A_j = \frac{Z_0 Z_j \epsilon^2 e^{\kappa a}}{kT(1+\kappa a)}. \tag{7}$$

The final form of $\tau_j(r)$ for $r \geq a$ given by equation (5) is consistent with the approximations made in the Debye-Hückel theory in accordance with condition (1), while the form for $\tau_j(r)$ given by equation (6) is consistent with the physical meaning of a. The second term in equation (5) and equation (6) can be considered as Debye-Hückel effect modifications to a random distribution, for which $\tau_0(r) \equiv 1$. It must be pointed out that no change in the normalization of $\tau_j(r)$ has been made to account for these modifications. In fact, the form of $\tau_0(r)$ for a random distribution prevents such normalizations. The integral of $\tau_0(r)$ over all r diverges, and so the Debye-Hückel modifications to $\tau_0(r)$ essentially combine a finite contribution with an infinite one. However, consistent with the approximations made in accordance with condition (1),

$$\sum_j N_j Z_j \epsilon\, \tau_j(r) = -\frac{\kappa^2}{4\pi}\psi(r). \tag{8}$$

This indicates that the probability function $\tau_j(r)$ does give the mean charge density of the ionic atmosphere, thereby insuring electrical neutrality.

The application of the Debye-Hückel theory to gases containing ions and free electrons raises two questions—the value of a and whether condition (1) is satisfied for the important regions of the ionic atmosphere. Seemingly, no direct method for determining a is known. Furthermore, any attempt to evaluate it by comparison between theory and experiment would probably lead to the same difficulties as those experienced with electrolytes, namely, that a must be considered "a parameter correcting for a whole variety of theoretical imperfections" rather than an effective radius. Starting with the requirement that classical mechanics is valid in the region $r \geq a$, Williamson (1946) sets a at that value of r for which the mean kinetic energy of translation of particles in the gas is equal to the potential energy of electrostatic interaction, i.e., when

$$\frac{|Z_j Z_0|\epsilon^2}{a_j} = \frac{3}{2}kT. \tag{9}$$

This gives an effective radius a_j for each type of charged particle. For stellar temperatures, equation (9) gives values of $a_j \sim 10^{-7}$ cm, which are somewhat larger than actual ionic radii. Equation (9) probably would hold with equal satisfaction for the higher temperatures of stellar interiors, but for lower temperatures it would give values of a_j which are probably too large. Determinations of a_j for electrolytes at room temperatures indicate values in the range 10^{-8}–10^{-7} cm. In this discussion values of a_j given by equation (9) will be used.

As indicated by equation (2), $\psi(r)$ monotonically increases with decreasing r. This means that condition (1) will not be satisfied for r sufficiently small; and in such a region of small r the use of $\psi(r)$ is not valid. A question pertinent to the use of $\psi(r)$ in the present discussion is, therefore, whether this region over which $\psi(r)$ is not valid extends into regions playing an important role in statistical theories of collision broadening. A related question which must be answered first is whether the ionic atmosphere itself extends into such regions. Let b_j be that value of r at which

$$\frac{|Z_j|\epsilon\psi(b_j)}{kT} = 10^{-1/2}. \tag{10}$$

Then, for $r > b_j$, $\psi(r)$ may be used with at least 10 per cent accuracy. One way of answering these questions concerning the valid use of $\psi(r)$ would be to compare r_m for various values of T and N_j with a_j, b_j, and d_j, the average distance of the nearest charged particle. The determination of d_j is discussed in Appendix I. This comparison is made in Table 1 for

$$|Z_j| = |Z_0| = 1 \qquad \text{and} \qquad N_j = \frac{1}{2}\sum_i N_j,$$

where d_- is for a particle with the same charge as the ion at $r = 0$ and d_+ is for a particle with opposite charge. From Table 1 the following conclusions can be made regarding this comparison.

1. For all values of T and N_j of astrophysical importance,

$$r_m > d_j > b_j > a_j. \tag{11}$$

This indicates that only a minor innermost portion of the ionic atmosphere lies in the small r region where $\psi(r)$ is not valid. Furthermore, the application of the Debye-Hückel effect to statistical theories of collision broadening will be valid, as the nearest charged particle or perturber will be located predominantly outside the small r region where $\psi(r)$ is not valid. Finally, the Debye-Hückel effect should be pertinent to statistical

theories of collision broadening, as the nearest charged particle or perturber will be located predominantly in the ionic atmosphere.

2. The first two inequalities in expression (11) increase with decreasing N_j for a fixed T or with increasing T for a fixed N_j, the dependence on T being much more critical. A lower limit for T or upper limit for N_j can be set at which these inequalities no longer hold and the application of the Debye-Hückel effect is no longer valid or pertinent. These limits are roughly indicated by

$$T \geq R N_j^{1/3}, \tag{12}$$

where, for the calculations performed in Table 1, $R \simeq 0.02$.

3. Though the portion of the ionic atmosphere for which $\psi(r)$ is not valid is a minor one, it is not negligible except for extremely low densities. The representation of $\tau_j(r)$ in this region poses a difficult problem. As Fowler and Guggenheim (1939) show in §§ 921 and 924 of their discussion, attempts to improve on the Debye-Hückel theory have not been successful. Since b_j never exceeds a_j by more than 4.75 (by less when the limits indicated by expression [12] are approached), perhaps the best working assumption would be to let $\psi(r)$ extend down to a_j, using the exponential form of equation (5). An alterna-

TABLE 1*

MEAN RADIUS (CM) OF THE IONIC ATMOSPHERE r_m FOR $|Z_0| = |Z_j| = 1$ AND $N_j = \frac{1}{2}\sum_j N_j$

ABSOLUTE TEMPERATURE (T °K)	NUMBER OF CHARGED PARTICLES PER CUBIC CENTIMETER (N_j)				
	10	10^{12}	10^{15}	10^{18}	10^{21}
10^2	15.5	4.90×10^{-5}			
	$=1.40\times10^{6}\ a_j$	$=4.42\ a_j$			
	$=2.94\times10^{5}\ b_j$	$=1.57\ b_j$			
	$=59.5\ d_+$	$=0.885\ d_0$			
	$=59.5\ d_-$				
	$=59.5\ d_0$				
3×10^2	26.9	8.40×10^{-5}	2.69×10^{-6}		
	$=7.27\times10^{6}\ a_j$	$=22.7\ a_j$	$=0.727\ a_j$		
	$=1.53\times10^{6}\ b_j$	$=5.95\ b_j$	$=0.604\ b_j$		
	$=105\ d_+$	$=1.52\ d_0$	$=0.486\ d_0$		
	$=105\ d_-$				
	$=105\ d_0$				
3×10^3	84	2.69×10^{-4}	8.40×10^{-6}	2.69×10^{-7}	
	$=2.27\times10^{6}\ a_j$	$=727\ a_j$	$=22.7\ a_j$	$=0.727\ a_j$	
	$=4.77\times10^{5}\ b_j$	$=153\ b_j$	$=5.95\ b_j$	$=0.604\ b_j$	
	$=327\ d_+$	$=4.80\ d_+$	$=1.52\ d_0$	$=0.486\ d_0$	
	$=327\ d_-$	$=4.92\ d_-$			
	$=327\ d_0$	$=4.86\ d_0$			
3×10^4	269	8.40×10^{-4}	2.69×10^{-5}	8.40×10^{-7}	2.69×10^{-8}
	$=7.27\times10^{6}\ a_j$	$=2.27\times10^{4}\ a_j$	$=727\ a_j$	$=22.7\ a_j$	$=0.727\ a_j$
	$=1.53\times10^{6}\ b_j$	$=4.77\times10^{3}\ b_j$	$=153\ b_j$	$=5.95\ b_j$	$=0.604\ b_j$
	$=1.05\times10^{3}\ d_+$	$=15.2\ d_+$	$=4.80\ d_+$	$=1.52\ d_0$	$=0.486\ d_0$
	$=1.05\times10^{3}\ d_-$	$=15.2\ d_-$	$=4.92\ d_-$		
	$=1.05\times10^{3}\ d_0$	$=15.2\ d_0$	$=4.86\ d_0$		

* For $T = 10^2$ and $N_j = 10^{18}$, $r_m = 1.55\times10^{-9} = 14.0\ a_j = 4.68\ b_j = 1.30\ d_0$.

tive with slightly less justification but with the advantage of mathematical simplicity would be to replace equations (5) and (6) by

$$\begin{aligned} \tau_j(r) &= 1 - \frac{A_j}{r}\, e^{-\kappa r} && (r \geq \tfrac{3}{2} a_j) \\ &\equiv 0 && (r < \tfrac{3}{2} a_j)\,. \end{aligned} \tag{13a}$$

For a_j given by equation (9), this insures that $\tau_j(r)$ will remain positive.

It has been established, therefore, that Debye-Hückel effect corrections to statistical-broadening theories are pertinent and valid. There remains the question of the importance or magnitude of these corrections. This question will be examined in Section III, but some indication might be given by the differences between d_+, d_-, and d_0, the average distance of the nearest charged particle when the Debye-Hückel effect is neglected. These differences, determined in Appendix I and given in Table 1, are small except near the limits imposed by inequality (12).

The expression for $\tau_j(r)$ given by equation (13*a*) will be used in this discussion. However, another possibility, though mathematically more complex, has the advantage that the value of a_j would not critically determine the form of $\tau_j(r)$. As indicated by equations (3) and (7), $\kappa \gg A_j$ and A_j is essentially independent of a_j, provided that a_j is small. The inequality holds without any restriction on T and N_j; the independence of A_j holds for values of T and N_j satisfying inequality (12). Hence, representing $\tau_j(r)$ for all values of r by

$$\tau_j(r) = 1 - \frac{A_j}{r + A_j}\, e^{-\kappa r} \tag{13b}$$

for A_j positive (Z_0 and Z_j of like sign) and by

$$\tau_j(r) = 1 - \frac{A_j}{r - A_j}\, e^{-\kappa r} - 2\, e^{r/A_j} \tag{13c}$$

for A_j negative (unlike sign) effectively removes the dependence of $\tau_j(r)$ on a_j by replacing the discontinuity at $r = \frac{3}{2}a_j$, as given by equation (13*a*), by a smooth approach to zero at $r = 0$. These representations closely approximate the results of the Debye-Hückel theory for $r > b_j$, and seemingly they are just as good representations as equations (5) and (6) or (13*a*) for $r < b_j$.

III. CORRECTIONS TO STATISTICAL-BROADENING PROFILES

The formulation of statistical-broadening theories to be considered in this discussion follows Holtsmark's theory for the linear Stark effect, in which the broadening profile is the probability function of a given electric field resulting from all possible ion configurations. This formulation, using a method first devised by Markoff, is described in chapters 1 and 4 of Chandrasekhar's review (1943), and its mathematics have been generalized to include various types of force fields (Chandrasekhar 1949). The force field due to a class of identical particles of charge $Z_j\epsilon$ may be represented by

$$\boldsymbol{F}_{nj} = C_{nj} \sum_{k=1}^{\infty} \frac{\boldsymbol{r}_k}{r_k^{n+1}}\,, \tag{14}$$

where $\boldsymbol{r}_k$ is the position vector to the kth particle, $r_k = |\boldsymbol{r}_k|$, and

$$\begin{aligned} C_{2j} &= Z_j\epsilon && \text{(linear Stark effect, } n = 2)\,, \\ C_{4j} &= (Z_j\epsilon)^2 && \text{(quadratic Stark effect, } n = 4)\,. \end{aligned} \tag{15}$$

The probability distribution of $\boldsymbol{F}_{nj}$ is given by

$$W(\boldsymbol{F}_{nj}) = \frac{1}{8\pi^3}\int_{-\infty}^{\infty} \exp\left[i\boldsymbol{\varrho}\cdot\boldsymbol{F}_{nj} - N_j D_j(\boldsymbol{\varrho})\right] d\boldsymbol{\varrho}\,, \tag{16}$$

where

$$D_j(\boldsymbol{\varrho}) = \int_{-\infty}^{\infty} \tau_j(\boldsymbol{r})\left[1 - \exp\left(iC_{nj}\frac{\boldsymbol{\varrho}\cdot\boldsymbol{r}}{r^{n+1}}\right)\right] d\boldsymbol{r}\,. \tag{17}$$

Use of spherical co-ordinates with the polar axis pointing in the direction of $\boldsymbol{\varrho}$ and substitution of the expression for $\tau_j(r)$ from equation (13a) give, after integration over the polar angles,

$$D_j(\boldsymbol{\varrho}) = 4\pi\int_{3a_j/2}^{\infty} r^2\left[1 - \frac{A_j}{r}\,e^{-\kappa r}\right]\left[1 - \frac{\sin(C_{nj}\rho/r^n)}{C_{nj}\rho/r^n}\right] dr\,, \tag{18}$$

where $\rho = |\boldsymbol{\varrho}|$.

In Appendix II this integral is compared with the integral evaluated by Chandrasekhar (1949),

$$\begin{aligned} D_0(\boldsymbol{\varrho}) &= 4\pi\int_0^{\infty} r^2\left[1 - \frac{\sin(C_{nj}\rho/r^n)}{C_{nj}\rho/r^n}\right] dr \\ &= (C_{nj}\gamma_n\rho)^{3/n}\,, \end{aligned} \tag{19}$$

corresponding to a random distribution of charged particles. In equation (19),

$$\gamma_2 = 2.6031\,, \qquad \gamma_4 = 4.9548\,. \tag{20}$$

This comparison is made for the values of Z_0, Z_j, N_j, T, and a_j considered in Table 1 for which the Debye-Hückel theory is valid or inequality (12) holds true. The differences between $D_j(\boldsymbol{\varrho})$ and $D_0(\boldsymbol{\varrho})$, which will give the Debye-Hückel effect corrections to $W(\boldsymbol{F}_{nj})$, have been estimated, and the results, as given by equations (42), (50), and (45), may be summarized as follows:

1. Appreciable differences between $D_j(\boldsymbol{\varrho})$ and $D_0(\boldsymbol{\varrho})$ exist from $\rho = 0$ to approximately

$$\begin{aligned} \rho = \rho_{22} &= \frac{10}{C_{2j}}\left(\tfrac{3}{2}a_j\right)^2 = \frac{5760}{T^2} && (n=2) \\ &= 10^4\rho_{24} = \frac{10^5}{C_{4j}}\left(\tfrac{3}{2}a_j\right)^4 = \frac{3.32\times 10^{11}}{T^4} && (n=4)\,. \end{aligned} \tag{21}$$

2. In general, the differences decrease with increasing ρ. For particles of the same charge, $D_j(\boldsymbol{\varrho}) < D_0(\boldsymbol{\varrho})$ throughout; for particles of opposite charge,

$$\begin{aligned} D_j(\boldsymbol{\varrho}) &< D_0(\boldsymbol{\varrho}) && (\rho < \tfrac{1}{10}\rho_{2n}) \\ &> D_0(\boldsymbol{\varrho}) && (\rho > \rho_{2n})\,. \end{aligned} \tag{22}$$

3. For $\rho > \rho_{2n}$ the differences seem to be due predominantly to the effects of $\tau_j(\boldsymbol{r})$ for $r \geq \frac{3}{2}a_j$, while for $\rho < \frac{1}{10}\rho_{2n}$ the effects of $\tau_j(\boldsymbol{r})$ for $r < \frac{3}{2}a_j$ seem to be of comparable importance.

These differences between $D_j(\boldsymbol{\varrho})$ and $D_0(\boldsymbol{\varrho})$ should produce negligible differences between the corresponding $W(\boldsymbol{F}_{nj})$ and $W(\boldsymbol{F}_{n0})$ because of the very small values of $C_{nj}\rho$ to which these differences are restricted. Using spherical co-ordinates with the polar axis

in the direction of $\boldsymbol{F}_{nj}$ and integrating over the polar angles change equation (16) to the following form:

$$W(\boldsymbol{F}_{nj}) = (2\pi^2 F_{nj})^{-1} \int_0^\infty \rho \sin(\rho F_{nj})\, e^{-N_j D_j(\rho)}\, d\rho\,, \tag{23}$$

where $F_{nj} = |\boldsymbol{F}_{nj}|$. Now equation (21) gives $D_j(\boldsymbol{\varrho}) \simeq D_0(\boldsymbol{\varrho})$ for

$$\begin{aligned} N_j D_j(\rho) &\geq 6.15 \times 10^{-13} \frac{N_j}{T^3} \qquad (n=2) \\ &\geq 4.89 \times 10^{-11} \frac{N_j}{T^3} \qquad (n=4)\,; \end{aligned} \tag{24}$$

these lower limits are smaller than 10^{-8} and 10^{-6}, respectively, for values of N_j and T for which the Debye-Hückel theory is valid. This means that differences between $\exp[-N_j D_j(\boldsymbol{\varrho})]$ and $\exp[-N_j D_0(\boldsymbol{\varrho})]$ will lie well below 10^{-8} for $n = 2$ and 10^{-6} for $n = 4$, and, therefore, the corresponding differences in the Fourier transforms $W(\boldsymbol{F}_{nj})$ and $W(\boldsymbol{F}_{n0})$ are equally negligible.

The differences between $W(\boldsymbol{F}_{nj})$ and $W(\boldsymbol{F}_{n0})$ will occur in the regions of large F_{nj} or far out in the wings of the collision-broadening profile. A rather crude determination of this range in F_{nj} is possible by using the criterion that the differences between $D_j(\boldsymbol{\varrho})$ and $D_0(\boldsymbol{\varrho})$ will not appear in $W(\boldsymbol{F}_{nj})$ as given by equation (23) unless $\sin(\rho F_{nj})$ goes through its first half-cycle for the range of ρ in which the deviations occur. This requires that

$$F_{2j} \geq \frac{\pi}{\rho_{22}}, \qquad F_{4j} \geq \frac{\pi}{10^4 \rho_{24}}. \tag{25}$$

Expressing F_{nj} in units of the "normal field," these lower limits become

$$\begin{aligned} \beta_{nj} = \frac{F_{nj}}{C_{nj}\gamma_n N_j^{n/3}} &\geq 4.37 \times 10^5 \frac{T^2}{N_j^{2/3}} \qquad (n=2) \\ &\geq 8.55 \times 10^7 \frac{T^4}{N_j^{4/3}}\,. \qquad (n=4)\,. \end{aligned} \tag{26}$$

For values of T and N_j for which the Debye-Hückel theory is valid, these lower limits have minimum values which are approximately 437 for $n = 2$ and 8550 for $n = 4$. That the Debye-Hückel effect corrections are restricted to these large values of β_{nj} is due to the fact that only near-by particles which produce large F_{nj} are affected.

APPENDIX I

Debye-Hückel Effect and Law for Distribution of Nearest Charged Particle

The law for distribution of the nearest neighbor in a random distribution of particles is discussed in Appendix VII of a review of stochastic problems by Chandrasekhar (1943), and this law can be generalized to account for the Debye-Hückel effect when the particles are charged. Let $W_j(r)dr$ be the probability that the nearest particle with a charge $Z_j\epsilon$ lies between r and $r + dr$. Then, in analogy to equation (669) of Chandrasekhar's discussion, $W_j(r)$ must satisfy the relation

$$W_j(r) = 4\pi r^2 N_j \tau_j(r) \left[1 - \int_{3a_j/2}^{r} W_j(r')\, dr'\right], \tag{27}$$

where $\tau_j(r)$ is given by equation (13a). This relation and the additional condition that

$$W_j(r) \to 4\pi r^2 N_j \tau_j(r) \qquad \text{as} \qquad r \to \tfrac{3}{2}a_j \tag{28}$$

are satisfied by the expression

$$\begin{aligned} W_j(r) &= 4\pi N_j r^2 \tau_j(r) \exp\left[-4\pi N_j \int_{3a_j/2}^{r} r'^2 \tau_j(r')\, dr'\right] \\ &= 4\pi N_j r^2 \left(1 - \frac{A_j}{r}\, e^{-\kappa r}\right) \exp\left\{-4\pi N_j \right. \\ &\qquad \left. \times \left[\frac{r^3 - (\frac{3}{2}a_j)^3}{3} + \frac{A_j}{\kappa^2}\left(\frac{\kappa r + 1}{e^{\kappa r}} - \frac{\frac{3}{2}\kappa a_j + 1}{e^{3\kappa a_j/2}}\right)\right]\right\} \qquad (r \geq \tfrac{3}{2}a_j) \\ &\equiv 0 \qquad\qquad (r < \tfrac{3}{2}a_j)\,. \end{aligned} \tag{29}$$

The average distance to the nearest charged particle is given by

$$d_j = \frac{\int_{3a_j/2}^{\infty} r W_j(r)\, dr}{\int_{3a_j/2}^{\infty} W_j(r)\, dr} = \frac{\frac{3}{2}a_j \int_1^{\infty} y^3 F(y)\, e^{-B_j y^3} dy}{\int_1^{\infty} y^2 F(y)\, e^{-B_j y^3} dy}, \tag{30}$$

since $W_j(r)$ is not normalized to unity because of the normalization problems of $\tau_j(r)$ discussed in Section II. In equation (30),

$$\begin{aligned} y &= \frac{r}{\frac{3}{2}a_j}, \qquad B_j = \tfrac{4}{3}\pi N_j (\tfrac{3}{2}\kappa a_j)^3, \\ F(y) &= \left(1 - \frac{A_j}{\frac{3}{2}a_j}\, \frac{e^{-3\kappa a_j y/2}}{y}\right) \exp\left[-\frac{Z_0 N_j Z_j}{\sum_i N_i Z_i^2}\, \frac{e^{\kappa a_j}}{\kappa a_j + 1} \right. \\ &\qquad \left. \times \left(\frac{\frac{3}{2}\kappa a_j y + 1}{e^{3\kappa a_j y/2}} - \frac{\frac{3}{2}\kappa a_j + 1}{e^{3\kappa a_j/2}}\right)\right]. \end{aligned} \tag{31}$$

For the values of Z_0, Z_j, N_j, T, and a_j considered in Table 1, for which inequality (12) holds true,

$$\begin{aligned} |A_j| &= \tfrac{3}{2}a_j\,, \qquad \frac{\frac{3}{2}\kappa a_j + 1}{e^{3\kappa a_j/2}} \simeq 1\,, \\ \frac{|Z_0 N_j Z_j|}{\sum_i N_i Z_i^2}\, \frac{e^{\kappa a_j}}{\kappa a_j + 1} &\simeq \tfrac{1}{2}\,. \end{aligned} \tag{32}$$

Equations (32), in turn, give

$$\begin{aligned} F(y) &\simeq 1 \pm (y^{-1} - \tfrac{3}{2}\kappa a_j) && [y \ll (\tfrac{3}{2}\kappa a_j)^{-1}] \\ &\simeq 1.14 && [y = (\tfrac{3}{2}\kappa a_j)^{-1}] \\ &\simeq e^{1/2} = 1.65 && [y \gg (\tfrac{3}{2}\kappa a_j)^{-1}]\,, \end{aligned} \tag{33}$$

where the plus sign is for opposite charge and the negative sign for the same charge. The integrals in equation (30) may be approximately evaluated by letting

$$\begin{aligned} F(y) &= 1 \pm (y^{-1} - \tfrac{3}{2}\kappa a_j) && [y \leq (\tfrac{3}{2}\kappa a_j)^{-1}] \\ &= 1.16 && [y \geq (\tfrac{3}{2}\kappa a_j)^{-1}]\,. \end{aligned} \tag{34}$$

This gives, for $T \geq N_j^{1/3}/3000$ with an accuracy of better than 5 per cent,

$$d_j = d_0 \pm \tfrac{3}{2} a_j \,, \tag{35}$$

where

$$d_0 = 0.55396\ N_j^{-1/3} \tag{36}$$

is the average distance for a random distribution of particles, as obtained by Chandrasekhar (1943).

These values of d_j are included in Table 1 as d_+ (opposite charge) and d_- (same charge). The differences between d_j and d_0 are negligible when N_j is considerably less than the limit imposed by inequality (12). Furthermore, $d_+ > d_0 > d_-$, which is just opposite to what might first be expected. Since $r_m \gg d_0$, which means that the major portion of the ionic atmosphere lies outside d_0, the additional probability of an oppositely charged particle due to the Debye-Hückel effect will be effective primarily for $r > d_0$, giving a $d_+ > d_0$. Similar reasoning for particles of the same charge shows that $d_- < d_0$. For $T < N_j^{1/3}/3000$, the approximate evaluation of the integrals in equation (30), using equation (34), becomes too crude to yield reliable results. The approximate evaluations show, however, that d_+ and d_- will be shifted outward (i.e., made larger) with respect to d_0 because d_0 is only slightly larger than $\frac{3}{2}a_j$, where $W_j(r)$ becomes zero, as indicated by equation (29).

A more accurate determination of d_j is possible by numerical integration of the integrals in equation (30). However, as indicated by equations (30) and (31), this determination will depend critically on the value assigned a_j. Hence a reliable determination of d_j must await a satisfactory resolution of the difficulties involved in fixing a_j, as discussed in Section II. One possible resolution would be to employ a $\tau_j(r)$, such as given by equations (13*b*) and (13*c*), which is essentially independent of a_j. When this is done, the following expressions are obtained for $W_j(r)$ by the same method as that used in obtaining equation (29):

$$W_j(r) = 4\pi N_j r^2 \left(1 - \frac{A_j}{r + A_j}\, e^{-\kappa r}\right) \qquad (A_j \text{ positive})$$

$$\times \exp\left[-4\pi N_j \left(\frac{r^3}{3} - \frac{A_j}{\kappa}\left[(A_j - \kappa^{-1} - r)\, e^{-\kappa r} - (A_j - \kappa^{-1})\right]\right.\right.$$

$$\left.\left. - A_j^3 e^{\kappa A_j}\left[E_1(\kappa A_j) - E_1(\kappa r + \kappa A_j)\right]\right)\right]$$

$$= 4\pi N_j r^2 \left(1 - \frac{A_j}{r - A_j}\, e^{-\kappa r} - 2\, e^{r/A_j}\right) \qquad (A_j \text{ negative}) \tag{37a}$$

$$\times \exp\left[-4\pi N_j \left(\frac{r^3}{3} - \frac{A_j}{\kappa}\left[(A_j + \kappa^{-1} + r)\, e^{-\kappa r} - (A_j + \kappa^{-1})\right]\right.\right.$$

$$+ A_j^3 e^{-\kappa A_j}\left[E_1(-\kappa A_j) - E_1(\kappa r - \kappa A_j)\right]$$

$$\left.\left. - 2A_j e^{r/A_j}\,(r^2 - 2A_j r + 2A_j^2)\right)\right],$$

where $E_1(x)$ is the exponential integral of order unity. Since $W_j(r)$ as given by equation (37*a*) holds for all r, equation (30) becomes

$$d_j = \frac{\int_0^\infty r W_j(r)\, dr}{\int_0^\infty W_j(r)\, dr}\,. \tag{37b}$$

APPENDIX II

Comparison of $D_j(\varrho)$ with $D_0(\varrho)$

For

$$\rho \leq \rho_{1n} = \frac{(\frac{3}{2}a_j)^n}{C_{nj}}, \tag{38}$$

it follows that

$$1 - \frac{\sin(C_{nj}\rho/r^n)}{C_{nj}\rho/r^n} \simeq \frac{1}{6}\left(\frac{C_{nj}\rho}{r^n}\right)^2 \tag{39}$$

with better than 10 per cent accuracy for $r \geq \frac{3}{2}a_j$. Therefore, in this range of small ρ, equation (18) gives

$$\begin{aligned} D_j(\varrho) &= \frac{2\pi}{3}(C_{nj}\rho)^2 \int_{3a_j/2}^{\infty} \left(1 - \frac{A_j}{r}\, e^{-\kappa r}\right) \frac{dr}{r^{2n-2}} \\ &\simeq \frac{2\pi}{3}\,\frac{(C_{nj}\rho)^2}{(\frac{3}{2}a_j)^{2n-2}}\left[\frac{\frac{3}{2}a_j}{2n-3} - A_j E_{2n-2}(\tfrac{3}{2}\kappa a_j)\right], \end{aligned} \tag{40}$$

where $E_k(x)$ is the exponential integral (Unsöld 1938),

$$\begin{aligned} E_k(x) &= x^{k-1}\int_x^{\infty} u^{-k}\, e^{-u}\, du \\ &\simeq \frac{1}{k-1} \qquad \text{(small } x\text{)}. \end{aligned} \tag{41}$$

When the conditions of equations (32) are applied, the following comparison can be made between $D_0(\varrho)$, as given by equations (19) and (20), and $D_j(\varrho)$, where use is made of the small argument approximation of the exponential integral:

$$\begin{aligned} D_j(\varrho) &\simeq 0.25 \left(\frac{\rho}{\rho_{12}}\right)^{1/2} D_0(\varrho) \qquad (n = 2, \text{ same charge}), \\ &\simeq 0.75 \left(\frac{\rho}{\rho_{12}}\right)^{1/2} D_0(\varrho) \qquad (n = 2, \text{ (opposite charge)} \\ &\simeq 0.021 \left(\frac{\rho}{\rho_{14}}\right)^{5/4} D_0(\varrho) \qquad (n = 4, \text{ same charge}) \\ &\simeq 0.23 \left(\frac{\rho}{\rho_{14}}\right)^{5/4} D_0(\varrho) \qquad (n = 4, \text{ opposite charge}). \end{aligned} \tag{42}$$

For large ρ, the term

$$\left[\frac{\sin(C_{nj}\rho/r^n)}{C_{nj}\rho/r^n}\right]\left(\frac{A_j}{r}\, e^{-\kappa r}\right) \tag{43}$$

in the integrand of equation (18) should contribute negligibly to $D_j(\varrho)$, since the second factor will be extremely small in the $r \to \infty$ range, where the first factor is not very small and is not rapidly oscillating. For

$$\rho \geq \rho_{4n} = \frac{10}{C_{nj}}(2r_m)^n, \tag{44}$$

the separation of these regions of possible interaction between the two factors in equation (42) should be sufficient to allow neglecting this term with better than 10 per cent accuracy. For this range of ρ,

$$D_j(\underline{\rho}) \simeq D_0(\underline{\rho}) - 4\pi\int_0^{3a_j/2} r^2\left[1-\frac{\sin(C_{nj}\rho/r^n)}{C_{nj}\rho/r^n}\right]dr - 4\pi A_j\int_{3a_j/2}^{\infty} r\,e^{-\kappa r}dr$$

$$\simeq D_0(\underline{\rho}) - \tfrac{4}{3}\pi(\tfrac{3}{2}a_j)^3 - \frac{4\pi A_j}{\kappa^2}\frac{\frac{3}{2}\kappa a_j+1}{e^{3\kappa a_j/2}}, \tag{45}$$

using equations (18) and (19). In the evaluation of the first integral in equation (45), the second term in the integrand can be neglected for $\rho \geq \rho_{4n}$ and $r \leq \frac{3}{2}a_j$. Under the conditions of equation (32), the last two terms on the right-hand side of equation (45) are negligible for $\rho \geq \rho_{4n}$.

A somewhat cruder comparison of $D_j(\rho)$ and $D_0(\rho)$ is possible for a limited range in ρ which lies at the lower end of the range $\rho_{1n} \leq \rho \leq \rho_{4n}$. The values of C_{nj} and κ pertinent to this discussion allow the approximation

$$\left(\frac{A_j}{r}\,e^{-\kappa r}\right)\left[1-\frac{\sin(C_{nj}\rho/r^n)}{C_{nj}\rho/r^n}\right] \simeq \frac{A_j}{r}\left[1-\frac{\sin(C_{nj}\rho/r^n)}{C_{nj}\rho/r^n}\right] \tag{46}$$

within the integrand of equation (18) for

$$\rho \leq \rho_{3n} = \frac{0.15}{C_{nj}}\left(\frac{r_m}{10}\right)^n$$

$$= 3.75\times10^{-5}\rho_{42} \qquad (n=2) \tag{47}$$

$$= 9.38\times10^{-8}\rho_{44} \qquad (n=4),$$

since A_j/r will cease to dominate the variation of the first factor only when the second factor is quite small. However, the second factor in expression (46) approaches zero when $r\longrightarrow\infty$ as r^{-2n}, as indicated by equation (39), and neglecting the pinching-off of this tail by $e^{-\kappa r}$ may introduce errors greater than 10 per cent into the integration. It is unlikely that these errors would be much larger than 10 per cent. Using equations (18) and (46), for $\rho \leq \rho_{3n}$, we obtain

$$D_j(\underline{\rho}) \simeq D_0(\underline{\rho}) - 4\pi A_j\int_0^{\infty} r\left[1-\frac{\sin(C_{nj}\rho/r^n)}{C_{nj}\rho/r^n}\right]dr$$

$$- 4\pi\int_0^{3a_j/2} r^2\left(1-\frac{A_j}{r}\right)\left[1-\frac{\sin(C_{nj}\rho/r^n)}{C_{nj}\rho/r^n}\right]dr \tag{48}$$

$$\simeq D_0(\underline{\rho}) - \frac{\pi^2 n A_j (C_{nj}\rho)^{2/n}}{(n+2)\,\Gamma(2/n)\sin(\pi/n)} - 4\pi\left[\tfrac{1}{3}(\tfrac{3}{2}a_j)^3 - \tfrac{1}{2}A_j(\tfrac{3}{2}a_j)^2\right].$$

The first integral in equation (48) was evaluated in a manner similar to that used by Chandrasekhar (1949) for evaluating $D_0(\underline{\rho})$. In the evaluation of the second integral, the second term in the third factor of the integrand has been neglected, which is valid for $r \leq \frac{3}{2}a_j$ only when

$$\rho \geq \rho_{2n} = \frac{10}{C_{nj}}(\tfrac{3}{2}a_j)^n = 10\rho_{1n}. \tag{49}$$

Hence equation (48) is a valid expression for $D_j(\underline{\rho})$ in the range of values $\rho_{2n} \leq \rho \leq \rho_{3n}$, and under the conditions of equations (32) it may be rewritten in the following form:

$$\frac{D_j(\underline{\rho})}{(\frac{3}{2}a_j)^3} \simeq 4200\left(\frac{\rho}{\rho_{22}}\right)^{3/2} \pm 49.3\left(\frac{\rho}{\rho_{22}}\right) - 4.19 \pm (-6.28) \quad (n=2)$$

$$\simeq 105\left(\frac{\rho}{\rho_{24}}\right)^{3/4} \pm 16.6\left(\frac{\rho}{\rho_{24}}\right)^{1/2} - 4.19 \pm (-6.28) \quad (n=4), \tag{50}$$

where the plus sign is used for opposite charge and the negative sign for same charge. In equations (50) the first and dominant term is $D_0(\underset{\sim}{\varrho})/(\frac{3}{2}a_j)^3$.

REFERENCES

Chandrasekhar, S. 1943, *Rev. Mod. Phys.*, **15**, 1.
———. 1949, *Proc. Cambridge Phil. Soc.*, **45**, 219.
Doherty, L., and Aller, L. H. 1954, in M. H. Wrubel (ed.), *Proceedings, NSF Conference on Stellar Atmospheres* (Indiana University), p. 98.
Fowler, R. H., and Guggenheim, E. A. 1939, *Statistical Thermodynamics* (Cambridge: At the University Press), chap. 9.
Kolb, A. C. 1954, in M. H. Wrubel (ed.), *Proceedings, NSF Conference on Stellar Atmospheres* (Indiana University), p. 63.
Margenau, H., and Meyerott, R. 1955, *Ap. J.*, **121**, 194.
Minnaert, M. 1953, in G. P. Kuiper (ed.), *The Sun* (Chicago: University of Chicago Press), chap. 3, § 3.35.
Unsöld, A. 1938, *Physik der Sternatmosphären* (Berlin: J. Springer), Appendix B.
Williamson, R. E. 1946, *Ap. J.*, **103**, 139, eq. (8).

RADIATIVE TRANSFER AND THERMODYNAMICS

RUPERT WILDT
Yale University Observatory
Received July 25, 1955

ABSTRACT

The irreversibility of radiative transfer is made manifest by analyzing the steady-state interaction of the nonisotropic field of nonequilibrium radiation with an isotropic atom gas. It is shown that the practice of substituting the Planck function for the source function contravenes the second law of thermodynamics. Consideration of the nonequilibrium entropy leads to rather general conjectures regarding the spectral distribution of the source function.

1. *Irreversibility of radiative transfer.*—At a conference on irreversible processes, convened at Syracuse University, March 31–April 2, 1955, a discussion of stationary transfer processes involving radiation was held. This paper reproduces, with minor revisions, a set of notes furnished as background for the discussion. Several statements offered here without proof require elaboration in their astrophysical context, and in this sense the paper is to be regarded as a preliminary report. However, radiative processes are of some interest in the wider setting of irreversible thermodynamics, and it is this aspect of the problem to which the present account is intended to draw attention.

The conventional theory of radiative transfer in stellar atmospheres and of continuous stellar spectra does not take explicit notice of the fact that the leaking of radiation from a star is an irreversible phenomenon par excellence. In practice, students of stellar atmospheres and spectra operate with what has been called, in discussions of irreversible processes, a pseudo-thermostatic theory. The limited accuracy of the observational data has not made it imperative to press forward to higher approximations.

2. *Basic concepts of the current astrophysical theory of radiative transfer in stellar atmospheres.*—The equation of transfer of radiant energy in a pencil of infinitesimal aperture and spectral band width is

$$\frac{1}{c}\frac{\partial I_\nu}{\partial t}+\mu_s\frac{\partial I_\nu}{\partial x_s}=-(\kappa_\nu+\sigma_\nu)I_\nu+\sigma_\nu I_{\nu 0}+\epsilon_{\nu 0}. \tag{2.1}$$

Definitions of the phenomenological variables:

$I_\nu d\nu$ (erg cm^{-2} sec^{-1} steradian^{-1}) = Specific intensity of radiant energy ; (2.21)

κ_ν (cm^{-1}) = Coefficient of absorption ; (2.22)

σ_ν (cm^{-1}) = Coefficient of (isotropic) scattering ; (2.23)

$\epsilon_{\nu 0}d\nu$ (erg cm^{-3} sec^{-1} steradian^{-1}) = Coefficient of spontaneous emission ; (2.24)

$$u_\nu d\nu=\frac{4\pi}{c}I_{\nu 0}d\nu=\frac{\int I_\nu d\omega d\nu}{c}=\text{Energy density}; \tag{2.25}$$

$$\pi F_\nu d\nu=\int I_\nu\mu d\omega d\nu\ (\text{erg cm}^{-2}\text{ sec}^{-1})=\text{Net flux of energy}. \tag{2.26}$$

Qualification of the state of radiative equilibrium ($\partial I_\nu/\partial t = 0$):

Steady-state interaction of nonisotropic, nonequilibrium radiation with isotropic atom gas ; (2.311)

Mean free path of photons $\gg$ mean free path of atoms ; (2.312)

Heat conduction demonstrably negligible ; (2.313)

Steady-state diffusion of the ionized gas ignored ; (2.314)

Convection, or stationary macroscopic motion of the gas, excluded . (2.315)

These assumptions jointly define the state of *strict radiative equilibrium*, which is characterized by the equality of the local rates of absorption (+ attenuation by scattering) and re-emission (including scattering), viz.,

$$\operatorname{div} \pi F = \int\int \mu_s \frac{\partial I}{\partial x_s}\, d\omega d\nu = 4\pi \int_0^\infty (\epsilon_{\nu 0} - \kappa_\nu I_{\nu 0})\, d\nu = 0\,. \tag{2.32}$$

Note that even in the monochromatic energy balance the terms proportional to σ_ν cancel out:

$$\operatorname{div} \pi F_\nu = 4\pi\, (\epsilon_{\nu 0} - \kappa_\nu I_{\nu 0})\,.$$

Additional restrictions result from specifying the mechanism of interaction. There are two limiting cases:

$\operatorname{div} F_\nu \neq 0$ for almost all frequencies implies redistribution of absorbed energy over the entire spectrum; (2.331)

$\operatorname{div} F_\nu = 0$ for all frequencies implies redistribution of "scattered" photons over all directions, but without change in frequency ; (2.332)

Intermediate cases will not be considered in this paper . (2.333)

If the absorption coefficient is zero everywhere and σ_ν, or, more generally, the scattering matrix, is prescribed, the physical aspect of the problem is defined without ambiguity; case (2.332) applies, and the analysis of radiative transfer then becomes a purely mathematical task. Its solution is far advanced because of the powerful methods created by Chandrasekhar (1950). On the other hand, if case (2.331) applies and if κ_ν (the spatial distribution of matter) and πF_s (the total energy flux emerging at the stellar surface) are given, the phenomenological theory of radiative transfer has to be completed by specifying the spectral distribution of the coefficient of spontaneous emission. Instead, it is often convenient to use $\epsilon_{\nu 0}/\kappa_\nu = I_\nu^*$, the so-called *monochromatic source function*.

Conventionally, the problem is now made determinate by introducing a pseudo-thermostatic principle, which is known as the "hypothesis of local thermodynamic equilibrium"; as a heuristic device, one assumes the validity of Kirchhoff's law of emission, though matter be exposed to nonequilibrium radiation,

$$I_\nu^* = \frac{2h\nu^3}{c^2}\left[\exp\left(\frac{h\nu}{kT}\right) - 1\right]^{-1}. \tag{2.4}$$

Attempts to validate the postulate of local thermodynamic equilibrium by kinetic considerations are likely to argue in circles. A novel approach to the problem follows under § 4. Hilbert (1912, 1913) designed the most sophisticated proof of Kirchhoff's law. The pivotal point of this proof is an appeal to the principle of *detailed balancing*.

The appellation "local thermodynamic equilibrium" is given indiscriminately, by some authors, to the physically distinct propositions (2.331) (div $F_\nu \neq 0$) and (2.4) ($I_\nu^* =$ Planck function). The use of the term, which, in the sense of case (2.331), is somewhat misleading, in this paper will be restricted to postulate (2.4).

Whenever it may be desirable to label (2.331), the antithesis to (2.332) should be stressed. Now Milne coined for (2.332) the term "monochromatic radiative equilibrium," which is descriptively appropriate and logically unobjectionable. By analogy, one might use for (2.331) the term "poecilochromatic radiative equilibrium," from ποικιλος, which suggests continual alteration of many hues.

3. *Radiative transfer reconsidered as a problem in photon diffusion.*—Definitions of further phenomenological variables:

$$\frac{I_\nu}{h\nu} = Q_\nu = \text{Specific intensity of photon diffusion} ; \tag{3.11}$$

$$\frac{I_\nu^*}{h\nu} = Q_\nu^* = \text{Source function of spontaneous photon emission} ; \tag{3.12}$$

$$\frac{I_{\nu 0}}{h\nu} = Q_{\nu 0} = \text{Average intensity (proportional to photon density)} ; \tag{3.13}$$

$$\pi\Phi_\nu d\nu = \int Q_\nu \mu d\omega d\nu = \text{Net flux of photons} . \tag{3.14}$$

The equation of photon transfer (cf. [2.1]) is

$$\frac{1}{c}\frac{\partial Q_\nu}{\partial t} + \mu_s \frac{\partial Q_\nu}{\partial x_s} = -(\kappa_\nu + \sigma_\nu) Q_\nu + \sigma_\nu Q_{\nu 0} + \kappa_\nu Q_\nu^* . \tag{3.2}$$

After integration over the complete sphere, the monochromatic photon balance is found to be

$$\frac{4\pi}{c}\frac{\partial Q_{\nu 0}}{\partial t} + \operatorname{div} \pi\Phi_\nu = 4\pi\kappa_\nu (Q_\nu^* - Q_{\nu 0}) . \tag{3.21}$$

The steady-state analogues to (2.331) and (2.332) are, respectively,

$$\operatorname{div} \pi\Phi_\nu \neq 0 , \tag{3.31}$$

$$\operatorname{div} \pi\Phi_\nu = 0 . \tag{3.32}$$

To equation (2.32) there corresponds the inequality

$$\operatorname{div} \pi\Phi = \int_0^\infty 4\pi\kappa_\nu (Q_\nu^* - Q_{\nu 0})\, d\nu \neq 0 , \tag{3.4}$$

which puts in evidence the chief physical characteristic of strict radiative equilibrium of type (2.331), namely, the steady-state generation or destruction of photons. The net flux of energy, because of the photon generation, changes in spectral composition with approach to the stellar surface. It is commonly held that this change must be a reddening, but this is not true in general. An example to the contrary can readily be constructed on suitable assumptions regarding the spectral variation of κ_ν. The intuitive expectation proves correct only for neutral absorption (so-called "gray atmosphere").

The fundamental significance of the inequality just stated has been obscured by the

preoccupation with Milne's integral equation for a gray atmosphere (stratified in parallel planes), which expresses only the total energy balance, i.e., equation (2.32),

$$I^*(\tau) = \tfrac{1}{2}\int_0^\infty I^*(t)\,E_1(|t-\tau|)\,dt. \tag{3.51}$$

The corresponding balance for photons, in a gray atmosphere stratified in parallel planes, namely,

$$Q^*(\tau) - \tfrac{1}{2}\int_0^\infty Q^*(t)\,E_1(|t-\tau|)\,dt + \frac{1}{4}\frac{d\Phi}{d\tau} = 0, \tag{3.52}$$

is a nonhomogeneous integral equation which has been considered, in another context, by Hopf (1934). He pointed out that its formal solution is the Neumann series. This observation does not shed any light on the mechanism of photon generation, which is an essentially atomistic problem and, as such, is beyond the reach of a merely phenomenological analysis of radiative transfer. At any rate, it is clear that an unbiased approach to the problem of radiative equilibrium in a gray atmosphere ought to take simultaneous account of the pair of integral equations.

4. *Kinetics of the interaction between atom gas and photons.*—Rosseland (1930) was the first to stress the distinction between the absorption coefficient κ_ν (eq. [2.22]), which appears in Kirchhoff's law, and a coefficient a_ν (cm^{-1}), which is an aggregate of the Einstein probability coefficients for upward transitions (so-called "true absorptions") weighted according to the populations of the lower states. Rosseland's analysis was too restrictive in one respect: he assumed that the excited atoms obey the Boltzmann distribution. It can be shown that the following relation holds quite generally, even for transient states:

$$\kappa_\nu = a_\nu - \frac{c^2\epsilon_{\nu 0}}{2h\nu^3} = a_\nu\left(1 + \frac{c^2 I_\nu^*}{2h\nu^3}\right)^{-1}. \tag{4.1}$$

This expression reduces to the one given by Rosseland for I_ν^* = Planck function, on the hypothesis of local thermodynamic equilibrium.

Greater symmetry and compactness can be achieved by combining the Einstein probabilities and atomic population as follows:

$$R_{ij} = n_i B_{ij}\left[1 + \left(\frac{1+s_{ij}}{2}\right)\frac{2h\nu^3}{c^2 I_{\nu 0}}\right]\frac{4\pi}{c}\,I_{\nu 0}\,d\nu\ (\mathrm{cm}^{-3}\,\mathrm{sec}^{-1}), \tag{4.21}$$

with

$$s_{ij} = -s_{ji} = \frac{E_i - E_j}{h\nu_{ij}} = \pm 1, \qquad (E_i - E_j \gtrless 0),$$

E_i being the energy and n_i the population of the state i. The new variables are the radiative reaction rates for transitions $i \to j$. The inverse reaction rate, R_{ji}, is obtained from equation (4.21) by interchanging the indices. Hence, by virtue of the Einstein relation $g_i B_{ij} = g_j B_{ji}$

$$\frac{R_{ij}}{R_{ji}} = \frac{g_j n_i}{g_i n_j}\left(1 + \frac{2h\nu^3}{c^2 I_{\nu 0}}\right)^{s_{ij}}. \tag{4.22}$$

The following equations are examples of the atomistic interpretation of phenomenological variables in terms of the reaction rates:

$$\kappa_\nu d\nu = \sum{}' \left[R_{ji} - R_{ij}\left(1 + \frac{2h\nu^3}{c^2 I_{\nu 0}}\right)^{-1}\right]\left(\frac{h\nu}{4\pi I_{\nu 0}}\right); \tag{4.31}$$

$$4\pi\epsilon_{\nu 0}\,d\nu = \Sigma' R_{ij}\left(\frac{h\nu}{4\pi I_{\nu 0}}\right)\left(1 + \frac{c^2 I_{\nu 0}}{2h\nu^3}\right)^{-1}; \tag{4.32}$$

$$I_\nu^* = \frac{2h\nu^3}{c^2}\left[\left(1+\frac{2h\nu^3}{c^2 I_{\nu 0}}\right)\frac{\Sigma' R_{ji}}{\Sigma' R_{ij}} - 1\right]^{-1}, \tag{4.33}$$

where

$$\Sigma' = \left(\sum_i \sum_{j<i} \cdots\right)_{E_i - E_j = h\nu_{ij} = \text{constant}}.$$

All interpretations given here hold likewise if the sums Σ' are understood to include the integrals properly representing transitions to and from continuous states. In a mixture of several elements, the R_{ij} should carry, moreover, an index identifying the atomic species. But this index will be omitted throughout, as no loss of generality will result.

Since I_ν^* has the physical dimension of a specific intensity of radiant energy, it can serve to define a *characteristic temperature of the monochromatic source function:*

$$\frac{1}{T_\nu^*} = \frac{k}{h\nu}\ln\left(1+\frac{2h^3}{c^2 I_\nu^*}\right) = \frac{k}{h\nu}\ln\left(1+\frac{2h^3}{c^2}\frac{\kappa_\nu}{\epsilon_{\nu 0}}\right). \tag{4.4}$$

This definition does *not* imply detailed balancing, as substitution of equation (4.33) in equation (4.4) will show. The hypothesis of local thermodynamic equilibrium amounts to setting T_ν^* equal to a constant, i.e., independent of ν. It can be shown that this heuristic device is thermodynamically unsound. The demonstration requires consideration of the entropy of the atom gas. This is associated with (*a*) the translational degrees of freedom and (*b*) the excitational degrees of freedom. It is assumed that there is no correlation between the partition functions *a* and *b*.

Under steady-state conditions, there are constant rates of transfer of energy and entropy between (A) the radiation field and the excitational degrees of freedom and (B) the excitational and translational degrees of freedom. The former are proportional to the rates R_{ij} (defined by eq. [4.21]), and the latter are proportional to analogous quantities C_{ij} ($\text{cm}^{-3}\,\text{sec}^{-1}$), which are the reaction rates due to inelastic and superelastic collisions. Elastic collisions do not affect the balance of population of the state i, viz.,

$$\frac{\partial n_i}{\partial t} = \sum_j (R_{ji} + C_{ji} - R_{ij} - C_{ij}). \tag{4.51}$$

The total density of entropy of excitation associated with a population $N = \Sigma n_i$ is, by definition,

$$S = k\sum_i n_i \ln\frac{g_i N}{n_i}, \tag{4.521}$$

and its rate of change, keeping $N = \text{Const.}$, is

$$\frac{\partial S}{\partial t} = k\sum_i \left(\ln\frac{g_i N}{n_i} - 1\right)\frac{\partial n_i}{\partial t}. \tag{4.522}$$

This expression is the sum of entropy transfer rates of types A and B and may be decomposed, according to equation (4.51), into

$$\left(\frac{\partial S}{\partial t}\right)_{\text{rad}} = k\sum_i \sum_j (R_{ji} - R_{ij}) \ln\frac{g_i N}{n_i}, \tag{4.5221}$$

$$\left(\frac{\partial S}{\partial t}\right)_{\text{coll}} = k\sum_i \sum_j (C_{ji} - C_{ij}) \ln\frac{g_i N}{n_i}. \tag{4.5222}$$

The net rate of loss of excitation entropy by radiative transitions is the negative of equation (4.5221), which may be contracted into

$$-\left(\frac{\partial S}{\partial t}\right)_{\text{rad}} = k \sum_i \sum_j R_{ij} \ln \frac{g_i n_i}{g_i n_i} = G. \tag{4.53}$$

Kinetic classification of steady states.—Conservation of the population of level i requires only that

$$\sum_j (R_{ji} - R_{ij} + C_{ji} - C_{ij}) = 0,$$

an equation satisfied under physically distinct conditions which appear to admit of exhaustive classification:

Detailed balancing: $R_{ij} = R_{ji}$, and $C_{ij} = C_{ji}$, all (i, j), (4.61)

"thermostatic equilibrium."

Over-all radiative balancing: $R_{ij} \neq R_{ji}$, but $\sum_j (R_{ji} - R_{ij}) = 0$, (4.62)

"fluorescent equilibrium," infinitely dilute gas, hence $C_{ij} = 0$.

Co-operative balancing: $\sum_j (R_{ij} - R_{ji}) = \sum_j (C_{ji} - C_{ij}) \neq 0$, (4.63)

"strict radiative equilibrium, with div $F_\nu \neq 0$."

Nonco-operative balancing: $\sum_j (R_{ij} - R_{ji}) = 0$, $\sum_j (C_{ji} - C_{ij}) = 0$; (4.64)

it is doubtful whether this case can be realized physically.

Thermodynamics of the steady state.—All state variables are time-invariant by definition. Hence, according to equation (4.522),

$$\frac{\partial S}{\partial t} = \left(\frac{\partial S}{\partial t}\right)_{\text{rad}} + \left(\frac{\partial S}{\partial t}\right)_{\text{coll}} = 0. \tag{4.7}$$

But, with the conditions laid down under equation (4.63), it follows by equations (4.5221) and (4.5222) that, in strict radiative equilibrium,

$$\left(\frac{\partial S}{\partial t}\right)_{\text{coll}} = -\left(\frac{\partial S}{\partial t}\right)_{\text{rad}} = G \neq 0. \tag{4.71}$$

Because the irreversible production of entropy can be discharged only into the radiation field, strict radiative equilibrium requires

$$G > 0. \tag{4.72}$$

Test of the hypothesis of local thermodynamic equilibrium: Elimination of $g_i n_j / g_j n_i$ from equation (4.53) by substitution of equations (4.23) and (4.33) gives

$$G = G_1 - G_2; \tag{4.81}$$

$$G_1 = k \sum_i \sum_j s_{ij} R_{ij} \ln \left(1 + \frac{2h\nu^3}{c^2 I_\nu^*}\right) = \int_0^\infty \frac{1}{T_\nu^*} (\epsilon_{\nu 0} - \kappa_\nu I_{\nu 0})\, d\nu; \tag{4.811}$$

$$G_2 = k \sum_i \sum_j s_{ij} R_{ij} \ln \left[\left(\frac{R_{ij}}{R_{ji}} \right)^{s_{ij}} \frac{\Sigma' R_{ji}}{\Sigma' R_{ij}} \right] = \Psi^2 > 0 . \tag{4.812}$$

The crucial point is that G_2 can be shown to be nonnegative; hence $G_2 = \Psi^2$; and G_2 vanishes identically for $(R_{ij}/R_{ji})^{s_{ij}} = f(\nu)$, i.e., a function solely of ν, apart from universal constants; this case appears to be physically unrealistic. By equations (4.72), (4.811), and (4.812), finally, we obtain

$$G = \int_0^\infty \frac{1}{T_\nu^*} \operatorname{div} F_\nu d\nu - \Psi^2 > 0 . \tag{4.82}$$

For $T_\nu^* = T = \text{Const.}$, equation (4.82) becomes negative, contravening the second law. Hence Kirchhoff's law of emission cannot hold, even approximately, with $\Psi^2 \neq 0$, that is to say, in strict radiative equilibrium.

5. *Transfer of radiant entropy.*—Planck (1906) gave the following definition of the specific intensity of entropy radiation:

$$L_\nu d\nu \text{ (erg degree}^{-1} \text{ cm}^{-2} \text{ sec}^{-1} \text{ steradian}^{-1}) = L_\nu(\nu, I_\nu)\, d\nu =$$
$$\frac{2k\nu^2}{c^2} \left[\left(1 + \frac{c^2 I_\nu}{2h\nu^3} \right) \ln \left(1 + \frac{c^2 I_\nu}{2h\nu^3} \right) - \frac{c^2 I_\nu}{2h\nu^3} \ln \frac{c^2 I_\nu}{2h\nu^3} \right] d\nu . \tag{5.1}$$

The partial derivative of L_ν with respect to I_ν is the *monochromatic temperature* of the pencil:

$$\left(\frac{dL_\nu}{dI_\nu} \right)_{\nu = \text{const}} = \frac{k}{h\nu} \ln \left(1 + \frac{2h\nu^3}{c^2 I_\nu} \right) = \frac{1}{T_\nu} . \tag{5.2}$$

The equation of entropy transfer,

$$\frac{1}{c} \frac{\partial L_\nu}{\partial t} + \mu_s \frac{\partial L}{\partial x_s} = \frac{\kappa_\nu}{T_\nu} (I_\nu^* - I_\nu) , \tag{5.3}$$

after integration over the complete sphere leads to the monochromatic entropy balance:

$$\frac{\partial s_\nu}{\partial t} + \operatorname{div} \pi E_\nu = \int \frac{\kappa_\nu}{T_\nu} (I_\nu^* - I_\nu)\, d\omega ; \tag{5.4}$$

$$s_\nu d\nu = \frac{4\pi}{c} L_{\nu 0} d\nu = \int \frac{L_\nu}{c}\, d\omega\, d\nu = \text{Density of radiant entropy} ; \tag{5.41}$$

$$\pi E_\nu d\nu = \int L_\nu \mu\, d\omega\, d\nu = \text{Net flux of radiant entropy} . \tag{5.42}$$

In several monographs on irreversible thermodynamics Jaumann (1911) is credited with having introduced the concept of the entropy flow vector; actually, it is due to Planck, who gave definition (5.42) many years before Jaumann. Although Planck used the entropy balances—equations (5.4) and (5.52)—he did not formulate the transfer equation (5.3).

Sundry inequalities concerning radiant entropy can be established by appeal to the second law of thermodynamics, or as consequences of equation (5.3). The most important ones are:

An upper bound to the entropy density, under nonequilibrium conditions, is given by the fictitious entropy density that would result from transformation of the original radiation into equilibrium radiation, the total energy density, $4\pi I_0/c$, being kept constant:

$$\int_0^\infty L_{\nu 0} d\nu = L_0 \leq \frac{4}{3} \left(\frac{\sigma}{\pi} \right)^{1/4} I_0^{3/4} , \tag{5.51}$$

σ = Stefan-Boltzmann constant .

The same argument applies to another nonequilibrium function, the virtual entropy density, L^*:

$$\int_0^\infty L_\nu^* \, d\nu = L^* \leq \frac{4}{3}\left(\frac{\sigma}{\pi}\right)^{1/4} I^{*3/4}, \qquad I^* = \int_0^\infty I_\nu^* \, d\nu, \tag{5.511}$$

$$L_\nu^* = \text{Function (5.1) of the argument } I_\nu^* .$$

The divergence of the net flux of radiant entropy is essentially nonnegative:

$$\operatorname{div} \pi E = \iint \frac{\kappa_\nu}{T_\nu}(I_\nu^* - I_\nu) \, d\omega d\nu \geq 0, \qquad \frac{\partial s}{\partial t} = 0. \tag{5.52}$$

The double integral is the exact expression for the rate of entropy production per unit volume. It can be shown, moreover, that the entropy production is always greater than the function G_1, defined by equation (4.811).

The entropy flux emergent at the surface of an infinitely deep atmosphere, stratified in parallel planes, cannot exceed the fictitious entropy flux that would emerge from an isothermal atmosphere in local thermodynamic equilibrium, the emergent energy flux being the same in either case:

$$\pi E_s < \frac{4}{3}\left(\frac{\sigma}{\pi}\right)^{1/4} (\pi F_s)^{3/4}. \tag{5.53}$$

An alternate form of the equation of transfer (5.1) is

$$\frac{1}{c}\frac{\partial L}{\partial t} + \mu_s \frac{\partial L}{\partial x_s} = -\kappa_\nu L_\nu + \kappa_\nu \left[\frac{I_\nu^*}{T_\nu} + \frac{2h\nu^2}{c^2} \ln\left(1 + \frac{c^2 I_\nu}{2h\nu^3}\right)\right]. \tag{5.54}$$

The expression in brackets is the (nonisotropic) source function characteristic of L_ν, which in a plane atmosphere has a minimum in the plane of stratification, whose value is L_ν^*. Because of this minimum, it is possible to establish divers inequalities. The most interesting one is, perhaps,

$$L_{\nu 0}(\tau_\nu) > \tfrac{1}{2}\int_0^\infty L_\nu^*(t_\nu) E_1(|t_\nu - \tau_\nu|) \, dt_\nu. \tag{5.55}$$

6. *Conjectures regarding the source function.*—

6.1. The spectral distribution of the source function, I_ν^*, reflects, as it were, the statistical equilibrium of the atom gas. Instead of trying to evaluate the latter, it is proposed to deal with the virtual photon gas, Q_ν^*, and to assume in particular that the steady-state nonequilibrium distribution of the virtual photons is characterized by the following conditions:

$$L^* = \int_0^\infty L_\nu^* \, d\nu = \text{Maximum}, \tag{6.11}$$

$$I^* = \int_0^\infty I_\nu^* \, d\nu = \text{Const.}, \tag{6.12}$$

$$Q^* = \int_0^\infty Q_\nu^* \, d\nu = \text{Const.} \tag{6.13}$$

The solution of this maximum problem represents the nondegenerate case (Kothari and Singh 1940) of relativistic Bose-Einstein statistics:

$$I_\nu^* = \frac{2h\nu^3}{c^2}\left[\exp\left(\frac{h\nu}{kT} + \text{const.}\right) - 1\right]^{-1}, \tag{6.14}$$

where $1/T$ and k·const. are the Lagrangian multipliers referring to equations (6.12) and (6.13), respectively.

A more transparent solution is obtained from the equivalent maximum problem,

$$L^* = \text{Maximum}, \tag{6.15}$$

$$\frac{4}{3}\left(\frac{\sigma}{\pi}\right)^{1/4} I^{*3/4} = \text{Const., multiplier } m_1, \tag{6.16}$$

$$Q^* = \text{Const., multiplier } m_2. \tag{6.17}$$

Condition (6.16) restricts the set of comparison functions to such spectra of I_ν^* as will yield the same entropy maximum on being transformed to equilibrium radiation, while I^* is kept constant (see eq. [5.511]). The solution is

$$I_\nu^* = \frac{2h\nu^3}{c^2}\left[\exp\left(\frac{h\nu}{k}\left\langle\frac{15}{\pi^5}\frac{\sigma}{I^*}\int_0^\infty \frac{x^3\,dx}{e^{x+m_2}-1}\right\rangle^{1/4} + m_2\right) - 1\right]^{-1}, \tag{6.18}$$

$$1 \geq m_1^4 = \frac{15}{\pi^4}\int_0^\infty \frac{x^3\,dx}{e^{x+m_2}-1} \geq 0, \qquad m_2 \geq 0.$$

The accessory condition (6.13) or (6.17) can be imposed only because the desired entropy maximum is to qualify nonequilibrium radiation. For thermostatic equilibrium this constraint, of course, is redundant; but for the steady nonequilibrium case, Q^* would appear to be a requisite parameter. This statement at any rate contains the gist of the hypothesis enunciated previously.

6.2. On the further hypothesis that the parameter m_2 in equation (6.18) is constant throughout the stellar atmosphere, the new source function can be injected in a straightforward manner into the theory of radiative equilibrium in a gray atmosphere ($\kappa_\nu = \bar{\kappa} =$ Const.). In particular, it can be shown that the parameter m_2 determines the total number of photons escaping at the surface ($= \pi\Phi_s$). On the hypothesis of local thermodynamic equilibrium, this very quantity was not a free parameter but was fixed automatically by the net flux of energy, πF.

This auxiliary hypothesis confers a deeper physical meaning upon the sequence of I_ν^* spectra representing the variation in the source function from one atmospheric level to the next. This sequence is generated by a continuous adiabatic transformation, in the sense of Wien's general displacement law,

$$V\frac{\partial I_\nu^*}{\partial V} = \frac{\nu}{3}\frac{\partial I_\nu^*}{\partial \nu} - I_\nu^*, \tag{6.21}$$

where V denotes the fiducial volume; and the volume, as function of the optical depth in the gray atmosphere, turns out to be inversely proportional to the fourth root of the solution of the integral equation (3.51).

6.3. The status of Wien's differential equation (6.21) is logically unrelated to the particular hypotheses 6.1 and 6.2. It is possible, therefore, to base upon the unrestricted validity of equation (6.21) a separate, third conjecture, namely, that the variation of the source function (from level to level in the same atmosphere) might at any rate admit of representation by a continuous adiabatic transformation.

Nowhere in the astrophysical literature has it been noted that Wien's displacement law, in its most general form (6.21), rules the adiabatic transformations of nonequilibrium radiation of *arbitrary* initial composition. It would be surprising, indeed, if a radiation law of such surpassing generality did not prove to be relevant, somehow, to the elusive transformation of stellar radiation.

REFERENCES

Chandrasekhar, S. 1950, *Radiative Transfer* (Oxford: Clarendon Press).
Hilbert, D. 1912, *Phys. Zs.*, **13**, 1056.
———. 1913, *ibid.*, **14**, 592.
Hopf, E. 1934, *Mathematical Problems of Radiative Equilibrium* (Cambridge: At the University Press).
Jaumann, G. 1911, *Sitz. Ber. Akad. Wiss. Wien, Math.-Nat. Kl.*, Abt. IIA, **120**, 385.
Kothari, D. S., and Singh, B. N. 1941, *Proc. R. Soc. London, A*, **178**, 135.
Planck, M. 1906, *Theorie der Wärmestrahlung* (Leipzig: J. A. Barth).
Rosseland, S. 1930, *Handb. d. Ap.*, **3**, Part I, 457.

ATMOSPHERES OF THE B STARS. I. THE SUPERGIANT EPSILON CANIS MAJORIS

LAWRENCE H. ALLER
University of Michigan Observatory
Received July 29, 1955

ABSTRACT

Three formulations of the curve of growth are applied to the analysis of line-intensity data for the B2 II supergiant ϵ Canis Majoris. These include the Schuster-Schwarzschild approximation (Menzel-Unsöld-Wrubel), the Milne-Eddington approximation with pure scattering (Wrubel), and a Milne-Eddington approximation with pure absorption. The turbulent velocities and the abundances depend on the curve of growth chosen for the analysis. The ionization equilibrium appears to be but little affected. The differences probably reflect the influence of the different basic assumptions that are made in the various curves of growth.

I. INTRODUCTION

The present paper is the first of a series on the problems of the atmospheres of the B stars. This article is concerned primarily with the use of the curve of growth and similar rough approximations, commonly referred to as *grobanalyses* in the first reconnaissance of a stellar atmosphere. Subsequent papers will deal with the calculation of model stellar atmospheres and the application of these model atmospheres to the detailed or "fine" analysis of the spectrum. The ultimate objective of the investigation is to determine as accurately as possible the compositions of the atmospheres of these early-type stars.

For main-sequence stars, at least, the model-atmosphere approach is probably superior to the curve-of-growth approach, but the amount of labor required for the interpretation of the spectrum of a single star is immense. For each choice of effective temperature, chemical composition, and surface gravity a different model must be computed, and the characteristics of a given star must be fitted in general to some interpolated model. In proceeding to analyze a given stellar spectrum, it is therefore desirable that we possess good guesses about the basic parameters, and such guesses may be provided by the curve of growth.

In dealing with supergiant atmospheres, we have no sound theoretical basis for calculating atmospheric models. It has long been known that the effective surface gravities of these stars are considerably lower than the values predicted from their radii and probable masses. Hence it is doubtful whether we can do much more in spectral interpretation than use a crude dependence of temperature on optical depth, and even the curve of growth may suffice.

Our first concern will be the application of the curve of growth to the problem. The immediate question arises: Which curve of growth? Those of Menzel (1936), of Unsöld (1938), and of Wrubel (1954), based on the Schuster-Schwarzschild model or those of Wrubel (1949) based on the Milne-Eddington approximation and pure scattering are the most popular. To these we may add a third family of curves, similar to Wrubel's but based on the hypothesis of pure absorption. We shall analyze our data with all three sets of curves to see what uncertainties are introduced into the analysis by the initial assumptions involved. It will be seen that the ionization equilibrium will be but little affected by our choice of the curve of growth but that the derived abundances may differ from one set of assumptions to another. The hydrogen-line intensities will be seen to provide further important clues, particularly to the atmospheric densities.

II. THE OBSERVATIONAL DATA

In the present paper we make detailed applications of the various curve-of-growth procedures to the star ϵ Canis Majoris, HD 52089, $\alpha = 6^h54^m7$, $\delta = -28°50'$ (1900), $m_{vis} = 1.63$. The Draper class of this star is B1, but Morgan's classification, B2 II, seems in better harmony with the results of the spectroscopic analysis.

Earlier work on this star, carried out on tracings of Mount Wilson coudé data made in Pasadena in 1946, involved a curve-of-growth analysis by the Unsöld (1941) method. The results were presented at the symposium on stellar atmospheres of the American Astronomical Society at Evanston, Illinois (1947). The limited data then available did not define the curve of growth very accurately. I carried out solutions on the basis of (*a*) no turbulence and (*b*) turbulence requiring a shift in log $wc/\lambda v$ of 0.50. Values of $T = 23000°$ K and log $P_e = 2.80$ were assumed. The preliminary values of the abundances may be compared as shown in the accompanying tabulation. The importance of

Element	log N		Element	log N	
	a	*b*		*a*	*b*
H.....	+3.25	+3.76	Mg.....	−0.24	−1.08
He.....	+2.11	+2.62	Al.....	−1.14	−1.91
C.....	−0.37	−0.89	Si.....	−0.44	−1.22
N.....	+0.19	−0.29	S.....	−2.37	−2.82

the determination of an accurate value of the turbulence as well as of other parameters is obvious.

In 1948, three McDonald coudé plates—689, 690, and 729—of this star were made available to me, permitting a strengthening of the analysis. The tracing of the plates and their reductions were carried out in the usual way. The McDonald material covered the region from λ 3980 to λ 4720, whereas the Mount Wilson material included the region of the Balmer limit. The second rediscussion, based on the Wrubel curve of growth, assumed no turbulence but the same electron densities and temperature as before (Hynek 1951). The same observational data are utilized here with the aid of improved *f*-values due to Garstang (1954). The curves of growth for the O II 3s–3p and 3p–3d transition arrays are sufficiently well defined to establish the turbulent velocities. The star has somewhat fuzzy lines, so that some turbulence must be present in the atmosphere. Table 1 summarizes the intensity data that have been used.

III. COMMENTS ON CURVES OF GROWTH

We shall discuss the line-intensity data with the aid of three theoretical curves of growth: (1) Milne-Eddington approximation with pure scattering (Wrubel 1949); (2) Milne-Eddington approximation with pure absorption; and (3) Schuster-Schwarzschild model with the empirical Minnaert equation (Unsöld 1938).

The application of the Wrubel curve of growth is very similar to that described elsewhere (Aller 1953). The ordinate is log $wc/\lambda v$, where v is the most probable velocity of the atoms, while the abscissa may be written as

$$\log \frac{\eta_c}{N} = \log \frac{\pi e^2}{m c} \frac{4 \times 10^{-5}}{v \sqrt{\pi}} + \log f - \theta (\chi - \chi_0) + \log \left(\frac{\lambda}{4000} \right) - \log k_{\text{eff}} + \Delta \log \eta , \quad (1)$$

which can be expressed as

$$\log \frac{\eta_c}{N} = \mathfrak{N}_e + \Delta_w , \quad (2)$$

TABLE 1

LINE INTENSITIES IN ϵ CANIS MAJORIS

Ion	Multiplet	Blend	λ	W (mA)	log f
C II	(4)	.....	3920.68	143	−1.04
.....	.....	.....	3918.98	145	−1.35
	(6)	.....	4267	240	−0.02
	(33)	.....	3876.2–.67	152	−0.34
C III	(1)	O II	4650.16:	57:	−0.60
.....	.....	.....	4647.40	66	−0.38
	(16)	.....	4069.0	10	−0.37
.....	.....	.....	4067.8	18	−0.47
	(18)	.....	4187.05	10	+0.13
N II	(5)	Si IV	4630.55	205	−1.00
.....	.....	.....	4613.98	110	−1.70
.....	.....	.....	4643.08	120	−1.48
.....	.....	.....	4621.39	95	−1.57
.....	.....	.....	4601.48	140	−1.48
.....	.....	Fe III	4607.15	125	−1.57
	30	.....	3856.06	85:	−2.28
	12	.....	3995.0	200	−0.88
	15	O II?	4447.02	107	−0.21
	33	.....	4227.75	70	−1.67
	39	O II	4041.32	110	−0.79
.....	.....	Fe III	4043.54	70	−0.90
.....	.....	O II	4035.09	70	−1.02
	42	.....	4176.16	70	−0.56
	48	.....	4241.79	95	−0.93
.....	.....	.....	4236.93 4237.05	75	−1.26
O II	3s–3p	.....	4649.14	275	−0.99
	(1)	.....	4641.81	230	−1.25
.....	.....	.....	4638.71	176	−1.64
.....	.....	.....	4676.24	165	−1.70
.....	.....	.....	4661.64	185	−1.57
.....	.....	.....	4673.75	51	−2.40
	(2)	2 per cent H	4349.43	234	−1.26
.....	.....	12 per cent H	4336.9	50	−2.15
.....	.....	.....	4325.7	50	−2.42
.....	.....	.....	4366.9	145	−1.61
.....	.....	8 per cent H	4345.5	125	−1.67
.....	.....	.....	4319.6	145	−1.70
.....	.....	.....	4317.2	145	−1.73
	(5)	.....	4414.91	185:	−1.11
.....	.....	.....	4416.98	155	−1.36
.....	.....	.....	4452.4	65	−2.11
	(6)	.....	3973.26	70	−1.35
.....	.....	He I	3954.3	160	−1.76
.....	.....	.....	3982.72	70	−2.08
.....	.....	.....	3945.05	125	−2.13
.....	.....	.....	4596.17	146	−1.15
	(15)	.....	4590.97	160	−0.99
	(16)	.....	4351.27	125	−1.14
.....	.....	4 per cent H	4347.43	90	−1.33
O II	3p–3d	.....	.....	.....	.....
	(12)	.....	3882.20	113	−1.90
.....	.....	.....	3865.45; .68	68	−2.22
.....	.....	S II	3851.04; 50.81	116	−2.38

TABLE 1—*Continued*

Ion	Multiplet	Blend	λ	W (mA)	log f
O II	.....	Si II N II	3856.01	99	−3.26
	10	Fe III	4075.87	182	−1.16
	.....	.....	4072.16	150	−1.31
	.....	.....	4069.90	185	−1.50
	.....	.....	4092.94	60	−2.17
	.....	.....	4085.12	75	−2.03
	.....	.....	4078.86	55	−2.14
	19	C III?	4156.54	55	−2.68
	.....	.....	4132.81	60	−1.96
	.....	S II	4153.30	112	−1.81
	.....	.....	4121.48	35:	−2.80
	20	.....	4119.22	120:	−1.41
	.....	15 per cent H	4105.00	65:	−2.01 −1.90
	.....	.....	4110.80	50:	−2.27
	26	.....	4395.88	90	−1.99
	25	.....	4705.36	135	−1.27
	.....	.....	4699.21	105	−1.46
	40	.....	4703.18	50	−1.59
	41	.....	4327.48	35	−1.67
	36	S II	4189.79	115	−1.16
	.....	.....	4185.5	.....	−1.27
	57	.....	4701.33	25	−1.75
O II	3d–3f	.....	.....	.....	.....
	54	.....	4276.71	45	−2.90
	.....	.....	4303.82	77	−1.53
	.....	S II	4294.8	50	−1.81
	.....	.....	4275.6	75	−1.41
	93	N II	4609.42	90	−1.50
	.....	N II	4602.11	140	−1.66
	101	O II S III	4253.74	72	−1.27 −1.36
	67	.....	4277.5	45	−1.96
	64	.....	4315.35	23	−3.16
	78	10 per cent H	4097.24	45	−1.39
	.....	.....	4087.14	47	−1.64
	.....	5 per cent H	4095.6	30	−1.52
Mg II	4	.....	4481	220	0.00
Al III	(8)	.....	4479.45	60	0.00
	(3)	.....	4529.6	140:	−0.11
	.....	.....	4513.2	115:	−0.37
P III	(3)	.....	4222.15	45	−0.12
Si III	5	.....	3806.56	238	−0.25
	.....	O III	3791.41	108	−0.87
	(2)	.....	4552.65	365	−0.17
	.....	.....	4567.8	295	−0.39
	.....	.....	4574.78	215	−0.86
Si IV	.....	.....	4116.1	60	−0.11
	.....	O II	4088.9	130	−0.41
S II	44	.....	4162.69	51	−1.16
	.....	.....	4217.23	15:	−2.10
S III	.....	.....	4285.04	96	−0.86
	.....	O II	4253.59	135	−0.58
	.....	.....	4332.71	50	−1.20
	.....	.....	4361.5	50	−1.33

where $\mathfrak{A}_e$, which involves the first three terms, changes from element to element and from line to line. The last three terms of equation (1) comprise Δ_w and involve factors that depend on the wave length and the atmospheric model—not the element or line in question. Here

$$k_{\text{eff}} = k'_\nu + \sigma \,, \tag{3}$$

where σ is the contribution of the electron scattering and k'_ν is the coefficient of continuous absorption corrected for the negative absorptions. The $\Delta \log \eta$ factor is required in order to utilize the same curve of growth for all lines. It depends on both the wave length and the intensity of the line, but for pure scattering the dependence on intensity is small and can generally be neglected.

The first term in $\mathfrak{A}_e$ can be computed for each element (it depends only on the temperature through v), the f is the Unsöld (1941) f, and $\theta(\chi - \chi_0)$,where $\theta = 5040/T$, is the correction necessary to reduce all terms or levels of a given configuration to a selected reference value. This correction changes slowly with the temperature.

The "pure absorption"-curve of growth is plotted, with the quantity

$$\log \frac{\eta_c}{N} = \mathfrak{A}_e + \Delta\lambda' \tag{4}$$

as abscissa. Here $\mathfrak{A}_e$ is the same as before, but

$$\Delta\lambda' = \log \frac{\lambda}{4000} + \log (1 - e^{-h\nu/kT}) - \log k_{\text{eff}} + \Delta \log \eta \tag{5}$$

includes the negative absorptions. The $\Delta \log \eta$ term, which is required if all lines are to be discussed with the aid of a single curve of growth, depends not only on the wave length but now strongly on the intensity as well.

In 1949 Miss Boutelle and the writer calculated a family of curves of growth for pure absorption. The computations were based on Chandrasekhar's solution of the transfer equation for the Milne-Eddington model and the assumption that the Planck function varies linearly with optical depth,

$$B = B_0 + B_1 \tau_\nu \,. \tag{6}$$

The curves are analogous to Wrubel's curves for pure scattering, but they exhibit some marked differences dependent upon the changed physical assumptions. Specifically, there is a pronounced difference between curves for different values of the ratio B_0/B_1. Table 2 summarizes the calculations of the theoretical curves.

The explanation for the sensitivity of the curves to the value of B_0/B_1 for the case of pure absorption is easy to understand. If a line is formed by the mechanism of pure scattering, its central intensity will always be zero. On the other hand, the central intensity of a line formed according to the mechanism of pure absorption will be fixed by the ratio B_0/B_1. A slow gradient of B_ν will yield a shallow line regardless of the number of atoms acting to produce it.

The curves of growth proposed by Menzel and by Unsöld and given in a more exact formulation by Wrubel have the advantage of simplicity and ease of application. We shall employ Unsöld's formulation of the problem, in which it is supposed that the profile of the line can be adequately represented by the empirical Minnaert formula,

$$\frac{1}{R} = \frac{1}{R_c} + \frac{1}{l_\nu} , \tag{7}$$

where $l_\nu = NH\alpha_\nu$, NH being the number of atoms "above the photosphere." We make an approximate correction for the variation of the depth of the photosphere with wave length by writing

$$NH = \frac{(NH)_0}{k_{\text{eff}}}. \tag{8}$$

To go from the scale of abscissae used by Wrubel and others to that employed by Unsöld, we must introduce a factor c_0 such that

$$\frac{\pi\epsilon^2}{mc}\frac{c\lambda}{v\sqrt{\pi}}f\frac{1}{k_{\text{eff}}} = c_0\frac{1}{R_c}\frac{\lambda f}{2\pi v k_{\text{eff}}}, \tag{9}$$

where

$$c_0 = \frac{\pi\epsilon^2}{mc}(2\sqrt{\pi}R_c) = 0.02654\sqrt{\pi} = 0.047, \tag{10}$$

TABLE 2

THEORETICAL CURVE OF GROWTH FOR PURE ABSORPTION
(MILNE-EDDINGTON MODEL)
($\log \eta$)

$\log W/b$	10/3	4/3	2/3	1/3	10/3	4/3	2/3	1/3
	$a=0$, B_0/B_1				$a=0.01$, B_0/B_1			
−1.0	−0.30	−0.68	−0.88	−1.02	−0.30	−0.68	−0.88	−1.02
−0.5	+0.60	−0.02	−0.29	−0.42	+0.59	−0.02	−0.39	−0.42
0.0		+1.35	+0.65	+0.31	+2.79	+1.26	+0.62	+0.31
+0.25		+3.77	+1.74	+0.99	+3.59	+2.51	+1.57	+0.99
+0.40			+3.15	+1.82	+3.78	+3.12	+2.38	+1.64
+0.50				+3.08	+3.96	+3.37	+2.80	+2.22
+0.60				+4.00		+3.59	+3.13	+2.66
+0.70						+3.80	+3.37	+3.04
+0.80						+3.98	+3.58	+3.30
+1.00							+3.96	+3.71
	$a=0.03$, B_0/B_1				$a=0.10$, B_0/B_1			
−1.0	−0.30	−0.68	−0.88	−1.02	−0.30	−0.68	−0.88	−1.02
−0.5	+0.59	−0.02	+0.29	−0.42	+0.49	−0.02	−0.29	−0.42
0.0	+2.40	+1.16	+0.59	+0.30	+2.07	+1.00	+0.50	+0.25
+0.25	+2.98	+2.12	+1.40	+0.91	+2.57	+1.70	+1.19	+0.78
+0.40	+3.29	+2.58	+2.07	+1.49	+2.84	+2.07	+1.76	+1.25
+0.50	+3.48	+2.86	+2.33	+1.96	+3.02	+2.29	+2.06	+1.63
+0.60	+3.68	+3.09	+2.59	+2.28	+3.19	+2.52	+2.30	+1.92
+0.70	+3.86	+3.30	+2.82	+2.54	+3.36	+2.73	+2.51	+2.15
+0.80		+3.50	+3.05	+2.76	+3.52	+2.93	+2.71	+2.53
+1.00		+3.86	+3.48	+3.20	+3.84	+3.32	+3.09	+2.73
+1.20			+3.88	+3.61			+3.44	+3.10
+1.40				+4.00				+3.46
+1.60								+3.81

since $R_c = 0.50$ for ϵ Canis Majoris. For this star the abscissa in the Unsöld curve of growth is

$$\log \frac{1}{R_c}\frac{\lambda f}{2\pi v k_{\text{eff}}} = \log \mathfrak{N}_e + 1.33 + \log \frac{\lambda}{4000} + \log (1 - e^{-h\nu/kT}) - \log k_{\text{eff}}. \quad (11)$$

Notice that, whereas the Milne-Eddington curves of growth yield the numbers of atoms of a given kind referred to a gram of stellar material, the Menzel, Wrubel, or Unsöld formulations, which are based on the Schuster-Schwarzschild model, give the "number of atoms above the photosphere." The mere division of log NH by k_{eff} does not change the log NH over to the number of atoms per gram of material; there is a zero-point shift between the Milne-Eddington and Schuster-Schwarzschild curves of growth.

TABLE 3

CONTINUOUS ABSORPTION COEFFICIENT, LOG k_ν
(log $P_e = 3.0$)

λ	T 28000 θ 0.18	25200 0.20	22900 0.22	21000 0.24	19350 0.26	18000 0.28	16800 0.30
3200	+0.28	0.45	0.62	0.77	0.93	1.06	1.20
3422 V	+ .33	.52	.69	.84	1.00	1.14	1.28
3422 R	+ .29	.47	.64	.79	0.94	1.09	1.23
3535	+ .32	.50	.67	.81	0.97	1.12	1.26
3650 V	+ .39	.54	.71	.86	1.02	1.16	1.29
3650 R	− .08	.07	.20	.32	0.41	0.52	0.60
3680 V	− .07	.08	.22	.32	0.42	0.53	0.61
3680 R	− .09	.05	.19	.29	0.38	0.49	0.57
3800	− .06	.08	.22	.32	0.42	0.52	0.60
4000	.00	.14	.27	.38	0.48	0.58	0.66
4200	+ .07	.20	.34	.45	0.55	0.65	0.73
4400	+ .11	.24	.38	.50	0.59	0.70	0.77
4600	+ .16	.29	.42	.55	0.64	0.74	0.82
4800	+ .20	.34	.47	.60	0.69	0.79	0.88
5000	+0.25	0.39	0.52	0.64	0.74	0.84	0.92

Wrubel's exact curves of growth for the Schuster-Schwarzschild model are based on the hypothesis of pure scattering. This theory predicts strong lines of zero central intensity, whereas these lines are observed to have central intensities of about 0.50. Unsöld's curve, based on the empirical Minnaert formula and applicable either for absorption or for scattering, seemed more appropriate for the present calculations. Nevertheless, it would be of interest to apply the Wrubel curves for the Schuster-Schwarzschild model and pure scattering, as they would probably represent an extreme departure from the physical conditions prevailing for the formation of the lines.

IV. APPLICATION OF CURVE-OF-GROWTH PROCEDURES TO OBSERVATIONAL MATERIAL

In order to apply the curve-of-growth procedure to the lines in ϵ Canis Majoris, we must first choose a tentative temperature value and calculate for each line the quantity log $wc/\lambda v$ and $\mathfrak{N}_e$. The kinetic velocity and the Boltzmann corrections have been computed for a temperature of 23000° K; the effect of the change in the corrections on the final results if the temperature is lowered to 20000° K is negligible.

The continuous absorption coefficient depends on both T and P_e. The first calcula-

tions were carried out with $T = 23000°$ K and log $P_e = 2.80$. The change in k_{eff} with P and T can easily be allowed for in the present analysis. In the calculation of k_ν I have assumed a hydrogen to helium ratio of 85/15 by numbers of atoms and have computed k'_ν with the aid of tables computed at Kyoto by Ueno, Saito, and Jugaku (1954). Table 3 gives the calculated values of log k'_ν for log $P_e = 3.0$.

The factor B_0/B_1 required in the Milne-Eddington curves of growth is often calculated from the approximation (cf., e.g., Wrubel 1949; Unsöld 1938)

$$B_\nu(T) = B_\nu(T_0)\left(1 + \frac{3}{8}\frac{e^{h\nu/kT_0}}{e^{h\nu/kT_0} - 1}\frac{h\nu}{kT_0}\frac{\bar{k}}{k_{\nu_0}}\tau_\nu\right). \tag{12}$$

Here T_0 is the boundary temperature, $\bar{k}$ is the mean absorption coefficient, and k_{ν_0} the absorption coefficient at the frequency under consideration. The formula involves the assumption that the temperature distribution approximates that of a gray body. Recent calculations of model atmospheres for hot stars show that near the surface the gray-body temperature distribution is strongly distorted by the blanketing effect of the Lyman continuum (see, e.g., Pecker 1951; Milligan and Aller 1954; Hunger 1955; Traving 1955). Accordingly, I have plotted B_ν as a function of τ_ν both for Milligan's model (which lies near B1) and for Miss McDonald's model (B2 or B3) (1953). The latter model has too high a boundary temperature, but the temperature distribution below about $\tau = 0.05$ seems reasonably satisfactory. The B_ν-τ_ν relationship cannot be represented by a

TABLE 4

VALUES OF B_0/B_1 DERIVED FROM MODEL-ATMOSPHERE CALCULATIONS

λ	B_0/B_1	λ	B_0/B_1	λ	B_0/B_1
3200	1.60	3800	0.95	4600	1.43
3420	1.85	4000	1.07	4800	1.56
3650 V	2.10	4200	1.18	5000	1.68
3650 R	0.86	4400	1.32		

straight line over the range in optical depth in which a line is formed. As a compromise, I passed a straight line through each B_ν-τ_ν-curve, with the slope and zero point so chosen as to give the best fit in the region $\tau = 0.05$ to $\tau = 0.6$. For the weaker lines whose effective optical depths may be of the order of 0.3, such an approximation may be adequate, but stronger lines (particularly those of atoms in the lower ionization stages) are formed in relatively shallow layers ($\tau < 0.1$), and the approximation tends to break down. Table 4 gives the adopted variation of B_0/B_1 of this ratio with wave length. The change with temperature is very small. Notice the sharp jump at the Balmer limit.

The calculation of log η_c/N or log $NHf/R_c\Delta\omega_D$ can be carried out in a straightforward fashion with the aid of the data for k_{eff}, Δ log η, and log f. For the Milne-Eddington approximation I have adopted as standard the curves for $B_0/B_1 = \frac{4}{5}$. The successive columns of Table 5 give the ion, the transition array or multiplet from the *Revised Multiplet Table* by Charlotte Moore (1945), the "reference term," i.e., the term or configuration to which log f is referred, the statistical weight of the term ϖ, and the energy difference $\chi_0 - \chi_{r,s}$ between the term and the continuum. We give log $N_{r,s}$ for the scattering- and absorption-curves of growth and, finally, log $(NH)^0_{r,s}$ derived from the Unsöld curve of growth. For a given choice of T and log P_e the calculation of the total number of atoms of a given element per gram of material or "above the photosphere" proceeds in a straightforward way (see, e.g., Unsöld 1941; Aller 1953).

The solution for the ionization equilibrium may be carried out with the aid of lines of elements that appear in two stages of ionization. If the measurements and interpretation are correct, the lines of C II and C III should yield the same abundance for carbon, while at the same temperature and density each ion of any other element that appears in two stages of ionization, e.g., S II and S III or Si III and Si IV, should give the same abundance. When this program is carried out, it is found that the sulphur and silicon lines require a lower temperature and/or a lower electron pressure than do the carbon lines. Each element observed in two stage of ionization gives its own curve in the log P_e-5040/T plane. If the isothermal approximation were sufficiently good, if the observations were not affected by errors, and if the f-values and damping constants were accurately known, all these curves would intersect at a point which would determine the ionization equilibrium. Unfortunately, the curves tend to lie parallel to one another and not too close together, so that, instead of lying along a line, the solution may be expected to fall in a region bounded, on the one hand, by the carbon solution and, on the other, by the silicon and sulphur solutions. Presumably, the C III and Si III lines are formed at very different layers in the stellar atmosphere.

TABLE 5

DATA FOR CALCULATION OF IONIZATION EQUILIBRIUM

Ion	Mult.	Ref. Term	ϖ	$\chi - \chi_{r,s}$	log $N_{r,s}$ W	log $N_{r,s}$ Abs.	log $N_{r,s}H$ U	log $N_{r+1}P_e$ W	log $N_{r+1}P_e$ Abs.	log $HN_{r+1}P_e$ U	Wt.
C II	4	3^2P	6	8.02	13.80	13.34	13.45	19.25	18.79	18.90	1
	6	3^2D	10	6.31	13.20	13.02	12.88	18.81	18.63	18.49	2
	33	$3d^4F$	28	6.56	13.10	12.50	12.43	18.20	17.60	17.53	11
C III	1	3^3S	3	18.28	12.56	12.50	12.16	16.19	16.13	15.78	2
	18	4^1F	7	7.83	11.05:	10.95	10.68	16.66	16.56	16.29	1
	16	4^3F	31	7.93	11.75:	11.60	11.32	16.86	16.71	16.43	1
N II	5,12	3P	12	11.08	14.02	13.97	13.58	19.15	19.10	18.71	10
	39,38	....	48	6.34	13.20	13.00	12.77	18.82	18.62	18.39	5
	15	....	2	9.17	12.65	12.54:	12.16	18.82	18.71	18.33	1
	33	....	36	8.42	13.92	13.66	13.56	19.18	18.92	18.76	1
	42	....	3	6.12	12.76	12.36:	12.35	19.61	19.21	19.20	1
O II	3s–3p	3s	30	12.12	14.33	14.25	13.90	19.36	19.28	18.93	10
	3p–3d	3p	90	9.25	14.08	14.00	13.68	19.08	19.00	18.68	5
	3d–4f	3d	150	6.17	13.80	13.67	13.40	19.26	19.13	18.86	2
Mg II	.....	3^2D	10	6.14	13.20	13.10	12.80	18.72	18.62	18.32	....
Al III	(5)	4^2D	10	7.86	13.00	12.86	12.50	18.13	17.99	17.63	....
	(8)	4^2F	14	7.64	12.13	12.03	11.72	17.17	17.07	16.76	....
Si III	2	4^3S	3	14.40	13.98	13.84	13.70	18.20	18.06	17.92	....
	5	4^3P	9	11.69	13.51	13.29:	13.21	18.15	17.93	17.85	....
Si IV	.....	4^2S	2	21.0	12.24	11.95	11.79	15.11	14.82	14.66	....
P III	(2)	4^2S	2	15.48	12.05	11.85	11.66	16.22	16.02	15.83	....
S II	.....	4P	90	7.42	13.32	13.00	12.85	18.67	18.35	18.20	....
S III	.....	$4s^3P$	12	16.73	13.25	13.13	12.90	17.20	16.98	16.75	....

Although the spectrum of the star contains a great number of lines of different elements in different stages of ionization, the determination of the ionization equilibrium is found to depend on only a very few lines. The strategic lines of C III seem rather strong compared with the other elements. There is essentially one good unblended line of C III;

the other lines are blended or weak, and their intensities are uncertain. The S II data consist of only two unblended lines, one of which is very weak and involves only a single observation. In computing the abundance of sulphur, we should employ the S III data rather than those of S II. There are numerous strong lines of Si III, but the only measurable unblended line of Si IV is λ 4116; the λ 4088 line is confused with O II. The damping constant, a, for the silicon lines is taken tentatively as 0.10. Ultimately, the ionization equilibrium is fixed by using carbon and silicon, giving greater weight to the latter, since the intensities of the silicon lines are more accurately fixed than are those of carbon.

The Al III lines also give a certain amount of trouble. The ratio of 4512 or 4529 to 4479 is much larger than in γ Pegasi, a star of the same excitation level, which lies near the main sequence. The 4479 line gives the lower abundance and a value more nearly in accord with that found in other stars. Calculations have been carried out with both sets of lines, however.

The ionization equilibrium fixes only a strip in the θ-log T plane, in which the solution may be expected to lie. We can choose either a higher temperature and electron pressure, as was tried earlier (e.g., $T = 23000°$ K, log $P_e = 2.80$), or a lower temperature and electron pressure, e.g., $T = 20600°$ K, log $P_e = 2.20$. The choice of the proper pair of values involves other considerations, which we shall review in Section V.

From a fitting of the observed points to the theoretical curves of growth it is found that (*a*) the scatter of the points about the theoretical curves is about the same for the three sets of curves; (*b*) the ionization equilibrium is about the same for the three theoretical curves, i.e., the discrepancy between the carbon and silicon solutions is not much affected by choosing the Unsöld curve of growth rather than that of Wrubel or the pure absorption-curve; and (*c*) the turbulence is determined essentially by the lines of the 3s–3p and 3p–3d configurations in O II; other elements give too few lines. The shift in ordinate, i.e., Δ log ($Wc/\lambda v$) differs for the three curves of growth, as shown in the accompanying table.

	M-E		SS (Unsöld) Approx.
	Scattering	Absorption	
Δ log $Wc/\lambda v$	0.20	0.60	0.35

The degree of microturbulence, i.e., the turbulence which is on such a scale as to affect the curve of growth but not the line profiles, would appear to depend on the curve of growth chosen for the analysis. The difference between the values inferred from the Wrubel and Unsöld curves is not great, but the pure absorption-curve appears to give much the largest turbulent velocities.

An application of the procedure proposed by Huang and Struve (1952) suggests that the small-scale turbulent velocities are of the order of 8 km/sec, whereas the "large-scale" velocities are of the order of 15 km/sec. No emphasis can be placed on these figures, because the McDonald coudé spectrograph, which yielded most of our information, was a prism instrument and the resolution of the tracing varied with the wave length. The proper discussion of the influence of turbulence on the profiles and total intensities of the lines in this star clearly requires additional observational data of high quality.

V. THE HYDROGEN AND HELIUM LINES

The strongest lines in the spectra of the B stars are those of hydrogen and helium. The lines of both these elements are broadened by the interatomic Stark effect. The hydrogen lines are widened by the first-order Stark effect; some helium lines are affected

by second-order Stark effect and others by the second-order Stark effect at low densities and the first-order effect at high densities.

The helium lines used in the present analysis are those affected by the quadratic Stark effect. Table 6 gives for each line, λ, the value of the damping constant, Γ, computed by the formula

$$\Gamma_e = 38.8 C^{2/3} T^{1/3} N_e , \tag{13}$$

where the Stark coefficient C is taken from the compilations of Unsöld (1944) and Mrs. Krogdahl. The temperature and electron density adopted for this particular computation are $T = 20600°$ K and $P_e = 100$ dynes. Calculations made for other temperatures and the higher electron pressure ($P_e \sim 630$ dynes) are not reproduced here. The third column gives log $\Delta\omega_D$ (Unsöld notation), and the fourth column the logarithm of the damping constant, a, as defined, for example, by Hjerting (1938). The measured equivalent width, W, is given in the last column. The f-values are taken from the work of Goldberg (1939) and are the same as those employed by Unsöld. The f-value for λ 4121 is probably too small. The λ 3964 line is affected by blending with Hϵ, and the number of

TABLE 6

DATA FOR HELIUM LINES

λ	log Γ	log $\Delta\omega_D$	log a	W
4713.3	9.26	11.09	−2.12	300
4437.5	9.98	11.11	−1.43	125
3964.7	10.02	11.16	−1.44	200
4388	11.15	11.10	−0.26	530
4121	9.80	11.15	−1.64	320

	Unsöld log NH_τ	Abs. (M-E) log N	Scat. (M-E) log N
Mean value	15.52	15.78	15.98

atoms derived from the line intensity has accordingly had to be corrected. The second half of the table gives the mean values of the number of atoms in the 2^3P level above the photosphere (Unsöld curve of growth) and the number in this level per gram of stellar material for both the hypothesis of pure absorption and that of pure scattering. The discordance between the latter two estimates amounts to a factor of 1.6.

The hydrogen lines are broadened by the first-order Stark effect. The profiles of the Balmer lines are insensitive to the temperature over a wide range of ΔT in the neighborhood of 22000° K. On the other hand, they are sensitive to the electron density. Hence we may employ the profiles of the hydrogen lines to establish the order of magnitude of the electron density by comparing observed and theoretical profiles calculated for different electron densities. The strong dependence of the absorption coefficient on the density means that a line profile computed for a fixed density cannot be expected to reproduce the observed profile in detail. One can secure a "best fit" such that the computed equivalent width is very close to the observed equivalent width. Such a procedure has been employed by Unsöld (1941).

Recent work at Kiel (Griem 1954) as well as the Michigan shock-tube experiments (Kolb 1954; Turner 1954) have indicated that line broadening by ions alone cannot account for the observed Balmer line profiles. The contributions of the electrons must

also be taken into account. We have employed the theory by Kolb to calculate line-broadening coefficients for Hγ as a function of temperature and density. This theory has been applied in the present instance to find the value of P_e appropriate for the broadening of the observed Hγ line. The theoretical profile (see Table 7) has been computed both with the empirical Minnaert formula, with the optical depth of the photosphere taken at $\tau = 0.50$, and with the Chandrasekhar solution of the transfer equation for pure absorption in the Milne-Eddington approximation. The value of B_0/B_1 is so chosen as correctly to reproduce the central intensity of the line. The profiles are calculated for $T = 20600°$ K, but there is no noticeable change if the temperature is taken as 23000° K.

Notice that the theoretical profiles for both the Milne-Eddington and the Schuster-Schwarzschild approximations are rather similar for the lower electron densities. The profile is sensitive to the electron density, and it is clear that the electron pressure must lie closer to 100 than to 800 dynes/cm². The theoretical cores are wider than the observed cores because the central parts of the line are formed in regions of lower electron densi-

TABLE 7

PROFILE OF Hγ

Δλ	Observed Residual Intensity in Line	Predicted Profile					
		Pure Absorption (M-E)			Minnaert Formula		
		$P_e = 800$	200	125	800	200	125
1.0	0.64	0.51	0.53	0.56	0.51	0.53	0.56
2.5	.79	.57	.70	.77	.56	.69	.77
5	.91	.72	.88	.93	.68	.88	.93
10	0.98	0.89	0.97	0.98	0.89	0.97	0.98

ties. On the other hand, if the electron density is so chosen that the theoretical and observed equivalent widths are equal, the theoretical profile is shallower in the wings. The Holtsmark theory gives somewhat narrower profiles and shallower wings for a given electron density; we would choose $P_e \sim 250$ dynes if the Holtsmark theory were adopted.

The hydrogen/helium ratio may be estimated from the curve-of-growth data. For the pure absorption- and pure scattering-curves of growth we can compute the number of helium atoms per gram of stellar material. At $\theta = 0.255$ and $\log P_e = 2.00$, we get a ratio of hydrogen to helium of 4.4 and 3 for the pure absorption- and pure scattering-curves, respectively. These values are unreliable because the helium lines are all strong lines, for some of which the damping constants are important and for all of which the value of B_0/B_1 is not the same as for the weaker lines used in most of the analysis.

The application of the Unsöld procedure gives, for the number of atoms in the second level of hydrogen "above the photosphere," $\log N_{0,2} H = 16.30$. Taking into account the variation of absorption coefficient with wave length for the hydrogen as well as the helium lines, we find a hydrogen/helium ratio of 7.9. The ratio is not sensitive to slight changes in the assumed temperature. This ratio differs from that obtained by Anne Underhill (1951) and Neven and De Jager (1954) by model-atmosphere methods but is in harmony with other analyses by curve-of-growth methods (Unsöld 1941; Aller 1946) and with Traving's results (1955) for an atmospheric model of τ Sco. We cannot regard the question of the hydrogen/helium ratio as settled by these curve-of-growth considerations, although it seems possible that this ratio may be closer to 10 than to 25.

VI. COMPARISON OF RESULTS

It is clear from the evidence of the hydrogen lines that the electron pressure is much lower than the value 630 dynes assumed in the earlier work. If the considerations of Griem and of Kolb are correct, a value near 100 dynes would appear appropriate. The ionization equilibrium of carbon and silicon suggests an excitation temperature of the order of 20000° K. Accordingly, I have carried out calculations for log $P_e = 2.00$ and $\theta = 0.245$ and 0.255. Probably the latter value is to be favored.

Table 8 gives log N_{r+1} for each of the observed ions for the Wrubel, pure absorption, and Unsöld curves of growth. The fifth column, labeled "I.C.," gives the correction for the effect of ionization to reduce the numbers found for each ion to the total number of a given element. The last three columns give log N, the number of atoms per gram of material, for the Milne-Eddington approximation, and log NH_0 for the Schuster-Schwarzschild approximation employed in the Unsöld curve of growth. The discordant values for S II and for C III are probably to be attributed to some degree to the effects

TABLE 8

CONCENTRATIONS OF ATOMS
($\theta = 0.255$; log $P_e = 2.00$)

	log N_{r+1}				log N		
	W	Abs.	U	I.C.	W	Abs.	U
He I	22.96	22.73	22.43	0.00	22.96	22.73	22.43
C II	19.63	19.27	19.23	+0.01	19.64	19.28	19.24
C III	16.73	16.67	16.33	+3.44	20.17	20.11	19.77
N II	19.86	19.67	19.43	+0.07	19.93	19.74	19.50
O II	19.77	19.70	19.38	+0.32	20.09	20.02	19.70
Mg II	19.63	19.53	18.23	0.00	19.63	19.53	18.23
Al III	18.03	17.93	17.62	+0.04	18.07	17.97	17.66
Si III	18.93	18.74	18.63	+0.20	19.13	18.94	18.83
Si IV	15.77	15.28	15.02	+3.43	19.00	18.71	18.55
P III	16.82	16.62	16.43	+0.14	16.96	16.76	16.57
S II	19.57	19.25	19.10	+0.09	19.67	19.35	19.20
S III	17.77	17.55	17.32	+0.73	18.50	18.28	18.05

of temperature stratification but also to possible errors in the intensities of the few observable lines.

Table 9 compares the abundances derived for the various elements on the assumptions of different electron densities and temperatures, on the one hand, and the different curves of growth, on the other. The last column of Table 9 gives some values based on previous studies of the sun and other hot stars. All values are expressed in terms of oxygen as standard (Aller 1953). From an inspection of the table the following conclusions may be drawn:

1. The carbon, nitrogen, and helium abundance ratios in this star appear to be more sensitive to the choice of T and P_e than do the ratios of magnesium, aluminum, and silicon.

2. The higher temperatures and electron pressures give abundance ratios for this particular star more nearly in accord with those found by previous investigators. On the other hand, the hydrogen-line data require the smaller values of T and P_e. The best values appear to be those for $\theta = 0.255$, log $P_e = 2.00$, although a still smaller temperature may be appropriate if the C III lines can be completely ignored. Nevertheless, it

TABLE 9

COMPANION OF DERIVED ABUNDANCES, LOG N/N_0

	$\theta=0.225$ LOG $P_e=2.80$			$\theta=0.245$									$\theta=0.255$ LOG $P_e=2.00$			PREVIOUS DATA
				log $P_e=2.80$			log $P_e=2.20$			log $P_e=2.00$						
	W	Abs.	U	W	Abs.	U	W	Abs.	U	W	Abs.	U	W	Abs.	U	
He	+2.53	+2.41	+2.44	+2.50	+2.37	+2.40	−2.93	+2.70	+2.72	+2.90	+2.77	+2.80	+2.86	+2.72	+2.73	+2.41
C	−0.67	−0.98	−0.58	−0.75	−0.97	−0.60	−0.41	−0.66	−0.30	−0.38	−0.61	−0.24	−0.44	−0.74	−0.46	−0.77
N	−0.43	−0.42	−0.39	−0.34	−0.43	−0.37	−0.11	−0.23	−0.17	−0.11	−0.20	−0.14	−0.16	−0.26	−0.20	−0.51
Mg	−0.71	−0.72	−0.69	−0.79	−0.81	−0.78	−0.43	−0.48	−0.45	−0.39	−0.41	−0.38	−0.46	−0.49	−0.47	−0.95
Al	−2.23	−2.24	−2.24	−2.30	−2.32	−2.30	−2.01	−2.03	−2.11	−1.94	−1.97	−1.95	−2.02	−2.05	−2.04	−2.33
Si	−1.15	−1.27	−1.07	−1.08	−1.24	−1.03	−1.14	−1.31	−1.22	−1.20	−1.28	−1.10	−0.96	−1.20	−1.02	−1.20
P	−3.06	−3.17	−3.03	−2.82	−2.94	−2.80	−2.96	−3.11	−2.97	−3.07	−3.09	−2.95	−3.13	−3.28	−3.13	−2.92
S	−1.59	−1.66	−1.52	−1.33	−1.50	−1.35	−1.30	−1.47	−1.37	−1.20	−1.30	−1.30	−1.30	−1.45	−1.35	−1.48

does not appear to be possible to reconcile the derived abundances with the "standard" values given in the last column.

3. The different curves of growth give different abundance ratios for different atoms. For example, we get somewhat different carbon/oxygen or nitrogen/oxygen ratios from the pure absorption-curve of growth than from the Wrubel or Unsöld curves. The differences are $\sim \pm 0.20$ in log N for certain elements.

4. From a comparison of Tables 8 and 9 the chief uncertainties would appear to lie in the values of log N derived from a few lines of a given element. Certain Al III lines, as previously noted, give discordant values for this star, and the C III lines appear to be unduly strong. Abundances or ionization equilibrium calculations that depend on one or two weak lines of uncertain intensities and f-values are to be avoided whenever possible. Blends with unknown contributors may play havoc with much of such data.

Many of our difficulties could have been avoided if we had confined our attention to stars with narrower, sharper, and more numerous lines whose intensities could be more accurately measured. On the other hand, we would thereby exclude the vast majority of "normal" B stars, which show somewhat broadened lines.

Some improvement could be obtained by taking some account of the temperature and density stratification in the atmosphere. There is no purely theoretical basis for constructing a model atmosphere for a supergiant; we should have to proceed by trial and error. Yet in this particular star, ϵ Canis Majoris, there is some indication that the range in excitation and ionization is such that it cannot be handled by an isothermal atmosphere approximation. A more extreme example in point is provided by γ Pegasi, where we simply cannot reconcile the observed intensities of the lines of Si II, Si III, and Si IV with the isothermal approximation.

As long as we restrict ourselves to rough analysis methods, there remains the question of which particular curve of growth ought to be chosen. Wrubel's curves, based on the Milne-Eddington approximation and the hypothesis of pure scattering for line formation, would appear to be ruled out for the observable, subordinate lines in the hotter stars. We might be inclined to employ the curves for pure absorption, but the theoretical equivalent widths are very sensitive to the approximation that the Planckian function varies linearly with optical depth throughout the strata where the lines are formed. This particular hypothesis is so poor that we would have to restrict ourselves to the comparison of lines over a very narrow range in total intensity. The rapid temperature drop near the surface of the star (cf., e.g., Unsöld 1943; Pecker 1951; Milligan and Aller 1954; Traving 1955) would appear to render the pure absorption-curves of growth of limited value.

The Schuster-Schwarzschild approximation embodied in the Menzel, Wrubel, and Unsöld curves of growth may be vulnerable to certain theoretical objections; it is certainly vulnerable for the lines formed in the deeper layers. In the application of curve-of-growth techniques, one is forced to adopt compromises, and, for such analyses as we have described here, the simple Unsöld procedure would appear to offer many advantages.

The chief use of rough analysis methods will be to provide starting approximations for more accurate treatments. Such refined methods are extremely laborious and worthwhile only for stars for which excellent observational data are available.

Thanks are due to Messrs. Bowen, Kuiper, and Struve, who made available to me the observational data used in this paper. The program is supported by a grant from the National Science Foundation.

REFERENCES

Aller, L. H. 1946, *Ap. J.*, **104**, 347.
———. 1948, *A.J.*, **53**, 105.
———. 1953, *The Atmospheres of the Sun and Stars* (New York: Ronald Press Co.), p. 293.

Garstang, R. H. 1954, *M.N.*, **114**, 118.
Goldberg, L. 1939, *Ap. J.*, **90**, 414.
Griem, H. 1954, *Zs. f. Phys.*, **137**, 280.
Hjerting, F. 1938, *Ap. J.*, **88**, 508.
Huang, Su-shu, and Struve, O. 1952, *Ap. J.*, **116**, 410.
Hunger, K. 1955, *Zs. f. Ap.*, **36**, 42.
Hynek, J. A. (ed.). 1951, *Astrophysics: A Topical Symposium* (New York: McGraw-Hill Book Co., Inc.), chap. 2.
Kolb, A. C. 1954, *Proceedings of the Indiana Conference on Stellar Atmospheres*, ed. M. Wrubel (1955), p. 63.
———. 1955, Ph.D. thesis, University of Michigan.
McDonald, J. K. 1953, *Pub. Dom. Ap. Obs. Victoria*, **9**, 269.
Menzel, D. H. 1936, *Ap. J.*, **84**, 462.
Milligan, J. E., and Aller, L. H. 1954, *Proceedings of the Indiana Conference on Stellar Atmospheres*, ed. M. Wrubel (1955), p. 93.
Moore, Charlotte. 1945, *Princeton Contr.*, No. 20.
Neven, L., and Jager, C. de. 1954, *B.A.N.*, **12**, 103.
Pecker, J. 1951, *Ann. d'ap.*, **13**, 294, 319, 433.
Traving, G. 1955, *Zs. f. Ap.*, **36**, 1.
Turner, E. B. 1954, *Proceedings of the Indiana Conference on Stellar Atmospheres*, ed. M. Wrubel (1955), p. 52.
Ueno, S., Saito, S., and Jugaku, J. 1954, *Contr. Kyoto Inst. Ap.*, No. 43.
Underhill, A. 1951, *Canad. J. Phys.*, **29**, 447.
Unsöld, A. 1938, *Physik der Sternatmosphären* (Berlin: Julius Springer).
———. 1941, *Zs. f. Ap.*, **21**, 22.
———. 1944, *ibid.*, **23**, 75.
Wrubel, M. 1949, *Ap. J.*, **109**, 66.
———. 1954, *ibid.*, **119**, 51.

ATMOSPHERES OF THE B STARS. II. THE SUPERGIANT 55 CYGNI

LAWRENCE H. ALLER
University of Michigan Observatory
Received July 29, 1955

ABSTRACT

The spectrum of the B3 I*a* supergiant 55 Cygni is discussed with the aid of a simple model atmosphere that reproduces the central intensities of the stronger lines and the intensities of the best Si II and Si III lines. The brightness temperature in the ordinary photographic region is near 18000° K, and the relative abundances of hydrogen, helium, carbon, nitrogen, oxygen, and silicon are more nearly in accord with values found for other hot stars than are those obtained previously by curve-of-growth methods. No secure evidence is found for the departures of the helium-line intensities from the values expected for thermodynamic equilibrium.

I. INTRODUCTION

Probably the curve of growth provides the best method for the quantitative analysis of the atmospheres of the supergiants of earlier spectral classes, O8–B1. In this spectral range the prevalence of turbulence and possibly of extended envelopes suggests that the atmospheres may not be in strict hydrostatic equilibrium or that the force exerted by the flux of radiation may be comparable with that exerted by gravity. The calculation of model atmospheres by the usual procedures, in which constancy of flux is required, is extremely laborious and may not even be justified theoretically. On the other hand, the assumption of an isothermal, isobaric atmosphere may not be capable of always giving even a rough representation of the observed state of ionization and excitation in the atmosphere. Accordingly, it has seemed worth while to investigate whether some procedure intermediate between the tedious complexity of a strict model-atmosphere calculation and a quick and rough curve-of-growth method may not be applicable to supergiants in certain spectral ranges. The method pursued in the illustrative calculation here is based on the following precepts:

a) The temperature distribution as a function of the optical depth, τ_0, at λ 5000 A is assumed to be the same as in a main-sequence star of about the same spectral class. For a particular star, slight modifications in the boundary temperature are made (if necessary) in order to reproduce the central intensities of the hydrogen lines.

b) The emergent flux in the continuum at any wave length is taken as

$$\pi F = 2\int B_\nu(\tau)\, E_2(\tau)\, d\tau\ , \tag{1}$$

where

$$d\tau_\nu = (\kappa_\nu + \sigma)\, \rho\, dx\ , \tag{2}$$

$$d\tau_0 = (\kappa_0 + \sigma)\, \rho\, dx\ , \tag{3}$$

for λ 5000 A, where κ_ν is the coefficient of continuous absorption and σ that of electron scattering. The difference between thermal and scattered continuous radiation is thus neglected, so that this method can be applied only to supergiants in which electron scattering is not the dominating cause of extinction throughout the layers principally responsible for the observed absorption lines.

c) The absorption lines are assumed to be produced by the mechanism of pure absorption.

d) Following the discussion by Traving (1955) for τ Scorpii, it is supposed that one may employ the empirical Minnaert formula,

$$\frac{1}{R}=\frac{1}{R_c}+\frac{1}{X_\nu}, \tag{4}$$

where R_c is the central depth in the line and X_ν is defined by

$$X_\nu = X_0 H(a, v), \tag{5}$$

where H is the line-broadening function discussed, for example, by Harris (1948) and

$$X_0=\frac{\pi e^2}{m c^2} N\lambda^2 f \frac{1}{\sqrt{\pi}\Delta\lambda_D} I_1. \tag{6}$$

The integral I_1 is defined below; N is the total number of atoms of the given kind per unit mass of stellar material; f is the Unsöld f (Unsöld 1941), and $\Delta\lambda_D$ is the Doppler breadth of the line (determined by thermal motion + microturbulence), and the other factors have their usual meanings.

e) The integral I_1 is defined as

$$I_1=\int \frac{N_{r,s}}{N}\frac{G(1-e^{-hc/\lambda kT})}{\kappa_0+\sigma} d\tau_0, \tag{7}$$

where $N_{r,s}$ is the number of atoms in the rth level of the sth stage of ionization of the atom in question. The weighting function, G, is that defined for pure absorption by Unsöld (1932), viz.,

$$G(\tau) = \frac{2}{F_c(0)}\left[\int_\tau^\infty B(t) E(t)\, dt - B(\tau) E_2(\tau)\right]. \tag{8}$$

Here F_c is the flux in the continuum at the wave length in question. The function G is strictly appropriate only for the wings of strong lines or for weak ones. In a more rigorous analysis one could use a more sophisticated approach, as suggested, for example, by Pecker (1951), but the lack of accuracy of the model-atmosphere theory in our present example does not appear to justify the extended labor involved.

f) One calculates from the observations the quantity $\log (W_\lambda/2R_c\Delta\lambda_D)$ for each line, using a value of the turbulent velocity derived from a conventional curve-of-growth analysis. As abscissa for the Unsöld curve of growth we can note

$$\log\frac{1}{R_c}\frac{N_{r,s}Hf}{\Delta\omega_D}=\log\frac{X_0}{R_c}+1.027. \tag{9}$$

For a given line and model atmosphere it is a straightforward task to compute $\log (X_0/NR_c)$ and use the Unsöld curve of growth to evaluate $\log N$. The method differs from that of Traving only in that a rough model atmosphere is employed. The criterion of applicability is that the model must represent the relative intensities of lines of a given element in different stages of ionization.

II. APPLICATION TO 55 CYGNI

The supergiant 55 Cygni, HD 198478, $\alpha = 20^h45^m5$, $\delta = +45°44'.6$ (1900), $m = 4.89$, provides an instructive illustration for our quasi-model-atmosphere procedure. The *Henry Draper* class, cB2, is definitely too early, and Morgan's assignment of B3 I*a* seems more accurate. Some years ago I carried out a curve-of-growth analysis for this star with the aid of Wrubel's (1949) curves, using intensity measurements from one coudé plate secured with the 100-inch. The temperature assumed was unfortunately too high (Hynek

1951). Subsequently, Voigt (1952) made a careful investigation of the curve of growth for this star by the strict method of Unsöld (1941). He determined the excitation temperature from the ionization equilibrium of silicon, utilizing the lines of Si II and Si III, obtaining a much lower value, namely, $T = 16250°$ K, but about the same electron pressure, $\log P_e = 1.55 \pm 0.30$. He found a turbulent velocity of about 36 km/sec from the line profiles and a value of $\log g = 2.87$.

The ionization potential of Si II is 16.27 ev, whereas those of most of the other ions represented in the spectrum of this star—He I, C II, N II, O II, and Al III—are substantially higher. Presumably, the Si II lines are formed predominantly at shallower layers than are those of Si III and O II, for example.

With a temperature distribution similar to that derived for a ~B1 star (Milligan and Aller 1954), I carried out a model-atmosphere computation in the usual way. The continuous absorption coefficients have been calculated from the tables by Ueno, Saito, and Jugaku (1954) for a hydrogen/helium ratio of about 5. In the calculation of the model atmosphere (first trial) the zero point of the temperature distribution was taken as 19000° K at $\tau_0 = 0.6$. The brightness temperature at 5000 A was 18000° K. The value

TABLE 1

APPROXIMATE MODEL ATMOSPHERE

τ_0	T	$\log P_e$	τ_0	T	$\log P_e$	τ_0	T	$\log P_e$
0.00	13650	...	0.20	16000	1.98	1.4	19400	2.56
.01	13800	1.04	0.30	16470	2.10	1.6	19750	2.60
.02	14200	1.26	0.40	16850	2.18	1.8	20000	2.64
.04	14600	1.48	0.50	17200	2.25	2.0	20300	2.67
.06	14850	1.61	0.60	17500	2.30	2.5	20900	2.73
.08	15100	1.70	0.80	18100	2.38	3.0	21600	2.79
.10	15250	1.76	1.0	18600	2.45			
0.15	15650	1.89	1.2	19000	2.51			

of the surface gravity was taken as 800 cm/sec^2 on the basis of Voigt's results. This first approximation did not reproduce the measured intensities of the Si II and Si III lines; the Si III/Si II ratio was still too large.

Accordingly, I again readjusted the temperature, this time taking $T(\tau_0 = 0.6) = 17500°$ K and choosing the boundary temperature as 13650° K so as to reproduce the central intensities of the strongest lines in the 4000–5000 A region of the spectrum. This time a calculation of the relative intensities of the silicon lines showed an agreement with the observations; hence the intensities of lines of other ions have been calculated as well.

Some characteristics of this simple "interpolation model" are summarized in Table 1, the arguments of whose columns are self-explanatory. The same surface gravity has been adopted as before, i.e., $\log g = 2.90$. The "brightness" temperatures at λλ 4100, 4684, and 5000 A are, respectively, 18100°, 17600°, and 17370° K.

The first test of the applicability of the model is that it must reproduce the intensities of the silicon lines. We calculate the weighting functions for the necessary wave lengths and compute $N_{s,\tau}/N_{\text{total}}$ as a function of the optical depth from the combined Boltzmann and Saha equations. Table 2 illustrates the computational procedure. I have chosen only those lines for which good observational data are available. The λλ 3853, 3856, and 3862 lines of Si II, for example, have measurable intensities, but the f-values are unknown. The Doppler half-width, $\Delta\lambda_D$, is next computed on the assumption of a turbulent velocity ξ of 36 km/sec, as suggested by Voigt from the evidence of the line profiles. The curve-of-growth data are indecisive on the turbulent velocities; the carbon data employed in

the present analysis suggest that a velocity about half as large, i.e., of 18 km/sec, may be more appropriate. Calculations have been carried out with both assumed velocities. The mean W_λ is taken from the measurements published by Voigt and those obtained by the present writer. In the computation of the quantity $\log [(1/R_c)(W_\lambda/2\Delta\lambda_D)]$, the value for the central depth, $R_c = 0.45$, found by Voigt, has been retained in the present calculation. The log f-values are based on the tables of Bates and Damgaard (1949). The reference term for Si II is $3d^2D$ and that for Si III is $4s^3S$. Next we calculate $\log 1/R_c\Delta\omega_D$. The integral I_1 is computed from the model atmosphere, and the quantity $\log \zeta'$ refers to the abscissa, $\log (f/R_c\Delta\omega_D)I_1$. A curve of growth is plotted in the usual way; its fit with the theoretical Unsöld curve then determines $\log N$, the total number of silicon atoms. If the approximate model atmosphere is to be regarded as useful for the analysis of this particular star, the lines of both Si II and Si III must fit the same curve. This they do, in the present instance, to within the errors of the observations. Before proceeding further, one should try to represent the hydrogen-line profiles. Unfortunately, the available observational profiles do not lend themselves to a clear-cut decision here. To establish the surface gravity to within a factor of 2, it is necessary to have pro-

TABLE 2

THEORETICAL INTENSITIES OF THE SILICON LINES

Ion	λ	$\Delta\lambda_D$	Mean W_λ	$\log [(1/R_c)(W_\lambda/2\Delta\lambda_D)]$	$\log f$	$\log (1/R_c\Delta\omega_D)$	$\log I_1$	$\log \zeta'$
Si II....	4128.05	0.496	113	−0.60	−0.40	−11.39	−7.03	18.82
	4130.88	.....	150	− .48	− .22	.....	.....	18.64
Si III....	4552.65	0.548	305	− .21	− .17	−11.35	−6.76	18.27
	4567.87	.....	212	− .37	− .39	.....	.....	18.50
	4574.78	.....	109	−0.66	−0.86	.....	.....	18.97

file measurements accurate to within about 2 per cent. There is some suggestion that the assumed surface gravity may still be a little high and that a value $\log g = 2.60$ may be better than the $\log g = 2.90$. We cannot settle this question until better observational data are available. For the present we shall retain the model atmosphere described in Table 1.

The supergiant star, 55 Cygni, offers a rich line spectrum of neutral helium. From his investigation by the Unsöld method, Voigt concluded that the population of the 2^3P level obtained from the lines of the 2^1S-n^1P and 2^3P-n^3D series was significantly less than the values derived from the 2^1P-n^1S, 2^3P-n^3S, and 2^1P-n^1D levels. He attributed these differences to departures from thermodynamic equilibrium. The lower values are all determined essentially by lines falling to the shortward of the Balmer limit, the high values from lines falling on the longward side of the Balmer limit. If we carry out the analysis by the approximate model-atmosphere method, we find the values given in Table 3. The departures from the 2^3P-n^3D level are substantially reduced but not entirely eliminated. If a turbulent velocity of 18 instead of 36 km/sec is assumed, the discrepancies are still further reduced. An improved model atmosphere, on the one hand, and improved line intensities, on the other, would be necessary to decide whether or not departures from thermodynamic equilibrium were real or fancied.

In the other elements, the analysis has been restricted to those lines for which good intensity and f-value data are available. Little can be gained by adding material of low weight. Table 4 lists the transitions employed. Throughout, I have used the f-values computed for the transition arrays from the tables of Bates and Damgaard. In O II,

Garstang (1954) has computed line strengths in intermediate coupling; unfortunately, similar calculations are not available for many of the other elements.

Finally, the ratio of hydrogen to helium must be established by some other means. Ideally, we could calculate the line intensities for selected lines of each element and juggle the abundances until the observed intensities were represented. The problem is complicated by the circumstance that the continuous absorption, as well as the line absorption, is determined by the elements involved. In a first examination of the question some approximate procedure might suffice.

TABLE 3

THE POPULATION OF THE 2^3P LEVEL IN HELIUM

Series	log NH	Departure from 2^3P-n^3D		Series	log NH	Departure from 2^3P-n^3D	
		Curve of Growth (Voigt)	Model Atmosphere			Curve of Growth (Voigt)	Model Atmosphere
2^1P-n^1D	23.30	+0.70	+0.20	2^3P-n^3S	23.23	+0.40	+0.23
2^1P-n^1S	23.57		+0.47	2^1S-n^1P	23.10	0.00	0.00
2^1P-n^3D	23.10	0.00	0.00				

TABLE 4

DATA FOR LINES OF CARBON, NITROGEN, AND OXYGEN

Ion	Transition	$\chi_0-\chi_{s,r}$	$\bar{\lambda}$	Reference Terms	$\varpi_{s,r}$
C II	$3p^2P-4s^2S$	8.04	3920	$(^1S)3p\,^2P^0$	6
	$3d^2D-4f^2F$	6.33	4267	$(^1S)3d\,^2D$	10
N II	3s−3p	11.12	.....	$3s(^1P+^3P^0)$	12
	3d−4f	6.36	.....	$3d(^3P^0+^3D^0+^3F^0)$	45
O II	3s−3p	12.15	.....	3s config.	30
	3p−4s	8.90	.....	3p config.	90

Unsöld's (1941) procedure for estimating the abundance of hydrogen and helium involves the determination of the number of atoms "above the photosphere." The determination of log NH for hydrogen by this procedure uses the confluence of the hydrogen lines near the Balmer series limit. We may compare log NH, determined by the Unsöld method from the 2^3P-n^3D or 2^1S-n^1P series of helium, with that from the Balmer series. The difference in the "depths of the photosphere" in the two spectral regions should be small. For these helium series Voigt gets log $NH = 14.80$, while for the hydrogen series log $NH = 15.80$. We assume $\theta = 5040/T = 0.3$ (since the photosphere is shallow in this spectral region) and find a hydrogen/helium ratio of 6.6.

Table 5 compares the results obtained by the model-atmosphere analysis with those found by the strict Unsöld procedure for several stars. The data for 55 Cygni are taken from the paper by Voigt, those for τ Scorpii from Unsöld, and the results for 10 Lacertae from the present writer's reductions (Aller 1946). The composition found from the model-atmosphere method is more nearly in accord with that of the hotter stars.

The conclusion that may be drawn is that although the *grobanalyse* methods may give

results similar to those of model-atmosphere methods for O9–B1 stars, they will not necessarily do so for stars around B3 if the ionization equilibrium is fixed by a single element such as silicon.

One further point must be mentioned. The total mass of the atoms contributing to the quantity NH turns out to be about 2.2 g. In other words, the use of the stratification integral in conjunction with the curve of growth leads to a total "mass above the photosphere" slightly in excess of 2 g. The exact value will depend on the hydrogen/helium ratio.

Further theoretical analyses of these data do not appear to be warranted until, on the one hand, better observational data have been secured and, on the other, a better theory is available for the atmospheres of supergiants.

We must emphasize that the present procedure amounts only to a device for introducing the principal effects of the temperature stratification into essentially the curve-of-growth method. Other limitations of the curve of growth are not removed. Specifically, it is assumed that all the lines have the same shape (i.e., that given by the Minnaert formula) and that they all follow exactly the same curve of growth. That the abundances derived by Traving's method or by the present very similar one are so close to those found by the Unsöld curve of growth does not necessarily prove that they are the correct abundances. We must still examine the effect of using a precise formulation such as that of Pecker rather than a rough interpolation formula. Günther Elste and I will examine this question in one of the next papers of this series.

TABLE 5

COMPARISON OF ABUNDANCE ESTIMATES
(log N/N_0)

Element	log NH	Model Atm.	Curve of Growth		
			55 Cyg	τ Sco	10 Lac
Hydrogen	23.92	+3.02	+2.82	+3.01	+3.31
Helium	23.10	+2.20	+2.21	+2.26	+2.24
Carbon	20.33	−0.57	−1.04	−0.75	−0.68
Nitrogen	20.55	−0.35	−0.64	−0.39	−0.64
Oxygen	20.90				
Silicon	19.38	−1.52	−1.62	−1.19	−1.07

REFERENCES

Aller, L. H. 1946, *Ap. J.*, **104**, 347.
Bates, D. R., and Damgaard, A. 1949, *Phil. Trans. R. Soc. A*, **242**, 101.
Garstang, R. 1954, *M.N.*, **114**, 118.
Harris, D. 1948, *Ap. J.*, **108**, 114.
Hynek, J. A. (ed.). 1951, *Astrophysics: A Topical Symposium* (New York: McGraw-Hill Book Co., Inc.), chap. 2.
Milligan, J., and Aller, L. H. 1954, *Proceedings of the Indiana Conference on Stellar Atmospheres* (1955), p. 93.
Pecker, J.-C. 1951, *Ann. d'ap.*, **14**, 383.
Traving, G. 1955, *Zs. f. Ap.*, **36**, 1.
Ueno, S., Saito, S., and Jugaku, J. 1954, *Contr. Kyoto Inst. Ap.*, No. 43.
Unsöld, A. 1932, *Zs. f. Ap.*, **4**, 339.
———. 1941, *ibid.*, **21**, 22.
Voigt, H. H. 1952, *Zs. f. Ap.*, **31**, 48.
Wrubel, M. 1949, *Ap. J.*, **109**, 71.

MODEL ATMOSPHERES

THOMAS L. SWIHART
Yerkes Observatory
Received July 1, 1955; revised August 17, 1955

ABSTRACT

A method is considered for correcting model stellar atmospheres so that the integrated flux conditions are satisfied. The method is applied to the sun and to a dwarf star of approximate spectral type F5. It is found that after only two integrations the desired distribution of flux with depth can be reproduced with an accuracy of about 1 per cent. Since the method is not restricted to cases in which the integrated flux is constant with depth, it can be applied to problems considering convection and the blanketing effect.

When one constructs a model stellar atmosphere, the integrated net flux must satisfy certain conditions. If one considers a plane-parallel atmosphere in radiative equilibrium and if the blanketing effect is neglected, then the integrated flux will be constant with depth and will be related to the effective temperature by the equation

$$\pi F = \sigma T_e^4 , \tag{1}$$

where πF is the integrated net flux and σ is Stefan's radiation constant.

It is well known that the continuous spectrum of the sun can be reproduced to a good first approximation by that of a gray atmosphere. This fact has led many investigators to adopt the gray-body temperature distribution for computing model atmospheres, including nonsolar types; although the accuracy of this technique is sufficient for many purposes, there are cases for which greater accuracy is desired.

Several methods for correcting the temperature distribution so that the flux is constant with depth have been published (see Unsöld 1951; Kourganoff 1952, and the references listed there). There are cases, however, for which a more efficient method is desired. The purpose of this paper is to present such a method, suggested by Dr. B. Strömgren. The atmospheres considered in the present paper are assumed to be plane-parallel and in radiative equilibrium. Also, the Kirchhoff-Planck relation and the equation of mechanical equilibrium have been used throughout.

If one expands the fourth power of the temperature in the form

$$T^4 = \tfrac{3}{4} T_e^4 [a + b\tau + cE_2(\tau) + dE_3(\tau)] , \tag{2}$$

where E_2 and E_3 are the second and third exponential integral functions, the problem is the determination of the coefficients a, b, c, and d such that the flux conditions are satisfied.

The integrated flux at any depth in a gray atmosphere is given by the well-known relation

$$F_g(\tau) = \Phi_\tau [B(t)] , \tag{3}$$

where

$$\Phi_\tau [f(t)] = 2\int_\tau^\infty f(t) E_2(t-\tau)\, dt - 2\int_0^\tau f(t) E_2(\tau - t)\, dt . \tag{4}$$

Expressing the integrated Planck function in terms of the temperature and using equation (2), one can write the gray-body flux in the form

$$F_g(\tau) = \frac{3\sigma}{4\pi} T_e^4 [a\phi_0 + b\phi_1 + c\phi_2 + d\phi_3] , \tag{5}$$

where

$$\phi_0 = \Phi_\tau [1] , \qquad \phi_1 = \Phi_\tau [t] ,$$
$$\phi_2 = \Phi_\tau [E_2(t)] , \qquad \phi_3 = \Phi_\tau [E_3(t)] . \tag{6}$$

Values of these ϕ functions are tabulated by Kourganoff (1952).

Equation (5) yields the gray-body solution as follows: for a gray atmosphere with constant flux, equation (1) is valid for F_g. Then equation (5) becomes

$$a\phi_0 + b\phi_1 + c\phi_2 + d\phi_3 = \tfrac{4}{3} , \tag{7}$$

which is independent of the value of τ. By choosing four values of τ, one immediately obtains the coefficients.

A more important characteristic of equation (5) is the fact that it determines the change of the gray-body flux, at any depth, consequent to any given change in the temperature distribution. Taking differences, we obtain

$$\Delta F_g(\tau) = \frac{3\sigma}{4\pi} T_e^4 [\phi_0 \Delta a + \phi_1 \Delta b + \phi_2 \Delta c + \phi_3 \Delta d] . \tag{8}$$

Apparently, equation (8) may be used to determine the correction to the temperature distribution necessary to change the gray fluxes by a given amount.

One might expect equation (8) to be a good approximation for a nongray atmosphere if departures from grayness are not large. We shall now consider numerical applications of this equation to nongray atmospheres. Two atmospheres were considered—the sun and a dwarf F5 star. For the solar atmosphere, the ionization tables used were those published by Strömgren (1944). For the other, improved tables were available (Strömgren, unpublished); however, an investigation showed that the inhomogeneities introduced by using two different tables were small compared with the effects under consideration. Tables of representative points and weights (cf. Underhill 1950), tables of the absorption coefficients, and tables of the Planckian function were kindly supplied by Dr. Strömgren (unpublished).

The Rosseland mean absorption coefficient was used throughout, but the final results are independent of this. As pointed out, for example, by Strömgren (1951), the physically important quantity is the relation between temperature and pressure. The mean optical depth is only a convenient quantity to use in order to obtain the T-p relation, and this relation does not depend on the manner in which τ or $\bar{\kappa}$ is defined.

Values of $\kappa_\nu/\bar{\kappa}$ were given for 23 wave lengths, from λ 912 to λ 58336. Six of these were the long- and short-wave-length sides of the hydrogen absorption edges at λλ 3646, 8204, and 14584. The intermediate values were chosen so that one had equal intervals in frequency between each two absorption edges. The integral over frequency to obtain the integrated flux was then performed by means of the Newton-Cotes formula.

The parameters for the solar atmosphere were taken as

$$\log A = 3.8 , \qquad \log g = 4.44 , \tag{9}$$

where A is the hydrogen-metal ratio and g is the gravity. For the first approximation to the temperature distribution, the gray-body solution, corresponding to a surface temperature function of

$$\theta_0 = \frac{5040^\circ}{T_0} = 1.069 , \tag{10}$$

was adopted.

The values of F determined from the model varied from 2.13×10^{10} at the surface to 2.00×10^{10} in the deep layers, the units being ergs cm^{-2} sec^{-1}. This is very similar to

the values obtained by Michard (1949), who also used the Rosseland mean absorption coefficient.

The accuracy of equation (8) was tested as follows: each of the coefficients in the temperature expansion was separately varied and a new model computed. The fluxes, computed at several depths, were then compared with the predictions of equation (8). The results for one case are shown in Table 1, in which F_c is the value computed from the atmosphere and F_p is the value predicted from equation (8). Both are in the units ergs cm^{-2} sec^{-1}. In all cases the agreement was such that one can expect the fluxes predicted by equation (8) for solar-type atmospheres to have an error of no more than about 1 per cent. It was found that the influence of the fourth term in the temperature expansion on the fluxes is very small, and so the coefficient d was not varied.

TABLE 1

PREDICTED AND COMPUTED FLUXES

τ	F_p	F_c	τ	F_p	F_c
0.0	2.27×10^{10}	2.27×10^{10}	1.5	2.26×10^{10}	2.28×10^{10}
0.5	2.28	2.29	2.0	2.26	2.23
1.0	2.26	2.26			

TABLE 2

FLUXES OF THE CORRECTED SOLAR ATMOSPHERE

τ	0.0	0.5	1.0	1.5	2.0
$10^{-10}F$	2.13	2.13	2.12	2.13	2.11

TABLE 3

FLUXES COMPUTED FROM THE F5 MODELS

τ	F_1	F_2	τ	F_1	F_2
0.0	3.53×10^{10}	3.45×10^{10}	1.5	3.60×10^{10}	3.49×10^{10}
0.5	3.54	3.45	2.0	3.55	3.48
1.0	3.58	3.48			

The next step was to correct the first atmosphere so that the flux was constant with depth. The chosen value of F was 2.12×10^{10}, and Table 2 shows how well this was satisfied. The F5 model provided an important check on the versatility of the foregoing method, as departures from grayness are greater for early-type stars. The same values of the hydrogen-metal ratio and gravity (eq. [9]) were used for the F5 model as were used for the solar models. In the solar atmospheres the absorption due to the H_2^+ molecule was included (Bates 1952); however, this was found to have very little influence on the structure of the models and was not included in the F5 models.

The solution found for the solar model was used as a first approximation for the F5 model, the only difference being the higher effective temperature. The predicted value of the flux was 3.46×10^{10}, and the values computed, denoted as F_1, are listed in Table 3. In spite of the large extrapolation, the errors in this first approximation are only about 3 or 4 per cent. The fluxes computed from the corrected F5 model are also shown in

Table 3. They are denoted as F_2, and for all depths they deviate from the predicted flux by less than 1 per cent. The structures of the solar and F5 atmospheres are published in another paper (Swihart 1956).

For stars not too early in spectral type, the method described in the present paper makes possible the construction of accurate model atmospheres after only two integrations. It should be emphasized that the method is not restricted to problems with a constant integrated flux, but any distribution of flux with depth can be reproduced within limits determined by the flexibility of the assumed temperature expansion. This is particularly important for problems considering convection and blanketing.

Although the present investigation concerned only stars as early as F5, unpublished work by K. Osawa indicated that the method gives a similar accuracy for early A-type stars. For very early-type stars, however, one would expect the efficiency to be less.

Böhm (1954) recently published a different method for correcting the temperature distribution so that the flux conditions are satisfied. He makes use of an iteration method for solving an integral equation that determines the correction function ΔB when the values ΔF are specified.

The author would like to thank Dr. B. Strömgren for suggesting this problem and for offering helpful advice.

REFERENCES

Bates, D. R. 1952, *M.N.*, **112**, 40.
Böhm, K.-H. 1954, *Zs. f. Ap.*, **34**, 182.
Chandrasekhar, S. 1950, *Radiative Transfer* (Oxford: Clarendon Press), chap. ii (on the method of representative points and weights).
Kourganoff, V. 1952, *Basic Methods in Transfer Problems* (Oxford: Clarendon Press).
Michard, R. 1949, *Ann. d'ap.*, **12**, 201.
Strömgren, B. 1944, *Pub. mind. med. Köbenhavns Obs.*, No. 138.
———. 1951, *Astrophysics*, ed. J. A. Hynek (New York: McGraw-Hill Book Co., Inc.), pp. 196–197.
Swihart, T. L. 1956, *Ap. J.*, **123**, 143.
Underhill, A. B. 1950, *Pub. mind. med. Köbenhavns Obs.*, No. 151.
Unsöld, A. 1951, *Naturwissenschaften*, **22**, 525.

MODEL ATMOSPHERES AND THE SOLAR CONTINUUM

THOMAS L. SWIHART
Yerkes Observatory
Received July 1, 1955; revised August 17, 1955

ABSTRACT

Standard models of the solar atmosphere are constructed, and their continua are compared with observations of the solar continuum. Three possible sources of the differences are investigated. It is found that deviations from the Kirchhoff-Planck relation are negligible. Convection improves the theoretical fluxes and intensities by a small amount, but it also causes the values of the limb darkening to be more discordant with the observations. An evaluation of the continuous absorption of the metals in the ultraviolet, by means of a formula which leaves a large uncertainty, shows promise in reproducing the observations.

I. INTRODUCTION

When one constructs a model atmosphere, one tries to represent the physical conditions in a real atmosphere. The test of how well one succeeds in this is a comparison with observations. If the differences are greater than one can ascribe to observational uncertainty, the model is not an exact representation of the real atmosphere. The purpose of the present paper is to try to find the sources of the discrepancies between observations of the solar continuum and the so-called "standard" models of the sun (see Chandrasekhar 1950, and references listed there; also Aller and Pierce 1952). In the next section values of the limb darkening and the monochromatic fluxes derived from two standard models are compared with observations. In subsequent sections the following possible sources of error in the standard models are separately considered: (1) deviations from the Kirchhoff-Planck relation, (2) convection, and (3) the continuous absorption of the metals. The influence of variations in temperature at a given depth, due to turbulent convective transport, and the effects of a more detailed theory of blanketing than has been taken into account in the standard models are not considered in this paper.

II. THE STANDARD MODELS

The standard models which are used in this paper are plane-parallel atmospheres in radiative and mechanical equilibrium. The Kirchhoff-Planck relation is used, and the continuous absorption is assumed to be due to hydrogen and the negative hydrogen ion (Chandrasekhar and Breen 1946) only. The values of gravity and the hydrogen-metal ratio are given by

$$\log g = 4.44 , \qquad \log A = 3.8 . \tag{1}$$

The ionization tables used were those published by Strömgren (1944).

Absorption lines subtract energy from certain wave lengths and redistribute it throughout the spectrum. The true integrated flux at any depth is equal to the integrated flux computed according to the theory of the continuous spectrum, minus the total flux ΔF that is subtracted through all the absorption lines. The latter quantity is known from observation for $\tau = 0$. Since a detailed theory of the blanketing effect, which would give ΔF as a function of τ, is not available, ΔF was assumed to be independent of depth and equal to the observed value for $\tau = 0$. Consequently, the integrated fluxes of the standard models, at all depths, were assumed to be equal to the observed flux increased by ΔF for $\tau = 0$, or by about 10 per cent.

Helium was not included in the atmospheres of this paper, since its abundance is some-

what uncertain. As helium is essentially an inert constituent of the solar atmosphere, its presence can easily be taken into account by modifying the value of gravity (cf. Strömgren 1944, p. 34; see also Aller and Pierce 1952).

The solar constant probably lies between 1.90 and 2.00 cal cm^{-2} min^{-1}. If the corresponding values of F are increased by about 10 per cent to allow for blanketing, one obtains for the limiting cases 2.13 and 2.27×10^{10} ergs cm^{-2} sec^{-1}. As these figures are significantly different, a standard model was computed for each, by the method described by Swihart (1956). These two models are illustrated in Table 1. The model with the lower effective temperature is denoted as model VI, while model II has the higher effective temperature. Notice that the temperature for model II at a given optical depth is greater than that of model VI by a factor which is nearly constant with depth. The gas pressures are about the same for the two models, while model II has the larger p_e.

TABLE 1

THE STANDARD MODELS

τ	Model VI			Model II		
	θ	log p	log p_e	θ	log p	log p_e
0.05	1.045	4.30	0.37	1.031	4.30	0.40
0.1	1.020	4.46	0.55	1.004	4.46	0.58
0.2	0.980	4.63	0.75	0.963	4.63	0.79
0.4	0.921	4.79	1.01	0.904	4.79	1.06
1.0	0.816	4.98	1.58	0.801	4.97	1.66
2.0	0.722	5.07	2.24	0.709	5.05	2.32

TABLE 2

RATIO OF OBSERVED TO COMPUTED FLUXES

λ	F_ν(Obs.)/F_ν(VI)	F_ν(Obs.)/F_ν(II)	F_ν(Obs.)/F_ν(C)	λ	F_ν(Obs.)/F_ν(VI)	F_ν(Obs.)/F_ν(II)	F_ν(Obs.)/F_ν(C)
3647	1.04	0.97	0.98	8206	1.16	1.10	1.15
4235	1.20	1.10	1.14	9214	1.14	1.08	1.14
5050	1.28	1.17	1.23	12213	1.08	1.04	1.07
6250	1.26	1.18	1.23	14588	1.03	1.00	1.01

Comparing these models with Münch's (1947), the pressures of model VI are larger by about 0.05 in the logarithm, and the electron pressures are larger by about 0.05 near the surface and by 0.10 at optical depth unity. Model II has larger differences, since Münch used an effective temperature lower than that of model VI. Münch defined his optical depth in a different manner than has been done in this paper. If one compares points of equal temperature, the differences are much smaller.

Values of the monochromatic flux, the intensity at the center of the disk, and the limb darkening were computed for both models. These were compared with observations taken from Minnaert (1953). Tables 2 and 5 of Minnaert's work were used for the fluxes, as the values in his Table 1 are affected by absorption lines.

The second and third columns of Table 2 give the ratio of observed to computed fluxes, for several wave lengths, for models VI and II, respectively. The corresponding ratios for the intensities showed almost identical behavior, and so are not given. The Balmer discontinuities of models VI and II, measured in the fluxes, are 0.076 and 0.086, respectively. Measured in the intensities, these figures are 0.103 and 0.115. The computed fluxes

of both models are apparently too small in the visual region, where the observations are the most accurate. The computed fluxes seem to converge to the correct values in the far infrared, but observations in this region are less accurate.

It is apparent that if the only source of error is the effective temperature, one needs an even higher temperature than that of model II. It was found that, by extrapolating the monochromatic fluxes of models VI and II to higher temperatures, a very good fit with the observations in the visible region could be made; however, the extrapolated effective temperature was almost 6100°, much higher than that of the sun. One therefore needs an agent which will depress the ultraviolet and perhaps the far infrared, so that the computed fluxes in the visible can match observations.

The second, third, and fourth columns of Table 3 give the limb darkening for $\cos\theta = 0.7$ for observations (Minnaert, 1953) for model VI and for model II, respectively. The sixth, seventh, and eighth columns are the same for $\cos\theta = 0.4$. It again appears that the best fit would be afforded by an atmosphere with a temperature somewhat higher

TABLE 3

LIMB DARKENING

λ	$\cos\theta = 0.7$				$\cos\theta = 0.4$			
	Obs.	VI	II	C	Obs.	VI	II	C
4500	0.78	0.76	0.76	0.76	0.55	0.52	0.53	0.51
5000	.81	.79	.80	.79	.59	.57	.58	.55
6000	.84	.83	.84	.82	.66	.64	.65	.62
7000	.86	.85	.86	.84	.71	.69	.69	.67
8000	.88	.87	.87	.86	.74	.73	.73	.71
10000	.90	.89	.90	.88	.78	.77	.77	.75
15000	0.94	0.92	0.92	0.92	0.84	0.80	0.80	0.80

than that of model II. Observations indicate that if the sun is to be represented by a standard model, the effective temperature will be much higher than is allowable. In the following sections several deviations from the standard models are investigated.

III. THE KIRCHHOFF-PLANCK RELATION

In thermal equilibrium the Kirchhoff-Planck relation,

$$j_\nu = \kappa_\nu B_\nu(T), \tag{2}$$

is valid. In order to test the validity of this equation in the solar atmosphere, it will be assumed that the emission and absorption coefficients are related by

$$j_\nu = V \kappa_\nu B_\nu(T), \tag{3}$$

where V is a quantity whose deviation from unity is a measure of the error introduced by using equation (2).

If collisional ionization of H^- is much more important than photoionization, then the Kirchhoff-Planck relation will be a very good approximation (cf., e.g., Strömgren 1951, pp. 197–199). The maximum deviation of this relation will therefore be obtained by evaluating V under the assumption that collisional ionization is unimportant. Then (Rudkjøbing 1941)

$$V = \frac{\int_{\nu_0}^{\infty} \kappa_\nu J_\nu \, (d\nu/\nu)}{\int_{\nu_0}^{\infty} \kappa_\nu B_\nu(T) \, d\nu/\nu}, \tag{4}$$

where J_ν is the mean intensity and κ_ν is the bound-free absorption coefficient of H^-, corrected for induced emission.

The quantity V was evaluated at several depths in the atmosphere of model VI, the absorption coefficient being taken from Chandrasekhar (1945). The value at the surface was 0.96, and at optical depth unity it was 1.00. Since the surface layers have very little influence on the emitted continuum, deviations from the Kirchhoff-Planck relation cannot explain the differences between theory and observation discussed in Section II.

IV. CONVECTION

Since there is no completely satisfactory theory of energy transport by convection, it was decided to construct a convective solar model by assuming values of the convective transport which seemed plausible and to evaluate the corresponding continuous emission from the atmosphere. The radiative and convective fluxes decided upon are given in Table 4, in which F_r is the radiative flux divided by π, and F_c is the value corresponding to the convective flux. The model is based on model VI in the sense that the total flux is 2.13×10^{10} ergs cm^{-2} sec^{-1}. The values in Table 4 can be obtained by modifying somewhat the velocities of the turbulent elements in the theory of Vitense (1953), still keeping them reasonable.

TABLE 4

RADIATIVE AND CONVECTIVE FLUXES

τ	$10^{-10} F_r$	$10^{-10} F_c$	τ	$10^{-10} F_r$	$10^{-10} F_c$
0.0	2.13	0.00	1.5	2.10	0.03
0.5	2.13	.00	2.0	1.89	.24
1.0	2.13	0.00	3.0	1.23	0.90

In the convective model, improved ionization tables were available (Strömgren, unpublished). Ionization potentials, based on the values of Birge (1941), were employed. Also the following relative abundances of the metals among themselves were used: magnesium, 0.34; silicon, 0.37; iron, 0.22; aluminum, 0.03; calcium, 0.02; sodium, 0.02. Investigation showed, however, that the changes in a model due to the use of the different ionization tables were very small compared with the effects under consideration.

The model was constructed by the method described by Swihart (1956); however, the four-term temperature expansion used in that paper was not sufficiently flexible for the present case, since the variations of the radiative flux with depth were rather large. A two-functional representation was used, in the form

$$\begin{aligned} T^4 &= a + b\tau + cE_2(\tau) + dE_3(\tau) && (\tau \lesssim 1); \\ T^4 &= a' + b'\tau + c'E_2(\tau) + d'E_3(\tau)\, e'\tau^2 + f'\tau^3 && (\tau \gtrsim 1). \end{aligned} \tag{5}$$

One does not expect this expansion to be valid for very large depths, for the term in τ^3 will eventually become dominant; however, this will not occur until a rather great depth, at which point the influence on the emitted radiation is small. In practice, therefore, an expression approximately equal to the adiabatic was substituted at the point where the second formula in equation (5) began to diverge.

There are ten coefficients to be determined in equations (5). Since the influence of the terms in E_3 is very small (Swihart 1956), d and d' were both given the same value as the coefficient of the E_3 term in the solution of model VI. This leaves eight coefficients to be evaluated. Two of these are fixed by requiring the temperature and the tempera-

ture gradient to be continuous at $\tau = 1$. The six remaining coefficients are used to satisfy the radiative flux conditions at the six depths listed in Table 4.

The equations for the changes of the radiative fluxes are much more complicated than the corresponding expressions in the case of a simple one-function temperature expansion. The general equation for optical depths less than unity is

$$\begin{aligned}\text{Const.} \times \Delta F(\tau) = {} & \Delta a\,[Q^{t}_{\tau}(1, \tau) - R^{\tau}_{0}(1, \tau)] \\ & + \Delta b\,[Q^{t}_{\tau}(t, \tau) - R^{\tau}_{0}(t, \tau)] \\ & + \Delta c\,\{Q^{t}_{\tau}[E_2(t), \tau] - R^{\tau}_{0}[E_2(t), \tau]\} \\ & + \Delta a' Q^{\infty}_{1}(1, \tau) + \Delta b' Q^{\infty}_{1}(t, \tau) + \Delta c' Q^{\infty}_{1}[E_2(t), \tau] \\ & + \Delta e' Q^{\infty}_{1}(t^2, \tau) + \Delta f' Q^{\infty}_{1}(t^3, \tau) \qquad (\tau \lesssim 1),\end{aligned} \tag{6}$$

with a similar equation for optical depths greater than unity. Here

$$\begin{aligned} Q^{\tau_2}_{\tau_1}[f(t), \tau] &= 2\int_{\tau_1}^{\tau_2} f(t) E_2(t - \tau)\, dt \qquad (\tau \leq \tau_1), \\ R^{\tau_2}_{\tau_1}[f(t), \tau] &= 2\int_{\tau_1}^{\tau_2} f(t) E_2(\tau - t)\, dt \qquad (\tau \geq \tau_2). \end{aligned} \tag{7}$$

The Q and R functions can be determined analytically in terms of the exponential integral functions, for the cases in which $f(t)$ is a simple power of t (see, e.g., Kourganoff 1952, pp. 43–45). For $f(t) = E_2(t)$, however, the functions must be evaluated numerically. This was greatly facilitated by the tables of Chandrasekhar and Breen (1948) and of Kourganoff (1952). When the Q and R functions have been determined, the six equations similar to equation (6) are solved simultaneously for six of the quantities Δa, Δb, . . . , $\Delta f'$, two of them having been eliminated by means of the continuity conditions at $\tau = 1$. The six values of $\Delta F(\tau)$ are minus the assumed values of F_c. The coefficients are then given by

$$\begin{aligned} a &= a_0 + \Delta a, \qquad b = b_0 + \Delta b, \qquad c = c_0 + \Delta c, \\ d &= d' = d_0, \qquad a' = a_0 + \Delta a', \qquad b' = b_0 + \Delta b', \\ c' &= c_0 + \Delta c', \qquad e' = \Delta e', \qquad f' = \Delta f', \end{aligned} \tag{8}$$

where a_0, b_0, etc., are the coefficients found in the solution of model VI.

After the temperature distribution had finally been determined, one could integrate the atmosphere. When the radiative fluxes were evaluated, they were found to differ by 3 or 4 per cent from the values desired. The reason for this was that, as explained previously, the Q and R functions were computed on the assumption that equation (5) is valid for all depths, whereas a nearly adiabatic expression was substituted at the depth in which equation (5) began to diverge. This occurred at about $\tau = 6$; however, the importance of the layers below this is not so great as this may seem to indicate, since the error in the surface flux was only 1 per cent and also because the term in τ^3 is purely artificial.

Since the errors in the fluxes computed from this model were somewhat larger than was desired, a second convective model was constructed from the first one. The procedure was the same as for the first model, but the actual work was much less, as the Q and R functions had already been evaluated. The T-τ relation of the form of equation (5) was again cut off at the depth at which it began to diverge, and a near-adiabatic form sub-

stituted. In this case, however, the influence of this on the fluxes could be taken into account. The errors in the computed fluxes for optical depths up to 1.5 were less than 1 per cent, while for the two deeper points the deviations from the predicted values were about 2 per cent.

The structure of the final convective model, to be called "model C," is shown in Table 5. Comparing this with the structure of model VI, in Table 1, one sees how the upper radiative layers of the atmosphere are modified when there is convection in the lower layers. The main differences are that the surface temperature of model C is less than that of model VI ($\theta_0 = 1.116$ for model C and 1.081 for model VI), while the temperature gradient is greater than that of the standard model. This agrees with the results of Rudkjøbing (1946). At greater depths than those listed in Table 5, the temperature gradient of model C becomes much less, as one would expect. The ratio of the observed solar fluxes to those computed from model C, for several wave lengths, is listed in the fourth column of Table 2. There is some improvement over the corresponding values of model VI, but it is not very much. The Balmer discontinuity of the convective model, measured in the flux, is 0.073, slightly less than that of the standard model.

One expects qualitatively that convection will cause the monochromatic fluxes in the visible region to be larger than in the corresponding standard model. For convection

TABLE 5

THE CONVECTIVE MODEL

τ	θ	$\log p$	$\log p_e$	τ	θ	$\log p$	$\log p_e$
0.05	1.062	4.30	0.34	0.4	0.917	4.80	1.02
0.1	1.029	4.47	0.53	1.0	0.810	4.99	1.60
0.2	0.981	4.63	0.75	2.0	0.709	5.07	2.30

modifies the deep layers more than those near the surface, and so the short wave lengths, for which the continuous absorption is small, will be most affected. Thus the energy in the ultraviolet will be smaller, and the fluxes in the visible will have to be increased to make the integrated flux the same.

One might expect to be able to reproduce the observed fluxes simply by increasing the convective transport over what has been assumed for model C. The fifth and ninth columns of Table 3, however, indicate that model C is in less agreement with the observed limb darkening than are the standard models. This should not be interpreted as meaning that convection does not exist, because in a true theory of turbulent convection the plane-parallel assumption is not strictly valid; however, it seems unlikely that the convective transport can be much greater than that assumed for model C.

V. THE CONTINUOUS ABSORPTION COEFFICIENT

When accurate values of the continuous absorption coefficient of the negative hydrogen ion became available (Chandrasekhar and Breen 1946), the discrepancies between theories of the solar atmosphere and observations were greatly reduced (see, e.g., Chandrasekhar 1950, pp. 307–311). There are indications, however, that there are additional sources of absorption in the ultraviolet which may be important (see, e.g., Woolley and Stibbs 1953, pp. 84–85).

The continuous absorption of the metals in the ultraviolet was investigated to see whether it could possibly affect the structure of the atmosphere. To simplify the calculations, the metal mixture was replaced by an average element with an ionization potential of 7.75 volts. The abundance was given by the hydrogen-metal ratio, $\log A = 3.8$. The simple hydrogen-like equation for the absorption coefficient was used (Unsöld 1938,

p. 122). The value Unsöld gives for the effective nuclear charge, 2.5, was also used. The results for several wave lengths and for $\theta = 0.860$ are given in Table 6. Here, $\kappa_\nu(M)$ is the absorption coefficient of the metals per gram matter (essentially per gram hydrogen), and $\kappa_\nu(H + H^-)$ is the corresponding quantity for hydrogen and H^-. The former is, of course, very uncertain; however, this should give at least an idea of the order of magnitude of the metallic absorption. Notice that, according to these simplified calculations, the metals contribute some 20 per cent to the absorption coefficient at the Balmer limit, while at shorter wave lengths they become dominant.

The wave lengths below the Balmer limit contribute nearly 20 per cent of the total energy emitted by model II, so the metals may appreciably alter the character of the continuous spectrum. In order to obtain a general idea of the effects of the metals, the following approximate procedure was carried out. Using model II as a basis, the metallic absorption was calculated at each wave length and for the temperature at optical depth 0.7. These values were added to the coefficients of H and H^-, computed for all depths, at each wave length. Although the metallic absorption varies appreciably with depth, the uncertainties involved do not warrant a more accurate procedure.

TABLE 6

MASS-ABSORPTION COEFFICIENTS

λ	$\kappa_\nu(M)$	$\kappa_\nu(H+H^-)$	λ	$\kappa_\nu(M)$	$\kappa_\nu(H+H^-)$
3647−	0.08	0.45	2084	2.4	0.21
2652	0.39	0.28	1459	130	0.18

This made possible the recalculation of the monochromatic fluxes in the ultraviolet region. The wave lengths above the Balmer limit are not affected, so the resulting atmosphere had a lower effective temperature than model II. The effective temperature of the metallic atmosphere (that is, the atmosphere in which metallic absorption was included) was made equal to that of model II by multiplying all the monochromatic fluxes of the metallic atmosphere by the ratio of the integrated fluxes. This ratio turned out to be 1.14.

The foregoing indicates that, for wave lengths greater than the Balmer limit, a metallic atmosphere will have fluxes about 14 per cent greater than the corresponding standard model. Referring to the second and third columns of Table 2, one sees that such an increase reduces very considerably the discrepancies between the observations and the standard models, particularly so for model II. This would apparently cause errors in the far infrared, but in this region both theory and observation are less certain.

Recent rocket observations of the solar spectrum are consistent with the belief that the energy in the very short wave lengths of both standard models is much too large. Using data given by Tousey (1953), the intensity at λ 2652 for model VI is too large by a factor of about 10, and the difference increases rapidly for the shorter wave lengths.

VI. SUMMARY

Two standard solar models, differing from each other in effective temperature, were constructed and compared with observation. The monochromatic fluxes and intensities of both models were systematically too small in the visible region of the spectrum. According to rocket observations, the ultraviolet regions of both models are much too high, while the agreement in the far infrared is satisfactory.

Deviations from the Kirchhoff-Planck relation were found to be negligible.

Since convection tends to depress the ultraviolet relative to the other parts of the spectrum, the convective model reduced slightly the errors in the fluxes of the standard

models; however, the changes were small, and a comparison with observed limb darkening indicated that a model with greater convective transport in the upper layers was not to be expected. Thus convection may help reduce the errors in the standard models somewhat, but it cannot completely remove them.

Finally, if the computed metallic absorption coefficients are correct to at least an order of magnitude, the continuous absorption of the metals may go a long way toward removing the differences between observations and the predictions of the standard models.

A more complete theory of blanketing than has been included in the standard models should also be investigated. For the highest layers in the photosphere and therefore in the theory of line absorption, this is quite important (cf. Münch 1946; Böhm 1954); however, this is not expected to influence appreciably the continuous spectrum discussed here. Also, the possible modifications due to temperature variations at layers of equal depth, mentioned earlier, should be looked into.

It is a pleasure to thank Dr. B. Strömgren for suggesting this problem and for the many interesting discussions which the author had with him during the progress of this work.

REFERENCES

Aller, L. H., and Pierce, A. K. 1952, *Ap. J.*, **116**, 176.
Birge, R. T. 1941, *Rev. Mod. Phys.*, **13**, 233.
Böhm, K.-H. 1954, *Zs. f. Ap.*, **34**, 182.
Chandrasekhar, S. 1945, *Ap. J.*, **102**, 395.
———. 1950, *Radiative Transfer* (Oxford: Clarendon Press).
Chandrasekhar, S., and Breen, F. H. 1946, *Ap. J.*, **104**, 430.
———. 1948, *ibid.*, **108**, 92.
Kourganoff, V. 1952, *Basic Methods in Transfer Problems* (Oxford: Clarendon Press).
Minnaert, M. 1953, *The Sun*, ed. G. P. Kuiper (Chicago: University of Chicago Press).
Münch, G. 1946, *Ap. J.*, **104**, 87.
———. 1947, *ibid.*, **106**, 217.
Rudkjøbing, M. 1941, *Zs. f. Ap.*, **20**, 288.
———. 1946, *Ann. d'ap.*, **9**, 7.
Strömgren, B. 1944, *Pub. mind. med. Københavns Obs.*, No. 138.
———. 1951, *Astrophysics*, ed. J. A. Hynek (New York: McGraw-Hill Book Co., Inc.).
Swihart, T. L. 1956, *Ap. J.*, **123**, 139.
Tousey, R. 1953, *The Sun*, ed. G. P. Kuiper (Chicago: University of Chicago Press).
Unsöld, A. 1938, *Physik der Sternatmosphären* (Berlin: Julius Springer).
Vitense, E. 1953, *Zs. f. Ap.*, **32**, 135.
Woolley, R. v. d. R., and Stibbs, D. W. N. 1953, *The Outer Layers of a Star* (Oxford: Clarendon Press).

MODEL ATMOSPHERES WITH HIGH HYDROGEN-METAL RATIO

THOMAS L. SWIHART
Yerkes Observatory
Received July 1, 1955; revised August 17, 1955

ABSTRACT

In an attempt to represent the atmospheres of F-type subdwarfs, two model atmospheres with large values of the hydrogen-metal ratio were constructed. For both the solar and the F5 dwarf models, the continuous spectra were very insensitive to rather large changes in the hydrogen-metal ratio; however, blanketing and the continuous absorption of the metals were not included in the calculations. Since both effects tend to depress the ultraviolet, this may be an explanation of the ultraviolet excess of the subdwarfs, if the latter differ from normal stars in the metal content only.

The work of Chamberlain and Aller (1951) indicates that the F-type subdwarfs are probably stars, somewhat hotter than the sun, which have a low metal content. It was thought worth while to consider models with a high hydrogen-metal ratio, A, in somewhat greater detail.

Such models, if they do represent the subdwarfs, will be desirable for several reasons. In the first place, they are the basis for quantitative determinations of the chemical

TABLE 1

SOLAR MODELS

τ	θ	S 38			S 50		
		τ_0	log p	log p_e	τ_0	log p	log p_e
0.05	1.045	0.05	4.30	0.37	0.05	4.79	−0.10
0.1	1.020	0.11	4.46	0.55	0.11	4.94	+0.11
0.2	0.980	0.22	4.63	0.75	0.22	5.08	+0.40
0.4	0.921	0.44	4.79	1.01	0.43	5.20	+0.83
1.0	0.816	1.13	4.98	1.58	1.09	5.29	+1.60
2.0	0.722	2.29	5.07	2.24	2.23	5.33	+2.33

abundances. Also, in connection with spectrophotometric data or color-index observations, they make possible the determination of the effective temperature. The latter is particularly important in obtaining values of the radii, essential in discussions of the internal structure of subdwarfs (Reiz 1954).

The structure of two solar atmospheres, obtained by the method described by Swihart (1956), are shown in Table 1. The models differ from each other only in the assumed value of A. The model denoted by S 38 has log $A = 3.8$, and model S 50 has log $A = 5.0$. The T-τ relation is the same for both models, but a given value of τ does not correspond to the same geometrical depth for both models; τ_0 is the monochromatic optical depth for λ 5050.

Table 2 lists two more models, both constructed for an effective temperature corresponding to that of an F5 dwarf. Again, log $A = 3.8$ for model F 38, and log $A = 5.0$ for model F 50. The solar value of gravity, log $g = 4.44$, was used for all models. The general effect of increasing A is seen to be an increase in the pressure and a decrease in the electron pressure. These differences become smaller at greater depths, since the

ionization of hydrogen is beginning to be important. Also, variations of A have a greater influence on the structure of the atmosphere for the solar models than for the models with higher temperature, as one would expect.

Table 3 lists the values of F_ν, the monochromatic emergent flux divided by π, for the four models considered. Notice that these quantities are quite insensitive to rather large changes in the value of A. The Balmer discontinuity, D, for both F models is 0.17, in agreement with the value obtained by Chamberlain and Aller (1951) and normal for a standard F5 dwarf (Chalonge and Divan 1952). The color temperature in the photographic and visual regions is also essentially the same as that obtained by Chamberlain and Aller. For the solar models, a Balmer discontinuity of 0.08 is indicated ($D = 0.10$, as measured in the intensity at the center of the disk).

TABLE 2

F5 MODELS

τ	θ	F 38			F 50		
		τ_0	log p	log p_e	τ_0	log p	log p_e
0.05	0.930	0.05	4.29	0.58	0.05	4.47	0.37
0.1	.907	0.11	4.45	0.78	0.10	4.63	0.61
0.2	.871	0.21	4.61	1.03	0.21	4.77	0.95
0.4	.819	0.43	4.74	1.39	0.43	4.88	1.37
1.0	.726	1.08	4.86	2.08	1.08	4.97	2.11
2.0	0.643	2.10	4.92	2.73	2.11	5.01	2.75

TABLE 3

MONOCHROMATIC FLUXES

λ (A)	$10^5 F_\nu$ (ergs cm^{-2} sec^{-1} $\Delta\nu^{-1}$)				λ (A)	$10^5 F_\nu$ (ergs cm^{-2} sec^{-1} $\Delta\nu^{-1}$)			
	S 38	S 50	F 38	F 50		S 38	S 50	F 38	F 50
3647$^-$	1.05	1.08	1.80	1.80	8206	3.03	3.06	4.42	4.44
3647$^+$	1.25	1.28	2.69	2.69	10503	3.14	3.14	4.23	4.24
4235	1.64	1.67	3.18	3.15	14588	3.03	3.04	3.68	3.68
5050	2.11	2.16	3.75	3.76	19450	2.18	2.18	2.54	2.53
6250	2.64	2.67	4.23	4.25					

These results indicate that, in the continuum, subdwarfs should appear the same as normal stars of the same effective temperature, and so the same relation which holds for normal stars between color and effective temperature should also be valid for the subdwarfs; however, the observed ultraviolet excess of the subdwarfs (Roman 1954) is not explained by these results.

Two factors, both of which would tend to give the subdwarfs an ultraviolet excess with respect to normal stars which have the same color in the visible region, have been neglected in the previous discussion. These are blanketing and the continuous absorption of the metals in the ultraviolet. The presence of both of these tends to lower the continuum in the ultraviolet, and so a metal-poor star should have an ultraviolet excess of some amount. This points to the conclusion that if a subdwarf has the same relative energy distribution in the visible as a normal star and if the red ends of the spectra are

not significantly different, then the subdwarf will have a somewhat higher effective temperature. Since the effects of blanketing and continuous absorption of the metals were not included in the construction of the models used in this paper, it may be that if these effects are very important, the models with large A are more representative of the subdwarfs than the models with smaller A are of the normal stars. In any event, recent rocket observations of the ultraviolet solar spectrum (Durand, Oberly, and Tousey 1949; Tousey 1953) indicate that the monochromatic fluxes obtained from the solar models are much too high below about λ 3000. All the foregoing comments assume that subdwarfs differ from normal stars in the metal content only. If other effects are operative, these comments may need modification.

It is again a pleasure to thank Dr. B. Strömgren for suggesting this problem and for many interesting discussions which the author had with him.

REFERENCES

Chalonge, D., and Divan, L. 1952, *Ann. d'ap.*, **15**, 201.
Chamberlain, J. W., and Aller, L. H. 1951, *Ap. J.*, **114**, 52.
Durand, E., Oberly, J. J., and Tousey, R. 1949, *Ap. J.*, **109**, 1.
Reiz, A. 1954, *Ap. J.*, **120**, 342.
Roman, N. G. 1954, *A.J.*, **59**, 307.
Swihart, T. L. 1956, *Ap. J.*, **123**, 143.
Tousey, R. 1953, *The Sun*, ed. G. P. Kuiper (Chicago: University of Chicago Press), p. 658.

THE SURFACE-TEMPERATURE CLIMATE OF MARS

FRANK GIFFORD, JR.

Lowell Observatory, Flagstaff, Arizona*

Received March 29, 1955; revised August 11, 1955

ABSTRACT

The Lowell Observatory radiometric measurements of Martian surface temperatures are analyzed, and surface-temperature climatological properties of Mars are obtained. Annual and diurnal temperature variations and seasonal isotherm maps are displayed and discussed.

INTRODUCTION

The climate of the planet Mars has been debated almost since the invention of the telescope. Until the time of the first radiometric work of Coblentz and Lampland (1923, 1927) at Lowell Observatory and Pettit and Nicholson (1924) at Mount Wilson, conclusions were largely conjectural. Theoretical calculations that at first involved only the planet's distance from the sun were later refined, culminating in Lowell's (1907) study of the Martian temperature. Nevertheless, Herschel's remark (1784) that "the planet has a considerable but moderate atmosphere . . . in many respects similar to ours" is still very much to the point; and the details of the Martian temperature climate are not at all certain. The results of the systematic program of Martian radiometry carried on by Lampland at Lowell Observatory between 1926 and 1943 were published (cf. Gifford 1953). These temperature determinations, about 1300 altogether, make it possible to delineate at least the broader features of the surface-temperature distribution of Mars, which is the aim of the present study.

INSTRUMENTATION, DATA REDUCTION, AND ERRORS

Details of radiometric instrumentation, observational procedure, and reduction of the data, together with a study of the sources of error, have been given by Gifford (1953). Briefly, tiny thermocouples, the receivers of which were made either by flattening a small globule of pure tin or by punching a small disk or rectangle from gold foil, were mounted in vacuum cells containing rock-salt or fluorite windows. The receivers were blackened with a mixture of platinum and carbon black in alcohol containing a little shellac or turpentine. One junction of the couple was exposed to the planetary image at a focus of the 42-inch Lowell reflector and the other to space, and a series of galvanometer deflections was obtained. The series of readings was then repeated, but with absorbing screens of various materials in front of the cell window, in order to isolate fairly narrow regions of the spectrum. In particular, a water cell, 1 cm thick, was used to separate the long-wave planetary radiation from the reflected solar radiation.

Several methods are available for obtaining planetary temperatures from radiometric measurements; these have been discussed in earlier papers and recently summarized by Sinton (1951). They depend on either Planck's or Stefan's laws and may make use of the reflected solar radiation from the planet, lunar reflected radiation, or stellar radiation as a calibration standard. The methods that depend on the shape of the Planck-curve are sensitive to small variations in the energy measurements; accordingly, the use of Stefan's law, into which the energy enters as a fourth root, seemed preferable, despite uncertainties in the various parameters that are needed, such as the Martian emissivity and the transmission of the earth's atmosphere. For this reason the writer used the "method of

* Present address: U.S. Weather Bureau, Oak Ridge, Tennessee.

water-cell transmissions" (cf. Russell and Menzell 1923; see also Milankovitch 1936) in the reduction of Lampland's radiometric data.

Analysis of the various sources of error indicated that the individual tabulated Martian temperature measurements have an observational relative standard error of about 10 per cent. Thus annual and seasonal averages, based in some instances on hundreds of individual measurements, will be reliable except for possible systematic errors. The general effect of all the known sources of systematic error is to produce temperature values that are too low, and so the calculated values may be thought of as lower limits. Since the atmosphere of Mars is largely transparent to planetary radiation, the calculated temperatures are interpreted as applying to Mars's surface, a fact that should be remembered when contrasting them with terrestrial temperature values.

The Martian radiometric measurements to be analyzed were made near opposition times, between 1926 and 1941. Although several different radiometer receivers were used from time to time, most of the work was done with one having a diameter of 0.22 mm. During the 1926 and 1928 oppositions the 53-foot Cassegrain focus of the Lowell 42-inch

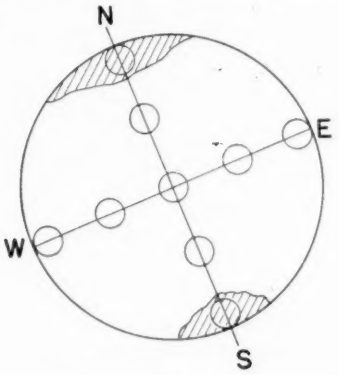

FIG. 1.—Location of radiometric observations on Mars's disk

reflector was most often used, whereas the 18.3-foot Newtonian was used for the bulk of the remaining observations. For the near oppositions of 1926 and 1939, the ratio of the receiver diameter to that of the Martian image (at the 53-foot focus) was about 1:8, whereas for the more distant oppositions, using the 18.3-foot focus, this ratio was as great as 1:2.

The locations of the radiometric observations discussed here are indicated in Figure 1. Other locations were systematically used (cf. Gifford 1953); but those along the central meridian, as well as those along the orthogonal to this line through the disk's center, are of greater interest. From these data, average diurnal and annual temperature-curves as well as seasonal isotherm maps can be obtained. When averaging temperatures for the various locations, the effect of the Martian phase has been taken into account, roughly, by determining its mean value during an opposition period, weighted by the distribution of observing nights. The variable planetocentric declination has been handled by assuming a mean value for all data obtained during a particular opposition. This treatment considerably simplifies the labor of averaging and, because observations were always made close to opposition, will introduce only small errors compared to other known sources.

DIURNAL SURFACE-TEMPERATURE VARIATION

Mars rotates at a speed very nearly equal to that of the earth and has an atmosphere. Although it is farther away from the sun and receives less solar radiation, Mars does not reflect so much of this back to space as does the earth. The actual amounts of energy available for heating do not differ greatly on a seasonal basis. Consequently, the temperature climate of Mars should exhibit certain similarities to our own. In particular, there should be a lag of the diurnal temperature maximum after Martian local noon. This diurnal lag was, in fact, detected by Coblentz and Lampland in 1924.

It should be realized that the Martian daily temperature maximum will lag behind the curve of incoming solar radiation *even in the absence of an atmosphere*. Milankovitch (1936)

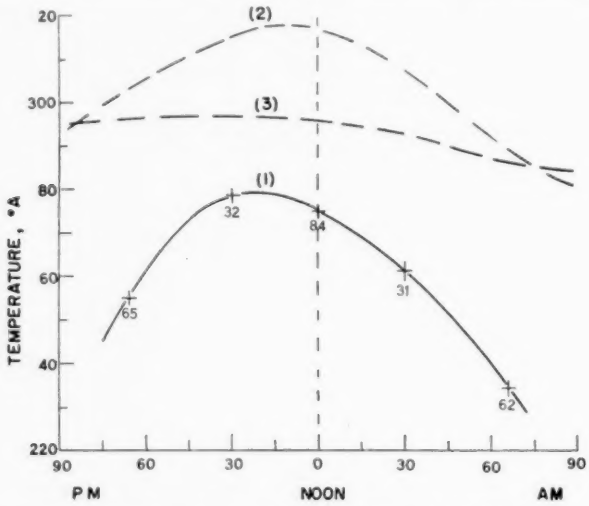

FIG. 2.—Average temperature variation near the Martian equator, i.e., the diurnal temperature variation; horizontal co-ordinate is degrees longitude east or west of the noon meridian; the number of individual observations averaged at each point is indicated; *2* and *3* are Haude's observations of the diurnal temperature variation at, respectively, zero and 2 meters above the Gobi Desert in June.

has analyzed the heat balance of a planet with no atmosphere; according to this investigation, the maximum lag should be 3 hours in the case of a perfect conductor and would vanish for an insulating surface. For a reasonable assumption about the composition of the surface of Mars, the diurnal lag might, in theory, exceed an hour (cf. De Vaucouleurs' [1951] discussion).

The diurnal temperature variation at the surface of Mars, obtained by averaging all the available Cassegrain data for the 1926 and 1928 oppositions and for the morning-to-evening locations of Figure 1, is presented in Figure 2, curve *1*. The location of the points has been corrected for the average phase during the observing periods, as described earlier. For these observations, the lag of the maximum temperature appears to be about 1–1½ hours. This, coupled with the extreme diurnal variation of perhaps 50° C., indicates a rigorous microclimate, but one with midday temperatures above 0° C. at the surface, at least in tropical latitudes.

The rigor of the Martian temperature climate, although undeniable, has perhaps been

overemphasized in comparisons with the earth. When interpreting Figure 2, one must remember that the measures give ground-surface temperature. This is not directly comparable with the instrument-shelter temperature, obtained at a height of about 2 meters, upon which standards of terrestrial climate are ordinarily based. Curves *2* and *3* of Figure 2 show, by way of comparison, Haude's observations of the diurnal temperature variation in the Gobi Desert during June, at the surface and at a height of 2 meters (according to Lettau 1951). The temperature variation at 2 meters of about 10° is in sharp contrast to that at the desert surface of nearly 40°. Note also the retardation with height of the time of the maximum. The temperature variation above the Martian surface must be, at least to some extent, similarly modified, both by reduction of the amplitude and delay of the time of maximum.

Owing to their finite size, radiometer receivers will exercise some averaging effect on the true Martian surface temperatures. This was studied for both rectangular and circular receiver shapes. It can be shown that, in either case, the amplitude and phase of the observed temperature-curve are a very close approximation to the true values for the receiver sizes used, provided only that the true curve is of a fairly simple shape.

It was thought that perhaps the location of the maximum temperature indicated by Figure 2 was due to some fortuitous, systematic positioning of the dark areas of Mars during the periods of observation. To test this, the same temperature data were separated into two groups on the basis of Martian longitude, one group including all observations made when the longitude of the central meridian was from 100° to 300° and the other containing the remainder of the data. This separates observations made on a primarily bright face from those made on one having many large dark markings. Temperatures averaged in this way indicate no great effect of the surface markings on the position of the maximum temperature.

Considering these points, it appears that the lag in the diurnal maximum temperature that Figure 2 exhibits is real. During the 1954 Martian opposition, some new radiometric observations were made by Dr. William Sinton, with the 200-inch telescope and instrumentation developed by Strong and Sinton at Johns Hopkins University. Dr. Sinton advised the writer that these observations tentatively indicate a diurnal lag of the Martian surface temperature amounting to about ½ hour. Sinton's work verifies the existence of a diurnal lag and must be regarded as the most reliable indication of its magnitude. One looks forward to more of these excellent observations.

ANNUAL SURFACE-TEMPERATURE VARIATION

Averaged Martian surface temperatures for the locations along the line connecting the north and south poles, separated according to the Martian *southern hemisphere* season, are shown in Figure 3. Spring is counted from the vernal equinox to the summer solstice, and so on. These curves illustrate the annual march of the seasons very nicely, particularly summer and fall. The winter-curve, based on observations at the Newtonian focus during the poor oppositions of 1935 and 1937, is naturally considerably flatter but does place the maximum temperature in the northern hemisphere. The spring-curve, based on only a few observations, was at first thought to be incorrect, and the alternative indicated by the dashed line has been suggested. A check revealed, however, that most of the springtime observations corresponding to the point at 16° S. had systematically chanced to fall near the longitude of the Hellas region, one of the brightest areas of the Martian southern hemisphere. It has been suggested that this region is an elevated plateau, and it is a well-known location of temporary bright markings, presumably frost or low cloudiness. Thus it seems that the low temperature near the equator on the spring-curve is real, although not representative of average conditions.

If there is a diurnal lag in the maximum temperature, then there should also be an annual lag, and the summer and fall curves of Figure 3 were examined with this possibil-

ity in mind. The average date of the summer curve was determined to be some 60 days after the southern-hemisphere summer solstice, and that of the fall curve about 20 days after the autumnal equinox. The curves are evidently consistent with an annual lag of about 3 weeks, a figure which is not unreasonable theoretically. Of course, a lag so short cannot be determined from the curves with much precision; and it may be said with confidence only that the annual lag cannot be much larger than this amount.

SEASONAL TEMPERATURE DISTRIBUTION

Hess (1950), using Coblentz and Lampland's few published 1926 data, produced a map of the Martian temperature distribution for the southern-hemisphere summer season. Such a display of the temperature observations is of great interest, both intrinsically

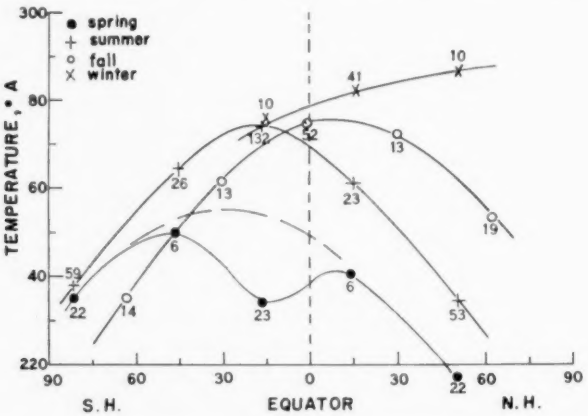

FIG. 3.—Average temperature variation along the Martian noon meridian for the various seasons; the number of individual observations averaged at each point is indicated.

and for the light it can throw upon the problem of the Martian general atmospheric circulation. Figures 4, 5, and 6 are seasonal isotherm maps obtained from the present much larger body of data.

To obtain the final charts, all the available temperatures for a particular one of the pole-to-pole locations were first plotted as a function of Martian longitude. A smooth curve was next interpolated by eye, the resulting smoothed temperature values entered at grid points of a Mercator projection, and isopleths of constant temperature were drawn for each 10° absolute. Once again, the summer and fall maps are based on data obtained during the 1926 and 1928 oppositions, and the winter map is made by combining the Newtonian observations of the 1933, 1935, and 1937 oppositions. Not enough data were available for the preparation of a (southern-hemisphere) spring-season map.

A rich variety of isotherm patterns is present in these figures, even by comparison with terrestrial isotherm maps. The summer map substantiates Hess's analysis, generally speaking. In the fall and winter maps we identify without difficulty the northerly march of the thermal equator. It is rather satisfying to discover, as well, that certain of the isotherm configurations are readily identifiable with well-known Martian surface markings. The closed 290° isotherm on the summer map (Fig. 4), for example, falls just over the dark area of Mare Cimmerium, and the Syrtis Major area is similarly outlined on the fall map (Fig. 5) by a closed 280° isotherm. On the other hand, Mare Cimmerium is com-

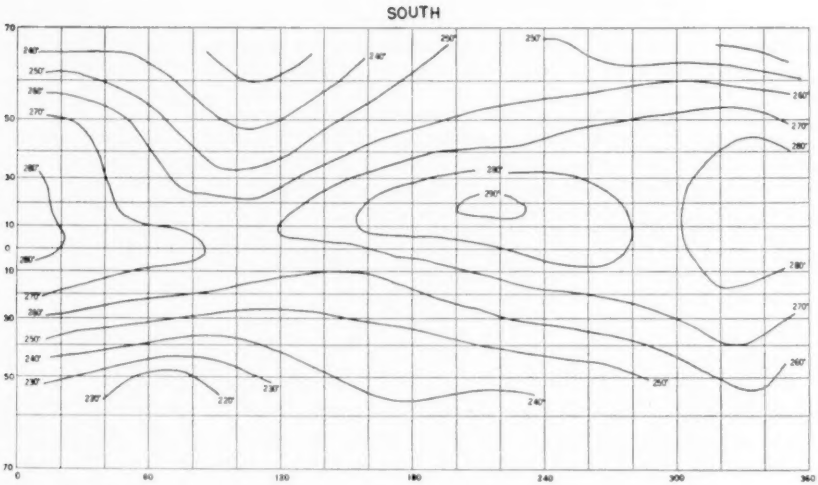

FIG. 4.—Average Martian southern hemisphere summer isotherms (deg. abs.)

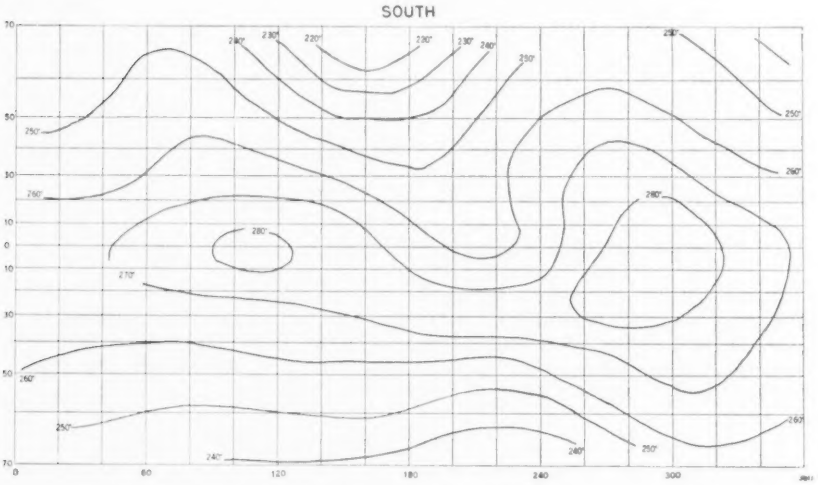

FIG. 5.—Average Martian southern hemisphere fall isotherms (deg. abs.)

paratively cold on both the fall and the winter map, perhaps indicating a real seasonal temperature change in this marking. Hess suggested, on the basis of his summer-season isotherm map and one cloud-drift observation, that the warm center at about latitude 30° S., longitude 340°, is an example of a *heat low*, that is, a low-pressure area present only during the summer season. It is interesting to verify that, in fact, this warm area is not present at the same location on the winter map.

Whereas the gross outlines of the isotherm configurations can in some cases be interpreted in terms of Martian surface markings, there is no slavish following by the isotherms of the details of the surface markings. This could not be expected, because the temperatures represent averages over large geographical areas. The chief utility of these isotherm maps will be in connection with study of the problem of the Martian general atmospheric circulation rather than with purely topographical interpretations.

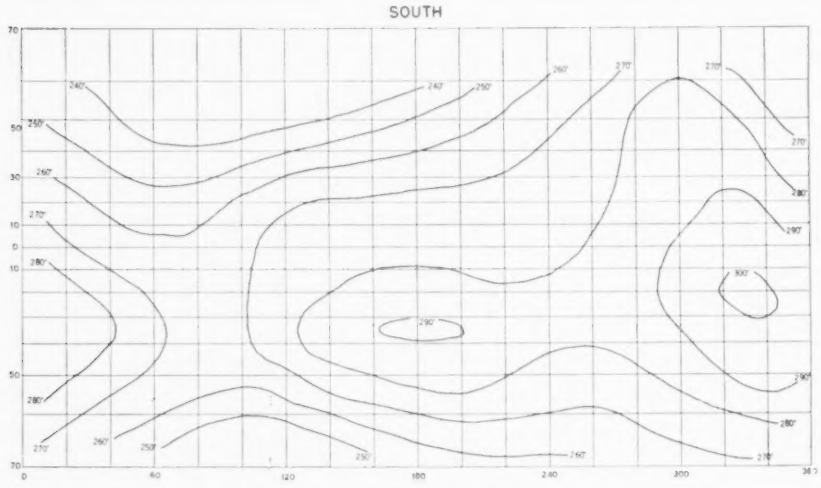

FIG. 6.—Average Martian southern hemisphere winter isotherms (deg. abs.)

The writer is deeply grateful for advice and encouragement given him by members of the staff of Lowell Observatory in connection with this work. Acknowledgment is also due to Mr. V. J. Oliver, U.S. Weather Bureau, who very kindly undertook to analyze the temperature data of Figure 4, in order to provide an independent test of its validity. The analysis presented in Figure 4 is Mr. Oliver's.

REFERENCES

Coblentz, W. W. 1925, *Temperature Estimates of the Planet Mars* ("Scientific Papers of the Bureau of Standards," No. 512).

Coblentz, W. W., and Lampland, C. O., 1923, "Measurements of Planetary Radiation," *Lowell Obs. Bull.*, No. 85.

———. 1927, *Further Radiometric Measurements and Temperature Estimates of the Planet Mars, 1926* ("Scientific Papers of the Bureau of Standards," No. 553).

Coblentz, W. W., and Menzel, D. H. 1927, "Temperatures of Mars, 1926, as Derived from the Water-Cell Transmissions," *Pub. Astr. Soc. South Pacific*, **39**, 97.

Gifford, F. 1953, *Surface Temperatures of the Planet Mars: 1926 to 1943*, Final Rept.: *The Study of Planetary Atmospheres* (Lowell Obs.).

Herschel, W. 1784, "On the Remarkable Appearances at the Polar Regions of the Planet Mars, etc.," *Phil. Trans. R. Soc. London*, pp. 531–539 (abridged ed., London, 1809).
Hess, S. L. 1950, "Some Aspects of the Meteorology of Mars," *J. Meteorol.*, **7**, 1.
Lettau, H. 1951, *Isotropic and Non-isotropic Turbulence in the Atmospheric Surface Layer* ("Geographical Research Papers," No. 1, U.S.A.F.).
Lowell, P. 1907, "Temperature of Mars, a Determination of the Solar Heat Received," *Proc. Amer. Acad. Arts and Sci.*, **42**, 651.
Menzel, D. H. 1923, "Water-Cell Transmissions and Planetary Temperatures," *Ap. J.*, **58**, 65.
Milankovitch, M. 1936, "Mathematische Klimalehre und astronomische Theorie der Klimaschwankungen," in *Handbuch der Klimatologie*, ed. W. Köppen and R. Geiger, Vol. **1**, Part A (Berlin: Verlag Gebrüder Borntraeger).
Pettit, E., and Nicholson, S. B. 1924, "Measurements of the Radiation from the Planet Mars," *Pop. Astr.*, **32**, 601.
Sinton, W. M. 1953, "Distribution of Temperatures and Spectra of Venus and Other Planets" (Diss., Johns Hopkins University).
Vaucouleurs, G. de. 1951, *Physique de la planète Mars* (Paris: Albin Michel).

LABORATORY EXCITATION OF THE BLUE-GREEN BANDS OBSERVED IN THE SPECTRA OF N-TYPE STARS

BENGT KLEMAN*

Division of Pure Physics, National Research Council, Ottawa, Canada

Received August 29, 1955

ABSTRACT

A complex band spectrum has been excited in a King furnace charged with silicon. The main features of the spectrum agree with those of the hitherto unidentified blue-green bands occurring in the spectra of some N-type stars. It is concluded from the complexity of the bands that the emitter is a polyatomic molecule. On the basis of a partial vibrational analysis and the experimental conditions for producing the bands, as well as the appearance in the spectra of cool carbon stars, the spectrum is tentatively ascribed to an Si-C-C molecule.

INTRODUCTION

In the spectra of certain N-type stars, there appears a system of blue-green bands which, in some stars such as RY Draconis, is very strong and dominates the spectrum. The band system was discovered by Merrill (1926) and by Sanford (1926). The molecule responsible for these bands has remained unidentified up to the present. In various comets, unidentified emission features have been observed in the same region. It has been suggested several times (see, e.g., Swings, McKellar, and Minkowski 1943; Jose and Swings 1950) that this emission originates from the same molecule that produces the band system in the N-type stars. The observed data for the comets, however, are very difficult to interpret in the region of the C_2 Swan bands, and the only safe statement at present, according to Swings (1951), seems to be that a hitherto unidentified molecule (or several) must play a role in the emissions in the range λλ 4600–6700 A.

Recently the bands that occur in the spectra of N-type stars have been excited in a laboratory source and photographed at high dispersion. There is considerable evidence to indicate that these bands arise from the SiC_2 molecule. The method used to excite these bands and a discussion of the spectrum are given.

LABORATORY EXCITATION OF THE BANDS

When silicon is inserted in the graphite tube of a King furnace and the temperature is raised to 2200°–2250° C, a red-degraded band can be observed in emission at λ 4977 A. As the temperature is increased to 2300°–2400° C, the gas space takes on a blue color, and weaker red-degraded bands can be observed at λλ 4640, 4867, 4906, 5128, and 5198 A. At the same time, a continuous background increases rapidly with the temperature, so that, at a temperature of 2450°–2500° C, all bands are masked by the continuum. This continuum is observed only when silicon is present. As a compromise between the intensity of the band system and that of the continuum, the bands have been photographed at temperatures between 2300° and 2400° C. The intensity of the bands gradually decreases with time, whereas the Swan bands of C_2, which are comparatively weak immediately after fresh silicon has been added, increase in strength. If the furnace is heated for an hour or more at a temperature of 2400° C, the bands and continuum disappear and give place to an intense C_2 spectrum. The same change in the spectrum occurs more quickly at higher temperatures.

For most of the exposures, the furnace was filled with argon or helium at a pressure of ½ atm, but the blue-green bands could be produced equally well with hydrogen,

* National Research Laboratories postdoctorate fellow.

deuterium, or nitrogen. The bands also appear in absorption, but since it proved more convenient experimentally to photograph the bands in emission, only emission plates were used in this work.

The bands were photographed in the second order of a 21-foot concave-grating spectrograph at a dispersion of 1.25 A/mm. The exposure times with Kodak III-O and III-F plates ranged between 1 and 15 minutes.

APPEARANCE OF BANDS AND COMPARISON WITH STELLAR SPECTRA

Under high resolution the bands appear very complex, and the single heads observed at low dispersion break into a number of heads. In addition to the stronger bands, which

TABLE 1

THE BLUE-GREEN BANDS

Laboratory Observations				Astrophysical Observations	
Est. Int.	λ (A)	ν (Cm^{-1})	Tentative Assignment $v_1', v_3'-v_1'', v_3''$	Est.* Int.	McKellar (1947) λ(A)
				0	4261
				0	4294
1	4350.87	22977.5	0,2–0,0	1	4352
				0	4482
				2	4540.9
1	4573.82	21857.5	2,1–1,0	1	4572
5	4639.79	21546.7	0,1–0,0	5	4639.9
1	4802.57	20816.4	1,1–2,0	1	4804.1
4	4866.99	20540.8	1,0–0,0	8	4866.8
3	4905.51	20379.6	2,0–1,0	5	4906.0
3	4909.35	20363.6	0,1–2,0		4909.8†
20	4977.44	20085.1	0,0–0,0	20	4977.1
1	5048.00	19804.3	0,1–0,1		
3	5128.19	19494.6	0,0–1,0	Overlapped by C_2	
1	5192.25	19254.1	2,0–0,1		5192.2‡
3	5198.05	19232.6			
1.5	5317.60	18800.3	1,0–0,1	McKellar's (1947) observations stop at λ 5212 A	
3	5450.04	18343.4	0,0–0,1		
1	5527.45	18086.5	0,1–0,2		
1	5632.41	17749.5	0,0–1,1		

* These are our estimates from McKellar's reproduction.

† In McKellar's observations, this band head is not resolved from the head λ 4906.0 A. The wave length given here has been obtained by measuring the separation of the two heads on the reproduction of Sanford's (1950) spectrum (see Fig. 1) and adding it to 4906.0 A.

‡ McKellar observes an absorption feature with rectangular profile extending from λ 5192.2 to λ 5211.7 A.

can be observed at low dispersion, there appear a number of weaker bands most of which are degraded to the red but a few of which are distinctly degraded the other way. Also, some of the stronger bands which seem to be degraded to the red show redward edges. The fine structure of the bands is not resolved except in a small region of the strongest band at 4977 A. It was found impossible to measure the weaker bands in a consistent way because of the poor contrast with the overlapping continuum and, in some regions, because of overlapping C_2 bands. In Table 1 only the more outstanding red-degraded bands are listed.

The blue-green bands observed by Merrill (1926) and by Sanford (1926) have been studied in detail by McKellar (1947). Also Sanford (1950) has more recently published

high-dispersion plates (10 A/mm) of VX Andromedae, showing the stronger bands. A part of the spectrum photographed by Sanford is shown, together with the laboratory spectrum, in Figure 1. The complete set of band heads as measured by McKellar (1947) is included in Table 1. From the agreement between the wave lengths of the outstanding bands observed in N-type stars and those observed in the laboratory, it seems certain that they represent the same band system.

VIBRATIONAL ANALYSIS AND DISCUSSION OF ORIGIN OF BANDS

The present laboratory spectrograms are not adequate for a detailed vibrational study. It does, however, seem possible to draw some conclusions about the vibrational structure. The characteristic groups of bands observed in the stellar spectra immediately suggest that there occurs a vibration in the upper electronic state (McKellar 1947), with the successive differences of 1461 and 1431 cm^{-1}. The corresponding differences for the vibration in the lower electronic state, as obtained from the laboratory spectrum, are 1742 and 1718 cm^{-1}.

From the method of exciting the blue-green bands in the laboratory, we do expect silicon to be a constituent of the emitting molecule. The possibility that impurities in the silicon samples were of any significance seems to be excluded by the fact that silicon from three different sources, one of which was specially purified, were used. The only diatomic molecule containing silicon which can have ω-values of the size given here is SiH. The blue-green bands, however, do not seem to depend on the presence of hydrogen, nor can any shift of the bands be observed when deuterium is used in the furnace. Also, from our knowledge of the SiH molecule, we do not expect an extended spectrum in this region. The ordinary SiH bands are weak in comparison with the blue-green bands when a gas other than hydrogen is used in the furnace. We can make the general observation that ω-values of the order of 1750 cm^{-1} are likely to occur only in vibrations between a hydrogen atom and an atom of another element or between two first-row elements. The spectra of diatomic molecules composed of cosmically abundant elements from the first period are sufficiently well known to exclude such a molecule as the emitter of the blue-green bands. We lack spectroscopic information of some diatomic hydrides, such as FeH and TiH, which may be likely emitters of the spectrum from the astrophysical point of view (McKellar 1947). The assumption of a diatomic hydride, however, contradicts our experimental evidence that silicon is a constituent of the emitting molecule and that hydrogen is not.

From the appearance of the blue-green bands on the high-resolution laboratory plates, it is also difficult to assume that the emitter is a diatomic molecule. The pattern of bands seems to be too complex. The spacing of the lines in the branches in that part of the λ 4977 band where the fine structure is resolved is too small to be produced by a light diatomic molecule with an ω-value of the order of 1750 cm^{-1}. Thus the only plausible assumption is that the observed frequencies (1742 and 1461 cm^{-1}) arise from a vibration between two first-row atoms in a polyatomic molecule. We do expect that only very simple polyatomic molecules are sufficiently stable to be of any significance at the high temperatures in the furnace. The simplest assumption that is also justified by the analysis is that the emitting molecule is triatomic. Nitrogen, as a constituent, can probably be excluded, since no intensity change of the spectrum was observed when the helium gas in the furnace was replaced by nitrogen. Also, oxygen does not seem likely because of the occurrence of the blue-green bands in cool carbon stars, where oxide spectra have not been observed. Thus the only assumption left is that the frequencies (1742 and 1461 cm^{-1}) arise from a vibration between two carbon atoms. (The ground-state frequency for the free C_2 molecule is $\omega_e = 1641$ cm^{-1}.) From the foregoing assumptions, we arrive at Si-C-C as the likely emitter. This would imply that we are dealing with an analogue of the C_3 spectrum, which appears under very similar conditions both in the furnace and in astrophysical sources.

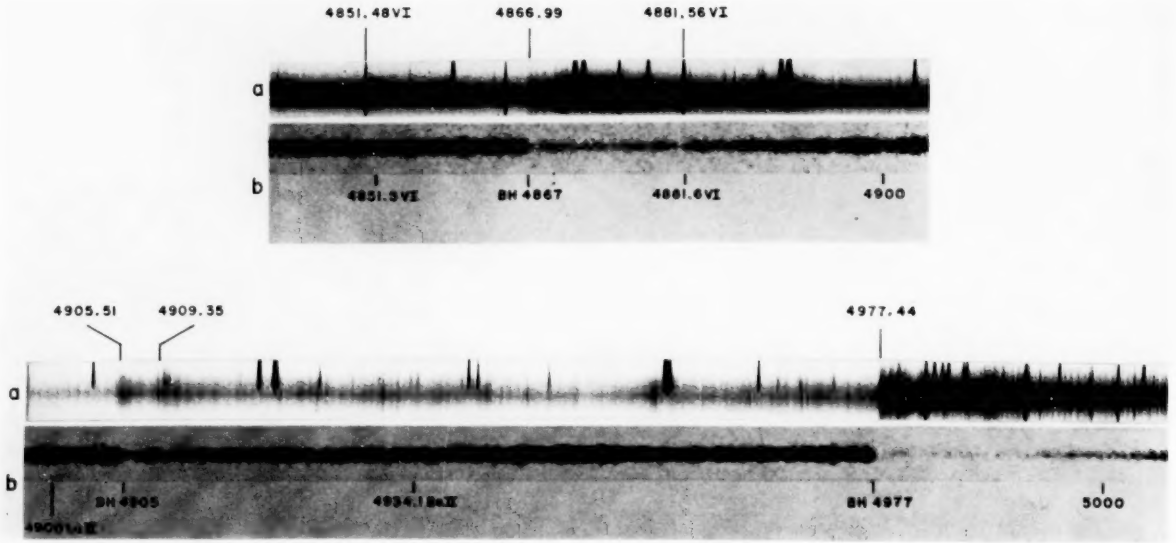

FIG. 1.—Photograph of the spectrum of the blue-green bands ascribed here to the SiC_2 molecule. (*a*) Part of the laboratory spectrum obtained in emission with a King furnace and photographed with a 21-ft grating; (*b*) the corresponding part of the spectrum of VX Andromedae reproduced from Sanford's (1950) *Stellar Atlas*.

An Si-C-C molecule will have three normal modes of vibration, and these can be approximately described as ν_1 (an Si-C stretching frequency), ν_2 (a bending frequency), and ν_3 (a C-C stretching frequency). If the molecule, similar to C_3, is linear in both electronic states, then during an electronic transition we should expect v_1 and v_3, but not v_2, to change. A given transition in v_1 and v_3 will, however, at the temperature used in this work, be complicated by the superposition of a large number of bands with different v_2, where, however, $v_2' = v_2''$. A tentative analysis, which accounts for the main features of the band system, is included in Table 1. The analysis gives the following vibrational frequencies: $\nu_1' = 456$, $\nu_1'' = 591$, $\nu_3' = 1461$, and $\nu_3'' = 1742$ cm^{-1}. There are some inconsistencies in this table in the assignment of the doubly excited levels of ν_1. It does not, however, seem profitable to discuss the finer details on the basis of the present experimental observations.

Future investigations of the blue-green bands emitted or absorbed in a furnace may probably be of interest for a comparison with stellar spectra, since the conditions in this light-source resemble those of the atmospheres of the carbon stars. Of special interest in this connection is the appearance of the strong continuum in the furnace, since this may be related to the abnormally strong absorption in the ultraviolet part of the spectrum in those stars where the blue-green bands appear. For a further analysis and an unambiguous assignment of the emitter of the blue-green bands, however, one would expect that a study of the bands in a cooler light-source would be more favorable.

I am very grateful to Dr. A. E. Douglas for his early suggestion of the identity of the bands obtained in the laboratory and those observed in the N-type stars. It is also a pleasure for me to acknowledge the advice received from Drs. G. Herzberg and A. E. Douglas during this investigation.

REFERENCES

Jose, P. D., and Swings, P. 1950, *Ap. J.*, **111**, 41.
McKellar, A. 1947, *J.R.A.S. Canada*, **61**, 147.
Merrill, P. W. 1926, *Pub. A.S.P.*, **38**, 175.
Sanford, R. F. 1926, *Pub. A.S.P.*, **38**, 177.
———. 1950, *Ap. J.*, **111**, 262.
Swings, P. 1951, *J. Opt. Soc. America*, **41**, 153.
Swings, P., McKellar, A., and Minkowski, R. 1943, *Ap. J.*, **98**, 142.

ANALYSIS OF THE (0, 1) AND (1, 2) BANDS OF THE $^2\Delta$–$^2\Pi$ SYSTEM OF CH*

NORMAN H. KIESS AND HERBERT P. BROIDA

National Bureau of Standards and University of Maryland

Received August 8, 1955

ABSTRACT

The (0, 1) and (1, 2) bands of the $^2\Delta$–$^2\Pi$ system of CH, lying in the region of 4890 A, have been measured and analyzed. Molecular constants for vibration, rotation, and term splitting have been determined.

INTRODUCTION

The $^2\Delta$–$^2\Pi$ system is the most easily excited transition of CH. Its most intense band, the (0, 0), lies in the region of 4315 Å and has been observed in such light-sources as burning hydrocarbons, electrical discharges where both carbon and hydrogen are present, and certain astrophysical sources. Fagerholm (1940) and Gerö (1941–1942) have measured and analyzed the rotational structure of the CH bands near 4315 A. These include the (0, 0), (1, 1), and (2, 2) bands of the $^2\Delta$–$^2\Pi$ system. A faint band system has been known, since 1916, to exist in the region of 4890 Å (Raffety 1916). This band system is present in some of the same sources as the $^2\Delta$–$^2\Pi$ system of CH. Vaidya (1941) showed that this system could be fitted into the vibrational schemes of the $^2\Delta$ and $^2\Pi$ states of CH, if it were assumed to be the (0, 1) band of the $^2\Delta$–$^2\Pi$ system of CH. A rotational analysis was not made, however, because of the faintness of this band. This paper deals with the development of a light-source with intense emission of these bands and their subsequent analysis.

EXPERIMENTAL

A survey of the spectra of various hydrocarbons burning with oxygen was made under medium dispersion with a Hilger E-2 spectrograph with glass optics. It was found that the source giving the 4890 A bands with highest intensity and contrast is the acetylene-oxygen flame with 1 part of acetylene to 8 parts of oxygen. More acetylene gives emission of the C_2 Swan bands, which submerge the 4890 A bands of CH; less acetylene increases exposure times. A medium-dispersion spectrogram of this region is given in Figure 1, *a*. A Kodak 103-F3 plate was used, with an exposure time of 15 minutes. In order to photograph this region under higher resolution, the flames were burned on a rectangular slot burner with port dimensions of 1.75×0.010 inches. When viewed end-on, it gives emission strong enough to use a 30000 lines-per-inch grating spectrograph. Several plates were taken in the first order, one of which, a Kodak II*a*-J exposed for 2 hours, is reproduced in Figure 1, *b*–*c*. Individual line measurements from the plates agree, on the average, to 0.07 cm^{-1}. An iron-arc comparison spectrum was used.

ROTATIONAL ANALYSIS

The twelve intense branches characteristic of $^2\Delta$–$^2\Pi$ transitions were found. These form the (0, 1) band, while twelve branches of moderate intensity form the (1, 2) band. Weak satellite branches were also found in both bands. The wave numbers of the lines of these bands are given in Tables 1 and 2. The *P* branches of the (0, 1) band form a head at 4940 A, while those of the (1, 2) band form a head at 4913 A. The headlike appearance at 4890 A is caused by the piling-up of the *Q* branches of the (0, 1) band. The analysis of the

* Based on a thesis presented by Norman H. Kiess in partial fulfilment for the degree of Master of Science, University of Maryland, January, 1955.

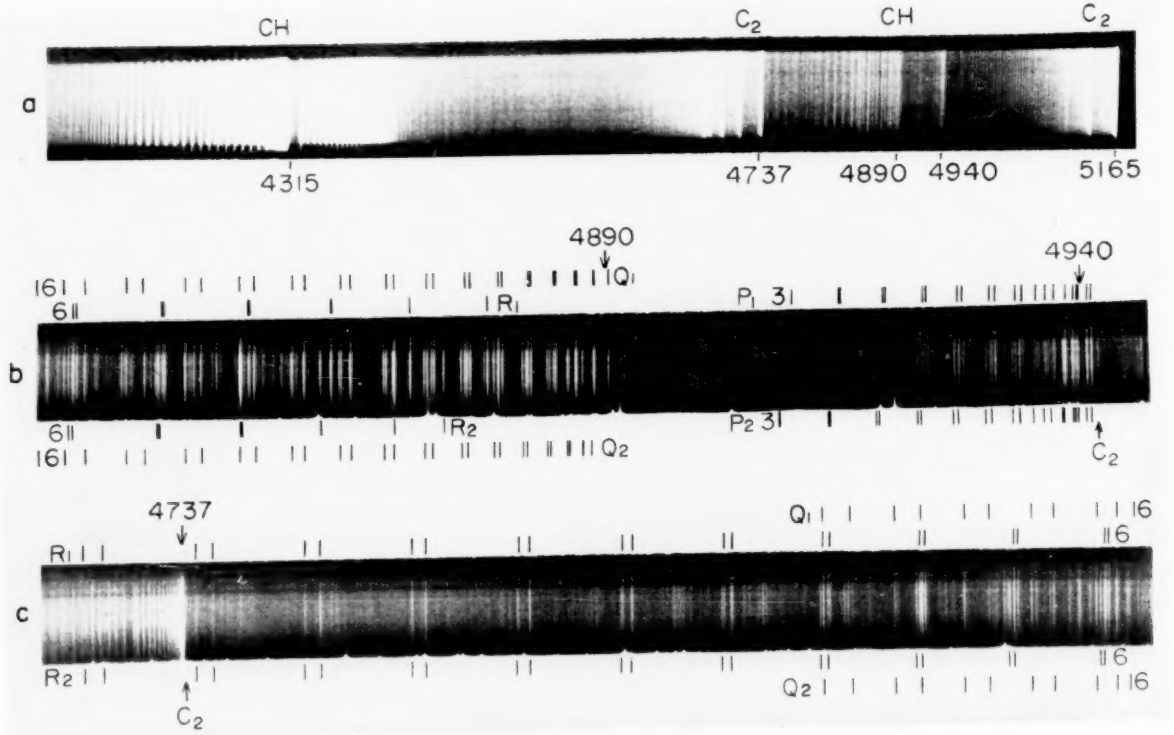

FIG. 1.—*a*: A lean acetylene-oxygen flame photographed under medium-glass dispersion. The $^2\Delta$–$^2\Pi$ system of CH and the Swan system of C_2 appear. *b* and *c*: The region of 4890 Å on *a*, photographed in the first order of a 30,000-lines-per-inch grating spectrograph. The main branches of the (0, 1) band of the $^2\Delta$–$^2\Pi$ system are marked. An iron-arc comparison spectrum appears at the bottom of each strip.

TABLE 1

WAVE NUMBERS OF THE LINES OF THE (0, 1) BAND (CM^{-1})

K	R_{1ed}	R_{1de}	Q_{1e}	Q_{1d}	P_{1ed}	P_{1de}
1	20496.23	20496.23	.....	.....	.....	.....
2	530.44	530.44	20442.89	20442.89	.....	.....
3	565.43	565.74	449.34	449.01	20361.46	20361.98
4	601.78	602.47	457.36	456.67	340.23	340.94
5	639.68	640.66	467.00	465.98	320.85	321.82
6	678.88	680.25	478.34	476.93	303.26	304.63
7	719.61	721.43	491.43	489.56	287.51	289.45
8	761.64	764.24	506.31	503.87	273.67	276.17
9	805.12	808.15	522.84	519.81	261.84	264.88
10	849.84	853.60	541.10	537.45	251.99	255.70
11	895.80	900.28	561.04	556.64	244.16	248.49
12	942.98	948.05	582.64	577.42	238.13	243.38
13	991.07	997.21	605.89	599.91	234.21	240.22
14	21040.28	21047.18	630.61	623.71	232.34	239.26
15	090.29	098.30	656.75	648.92	232.34	240.22
16	141.13	150.36	684.56	675.54	234.21	242.97
17	.....	.....	713.57	703.79	238.13	248.07
18	.....	.....	743.87	733.14	244.16	254.61
19	.....	.....	775.59	763.51	251.35	263.12
20	.....	.....	808.15	795.31	260.69	273.67
21	.....	.....	842.57	827.31	272.33	285.93
22	.....	.....	878.04	860.86	285.35	301.04
23	.....	.....	914.78	896.39	.....	.....
24	.....	.....	952.79	.....	.....	.....

K	R_{2ed}	R_{2de}	Q_{2e}	Q_{2d}	P_{2ed}	P_{2de}
1	20515.74	20515.74	.....	.....	.....	.....
2	537.45	537.45	20450.57	20450.57	.....	.....
3	570.13	570.66	454.60	454.11	20367.11	20367.91
4	605.36	605.89	461.26	460.46	344.31	345.30
5	642.36	643.44	470.05	468.83	323.98	325.13
6	681.02	682.62	480.80	479.27	305.76	307.32
7	721.43	723.41	493.48	491.43	289.45	291.61
8	763.02	765.81	508.01	505.26	275.20	277.97
9	806.18	809.64	524.30	520.91	263.12	266.41
10	850.71	854.80	542.32	538.26	252.96	256.94
11	896.39	901.20	562.10	557.26	244.80	249.64
12	943.28	948.90	583.50	577.87	238.70	244.16
13	991.33	998.06	606.45	599.91	234.42	241.03
14	21040.28	21047.63	631.09	623.71	232.34	239.85
15	090.29	098.50	657.22	648.92	232.34	240.55
16	141.13	150.36	684.76	675.54	234.21	243.38
17	.....	.....	713.57	703.31	238.13	248.07
18	.....	.....	743.87	732.67	243.38	254.61
19	.....	.....	775.59	763.02	250.77	263.12
20	.....	.....	808.15	794.70	260.04	273.67
21	.....	.....	841.93	827.31	271.16	285.35
22	.....	.....	876.51	860.86	284.55	299.58
23	.....	.....	912.79	895.80	.....	.....
24	.....	.....	.....	931.95	.....	.....

K	RQ_{2d1e}	RQ_{2e1d}	QP_{21e}	QP_{21d}	QR_{12e}	QR_{12d}	PQ_{1d2e}	PQ_{1e2d}
1	20497.98	20497.98	.....	.....	.....	.....	.....	.....
2	531.58	531.58	20444.50	20444.50	20449.01	20449.01	.....	.....
3	566.39	566.39	450.57	450.57	453.37	453.37	20366.17	20365.41
4	.....	.....	458.12	457.36	460.46	459.83	.....	443.19
5	.....	.....	.....	.....	.....	468.24	.....	423.26

R branches could not be carried far beyond 4737 A, because of the intense (1, 0) sequence of the C_2 Swan system in this region.

The origins of the (0, 1) and (1, 2) bands were determined from the relation

$$Q(K) = \nu_0 + (B_v' - B_v'')\, K\,(K+1).$$

TABLE 2

WAVE NUMBERS OF THE LINES OF THE (1, 2) BAND (CM^{-1})

K	R_{1cd}	R_{1dc}	Q_{1c}	Q_{1d}	P_{1cd}	P_{1dc}
1	20626.65	20626.65	.....	.....	.....	.....
2	659.09	659.09	20575.52	20575.52	.....	.....
3	691.71	692.14	581.17	580.69	20496.23	20497.27
4	725.64	726.33	587.97	587.27	475.50	476.93
5	760.55	761.64	596.06	595.01	456.67	457.36
6	796.78	798.14	605.36	604.23	438.76	439.97
7	834.15	835.83	616.61	614.78	422.38	424.13
8	872.56	874.73	629.01	626.65	407.41	409.71
9	911.85	914.78	642.80	639.87	394.16	397.08
10	951.91	955.52	658.03	654.55	382.60	386.24
11	992.87	997.21	674.45	670.20	372.53	376.83
12	21034.82	21040.28	692.14	686.99	364.14	368.99
13	077.49	083.78	710.99	705.27	357.56	363.15
14	.....	.....	730.92	724.38	352.25	358.74
15	.....	.....	751.93	744.41	348.75	356.01
16	.....	.....	774.31	765.81	346.28	354.36
17	.....	.....	796.78	787.35	346.28	355.21

K	R_{2cd}	R_{2dc}	Q_{2c}	Q_{2d}	P_{2cd}	P_{2dc}
1	20639.87	20639.87	.....	.....	.....	.....
2	665.81	665.81	20582.64	20582.64	.....	.....
3	695.97	696.75	585.87	584.67	20501.28	20502.61
4	728.91	729.75	591.61	590.65	479.27	480.80
5	763.02	764.24	598.95	597.80	459.59	460.87
6	798.97	800.39	607.97	606.45	441.13	442.89
7	835.83	837.84	618.58	616.61	424.13	426.06
8	873.82	876.26	630.61	627.96	408.61	411.40
9	912.79	916.02	644.23	641.02	395.39	398.60
10	952.79	956.62	659.09	655.35	383.50	387.46
11	993.57	998.22	675.54	670.88	373.31	377.89
12	21034.82	21040.28	692.96	687.60	364.85	370.00
13	077.49	083.78	711.85	705.27	357.79	364.14
14	.....	.....	731.59	724.38	352.25	359.49
15	.....	.....	752.52	744.41	348.75	356.53
16	.....	.....	774.31	765.81	346.28	354.79
17	.....	.....	796.78	787.35	346.28	355.21

K	RQ_{2d1c}	RQ_{2c1d}	PQ_{1d2c}	PQ_{1c2d}
1	20628.34	20628.34	.....	.....
2	660.10	660.10	.....	.....
3	692.96	.....	20501.28	20500.65
4	.....	.....	.....	478.34
5	.....	.....	.....	458.64

Here $Q(K)$ is the average of the wave numbers of the four Q branches, $Q_{1e}(K)$, $Q_{1f}(K)$, $Q_{2e}(K)$, and $Q_{2f}(K)$. The wave number $Q(K)$ was plotted against $K(K+1)$ with ν_0, the band origin, as the ordinate intercept. The origins are given in Table 4.

The rotational constants, B_v and D_v, were determined for each vibrational level from the relation

$$\Delta_2 F(K) = 4B_v(K+\tfrac{1}{2}) - 8D_v(K+\tfrac{1}{2})^3 .$$

Here $\Delta_2 F(K)$ is the average of the four combination double differences obtained by combining the four R branches with the four P branches. The quantity $[\Delta_2 F(K)]/[K+\tfrac{1}{2}]$

TABLE 3

OBSERVED SPIN-DOUBLINGS OF THE ROTATIONAL TERMS (CM^{-1})

K	$^2\Delta$ STATE $F_1(K)-F_2(K)$		$^2\Pi$ STATE $F_1(K)-F_2(K)$		
	$v=0$	$v=1$	$v=0$	$v=1$	$v=2$
1			17.83	17.76	11.53
2	−1.73	−1.72	6.22	6.07	5.71
3	−1.14	−1.12	4.14	4.07	3.94
4	−0.74	−0.74	3.05	3.09	2.84
5	−0.59	−0.58		2.34	1.97
6				2.04	

TABLE 4

CONSTANTS OF TRANSITIONS (CM^{-1})

A. $^2\Delta$–$^2\Pi$ transition: $\nu_e = 23151.8 \pm 1.0$
B. (0, 1) band: $\nu_0 = 20440.7 \pm 1.0$
C. (1, 2) band: $\nu_0 = 20574.2 \pm 1.0$

TABLE 5

VIBRATIONAL CONSTANTS (CM^{-1})

A. $^2\Pi$ state:
$\omega_e = 2868.5 \pm 1.0$ $\qquad \omega_e\chi_e = 64.4 \pm 0.5$
B. $^2\Delta$ state:
$\omega_e = 2943.0 \pm 1.0$ $\qquad \omega_e\chi_e = 99.3 \pm 0.5$

was plotted against $(K+\tfrac{1}{2})^2$, with $4B_v$ as the ordinate intercept and $-8D_v$ as the slope. The rotational constants B_e, α_e, D_e, and β_e were determined from the equations

$$B_v = B_e - \alpha_e(v+\tfrac{1}{2}) \qquad \text{and} \qquad D_v = D_e + \beta_e(v+\tfrac{1}{2}) .$$

The rotational constants B_0 and D_0 of the $^2\Pi$ state and B_2 and D_2 of the $^2\Delta$ state used in this determination are those given by Gerö (1941–1942). The rotational constants are given for both electronic states in Table 6.

The spin-doubling of the rotational levels was calculated from the combination relations involving the main and satellite branches and is given in Table 3. The formula of Hill and Van Vleck for the rotational levels of doublet states is

$$F_1(K) = B_v[(K+1)^2 - \Lambda^2 - \tfrac{1}{2}\sqrt{\{4(K+1)^2 + Y_v(Y_v-4)\Lambda^2\}}] - D_vK^2(K+1)^2,$$

$$F_2(K) = B_v[K^2 - \Lambda^2 + \tfrac{1}{2}\sqrt{\{4K^2 + Y_v(Y_v-4)\Lambda^2\}}] - D_vK^2(K+1)^2,$$

where Λ is the component along the internuclear axis of the electronic orbital angular momentum and Y_v is the ratio of the coupling constant to the rotational constant (Herzberg 1950). This formula can be written in the form

$$F_2(K) - F_1(K-1) = B_v \sqrt{\{4K^2 + Y_v(Y_v-4)\Lambda^2\}} - 4D_vK^3,$$

where the term in D_v is an order-of-magnitude correction only (Dieke and Crosswhite 1948). Knowledge of the spin-doubling, or $F_1(K) - F_2(K)$ differences, allowed the computation of $Y_v(Y_v-4)$ from this equation. This was done both by including and by excluding the term in D_v, so that the selected value of $Y_v(Y_v-4)$ is a weighted average. It was possible in the $^2\Delta$ state to compute the coupling constant A_v from $Y_v(Y_v-4)$, since it is known to be an inverted state for low values of K. Thus negative values of A_v were obtained for this state. No such decision was possible in the $^2\Pi$ state, as the value of $Y_v(Y_v-4)$ is near 4, thus yielding two close possible values for Y_v.

The $\Delta_1F'_{cd}$ and $\Delta_1F'_{dc}$ combination single differences were computed for the $^2\Delta$ state and were found to be equal within the experimental error. This shows that the Λ-doubling

TABLE 6

ROTATIONAL CONSTANTS (CM^{-1})

A. $^2\Pi$ state:	
$B_1 = 13.655 \pm 0.004$	$D_1 = (1.39 \pm 0.01) \times 10^{-3}$
$B_2 = 13.130 \pm 0.005$	$D_2 = (1.38 \pm 0.02) \times 10^{-3}$
$B_e = 14.448 \pm 0.010$	$D_e = (1.43 \pm 0.02) \times 10^{-3}$
$\alpha_e = 0.530 \pm 0.005$	$\beta_e = (-2.6 \pm 1.4) \times 10^{-5}$
B. $^2\Delta$ state:	
$B_0 = 14.572 \pm 0.001$	$D_0 = (1.52 \pm 0.00) \times 10^{-3}$
$B_1 = 13.901 \pm 0.004$	$D_1 = (1.56 \pm 0.03) \times 10^{-3}$
$B_e = 14.930 \pm 0.025$	$D_e = (1.47 \pm 0.03) \times 10^{-3}$
$\alpha_e = 0.696 \pm 0.015$	$\beta_e = (+6.4 \pm 2.4) \times 10^{-5}$

of the $^2\Delta$ state is unresolved. Thus the Λ-doubling of the $^2\Delta$–$^2\Pi$ bands is due entirely to the $^2\Pi$ state. It was found to follow the relation

$$\Delta\nu_{idc} = q_iK(K+1) - 4u_i^2K^2(K+1)^2 \qquad (i = 1, 2),$$

where q_i and u_i^2 are constants and $i = 1$ means Λ-doubling of F_1 levels and $i = 2$ means Λ-doubling of F_2 levels. The constants of spin- and Λ-doubling are given in Table 7.

VIBRATIONAL ANALYSIS

The equation

$$\nu_0 = \nu_e + \omega'_e(v'+\tfrac{1}{2}) - \omega'_ex'_e(v+\tfrac{1}{2})^2 - \omega''_e(v''+\tfrac{1}{2}) + \omega''_ex''_e(v+\tfrac{1}{2})^2,$$

involving the band origin ν_0, was used to determine the wave number ν_e of the electronic transition and the vibrational constants ω'_e, $\omega'_ex'_e$, ω''_e, and $\omega''_ex''_e$. Knowledge of the origins of the (0, 0), (1, 1), (2, 2), (0, 1), and (1, 2) bands allowed a unique solution to be made for these constants. They are given in Table 5.

DISCUSSION AND CONCLUSIONS

Estimates of error are given for all the molecular constants. In some cases these are based on the scatter of points in the direct computation of the constants and in other cases on the scatter of points in the plots used to determine the constants. The constants

pertaining to the $v = 0$ level of the $^2\Pi$ state were determined from the data of Gerö (1941–1942). In general, the present results agree more closely with those of Gerö (1941–1942) than with those of Fagerholm (1940). If the coupling constants of the $^2\Pi$ state are calculated from the values of $Y_v(Y_v - 4)$, the most precise result obtainable is $A_1 = 27.3 \pm 3.0$. This is, however, in close agreement with the value $Y = 2.0$ given by Mulliken (1928) on the basis of an early analysis of the CH spectrum (Heurlinger and Hulthén 1918–1919; Kratzer 1924). The vibrational constants are in close agreement with those given by Herzberg, as determined from the isotope relations applied to the spectrum of CH and CD (Herzberg 1950).

A calculation from the vibrational constants of the origin of the (1, 0) band of the $^2\Delta$–$^2\Pi$ system places it at 3856 A; that of the (0, 2) band is at 5607 A. Neither of these

TABLE 7

SPLITTING CONSTANTS

A. $^2\Pi$ state (spin-splitting)

$Y_0(Y_0 - 4) = -4.02 \pm 0.05$

$Y_1(Y_1 - 4) = -4.00 \pm 0.05$

$Y_2(Y_2 - 4) = -3.95 \pm 0.20$

B. $^2\Pi$ state (Λ-doubling, cm^{-1})

v	q_1	q_2	w_1^2	w_2^2
0	$(3.66 \pm 0.03) \times 10^{-2}$	$(3.98 \pm 0.02) \times 10^{-2}$	$(2.8 \pm 0.1) \times 10^{-6}$	$(3.5 \pm 0.1) \times 10^{-6}$
1	$(3.41 \pm 0.03) \times 10^{-2}$	$(3.88 \pm 0.10) \times 10^{-2}$	$(1.0 \pm 0.3) \times 10^{-6}$	$(3.8 \pm 0.8) \times 10^{-6}$
2	$(3.30 \pm 0.10) \times 10^{-2}$	$(3.83 \pm 0.05) \times 10^{-2}$	$(2.0 \pm 2.5) \times 10^{-6}$	$(7.0 \pm 1.2) \times 10^{-6}$

C. $^2\Delta$ state (spin-splitting, cm^{-1})

$A_0 = -0.96 \pm 0.04 \quad A_1 = -1.15 \pm 0.04$

bands has been reported. The (1, 0) band seems to be completely absent from hydrocarbon flame spectra. The (0, 2) band, however, falls on the (0, 1) sequence of the C_2 Swan system and possibly is not absent from hydrocarbon flame spectra. A recent calculation of vibrational transition probabilities by Pillow indicates that these bands should be very weak (Pillow 1955).

We wish to thank the spectroscopy section of the National Bureau of Standards for the use of their large grating spectrograph.

REFERENCES

Dieke, G. H., and Crosswhite, H. M. 1948, *The Ultra Violet Bands of OH* ("Bumblebee Series Report," No. 87).
Fagerholm, E. 1940, *Ark. f. mat., astr., fys.*, Vol. **27A**, No. 19.
Gerö, L. 1941–1942, *Zs. f. Phys.*, **118**, 27.
Herzberg, G. 1950, *Spectra of Diatomic Molecules* (New York: D. Van Nostrand Co.).
Heurlinger, T., and Hulthén, E. 1918–1919, *Zs. f. wissensch. Photographie*, **18**, 241.
Kratzer, A. 1924, *Zs. f. Phys.*, **23**, 298.
Mulliken, R. S. 1928, *Phys. Rev.*, **32**, 388.
Pillow, M. E. 1955, *Proc. Phys. Soc.*, **48**, 547.
Raffety, C. W. 1916, *Phil. Mag.*, **32**, 546.
Vaidya, W. M. 1941, *Proceedings of the National Institute of Sciences of India*, **7**, 89.

THE HYDROGEN-LINE RED SHIFT OF RADIO SOURCE CYGNUS A

A. E. Lilley and E. F. McClain

Radio Astronomy Branch, Naval Research Laboratory, Washington, D.C.

Received December 31, 1955

ABSTRACT

A measure of the red shift has been obtained on radio source Cygnus A by means of the hydrogen-line absorption effect in the continuous microwave spectrum of the source. The measured microwave red shift agrees in magnitude with the optical red shift, and, within the limits imposed by the experiment, $\Delta\lambda/\lambda$ is constant over an interval of 500000 to 1 in the electromagnetic spectrum.

The possibility of measuring the red shift over a wide base line in the electromagnetic spectrum is of interest in cosmology. The H I 21-cm emission from all but a few extragalactic objects is hopelessly below the over-all sensitivity of current instrumentation; but, with a significant decrease in minimum detectable H I opacities by means of 21-cm absorption effects in the spectra of discrete sources, it becomes possible to attempt a red-shift measurement with existing radio telescopes.

Cygnus A was selected as a source to attempt a measurement because the source is strong (it is a collision of galaxies), and there exists the possibility of comparing radio and optical red-shift measurements for a significantly large radial velocity.

If peripheral H I gas is associated with the collision, then there is a chance that the intense radio continuum radiation may first shine through the associated H I gas before passing into intergalactic space. If the red shift has $\Delta\lambda/\lambda$ as a constant, then there possibly should be an H I absorption effect in the continuous spectrum of Cygnus A, displaced to the red approximately 17000 km/sec (Baade and Minkowski 1954) or a shift of about 81 Mc/s from the undisplaced 21-cm line frequency of 1420.405 Mc/s.

QUANTITATIVE POSSIBILITY

We shall write an approximate expression for the apparent antenna temperature presented to a straight radiometer which has a bandwidth $\Delta\nu$, accounting for the H I 21-cm emission from the source and the continuum radiation interaction of the source. The apparent antenna temperature presented to the antenna and receiver at frequency ν and bandwidth $\Delta\nu$ is essentially

$$T \cong \{T(\mathrm{H})_{\Delta\nu} + T_B \exp[-\bar{\tau}(\mathrm{H})_{\Delta\nu}]\} \frac{\Omega_S}{\Omega_B}, \tag{1}$$

where $T(\mathrm{H})_{\Delta\nu}$ is the hydrogen-line brightness temperature of the galaxies in the frequency interval $\Delta\nu$; T_B is the continuum brightness temperature; $\bar{\tau}(\mathrm{H})_{\Delta\nu}$ is the mean projected H I opacity over the source; and Ω_S and Ω_B are, respectively, the solid angles subtended by the source and the antenna beam. If we take an angular diameter of $\sim 30''$ of arc as determined by Baade and Minkowski (1954), then Ω_S/Ω_B is $\sim 1/3600$ for the Naval Research Laboratory 50-foot antenna. With $T(\mathrm{H})$ of the order of $10^{2\circ}$ K, equation (1) reduces to

$$T \cong T_B \frac{\Omega_S}{\Omega_B} \exp[-\bar{\tau}(\mathrm{H})_{\Delta\nu}] \cong T_A \exp[-\bar{\tau}(\mathrm{H})_{\Delta\nu}], \tag{2}$$

where T_A is the unabsorbed apparent antenna temperature of the source in the vicinity of the hydrogen-line opacity $\tau(\mathrm{H})_{\Delta v}$. The minimum detectable temperature $\Delta T_{\min}$ of the Naval Research Laboratory equipment is approximately 1° K; therefore, equation (2), for small opacities, may be rewritten in the form

$$\Delta T_{\min} \cong T_A - T \cong T_A \bar{\tau}\,(\mathrm{H})_{\Delta v} . \tag{3}$$

If $\Delta T_{\min}$ is approximately 1° K, then the minimum detectable mean opacity projected over the Cygnus A source will be $1/T_A$, or about 0.016 for the Naval Research Laboratory equipment. One of the authors has pointed out that when the hydrogen kinetic temperature can be neglected in comparison to T_A, the resulting minimum detectable opacities are $\sim 1/T_A$; the same result is true here because of the strong geometrical reduction of the observed H I emission (Lilley 1955).

EQUIPMENT

The antenna and radiometer employed were identical with those described by Hagen, Lilley, and McClain (1955), with the exception of the bandwidth and the way in which the system was used. The signal band was changed to have a width of 150 kc and was used as a straight radiometer. The comparison band was not utilized in the measurements. Antenna declination scans were used to determine the temperature of Cygnus A against Cassiopeia A as a control. All scans were made between identical values of declination on successive runs, in order to eliminate any effect of background radiation.

THE MEASUREMENTS

Since the magnitude of a possible absorption effect was unknown, it was considered that the usual methods of radiometer calibration were unsatisfactory, and, if possible, a method was desired which would eliminate radiometer-noise figure and gain as first-order considerations. The relatively large part of the spectrum over which measurements were planned made this requirement practically mandatory. The most obvious method of accomplishing the desired result was the use of a second radio source as a control on the Cygnus measurements. Fortunately, the most intense radio source at these wave lengths, Cassiopeia A, differs by only 3 hours and 23 minutes in right ascension and 18° in declination from the Cygnus source. The relative positions of the two sources permitted a system of interleaved observations at periods of about 1 hour, which would tend to cancel out any effects of ground reflections, altitude of antenna, and atmospheric extinction. From measurements made at 9.4 and 21 cm, it appears that Cassiopeia and Cygnus have approximately the same spectral slope, and, based on this assumption, it is necessary only to look for departures in the ratio of the Cygnus-Cassiopeia temperatures. If the spectral slopes are different, it is necessary only to assume that a second derivative exists in the Cygnus spectrum and not in the Cassiopeia spectrum. In general, one source was observed for about 45 minutes; then the antenna was repositioned (requiring approximately 10–15 minutes), and the same set of observations was made on the second source. The antenna was then repositioned on the first source and the process repeated.

The measurements were of two kinds. In the first method the antenna temperature of one of the sources was measured at a number of frequencies. The antenna was then positioned on the second source, and identical measurements were made. This process was repeated a number of times in any one day and on successive days. The same frequencies ($\pm$ 10 kc) were employed on all runs, with the exception that the frequency interval was increased from that initially employed, to give more statistical weight to the remaining points. The points with few observations are not included in Table 1 and Figure 1. In the second measurement the receiver was tuned to a particular frequency, and a large number of measurements were made of the temperature of one source. The

antenna was then moved to the second source, and a comparable number of measurements was made at the same frequency. In all, approximately a thousand determinations of temperature were taken.

In reducing the data, there was no attempt to obtain a true antenna temperature for either source. Instead, the chart deflections on adjacent runs were compared, and the Cassiopeia-Cygnus ratio was noted. In order to eliminate any personal bias, a third party

TABLE 1

WAVE-LENGTH MEASUREMENTS

Point No.	Frequency (Mc/s)	No. of Measurements	Statistical Weight	Cass/Cygnus Ratio
Blue mean (A)	1348–1358	132	5	1.579
B	1346.25	24	1	1.538
C	1344.25	40	2	1.577
D	1342.25	36	2	1.639
E	1341.25	36	2	1.620
F	1341.00	44	2	1.591
G	1340.75	40	2	1.620
H	1341.50	44	2	1.614
I	1341.25	40	2	1.624
J	1337.25	44	2	1.580
K	1336.25	28	1	1.554
Red mean (L)	1324–1334	124	5	1.558

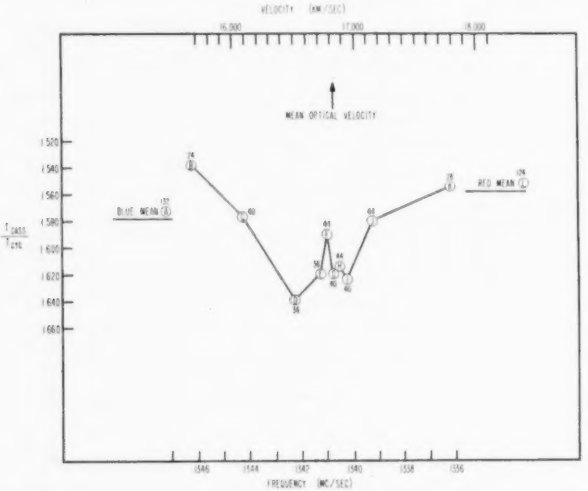

FIG. 1.—The lettered circles are a plot of the Cassiopeia-to-Cygnus antenna temperature ratios as a function of recessional velocity and observed frequency. These values are given in Table 1. Beside each lettered circle is a number which denotes the number of observations that were used in determining the ratio. Points *A* and *L* have been called the "Blue" and the "Red" means, for convenience. They represent a mean value over intervals of frequency which are specified in Table 1. The mean optical recessional velocity of Cygnus A as determined by Baade and Minkowski (1954) is indicated at the top of the figure.

reduced the data independently, and it was found that the results were practically identical with the authors' reduction.

Table 1 is a listing of the results of the measurements, and Figure 1 is a plot of the same data. The red and blue means were obtained at frequencies of from 5 to 10 Mc outside the suspected absorption range.

In order to obtain a statistical picture of the data, they were subjected to the t-test (Fisher 1950). Points A, B, C, J, K, and L were considered as one set located outside the absorption range, and points D, E, F, G, H, and I were considered as a second set within the absorption range. The standard deviation of a point having a statistical weight of 1 was found to be 0.014. The difference between the means of the two sets was 0.050, with a standard deviation of 0.0053. The t-test reveals that the probability of the observations' being due to random scatter is $\ll 10^{-2}$. We therefore take the difference between the means and find $0.050/1.618 \times 100 = 3.1$ per cent absorption. Since the receiver used does not employ image rejection, this figure must be doubled, yielding a true absorption of about 6.2 per cent. For small opacities the percentage reduction in temperature is approximately equal to the opacity, from which we conclude that the mean opacity of that hydrogen gas effective in absorbing energy from the collisional zone of the two galaxies is between 0.06 and 0.07. We find the observed absorption centered at a recessional velocity of approximately 16700 km/sec, with an approximate half-width of 850 km/sec. These figures are in good agreement with those determined by Baade and Minkowski (1954) in the optical range.

The major source of error in the measurements reported is probably due to interference and drift in receiver-noise figure and gain. We feel the precautions taken in interleaving the observations should have largely eliminated errors due to receiver drift, but interference was particularly bad at frequencies above 1350 Mc, casting some doubt on the value of the blue mean. This value is therefore considered tentative. Intergalactic hydrogen would have caused a lower value for the blue mean, but the measurement uncertainties preclude ascribing the somewhat lower value to this cause. The slight difference between the red and blue means may also be accounted for by a difference in the spectral slopes of Cygnus A and Cassiopeia A.

The measurements indicate an H I opacity of ~ 0.06 over a velocity interval of about 850 km/sec. Using this information and an assumed H I temperature of $\sim 10^{2\circ}$ K, one can estimate the total mass of H I which is effective in producing the observed absorption. We find approximately $7 \times 10^7 \times A$ solar masses, where A is the area in square kiloparsecs of the continuous source. However, since the absorption is barely detectable with our equipment, the results concerning the involved H I mass are tentative.

The authors are indebted to W. S. Ament for his suggestions about the statistical handling of the data; to F. T. Haddock for encouraging discussions; and to C. H. Mayer for his independent reduction of all the data as a check on the personal equation. Finally, the authors express their appreciation to H. H. Corbett, C. R. Grant, W. E. Grimes, J. H. Nichols, and B. S. Yaplee for their generous assistance in operating the antenna mount on a continuous basis.

REFERENCES

Baade, W., and Minkowski, R. 1954, *Ap. J.*, **119**, 206.
Fisher, R. A. 1950, *Statistical Methods for Research Workers* (London: Oliver & Boyd).
Hagen, J. P., Lilley, A. E., and McClain, E. F. 1955, *Ap. J.*, **122**, 361.
Lilley, A. E. 1955, *Ap. J.*, **122**, 197.

NOTES

THE PHASE VARIATION OF URANUS

The maximum phase angle which the planet Uranus can attain is about 3°. Recently, a few observers have made photoelectric measurements of the magnitude of this planet (Wilson 1955), and the question naturally arises as to the amount of phase variation to be expected.

The albedo of Uranus is very high; apparently, the incident light is reflected by Rayleigh scattering. The theory of radiative transfer has been developed by Chandrasekhar (1950, 1954) to include this type of scattering, and the application to the problem of planetary atmospheres is quite direct (Horak 1950). However, the amount of computation is considerable, and it was felt that the adoption of the phase function for isotropic scattering would materially reduce the length of the calculations, yet still be sufficiently close to the truth as far as phase variation is concerned. Accordingly, we adopted as a model for the atmosphere of Uranus a semi-infinite atmosphere which scatters light in accordance with the theory of isotropic scattering with albedo unity.

In order to compute the magnitude, it is necessary to integrate the intensity over the visible disk. For phase angles 0°, 1°, 3°, 6°, 8°, and 10° the integration was carried out by using a network of sixty-four points; for the other phase angles a network of only six-

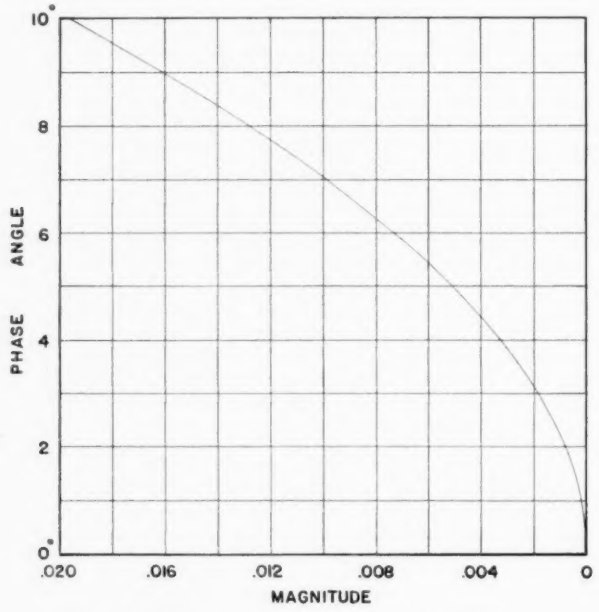

FIG. 1.—The theoretical phase variation from 0° to 10°

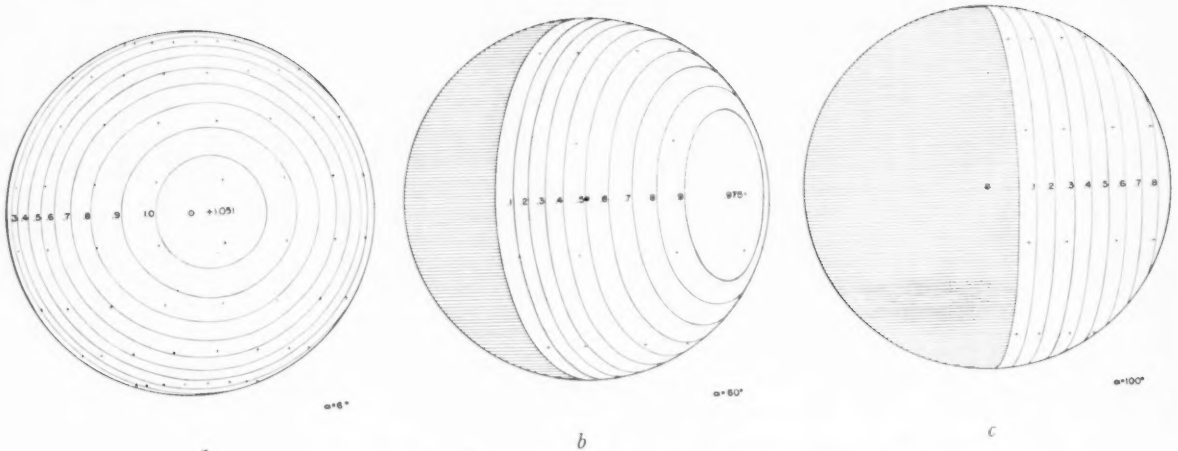

a *b* *c*

FIG. 2.—The isophotes at three different phase angles. The intensities are expressed in relative units

teen points was adopted. The numerical values of the $H(\mu)$-functions were taken from a table of Placzek (1947).

The results are given in Table 1 and shown graphically in Figure 1. It is seen that the phase variation to be expected from 0° to 3° is very small indeed, amounting to roughly 0.0006 mag/° and its detection by observation would require very high precision. The isophotes are shown at three different phases in Figure 2.

TABLE 1

ISOTROPIC SCATTERING ($\varpi = 1$)

Phase Angle	Magnitude	Phase Angle	Magnitude
0°	0.00000	40°	0.267
1	.00021	60	0.582
3	.00189	80	1.024
6	.00730	100	1.623
8	.01278	120	2.433
10	.01963	140	3.581
20	0.069	160	5.467

We are indebted to Drs. R. H. Hardie, H. L. Johnson, and G. P. Kuiper for encouraging us to carry out these computations and to the National Science Foundation for financial support.

ROBERT L. TALLEY
HENRY G. HORAK

UNIVERSITY OF KANSAS

REFERENCES

Chandrasekhar, S. 1950, *Radiative Transfer* (Oxford: Clarendon Press).
Chandrasekhar, S., and Elbert, D. D. 1954, *Trans. Amer. Phil. Soc.*, **44**, 643. This paper contains an extensive table of Raleigh-scattering functions.
Horak, H. G. 1950, *Ap. J.*, **112**, 445.
Placzek, G. 1947, *Phys. Rev.*, **72**, 557.
Wilson, A. G., Hardie, R. H., Giclas, H. L., and Johnson, H. L. 1955, *Scientific Report No. 1* (Lowell Observatory).

THE HALO DISTRIBUTION OF RADIO EMISSION AND EXTENDED MAGNETIC FIELDS IN OUR GALAXY AND M31

Some of the most interesting and important observational results recently obtained in radio astronomy concern the distribution of radio sources away from the galactic planes, in M31 and in our Galaxy. Baldwin (1954) has shown that in M31 there are sources extending to very great distances normal to the spiral plane. As a crude model he has considered that the observations can be explained by a distribution of sources following the stellar distribution in the spiral plane of the Galaxy which contributes about one-third of the total intensity, together with a distribution of sources having spherical symmetry, and extending to radial distances greater than 10 kpc, which contributes the remaining two-thirds. More recently an analysis of the background radiation in our Galaxy, made by Baldwin (1955), has shown that, apart from a small fraction from sources in the plane, the distribution of this radiation is also spherical. The approximate radii of the spheres and the power emitted at 81.5 Mc/s are: M31, 0.5×10^8

watts ster^{-1}(c/s)$^{-1}$/pc^3, $R \gtrsim 10$ kpc; Galaxy, 1.8×10^8 watts ster^{-1}(c/s)$^{-1}$/pc^3, $R \approx 11$–16 kpc. The centers of the spheres are approximately coincident with the disk centers.

We consider that the most plausible explanation of this radiation is that it is radiation emitted by high-energy electrons moving in magnetic fields (synchrotron radiation); such an explanation was earlier proposed by Shklovsky (1952) when he attempted to explain earlier observational data (see also Ginsberg 1953 and Pikel'ner 1955; I am indebted to Dr. J. H. Oort for these latter references). We shall suppose (*a*) that there is a roughly spherical distribution of very diffuse gas (which may in part be gas ejected from the galactic-plane regions, or gas which is a relic of the very early stages of galactic condensation); (*b*) that there is a roughly spherical distribution of magnetic field in equilibrium with this diffuse gas distribution; and (*c*) that in this volume a flux of high-energy electrons is continuously circulating.

For an electron having relativistic energy ($\gamma = E/mc^2 \gg 1$) moving in a magnetic field of strength H, the approximate formulae for the frequency, ν, and power radiated, P_ν, are (Hoyle 1954)

$$\nu = 4.19 \times 10^6 H\gamma^2 \,(\mathrm{c/s}), \qquad P_\nu = 1.58 \times 10^{-15} H^2\gamma^2 \,(\mathrm{erg/sec}).$$

If $\nu = 8.15 \times 10^7$, then

$$\sqrt{H}\gamma = 4.41, \tag{1}$$

$$P_\nu = 3.07 \times 10^{-14} H. \tag{2}$$

Now we can in the first instance suppose that the electrons have a cosmic-ray energy distribution, so that $N(E)$, the number having energies between E and $E + dE$, has the form

$$N(E)\,dE \propto \frac{dE}{E^n},$$

where $2.5 < n < 3$. A mean number density of electrons, n_0, and a mean energy, $\bar{E}$, are then defined by the condition that

$$n_0\bar{E} = k\int_{E_0}^{E_c} N(E)\,E\,dE,$$

where E_0 and E_c are the low- and high-energy cutoffs. The corresponding frequency-power spectrum of the emission is

$$P_\nu\,d\nu \propto \frac{d\nu}{\nu^{(n-1)/2}}.$$

Since we do not have any observational data on this frequency dependence for normal galaxies, we can only put

$$\int_{\nu_0}^{\nu_c} P_\nu\,d\nu = \bar{P}\Delta\nu,$$

where ν_0 and ν_c are the low- and high-frequency cutoffs. Following the treatment of Minkowski and Greenstein (1954) for other radio sources, we put $\Delta\nu \approx 10^8$ c/s, and $\bar{P} = P_{81.5}$. Then, if p is the power emitted per cubic centimeter in the sphere, we have, from equation (2), $p = n_0 H \times 3.07 \times 10^{-14}$; and if we use the observational values for p given earlier, then

$$n_0 H = 10^{-18} a, \tag{3}$$

where $a = 2.52$ (Galaxy) and $a = 0.70$ (M31).

The energy density of the electrons must be very much smaller than the total space-energy density of cosmic radiation ($\approx 10^{-12}$ erg/cc); the observations suggest that they

comprise less than 1 per cent of the primary particles (Critchfield, Ney, and Oleska 1952). Thus $n_0 \bar{E} \leq 10^{-14}$. Because of the form of the assumed energy spectrum, $\bar{E}$ will be near to the low-energy cutoff, E_0. No information is available, but if we put, as a very low limit, $E_0 = 10\ mc^2$, then

$$n_0 \leq 10^{-9}\ . \tag{4}$$

Finally, we have to consider the stability of the low-density neutral gas making up the bulk of the sphere. The mean density of this region must be very much lower than the mean density of the gas in the disk but rather larger than the mean density of the material in the universe. We shall put $10^{-24} \gg \rho > 10^{-27}$ g/cc. Now, for equilibrium,

$$p_{\text{grav}} = p_{\text{tur}} + p_{\text{mag}}\ , \tag{5}$$

where

$$p_{\text{grav}} \approx \frac{GM\rho}{R}; \qquad p_{\text{tur}} = \tfrac{1}{3}\rho v^2; \qquad \text{and} \qquad p_{\text{mag}} = \frac{H^2}{8\pi}.$$

Here H is the mean magnetic field, M can be taken to be the total mass of the Galaxy ($M \approx 10^{44}$ g), R is a dimension of the order of the radius of the sphere ($R = 3 \times 10^{22}$ cm), and v is the turbulent velocity of the gas. Thus $p_{\text{grav}} = 2 \times 10^{14}$ dynes, and, provided that the magnetic field is not completely negligible, the turbulent pressure can be neglected if $v \ll (3GM/R)^{1/2} = 240$ km/sec. We have no direct knowledge concerning such turbulent velocities, though detection might not be possible for such low densities. Two cases will be considered: (*a*) we shall suppose that the turbulent motions can be neglected, and (*b*) we shall put $v = 200$ km/sec. Then, from equation (5), we find that (*a*) if $\rho = 10^{-26}$ and 10^{-27} g/cc, $H = 7$ and 2×10^{-6} gauss, respectively; and (*b*) if $\rho = 10^{-26}$ and 10^{-27} g/cc, $H = 4$ and 1×10^{-6} gauss, respectively. Thus it is reasonable to suppose that the magnetic field is of the order of 10^{-6} gauss. From other considerations discussed later, it seems that case *b* is the more probable. If we now put $H = 2 \times 10^{-6}$ gauss in equation (1), we find $E = 1.6$ Bev, and, from equation (3), $n_0 \approx 10^{-12}$, so that inequality (4) is easily satisfied.

The origin of the flux of high-energy electrons is uncertain. If we supposed that the magnetic field were smaller than 10^{-6} gauss, there would no longer be rough equipartition between the magnetic and turbulent energies, and also the electron energies demanded would increase as $H^{-1/2}$. We might suppose that the electrons are accelerated in the galactic-plane region and are then continuously ejected into the halo, where they radiate but do not gain further energy. In this case a concentration of radio brightness toward the disk, apart from other sources, might be expected. However, we wish to explain a fairly uniform brightness distribution extending to great distances away from the plane, and it is therefore more probable that the electrons have a fairly uniform space density in the sphere. This can be achieved only if they are both gaining energy and losing it by radiation during their circulation. The most plausible way in which energy can be gained is by collisions with magnetic turbulent elements (Fermi 1949). It is this argument which suggests that the gas has large turbulent velocities. If $v = 200$ km/sec, the energy gained by an electron in a collision with a magnetic turbulent element, δE, is given by $\delta E = (v/c)^2 E$, so that, if $E = 1$ Bev, the energy gained is about 400 ev. From equation (2) the distance traveled by an electron while radiating this energy in a field of 10^{-6} gauss is of the order of 100 pc. The electron will, in general, follow a very tortuous path, but in most favorable circumstances the energy gain by collision will equal or exceed that lost by radiation if the "cores" of the turbulent elements from which the electron is totally reflected are ≤ 100 pc apart.

In assuming that we initially have electrons of energies near 1 Bev, we have neglected the difficulty in accelerating them to these energies where energy loss by radiation dominates. As Fermi pointed out, loss by ionization and bremsstrahlung will always be greater than gain by collisions for energies <300 Mev, where these losses are most im-

portant. This appears to be the case for both the galactic-plane regions and the diffuse sphere. Thus we need a source of electrons with a threshold above 300 Mev (if 300 Mev were the low-energy cutoff, inequality [4] would still be satisfied). The source may be electron-positron pair production in primary proton–thermal photon interaction. The calculations made by Feenberg and Primakoff (1948) suggest that the average energy of a pair will be about 100 Bev for primary proton energies near 10^5 Bev. This is considerably higher than the 1 Bev that we considered probable in the earlier discussion. Also for this energy range the photons in the primary interaction must have energies in the far-ultraviolet part of the spectrum. In addition to pair production, a small contribution to the flux will come from the electrons and positrons which are the stable end products following meson production in nuclear collisions.

Pikel'ner (1953) and Shklovsky (1952) have already suggested that in this Galaxy a more extended distribution of diffuse gas and magnetic field than that in the disk is necessary to explain both the isotropy of cosmic radiation and some of the earlier data on radio brightness. The importance of the model for theories of the origin of cosmic rays will be discussed elsewhere. As Pikel'ner has pointed out, if high turbulent velocities are present, the major difficulty of the acceleration process in Fermi's mechanism will be removed. Recent 21-cm work by Helfer and Tatel (1955) suggests that there is considerable material away from the plane in our Galaxy.

The model described here may quite generally apply to normal late-type spiral galaxies. Hoyle (1953) has supposed that conditions of high velocity turbulence and magnetic field may exist in a proto-galaxy, so that on his viewpoint we might suppose that this halo is a relic of the proto-galaxy.

A number of arguments suggest that in the disk the magnetic lines of force lie along the spiral arms and are important factors in maintaining their stability (Chandrasekhar and Fermi 1953). At some points, however, there are indications that there are bulges and leakages of field out of the arms (Davis 1954), and it is probable that it is in these regions that the lines of force defining the magnetic fields in the disk are linked to of those the surrounding sphere.

I am indeted to Mr. M. Ryle and Mr. J. E. Baldwin for discussions and for unpublished observational results of the Cambridge group, and to Dr. J. H. Oort and Dr. E. M. Burbidge for helpful criticism. This study has been made as part of the program of radio astronomical research currently being carried on at the Cavendish Laboratory, and I am grateful to the Royal Society for financial support.

G. R. Burbidge

Cavendish Laboratory
University of Cambridge

REFERENCES

Baldwin, J. E. 1954, *Nature*, **174**, 320.
———. 1955, in preparation.
Chandrasekhar, S., and Fermi, E. 1953, *Ap. J.*, **118**, 113, 116.
Critchfield, C. L., Ney, E. P., and Oleska, S. 1952, *Phys. Rev.*, **85**, 461.
Davis, L. 1954, *Phys. Rev.*, **96**, 743.
Feenberg, E., and Primakoff, H. 1948, *Phys. Rev.*, **73**, 449.
Fermi, E. 1949, *Phys. Rev.*, **75**, 1169.
Ginsberg, V. 1953, *Uspekhi Phys. Nauk*, **51**, 343.
Helfer, H. L., and Tatel, H. E. 1955, *Ap. J.*, **121**, 585.
Hoyle, F. 1953, *Ap. J.*, **118**, 513.
———. 1954, *Nature*, **173**, 482.
Minkowski, R., and Greenstein, J. L. 1954, *Ap. J.*, **119**, 238.
Pikel'ner, S. B. 1953, *Doklady Akad. Nauk SSSR*, **88**, No. 2, 229.
———. 1955, *Les particules solides dans les astres* (Cointe-Liège, Belgium: Institut d'Astrophysique).
Shklovsky, I. S. 1952, *Astr. J. SSSR*, **29**, 418.
———. 1953, *ibid.*, **30**, 15.
———. 1954, *ibid.*, **31**, 533.

RELATIVISTIC DEFLECTION OF SUN'S LIGHT BY THE MASS OF THE SUN

One of the well-known predictions of the general theory of relativity is that the light from a distant star just grazing the limb of the sun will be deflected through an angle of 1.75 seconds of arc. Now the sun's light will also be deflected, and it is the purpose of this note to calculate the effect of this deflection on the apparent diameter of the sun as observed from a distance r. Employing the Schwarzschild line element, the general relativity equation for a ray of light emitted by the sun and traveling in the sun-earth plane is (Tolman 1934)

$$\frac{d^2u}{d\theta^2} + u = 3mu^2, \tag{1}$$

where $r = 1/u$ and θ are polar co-ordinates in the sun-earth plane, origin at center of sun, and the mass m of the sun is expressed in relativistic units.

Let R be the radius of the sun, and specify a particular ray by the condition $dr/d\theta = A$ for $r = R$. Then the observed angle β' between the undeflected ray ($A = \infty$) from the center of the sun's disk and a ray from any other point on the disk is given by a first integration of equation (1), with the following result:

$$\tan \beta' = r\frac{d\theta}{dr} = r^{-1}\left(\frac{2m}{r^3} - \frac{2m}{R^3} - \frac{1}{r^2} + \frac{1}{R^2} + \frac{A^2}{R^4}\right)^{-1/2}. \tag{2}$$

Now the observed angular radius β will be the maximum value of β', given by equation (2) with $A = 0$. The apparent limb ray is tangential to the sun's surface, but consideration shows that it comes from a point behind the geometrical limb; in other words, the observer sees around the edge of the sun. The difference $\delta = \beta - \alpha$ between the observed β and the true angular radius α [$\tan \alpha = R/(r^2 - R^2)^{1/2}$] is obtained from equation (2),

$$\tan \delta = \frac{R(r^2 - R^2)^{1/2}\left[\left\{1 - 2m(r^3 - R^3)\left[rR(r^2 - R^2)\right]^{-1}\right\}^{-1/2} - 1\right]}{r^2 - R^2 + R^2\left\{1 - 2m(r^3 - R^3)\left[rR(r^2 - R^2)\right]^{-1}\right\}^{-1/2}}. \tag{3}$$

At the earth's distance from the sun, $R/r \approx 5 \times 10^{-3}$, giving $2\delta \approx 2m/r$. Thus, according to the theory of relativity, the sun's true angular diameter is smaller than the one observed by the amount $2\delta \approx 4 \times 10^{-3}$ seconds of arc. This is negligible, since the observed angular diameter is 1919.3 ± 0.1 sec at the mean distance of the sun. As an observer approached the sun, the value of 2δ would increase to a maximum value of the order of 1 second of arc and would then decrease to zero at the surface of the sun. For other stars, e.g., white dwarfs, the ratio δ/β can be considerably larger than for the sun, but this has no practical importance, since β cannot be known accurately for the large r involved.

I am indebted to St. John's University for a summer research grant.

S. N. Milford

Physics Department
St. John's University

REFERENCES

Tolman, R. C. 1934, *Relativity, Thermodynamics, and Cosmology* (Oxford: Oxford University Press), p. 210.

ABSTRACTS OF ASTROPHYSICAL JOURNAL SUPPLEMENT SERIES

Supplement No. 17, Volume II

NUCLEAR REACTIONS AND ELEMENT SYNTHESIS IN THE SURFACES OF STARS

W. A. Fowler, G. R. Burbidge, and E. Margaret Burbidge

Cavendish Laboratory, Cambridge, England

The astronomical evidence suggests that the anomalous overabundances, particularly of some heavy elements, in peculiar A stars with magnetic fields (Apm stars) are unlikely to be due to synthesis in the stellar interior. It is suggested in this paper that regions develop in which sufficient magnetic energy is available to accelerate particles on the stellar surface so that nuclear reactions can take place there. As a model it is supposed that the particles are accelerated in regions of changing magnetic field by the Swann betatron mechanism, modified to take account of the plasma and collision properties of the gas. The conditions necessary for element synthesis are plausible. They are, depending on the efficiency of the acceleration and nuclear processes, that the spot regions (assumed to have radii of 10^9–10^{10} cm) have densities $\rho = 10^{-8}$–10^{-7} g/cc and local magnetic fields $H = 5 \times 10^5$–10^7 gauss and that average particle energies of $\sim$1 Mev are attained. One to 10 per cent of the spot is involved (or a much smaller fraction for the very large spots), and a fraction 0.01–0.5 of the magnetic energy is converted into kinetic energy. The anomalous abundances occur in a surface layer reaching down to $\rho = 10^{-4}$ g/cc. It is assumed that the time scales over which the mechanism is effective are 10^4–10^6 seconds. Radiative effects may limit the time scale to the order of 1–10 seconds, but favorable choices for the other parameters involved will compensate for this.

Depending on the details of acceleration, energy loss, and energy-sharing mechanisms, we discuss two specific models: (*a*) An energy spectrum of the accelerated particles given by $f(E) \propto E^{-3}$, with about 1 per cent of the particles accelerated to 10–100 Mev. The still higher-energy particles in the spectrum may contribute to the primary cosmic radiation injected into the interstellar medium. Direct synthesis then takes place by (α, n) . . . (α, 3 nucleons) and by (d, p) and (d, n) reactions. This model can be criticized on the grounds of energy loss to electrons by the accelerated nuclei at $\rho = 10^{-8}$–10^{-7} g/cc, and it can be ruled out observationally if the D/H ratio in the Apm stars $\ll$0.01, since theoretically it builds up to $\sim$0.01. (*b*) A Maxwell-Boltzmann energy distribution in a "hot spot" within the magnetic spot, with $kT \sim 1$ Mev ($0.3 < kT < 1.5$), and all the particles involved. Synthesis then takes place by neutron production through (p, n) processes, principally on the light nuclei, followed by (n, γ) capture processes on the metals. In the primary (p, n) process each stable target nucleus, X, serves catalytically to change protons into neutrons. The unstable residual isobar, Y, produced in the reaction $X + p \rightleftarrows Y + n$ decays back to X by positron-neutrino emission or electron capture, i.e.,

$$Y \rightarrow X + \beta^+ + \nu \qquad \text{or} \qquad Y + e^- \rightarrow X + \nu\,.$$

In this case the theoretical D/H ratio might be as low as $\sim 10^{-5}$.

These results are applied to the observed anomalies in α^2 CVn and HD 133029. By making plausible estimates about the spot activity and the amount of mixing, the over-

abundances of Sr, Y, Zr, La, the rare earths, and Pb can reasonably be explained if the activity has gone on for $\sim 5 \times 10^8$ years. Other anomalies, i.e., of O, Si, and Ca, may also be explicable. Stellar surface synthesis of the cosmical D, Li, Be, and B is discussed, since these are unstable at the temperatures of stellar interiors. It is suggested that they are produced by spallation reactions on C, N, and O, either high up in the stellar atmospheres ($\rho \sim 10^{-9}$) or, less probably, in "hot spots" similar to case *b*, but where $kT \sim 5$ Mev. The postulated amount of magnetic activity in Apm stars is insufficient to produce reasonable abundances. If much smaller-scale activity on a larger number of stars (red dwarfs) is considered, then in $\sim 10^9$ years a D/H ratio of $\sim 10^{-6}$–10^{-9} and the cosmical abundances of Li, Be, and B can be produced, if a fairly high efficiency of production and ejection in these stars is assumed.

Supplement No. 18, Volume II

A CATALOGUE OF HIGH-VELOCITY STARS

NANCY G. ROMAN

Yerkes and McDonald Observatories

The catalogue contains new spectral types, photoelectric magnitudes and colors, and spectroscopic parallaxes for about six hundred high-velocity stars. For most of these, the space velocities and the eccentricities and semimajor axes of their galactic orbits are also given.

The basis for the new catalogue is all nonvariable stars north of declination $-20°$, brighter than 9.5 m_v, and not later than M0 in Miczaika's catalogue of high-velocity stars (1940). To these were added other stars from radial-velocity lists published since 1938, a few stars from a list of space motions of the bright stars, nineteen stars whose velocities were measured at the David Dunlap Observatory but which have not been published, and a number of stars from the Yale catalogues of proper motions. For the latter source, tangential velocities were estimated from the proper motions, magnitudes, and the published spectral types, assuming that all stars were dwarfs.

Although, on the basis of modern data, an appreciable number of stars from Miczaika's catalogue have velocities smaller than the 63-km/sec limit which he set, these have been included in the present catalogue also, as were some stars selected from other lists whose large velocities later proved to be spurious. For selecting stars from the proper-motion catalogues, a lower limit of about 100 km/sec was used. Thus there is no definite limit above which the catalogue is complete or below which all stars are omitted. Nevertheless, the catalogue should provide a source of data for a large group of typical high-velocity stars, from which smaller groups can be selected for further investigation.

The classification spectra were taken with either the small spectrograph on the Yerkes 40-inch refractor or the 110-mm camera on the Cassegrain spectrograph on the McDonald 82-inch reflector. The dispersion of both combinations is near 120 A/mm at Hγ. A few of the Yerkes spectrograms were taken by other observers, primarily Guido Münch, while W. A. Hiltner took several of the McDonald spectrograms. The types are on the MK system (Johnson and Morgan 1953).

As is well known, the spectra of many high-velocity stars are not normal, and some compromise must be made in their classification. In the present catalogue, the practice has been to use the strength of the ionized strontium line, λ 4077, to determine the luminosity of all stars later than F5. For stars with decidedly weakened lines, the type has been determined from the usual line ratios whenever possible; among the A- and F-type stars, the strength of the hydrogen lines has been given high weight. Usually, this procedure leads to luminosities and predicted colors in agreement with the measured

parallaxes and observed colors. The exceptions are indicated in the notes to the catalogue, as are extreme peculiarities in the spectra. Except for these stars, no attempt has been made to indicate weak cyanogen, a strong G band, or weakened metallic lines, as these effects are present to some extent in the spectra of almost all high-velocity stars. An indication of the weakness of the metallic lines in the F- and G-type spectra can be found from a comparison of the $B - V$ and $U - B$ colors for each star. An ultraviolet excess ranging from 0.0 to more than 0.2 mag., which is found in most high-velocity stars, is well correlated with the weakness of the lines. Moreover, both anomalies are correlated with velocity, in the sense that the stars with the weakest lines also have the largest ultraviolet excesses and the largest space velocities.

Most of the photometric observations were made with the 13-inch reflector at the McDonald Observatory. All material was reduced immediately to the B, V, U system, and no systematic difference is noticeable between various seasons or telescopes. Except in the cases specifically mentioned in the notes, at least two observations were obtained for each star; the average number is $2\frac{1}{2}$. The average internal mean errors per star are: V, $\pm 0^m022$; $B - V$, $\pm 0^m018$; and $U - B$, $\pm 0^m027$. Since the observations were made with a small telescope, magnitudes fainter than 11.0 were difficult to measure accurately with the available equipment. Therefore, the $U - B$ colors of the faint red stars are somewhat uncertain. This probably accounts for the unusually large average mean error for the $U - B$ colors.

As far as possible, the radial velocities are from the *General Catalogue of Radial Velocities*. The remainder are from the radial-velocity lists from which the stars were taken or from the author's measurements of David Dunlap Observatory plates. The sources of the proper motions are indicated in Table 1 by the standard abbreviations. The trigonometric parallaxes are from the 1950 parallax catalogue.

U, V, and W are the velocities relative to the centroid of motions of the near-by stars in the directions ($l = 57°.5$, $b = 0°$), ($l = 147°.5$, $b = 0°$), and ($b = 90°$); and Q is the vectorial sum of these components. On the assumption that this local centroid represents a circular velocity of rotation of 216 km/sec at a distance of 8.2 kpc from the center of the Galaxy, U and V have been used to compute the eccentricities and semimajor axes of the Newtonian orbits described by the projection of the star's motion on the galactic plane. At best, these orbits are only approximations, since we have ignored both the W component of the velocity and the lack of an exact inverse-square force field near the center of the Galaxy. However, their size and shape should provide more useful parameters for statistical discussions of these stars than Q alone.

It seems fairly definite that four of the stars in Table 1 move in hyperbolic orbits. These are BD+21°607, sd F5; BD+6°2932, G6 V; BD+2°3375, sd F5; and HD 134439, K0 VI, with orbits whose eccentricities are 1.10, 1.19, 1.15, and 1.37, respectively. A circular velocity near the sun of 270 km/sec would be necessary to account for the motions of these stars by elliptical orbits.

Visual double stars and spectroscopic binaries have been indicated in the notes to the catalogue. If both components of a visual double were observed as one star photometrically, the measured magnitude was corrected to give the true magnitude of the brighter one. In these cases the magnitude difference is from Aitken's *New General Catalogue of Double Stars* (1932) and is given in the notes. Among the spectroscopic binaries, only the one with double lines was corrected for the presence of a second component; in this case it was assumed that the stars were equally bright.

REFERENCES

Aitken, G. R. 1932, *New General Catalogue of Double Stars* (Washington, D.C.: Carnegie Institution of Washington).
Johnson, H. L., and Morgan, W. W. 1953, *Ap. J.*, **117**, 313.
Miczaika, G. 1950, *A.N.*, **270**, 249.

Supplement No. 19, Volume II

REVISED LIST OF ABSORPTION LINES IN THE SPECTRUM OF R ANDROMEDAE

PAUL W. MERRILL AND JESSE L. GREENSTEIN
Mount Wilson and Palomar Observatories
Carnegie Institution of Washington, California Institute of Technology

The spectrum of R Andromedae, a red variable of period 407 days, is typical of class S. Spectrograms, dispersion 4.5 A/mm in the blue region, 6.8 A/mm in the visual, recently obtained with the 200-inch telescope, form the basis of this article. A table lists the wave lengths, intensities, and chemical identifications of 1500 absorption lines between 4000 and 6900 A. The accuracy of the wave lengths approaches 0.01 A. The general behavior of lines of the rare earths and of other heavy elements, including technetium, is briefly described. The measurements show that displacements of lines of six neutral metals increase algebraically with excitation potential of the lower level.

Supplement No. 20, Volume II

PHOTOMETRY OF SOLAR FLARES

HELEN W. DODSON, E. RUTH HEDEMAN, AND ROBERT R. MCMATH
McMath-Hulbert Observatory of the University of Michigan

Photometric measures of Hα spectroheliograms provide the observational data for studies of the intensity, area, and duration of 194 flares and subflares and the ionospheric disturbances associated with them. Implications of these studies have been tested whenever possible by auxiliary studies of duration, disk distribution, and associated ionospheric disturbances for the much larger number of flares in the *Quarterly Bulletin of Solar Activity*.

Hα flare intensities have been measured in units of both the local and the central continuum at λ 6590. In the former, the *average* Hα intensity at flare maximum ranged from 0.66 for subflares and 0.88 for flares of importance 1, to intensity 1.17 and 1.28 for flares of importance 2 and 3, respectively. In units of the central continuum, the average values are about 0.1 lower. The brightest measured maximum was 1.9 times the local continuum for a flare at CMD 72°.

Hα intensity often varies differently in different parts of the same flare. At any one point in the flare, the change of Hα intensity with time can be well represented by the series of curves given by the equation

$$\log \frac{I_t}{I_0} = \left(\log \frac{I_{\max}}{I_0} \right) 10^{\pm a(t - t_{\max})},$$

where t is measured in minutes and a is positive for the ascending branch, negative for the descending branch, and takes values between 0.40 and 0.00313. Parameter a is always larger for the ascending than for the descending branch of the light-curve. The most usual value of a for the ascending branch is 0.10; for the descending branch a is $\gtrsim 0.025$ for 87 per cent of the cases.

No convincing relationship has been found between the rate of increase in intensity and the maximum intensity attained by the flare. However, the slowest rate of increase

apparently diminishes the chance of attaining a maximum as bright as the continuous spectrum.

Although, *in general*, the flare area and intensity increase together, the correlation coefficient of these two measures for the flares in this study is only 0.58 ± 0.03 p.e. The duration was associated more closely with the area than with the maximum intensity of the flare. The duration of flares as measured by photometric light-curves is much longer than the average duration of flares reported in the *Quarterly Bulletin of Solar Activity*.

There is evidence for center-to-limb variation in numerous characteristics of the Hα flares in this study. The slowest rates of rise and decline were observed only for flares within 55° of the central meridian, and the fastest rates of decline only for flares within 40° of the solar limb. The average intensity in units of the local continuum increased with increasing central meridian distance of the flares. In units of the central continuum, the average intensity diminished from center to limb. "Limb-darkening" equations for the flares and subflares are as follows:

$$\text{Flares: } I_c = 0.63 + 0.34 \cos \theta$$

$$\text{Subflares: } I_c = 0.36 + 0.26 \cos \theta .$$

For flares of the same importance, the average duration diminished with increasing distance from the center of the disk. Near the center of the disk, the Hα flare usually lasted as long as, or longer than, the associated ionospheric disturbance, but for flares far from the center the reverse was true.

The reported starting times of sudden ionospheric disturbances (SID) usually fell during the period of increasing intensity in the flare. Except in unusual cases, SID's were not reported unless the flare intensity was at least 0.8 of the local continuum and the area was of the order of 200 millionths of the solar disk. Near the limb the SID often lasted longer than the Hα flare. Furthermore, there is apparently less diminution from center to limb in the ionizing radiation from flares than in Hα. The ionospheric disturbances were unusually small for certain large and relatively bright flares associated with the onsets of 200-Mc/s noise storms.

Direct examination of ionospheric records for the times of the flares and subflares in this photometric study has provided evidence for a new type of flare-associated ionospheric effect, a gradual ionospheric disturbance (GID) in contradistinction to the sudden SID or Dellinger effect. The 45 originally reported SID's have been augmented by 19 additional, well-confirmed ionospheric disturbances and by 23 less certain events.

There is no evidence to indicate that subflares are not merely smaller, fainter examples of the flare phenomenon. Flares and subflares in this study have similar disk distributions and rates of increase and decrease in intensity. Ionospheric disturbances accompanied at least four of the brightenings here classified as subflares.

ERRATA

On page 44, Volume **122,** in equation (13), for $-GM(x)$ read $-3GM(x)$; in equation (15), for $\frac{g^2}{x^2}$ read $\frac{2}{9}\frac{g^2}{x^2}$; and for $\left[\frac{4}{3}\frac{g}{x} - (\gamma+1)\,g'\right]$ read $\left[\frac{4}{3}\frac{g}{x} - (\gamma+1)\,g'\right]g''$.

On page 45, in equation (19), for P_6 read $-P_6$; in equation (19), right-hand side of $-P_6$, for

$$\left(\frac{8+30\gamma-189\gamma^2+243\gamma^3}{6}\right) \text{ read } \left(\frac{8+30\gamma+189\gamma^2+243\gamma^3}{6}\right).$$

In equations (21), (24), (25), (26), and (27), coefficient of cubed term should read "minus."

THE OBSERVATORY

FOUNDED 1877

* * *

A Magazine presenting current developments in Astronomy by means of Articles, Correspondence, Notes on discoveries and Reviews of important astronomical books. The papers read at the Meetings (Astronomical & Geophysical) of the Royal Astronomical Society and the discussions which follow are also fully reported.

* * *

Annual subscription for 6 issues, post free, £1 (U.S.A. and Canada, $3.00) should be sent to

***The Editors,* ROYAL GREENWICH OBSERVATORY**

Herstmonceux Castle, Hailsham, Sussex, England

THE ASTROPHYSICAL JOURNAL

announces the publication of

A GENERAL INDEX, Volumes 76–100

Price: $6.00*

ORDERS NOW ACCEPTED

Also available:

GENERAL INDEX, Volumes 1–25 .....$3.00
GENERAL INDEX, Volumes 26–50 .....$3.00
GENERAL INDEX, Volumes 51–75 .....$3.00

* Postage $0.15 per copy extra to foreign addresses.

THE UNIVERSITY OF CHICAGO PRESS

5750 ELLIS AVENUE CHICAGO 37 • ILLINOIS

THE ASTROPHYSICAL JOURNAL SUPPLEMENT SERIES

These *Supplements* are intended to provide a medium for the publication of extensive investigations, such as wave-length lists of stars of special interest, photometric data, results of numerical integrations pertaining to stellar interiors, model stellar atmosphere calculations, and original memoirs.

Supplement No. 18

"A Catalogue of High-Velocity Stars." NANCY G. ROMAN.

The catalogue contains new spectral types, photoelectric magnitudes and colors, and spectroscopic parallaxes for about 600 high-velocity stars. For most of these, the space velocities and the eccentricities and semimajor axes of their galactic orbits are also given.

(Published December, 1955. Price, $1.25)

Supplement No. 19

"Revised List of Absorption Lines in the Spectrum of R Andromedae." PAUL W. MERRILL and JESSE L. GREENSTEIN

This article lists the wave lengths, intensities, and identifications of 1500 absorption lines from 4000 to 6900 A in the spectrum of the S-type long-period variable star R Andromedae. The behavior of lines of various metals, including technetium, and of the rare earths is briefly described.

(Published January, 1956. Price, $1.25)

Supplement No. 20

"Photometry of Solar Flares." HELEN W. DODSON, E. RUTH HEDEMAN, and ROBERT R. MCMATH

Photometric measures of $H\alpha$ spectroheliograms provide observational data for studies of intensity, area, and duration of 194 flares and subflares. Rates of increase and decrease of intensity, center-to-limb variations, and associated ionospheric disturbances are determined and compared. Whenever possible, the implications of these analyses are tested by auxiliary studies of the larger number of flares in the *Quarterly Bulletin of Solar Activity*.

(Ready February, 1956. Price, $1.25)

An abstract of each supplement will be published in THE ASTROPHYSICAL JOURNAL. The *Supplements* will appear irregularly and may be purchased separately or by subscription. Each volume of *Supplements* will consist of approximately 500 pages.

Subscriptions

$8.00 per current volume

Canada, $8.75. Foreign, $9.50.

To members of the American Astronomical Society, $6.00 per current volume.

Orders now accepted.

THE UNIVERSITY OF CHICAGO PRESS

5750 ELLIS AVENUE CHICAGO 37, ILLINOIS